

# Conceptual Design for a Supersonic Advanced Military Trainer

A project presented to  
The Faculty of the Department of Aerospace Engineering San José State University

In partial fulfillment of the requirements for the degree  
Master of Science in Aerospace Engineering

by

Royd A. Johansen

May 2019

approved by

Dr. Nikos Mourtos  
Faculty Advisor



© 2019  
Royd A. Johansen  
ALL RIGHTS RESERVED

## **ABSTRACT**

### **CONCEPTUAL DESIGN FOR A SUPERSONIC ADVANCED MILITARY TRAINER by Royd A. Johansen**

The conceptual aircraft design project is based off the T-X program requirements for an advanced military trainer (AMT). The design process focused on a top-level design aspect, that followed the classic aircraft design process developed by J. Roskam's *Airplane Design*. The design process covered: configuration selection, weight sizing, performance sizing, fuselage design, wing design, empennage design, landing-gear design, Class I weight and balance, static longitudinal and directional stability, subsonic drag polars, supersonic area rule applied to supersonic drag polars, V-n diagrams, Class II weight and balance, moments and products of inertia, and cost estimation. Throughout the process other materials and references are consulted to verify or develop a better understanding of the concepts in the *Airplane Design* series.

## ACKNOWLEDGEMENTS

I would like to express my deep gratitude to Dr. Nikos Mourtos for his support throughout this project and his invaluable academic advisement throughout my undergraduate and graduate studies. I would also like to thank Professor Gonzalo Mendoza for introducing Aircraft Design to me as an undergraduate and for providing additional insights throughout my graduate studies. My thanks are also extended to Professor Jeanine Hunter for helping me develop my theoretical foundation in Dynamics, Flight Mechanics, and Aircraft Stability and Control.

I would also like to thank Heidi Eisips for her help with utilizing Microsoft Word's capabilities and additional editorial recommendations. My thanks also goes to Reine Dominique Ntone Sike for providing feedback and editorial recommendations.

Finally, I would like to thank my friends and family that have continued to give me support and encouragement throughout my academics.

# Contents

1.	Introduction.....	1
1.1	Mission Requirements.....	1
1.2	Mission Profile .....	1
1.3	Market Analysis .....	2
1.4	Technical and Economic Feasibility .....	2
1.5	Comparative Study of Similar Airplanes.....	3
1.5.1	Mission Capabilities and Configuration Selection.....	3
1.5.2	Comparison of Important Design Parameters.....	5
1.5.3	Discussion and Conclusion .....	5
2.	Configuration Design.....	7
2.1	Comparative Study of Similar Airplanes.....	7
2.1.1	Wing Configuration .....	7
2.1.2	Empennage Configuration .....	7
2.1.3	Propulsion System .....	8
2.1.4	Landing-Gear .....	8
2.1.5	Proposed Configuration .....	8
3.	Weight Sizing.....	9
3.1	Mission Weight Estimates.....	9
3.1.1	Database for Takeoff and Empty Weights from Similar Airplanes .....	9
3.1.2	Determination of Weight Regression Coefficients A and B.....	9
3.1.3	Determination of Mission Weights .....	10
3.2	Takeoff Weight Sensitivities .....	13
3.2.1	Manual Calculation of Takeoff Weight Sensitivities.....	13
3.2.2	Calculation of Takeoff Weight Sensitivities using the AAA Program .....	15
3.2.3	Trade Studies .....	16
3.3	Conclusion.....	18
4.	Performance Sizing.....	19
4.1	Manual Calculation of Performance Constraints.....	20
4.1.1	Stall Speed .....	20
4.1.2	Takeoff Distance.....	20
4.1.3	Landing Distance .....	21
4.1.4	Drag Polar Estimation.....	21
4.1.5	Climb Constraints .....	23
4.1.6	Speed Constraint .....	24
4.1.7	Maneuvering Constraint.....	25
4.2	Calculation of Performance Constraints with the AAA Program.....	26
4.2.1	Stall Speed .....	26
4.2.2	Takeoff Distance.....	27
4.2.3	Landing Distance .....	27
4.2.4	Drag Polar Estimation.....	28
4.2.5	Climb Constraints .....	30
4.2.6	Speed Constraint .....	31
4.2.7	Maneuvering Constraint.....	31
4.3	Summary of Performance Constraints.....	32
4.4	Propulsion System Selection .....	33
4.4.1	Propulsion System Type .....	33
4.4.2	Number of Engines .....	34
4.5	Summary of Performance Sizing.....	35
5.	Fuselage Design.....	36

5.1	Layout Design of the Cockpit.....	36
5.1.1	Dimensions and Weights for Crew Members .....	36
5.1.2	Layout of Cockpit Seating and Cockpit Controls .....	38
5.1.3	Determination of Visibility from the Cockpit.....	41
5.1.4	Cockpit Layout .....	43
5.2	Layout Design of the Fuselage.....	44
5.3	Summary of Fuselage Design.....	45
6.	Wing Design .....	46
6.1	Wing Planform .....	46
6.2	Airfoil Selection .....	47
6.3	Wing Geometry .....	49
6.4	Wing Design Evaluation.....	50
6.5	Design of the High-Lift Devices .....	52
6.5.1	Trailing-Edge Flaps .....	53
6.5.2	Leading-edge Flaps.....	55
6.5.3	High-Lift Devices Evaluation.....	56
6.6	Design of the Lateral Control Surfaces .....	57
6.7	Drawings .....	57
6.8	Discussion and Conclusion.....	58
7.	Empennage Design .....	61
7.1	Overall Empennage Design.....	61
7.2	Design of the Horizontal Stabilizer .....	61
7.3	Design of the Vertical Stabilizer .....	62
7.4	Design of the Longitudinal and Directional Controls.....	63
7.5	Horizontal Stabilizer and Vertical Fin Geometry Drawings .....	63
7.6	AMT Views with Horizontal and Vertical Stabilizers .....	64
7.7	Discussion and Conclusion.....	65
8.	Class I Weight and Balance and Landing-Gear Design .....	66
8.1	Weight and Balance.....	66
8.1.1	Estimation of the Center of Gravity Location for the AMT.....	66
8.1.2	Center of Gravity Location for Various Loading Scenarios .....	68
8.2	Landing-Gear Design .....	69
8.2.1	Landing-Gear Configuration, Tip-Over, and Ground Clearance Criteria.....	69
8.2.2	Length and Diameter of Struts, and Tire Specifications .....	70
8.2.3	Landing-Gear Drawings.....	71
8.3	Discussion and Conclusion.....	72
9.	Longitudinal and Directional Stability and Control.....	73
9.1	Static Longitudinal Stability.....	73
9.1.1	Determination of Wing-Fuselage Aerodynamic Center with Monk's Method.....	74
9.1.2	Wing and Horizontal Lift-Curve Slopes .....	76
9.1.3	Downwash Gradient at Horizontal Stabilizer .....	77
9.1.4	Static Margin.....	78
9.1.5	Longitudinal X-plot .....	78
9.2	Static Directional Stability .....	80
9.2.1	Fuselage Contribution to the Yawing Moment Coefficient due to Sideslip .....	80
9.2.2	Vertical Fin Lift-Curve Slope .....	82
9.2.3	Directional X-plot.....	82
9.2.4	Sideslip to Rudder Feedback Gain.....	82
9.3	Discussion and Conclusion.....	83
10.	Refined Drag Polars.....	84
10.1	Airplane Zero-Lift Drag .....	84

10.2	Low Speed Drag Increments .....	86
10.2.1	High-lift Devices Drag Increment .....	86
10.2.2	Deployed Landing-Gear Drag.....	87
10.3	Compressibility Drag.....	87
10.3.1	Supersonic Contributions.....	88
10.3.2	Area Ruling.....	95
10.4	AMT Drag Polars .....	98
10.4.1	Clean .....	98
10.4.2	Takeoff and Landing.....	98
10.4.3	Supersonic.....	98
10.4.4	Drag Polars .....	99
10.5	Discussion and Conclusion.....	100
11.	V-n Diagram .....	101
11.1	Load Limits .....	101
11.2	Stall Speed.....	101
11.3	Design Maneuvering Speed.....	101
11.4	Maximum Level Flight Speed .....	102
11.5	Dive Limit Speed.....	103
11.6	V-n Plot .....	103
11.7	Discussion and Conclusion.....	104
12.	Class II Weight and Balance .....	105
12.1	Known and Previous Weights .....	105
12.2	Revised Weight Estimates.....	105
12.2.1	Structural Weight.....	105
12.2.2	Powerplant Weight.....	106
12.2.3	Fixed Equipment Weight .....	107
12.3	Iterated Weight Summary.....	109
12.4	Component Centers of Gravity.....	110
12.4.1	Discussion.....	112
12.5	Aircraft Moments and Products of Inertia.....	113
12.6	Performance Reevaluated.....	114
13.	Life-Cycle Cost Analysis .....	115
13.1	Research, Development, Testing, and Evaluation Costs .....	115
13.1.1	Airframe, Engineering, and Design Cost .....	116
13.1.2	Development, Support, and Testing Cost .....	116
13.1.3	Prototype Test Airplanes Cost .....	116
13.1.4	Flight Test Operation Cost.....	118
13.1.5	Test and Simulation Facilities Cost .....	118
13.1.6	RDTE Profit.....	118
13.1.7	RDTE Finance Cost.....	119
13.1.8	Summary of RDTE Costs .....	119
13.2	Manufacturing and Acquisition Cost.....	119
13.2.1	Airframe, Engineering, and Design Cost .....	120
13.2.2	Aircraft Production (APC <sub>m</sub> ) Cost.....	120
13.2.3	Production Flight Test Operations Cost.....	121
13.2.4	Manufacturing Finance Cost.....	122
13.2.5	Manufacturing Profit Cost .....	122
13.2.6	Summary of Manufacturing and Acquisition Cost .....	122
13.3	Operating Cost.....	123
13.3.1	Fuel, Oil, and Lubricants (FOL) Cost .....	123
13.3.2	Direct Personnel Cost .....	123
13.3.3	Indirect Personnel Cost.....	viii

13.3.4	Consumable Materials Cost .....	124
13.3.5	Spares Cost .....	124
13.3.6	Miscellaneous Costs.....	124
13.3.7	Summary of Operating Costs.....	124
13.4	Disposal Cost.....	125
13.5	Summary of Life-Cycle Cost.....	125
13.6	Discussion .....	126
14.	Final Design .....	127
14.1	Environmental and Economic Tradeoffs.....	127
14.2	Safety and Economic Tradeoffs .....	127
14.3	Summary of Design Parameters and Drawings .....	129
14.4	Boeing/Saab T-X Trainer .....	131
14.5	Recommendations and Future Work Opportunities .....	132
	References.....	133

## Figures

Figure 1. Flight profiles of AMT .....	2
Figure 2. Initial AMT design sketches .....	8
Figure 3. Determining A and B coefficients .....	9
Figure 4. Basic flight profile .....	11
Figure 5. AAA – Flight profile weight fractions.....	12
Figure 6. AAA – Regression coefficients from comparable aircraft.....	12
Figure 7. AAA – LogLog plot of comparable aircraft for $W_E$ and $W_{TO}$ .....	12
Figure 8. AAA – weight output.....	13
Figure 9. AAA – sensitivity output .....	16
Figure 10. Range versus payload and fuel mass .....	17
Figure 11. Endurance versus payload and fuel mass. ....	17
Figure 12. Stall speed performance sizing graph .....	20
Figure 13. Takeoff distance performance sizing graph.....	21
Figure 14. Landing distance performance sizing graph .....	21
Figure 15. Takeoff and landing drag polar.....	22
Figure 16. Clean drag polar.....	22
Figure 17. Supersonic drag polar .....	23
Figure 18. Climb requirement performance sizing graph .....	24
Figure 19. Speed requirement performance sizing graph.....	25
Figure 20. Maneuvering performance sizing graph .....	26
Figure 21. AAA – Stall T/W versus W/S.....	26
Figure 22. AAA – Takeoff distance T/W versus W/S .....	27
Figure 23. AAA – Landing distance T/W versus W/S.....	27
Figure 24. AAA – Takeoff drag polar.....	28
Figure 25. AAA – Clean drag polar .....	29
Figure 26. AAA – Takeoff climb T/W versus W/S .....	30
Figure 27. AAA – Speed T/W versus W/S .....	31
Figure 28. AAA – 7g maneuver T/W versus W/S .....	31
Figure 29. AAA – Performance sizing graph.....	32
Figure 30. Hand calculation performance sizing graph .....	32
Figure 31. Mach altitude plot.....	34
Figure 32. Mach versus altitude .....	34
Figure 33. Standing crewman dimension relations .....	36
Figure 34. Sitting crewman dimension relations.....	37
Figure 35. Crewman space sitting position .....	38
Figure 36. Recommended seat arrangement for military .....	39
Figure 37. Recommended clearances for ejection seats.....	39
Figure 38. Typical ejection seat dimensions .....	40
Figure 39. Fighter/attack cockpit arrangement .....	40
Figure 40. Port and starboard visibility requirements .....	41
Figure 41. Definition of radial eye vectors .....	42
Figure 42. Recommended seat arrangement .....	42
Figure 43. Cockpit cutaway side view .....	43
Figure 44. Cockpit cutaway top view .....	43
Figure 45. Cockpit cutaway front view.....	43
Figure 46. Fuselage cutaway side view.....	44
Figure 47. Fuselage side view .....	44
Figure 48. Fuselage top view .....	44
Figure 49. Fuselage front view .....	44

Figure 50. Preliminary engine intake ducts.....	45
Figure 51. Fuselage isometric view .....	45
Figure 52. Wing sweep versus airfoil thickness ratio .....	47
Figure 53. Wing weight percent of takeoff weight versus wing sweep angle.....	47
Figure 54. NACA 0008.....	48
Figure 55. NACA 0008 aerodynamic polars.....	48
Figure 56. NACA 0008 aerodynamic polars.....	49
Figure 57. NACA 0008 coefficient polars from XFLR5 .....	49
Figure 58. AAA – Airfoil $c_{l,max}$ .....	51
Figure 59. AAA – Wing geometry.....	52
Figure 60. AAA – Wing $C_{L,max}$ .....	52
Figure 61. Wing flapped area.....	53
Figure 62. Relation of flap chord ratio and K factor .....	54
Figure 63. Effect of thickness ratio and flap chord ratio on $c_{l,\delta f}$ .....	54
Figure 64. Effect of trailing-edge flap deflection and flap chord ratio on K' .....	55
Figure 65. Effect of leading-edge flap chord ratio on $c_{l,\delta}$ .....	56
Figure 66. Effect of $\delta_{nf}$ and $c_{nf}/c$ on $\Delta c_l$ .....	56
Figure 67. Proposed wing geometry .....	57
Figure 68. Aviation jet fuel densities versus temperature .....	58
Figure 69. AMT front view fuselage and wing.....	59
Figure 70. AMT side view fuselage and wing .....	59
Figure 71. AMT top view fuselage and wing.....	59
Figure 72. X-1 aircraft .....	63
Figure 73. NACA 0010 profile .....	63
Figure 74. Horizontal stabilizer geometry drawing .....	64
Figure 75. Vertical stabilizer geometry drawing.....	64
Figure 76. AMT front view with empennage.....	64
Figure 77. AMT side view with empennage .....	65
Figure 78. AMT top view with empennage .....	65
Figure 79. Aircraft side view with coordinate system .....	67
Figure 80. Top view with component center of gravity.....	68
Figure 81. Side view with component center of gravity .....	68
Figure 82. $X_{cg}$ travel from ref. point for different loading scenarios.....	68
Figure 83. Tricycle gear longitudinal tip-over criterion.....	69
Figure 84. Tricycle gear lateral tip-over criterion .....	69
Figure 85. Ground clearance criterion .....	70
Figure 86. Landing-Gear position and symbols.....	70
Figure 87. Side view of landing-gear.....	71
Figure 88. Back view of nose landing-gear .....	71
Figure 89. Back view of main landing-gear.....	72
Figure 90. Parameter definitions for Monk's method.....	74
Figure 91. Effect of fuselage (or nacelle) segment location on upwash gradient .....	75
Figure 92. Layout of AMT's fuselage for Monk's method .....	75
Figure 93. Wing parameter relations.....	76
Figure 94. Change in wing and horizontal lift-curve slope due to Mach number.....	77
Figure 95. Change in tail downwash due to Mach number.....	78
Figure 96. Effect of Mach number on static margin .....	78
Figure 97. X-plot for change in horizontal position.....	79
Figure 98. X-plot for change in horizontal area .....	80
Figure 99. Wing-fuselage interference with directional stability.....	81
Figure 100. Fuselage Reynolds number versus $K_{R1}$ .....	81

Figure 101. Mach number effect on vertical fin lift-curve slope .....	82
Figure 102. Mach effect on change in yawing moment wrt sideslip angle.....	82
Figure 103. Control surface effectiveness parameter $\tau_{\square}$	83
Figure 104. Mach number effect on $K_{\beta}$	83
Figure 105. Definition of fuselage variables.....	84
Figure 106. Nacelle geometry.....	85
Figure 107. Effect of equivalent skin friction on wetted and parasite area.....	85
Figure 108. Plain flap profile drag increase.....	86
Figure 109. Interrupted flap induced drag factor.....	87
Figure 110. Zero-lift drag rise versus Mach number for various aircraft.....	88
Figure 111. Reynolds number effect on turbulent mean skin-friction coefficient.....	88
Figure 112. Definition of supersonic and subsonic leading-edge.....	89
Figure 113. Definition of basic wing.....	89
Figure 114. Leading-edge pressure drag.....	90
Figure 115. Supersonic drag due to lift for straight tapered wings.....	91
Figure 116. Fuselage parameters defined.....	92
Figure 117. Drag of slender fore or aft bodies.....	92
Figure 118. Interference drag of pointed forebody with truncated aftbody.....	93
Figure 119. Bodies of revolution base drag.....	93
Figure 120. Steady-state cross flow drag coefficient.....	94
Figure 121. AMT Solidworks model.....	95
Figure 122. Solidworks cut view and measure feature.....	95
Figure 123. AMT, cut at wing-fuselage intersection.....	96
Figure 124. AMT area distribution.....	96
Figure 125. AMT non-dimensional diameter comparison to Sears-Haack type-I.....	97
Figure 126. AMT's cross-sectional area distributions.....	97
Figure 127. AMT drag polars.....	100
Figure 128. AMT clean configuration V-n diagram.....	104
Figure 129. AMT deployed HLD configuration V-n diagram.....	104
Figure 130. $X_{cg}$ travel for Class II W&B from reference point for different loading scenarios.....	111
Figure 131. AMT wing fuel cell.....	112
Figure 132. AMT fuselage fuel cell.....	112
Figure 133. Change in CEF over time.....	115
Figure 134. Prototype test airplanes cost percentages.....	118
Figure 135. Research, development, testing, and evaluation cost percentages.....	119
Figure 136. Aircraft production cost percentages.....	121
Figure 137. Manufacturing and acquisition cost percentages.....	122
Figure 138. Operational cost percentages.....	125
Figure 139. Life-cycle cost percentages.....	126
Figure 140. T-38 structure upgrades.....	128
Figure 141. AMT 3-view drawing.....	131
Figure 142. Boeing/Saab T-X aircraft.....	131

## Tables

Table 1. Comparable aircraft configurations and capabilities.....	4
Table 2. Comparable aircraft parameters.....	5
Table 3. Empty and takeoff weights of comparable aircraft.....	9
Table 4. Weight sensitivities.....	15
Table 5. Sensitivity comparison.....	16

Table 6. Aircraft performance requirements.....	19
Table 7. Performance at design point.....	33
Table 8. Possible engines.....	35
Table 9. Summary of critical parameters.....	35
Table 10. Dimensions for male crew members.....	37
Table 11. Sitting dimensions for male crew members.....	38
Table 12. Wing sweep angle versus thickness ratio.....	46
Table 13. Preliminary wing geometry.....	50
Table 14. Effect of flap chord ratio and K factor on $\Delta c_1$ .....	55
Table 15. Nose flap parameters.....	56
Table 16. Summarized wing geometry.....	60
Table 17. Tail volumes of comparable aircraft.....	61
Table 18. Horizontal stabilizer geometry.....	62
Table 19. Vertical fin geometry.....	63
Table 20. Similar aircraft component weights.....	66
Table 21. Component weights, coordinates from reference point, and weight fractions.....	67
Table 22. Center of gravity location for loading and unloading scenarios from reference point.....	69
Table 23. Landing-Gear parameters.....	72
Table 24. Values of wing and horizontal lift-curve slopes for Mach number correction.....	77
Table 25. Incremental change in horizontal position for X-plot.....	79
Table 26. Incremental change in horizontal area for X-plot.....	79
Table 27. Aircraft parameters for fuselage yawing-moment coefficient due to sideslip.....	80
Table 28. AMT's equivalent bodies of revolution thickness ratio for Mach condition.....	98
Table 29. AMT stall speed for given altitudes for clean and HLD configurations.....	101
Table 30. AMT minimum maneuver speed for given altitudes for clean and HLD configurations.....	101
Table 31. Dynamic pressure solution to equation (11.7) and $V_H$ .....	103
Table 32. Known and previous weights.....	105
Table 33. AMT structure weight summary.....	106
Table 34. AMT powerplant weight summary.....	107
Table 35. AMT fixed equipment weight summary.....	109
Table 36. Summary of class I and class II AMT component weights with percent change.....	110
Table 37. Class II component weights and coordinates from reference point.....	111
Table 38. Class II W&B center of gravity location for loading and unloading scenarios from reference point.....	112
Table 39. Moments and products of inertia.....	113
Table 40. AMT performance revaluated.....	114
Table 41. Summary of prototype test airplanes costs.....	118
Table 42. Summary of RDTE.....	119
Table 43. Summary of APC costs.....	121
Table 44. Summary of manufacturing and acquisition cost.....	122
Table 45. Summary of operational costs.....	125
Table 46. Summary of LCC.....	126
Table 47. AMT design parameters.....	129
Table 48. Boeing/Saab T-X- aircraft specs.....	132

## Abbreviations and Symbols

### Abbreviations

AR	Aspect ratio
A	Regression coefficient
A/C	Aircraft
AMT	Advanced military trainer
b	Wing span
B	Regression coefficient
$\bar{c}$	Mean chord
$c_f$	Skin friction coefficient
cg/CG	Center of gravity
$c_j$	Specific fuel consumption
$c_l$	Section lift coefficient
C	Fuel fraction parameter
$C_d$	$C_D/\text{span}$
$C_D$	Coefficient of drag
$C_{D_0}$	Zero-lift drag coefficient
CGR	Climb gradient
$C_l$	$C_L/\text{span}$
$C_L$	Coefficient of lift
$C_P$	Coefficient of pressure
D	Weight parameter $W_{PL} + W_{crew}$
e	Oswald's efficiency factor
E	Endurance
F	Breguet factor
h	Altitude
h	Change in altitude (m/s)
inv	inverse
$l$	Length
L/D	Lift-to-drag ratio
M	Mach number
M	Mission weight fraction
MAC	Mean aerodynamic chord
$n_s$	Number of struts
n	Load factor (g's)
N	Number
NES	Never exceed speed
P	Power
$P_m$	Main landing-gear maximum load
$P_n$	Nose landing-gear maximum load
$q_\infty$	Dynamic pressure
R	Range
$R_{bank}$	Turn radius
$\mathcal{R}$	Specific gas constant
RC	Rate of climb
Re	Reynolds number
s	Distance on TO and Landing
S	Wing area
$S_{wet}$	Wetted wing area
SM	Static margin

S&C	Stability and Control
t	time
$t_r$	Wing root thickness
T	Thrust
TSFC	Thrust specific fuel consumption
T/W	Thrust loading
V	Velocity
$V$	Tail volume coefficient
W	Weight
W/S	Wing loading
W&B	Weight and balance
x	Position from design ref. point
$\bar{x}$	Nondimensional x-position $x/\bar{c}$

### Greek

$\alpha$	Angle of attack
$\beta$	Sideslip angle, or Mach parameter
$\Gamma$	Dihedral angle
$\gamma$	Specific heat ratio
$\epsilon$	Downwash angle
$\eta$	Non-dimensional wing span location
$\Lambda$	w, h, v, c sweep angle
$\lambda$	Taper ratio
$\rho$	Air density
$\sigma$	Air density ratio ( $\rho_{alt}/\rho_{sea}$ )
$\omega$	Turn rate

### Subscripts

abs	Absolute
ac	Aerodynamic center
ai	Air induction
av	Available
A/C	Aircraft
AB	Afterburner
Ap	Approach
Alt	Altitude
c/4	Quarter chord
cle	Clean
cli	Climb
cr	Cruise
crew	Crew
dL	Dive Limit
eng	Engine
E	Empty
ff	Fuel fraction
F	Fuel
FEQ	Fixed equipment
FL	Field length

fus	Fuselage	$C_{L_{\alpha_h}}$	Horizontal stabilizer lift slope, $\partial C_L / \partial a$
guess	Guessed value	$C_{L_{\alpha_w}}$	Wing lift slope, $\partial C_L / \partial a$
h	Horizontal stabilizer	$C_{n_\beta}$	Variation in yawing moment due to sideslip $\partial C_n / \partial b$
H	Maximum level flight speed/Mach		
L	Lift		
La	Landing		
LE	Leading-edge		
LG	Landing-Gear		
LO	Lift off		
Ltr	Loiter		
m	Main gear		
max	Maximum		
ME	Manufacturer's empty		
n	Nose gear		
OE	Operating empty		
plf	Planform		
PL	Payload		
res	Reserve fuel		
req	Required		
r	Root		
R	Range		
RC	Rate of climb		
sub	Subsonic		
sup	Supersonic		
ss	Supersonic		
ST	Stall		
t	Tip		
tent	Tentative		
tfo	Trapped fuel/oil		
TE	Trailing-edge		
TO	Takeoff		
used	Used (fuel)		
v	Vertical stabilizer		
w	Wing		
wet	Wetted		
wrt	With respect to		
wf	Wing + fuselage		

#### Multiple subscripts

$\Delta c_{l_{req}}$	Required change in sectional lift coefficient
$\Delta c_{l_{des}}$	Design sectional lift coefficient incremental increase
$c_{l_\alpha}$	Airfoil/section lift-curve slope, $\partial c_l / \partial a$
$c_{l_{\delta_f}}$	Airfoil/section change in lift coefficient with respect to flap deflection, $\partial c_l / \partial \delta_f$

# 1. Introduction

The purpose of this project is to explore the aircraft design process to develop a design for an advanced military trainer (AMT). There are two classes of trainers, basic and advanced. Basic trainers are for the introduction of flying at low subsonic speeds. Advanced trainers are for pilots that will progress to faster aircraft, such as fighters or bombers. Advanced trainers are similar to the fighter class of aircraft in that they are smaller and more maneuverable than other military aircraft.

Aircraft design is a complex engineering process that requires knowledge and skills from multiple disciplines, and an artistic mind to blend the different aspects together. The process requires an analysis of the design space while considering mission requirements. Through the design process, compromises are made in favor of critical requirements to achieve a design that meets the mission specifications and looks appealing. If an aircraft cannot perform as expected by the customer or “look” good, then no consumer would buy the aircraft.

The motivation for this type of design comes from fighter planes. Fighters are fast, maneuverable, and help develop new technologies to meet engineering challenges. An advanced trainer was chosen for the design because it is a smaller-scale version of a fighter plane. Many of the advanced trainers in the military are based on 30-plus-year-old technology, with many modifications to keep up with training program demands, and will soon be meeting the end of their life-cycle. The United States Air Force (USAF) is in the process of replacing their aging trainer, the T-38 Talon, with a program called the T-X trainer. In 2017, the USAF requested proposals for the program from various manufacturers, such as Boeing, Lockheed Martin, etc. Through this project, the proposed design can be measured up against the well-known aircraft manufactures, which will help reveal the differences of aircraft design from the aerospace industry and the theoretical teachings.

## 1.1 Mission Requirements

The following mission specifications are based on the requirements set by the USAF for the T-X trainer proposals and military specification documents [1], [2], [3], and [4].

- **Crew:** Two, pilot and instructor
- **Range:** 500 nautical miles (926 km)
- **Cruise speed:** 510 knots (260m/s) at an altitude of 15,000ft (4.57km)
- **Mach number:** Capable of Mach 1.5 above 15,000ft
- **Cruise altitude:** 15,000ft (4.57km)
- **TO and Landing field requirements:** 8,000ft (2,400m) runway at an altitude of 7,400ft (2,250m) with a tail wind of 10 knots (5.1m/s)
- **Load-factor:** 6.5 at 80% max weight, altitude of +15,000ft
- **Maneuvering:** Turn rate of 12.5°/s with less than a 4,500ft (1,370m) turn radius at an altitude of more than 15,000ft
- **Climb gradient TO:** 200ft/nautical mile (32.9m/km)
- **Rate of climb:** Subsonic 500ft/min (2.54m/s), Supersonic 1,000ft/min (5.08m/s)
- **Engine efficiency:** Without AB 0.864lbm/(lbf-hr) {0.0881kg/(N-hr)}, With AB 1.98lbm/(lbf-hr) {0.202 kg/(N-hr)}

## 1.2 Mission Profile

There are twelve flight profiles given in the T-X Trainer guidelines document [2]. The USAF, in the list of requirements, have declared most maneuvers and training will occur between 10,000 and 18,000ft (3-5.5km). This would include aircraft maneuvering, high g-pulls, air-to-air, air-to-ground, and other

training exercises. The general profile of the twelve flights would consist of TO, 90 nautical miles cruise climb, flight exercise, decent, and landing. Each profile would be adjusted to fit the necessary requirements of the training missions. Three general flight profiles are shown in Figure 1.

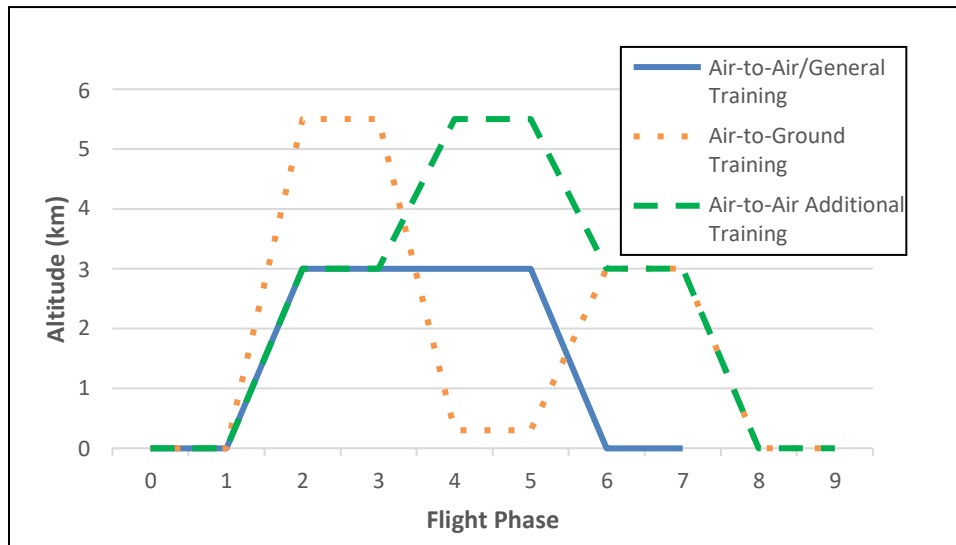


Figure 1. Flight profiles of AMT

### 1.3 Market Analysis

The market for such an aircraft is very good. The USAF is asking for 350 T-X trainers, worth a contract price of up to \$16 billion, to replace approximately 400 T-38 Talons in the AF service [5]. The success of such an aircraft could lead to additional procurements from the USAF and add the interest of the other military branches in replacing their aging advanced trainers. This could also lead to other countries wanting to procure the new modern trainer.

Modern aircraft are outfitted with many computers and advanced technologies. Today's military pilot demands are much more sophisticated than the simple stick, throttle, and rudder pedals of WWII. A new advanced trainer can be properly designed with all the modern features that are required. This will be able to prepare pilots better for the modern aircraft such as the B-2, F-22, F-35, etc. Based on the state of current aging trainers and modern aircraft demands, the market for a modern advanced military trainer is, that it is needed and wanted.

### 1.4 Technical and Economic Feasibility

An AMT is a very feasible design to achieve technically and economically. An AMT does not need all the advanced systems and weapons that a modern fighter or bomber aircraft requires, such as stealth, range, etc. The purpose of the trainer is to prepare pilots for the future aircraft they will be assigned for service. This includes advanced flight maneuvers, formation flying, supersonic flight, and mission exercises.

The technology required for an AMT has been well established through the development of modern aircraft. Composite design and technology have been proven in various aircraft across the design spectrum and offer potential weight reduction to the overall design. Circuit systems and computers have greatly improved since when the T-38 Talon was designed. This offers more capabilities in the cockpit and will better prepare pilots for their future services. Modern computers also improve the design process to make a more efficient design through utilization of software like computational fluid dynamics (CFD), finite element analysis (FEA), and computer aided design (CAD).

A complete ground-up design costs more than modification of an already-produced plane, which is some of the manufacturers plans to bid for the T-X contract. The benefit of a new design is that it offers the capability to have a purpose-built design, which meet mission requirements and include design features to better accommodate future technologies.

## **1.5 Comparative Study of Similar Airplanes**

### **1.5.1 Mission Capabilities and Configuration Selection**

Ten aircraft were selected based on their similarities in size and performance. The T-38 Talon and T-45 Goshawk are current trainers for the USAF and USN, respectfully. The scorpion was initially a design by Textron to bid on the T-X contract, but for unspecified reasons the company withdrew its proposal. The M-346 is a design by Aermacchi, an Italian company. The T-50 Golden Eagle is an already-produced plane by Lockheed Martin and Korean Aerospace Industries. The companies have made modifications to the previous T-50 to better meet the requirements given by the USAF. The Yakovlev Yak-130 is a Russian design that is categorized as a light attack aircraft. The Northrop F-5, Dassault Mirage III, and Douglas A-4 are light attack aircraft. Finally, the Aero L-39 was developed for advanced pilot training and later modified for light attack missions. Table 1 outlines the aircraft configurations and capabilities.

Table 1. Comparable aircraft configurations and capabilities

Name	Image	Configuration	Capabilities
M-346 (2004)		<ul style="list-style-type: none"> <li>• Mid/high-wing</li> <li>• Conventional tail</li> <li>• 2-engines</li> <li>• 2 crew</li> </ul>	<ul style="list-style-type: none"> <li>• Fly-by-wire</li> <li>• Night vision display</li> <li>• Autopilot recovery system</li> <li>• 9 armaments points</li> </ul>
Scorpion (2013)		<ul style="list-style-type: none"> <li>• High-wing</li> <li>• Twin vertical</li> <li>• 2 engines</li> <li>• 2 crew</li> </ul>	<ul style="list-style-type: none"> <li>• Ground support</li> <li>• Maritime patrol</li> <li>• Airspace control</li> <li>• 6 armaments</li> <li>• Night vision capable</li> </ul>
T-38 Talon (1961)		<ul style="list-style-type: none"> <li>• Low-wing</li> <li>• Conventional tail</li> <li>• 2 engines</li> <li>• 2 crew</li> </ul>	<ul style="list-style-type: none"> <li>• No armament</li> <li>• Safety chase plane</li> <li>• Aerial photography</li> </ul>
T-45 Goshawk (1991)		<ul style="list-style-type: none"> <li>• Low-wing</li> <li>• Conventional tail</li> <li>• 1 engine</li> <li>• 2 crew</li> </ul>	<ul style="list-style-type: none"> <li>• Carrier-capable</li> <li>• External payload capable (practice armaments, fuel pods)</li> </ul>
T-50 Golden Eagle (2002)		<ul style="list-style-type: none"> <li>• Mid-wing</li> <li>• Conventional tail</li> <li>• 1 engine</li> <li>• 2 crew</li> </ul>	<ul style="list-style-type: none"> <li>• Easy transition to modern fighters</li> <li>• Air-to-air and air-to-ground capable</li> <li>• Light attack and multi-role</li> </ul>
Yak-130 (1996)		<ul style="list-style-type: none"> <li>• Mid-wing</li> <li>• Conventional tail</li> <li>• 2 engines</li> <li>• 2 crew</li> </ul>	<ul style="list-style-type: none"> <li>• 9 external armament points</li> <li>• Light attack</li> <li>• Air-to-air and air-to-ground capable</li> </ul>
F-5 Tiger		<ul style="list-style-type: none"> <li>• Low-wing</li> <li>• Conventional tail</li> <li>• 2 engines</li> <li>• 1 crew</li> </ul>	<ul style="list-style-type: none"> <li>• 7 external armament points</li> <li>• Light-fighter</li> </ul>
Mirage III		<ul style="list-style-type: none"> <li>• Low-delta-wing</li> <li>• Tailless</li> <li>• 1 engine</li> <li>• 1 crew</li> </ul>	<ul style="list-style-type: none"> <li>• Early delta-wing development</li> <li>• Interceptor</li> <li>• Poor low-speed performance</li> <li>• 5 external armament points</li> </ul>
A-4 Skyhawk		<ul style="list-style-type: none"> <li>• Low-wing</li> <li>• Conventional tail</li> <li>• 1 engine</li> <li>• 1 crew</li> </ul>	<ul style="list-style-type: none"> <li>• Carrier-capable</li> <li>• Light attack aircraft</li> <li>• Various armament types</li> </ul>
L-39 Albatros		<ul style="list-style-type: none"> <li>• Low-wing</li> <li>• Conventional tail</li> <li>• 1 engine</li> <li>• 2 crew</li> </ul>	<ul style="list-style-type: none"> <li>• 2 external armament points</li> <li>• Light attack capable</li> <li>• Designed for advanced pilot training</li> </ul>

### 1.5.2 Comparison of Important Design Parameters

The ten aircraft selected were investigated for their flight parameters and specifications. Table 2 presents the performance parameters and specifications for the aircraft. The wing and thrust loading of the aircraft were approximated from the average of the empty and maximum weights for the aircraft that did not have reported values. The tabulated parameters were found in [6] through [17].

Table 2. Comparable aircraft parameters

Parameter	Units	M-346	Scorpion	T-38 Talon	T-45 Goshawk	T-50 Golden Eagle
$W_{TO}$	kN	93.2	97.9	53.9	62.7	120
$W_E$	kN	45.2	56.5	32.1	43.7	63.5
T	kN	56	36	18.2	26	53
$V_{ST}$	km/hr	176	176	240	130	167
Range	km	1,980	2,960	1,835	1,290	1,850
RC	km/min	6.7	N/A	10.2	2.44	11.8
S	m <sup>2</sup>	23.5	16.3	15.8	17.7	23.7
b	m	9.72	10.4	7.6	9.39	9.45
AR	---	4.0	6.6	3.6	5.0	3.8
W/S	N/m <sup>2</sup>	2,795	4,737	3,325	3,001	3,884
T/W	---	0.84	0.47	0.65	0.49	0.96
Load limits	g	-3/+6	N/A	-3/+7.3	-3/+7.3	-3/+8
Ceiling	km	13.7	13.7	15.2	13.0	14.6
Parameter	Units	Yak-130	F-5 Tiger	Mirage III	A-4 Skyhawk	L-39
$W_{TO}$	kN	101	110	134	109	44.7
$W_E$	kN	45.1	42.7	69.1	46.5	34.9
T	kN	49.0	44.4	60.8	41.0	16.9
$V_{ST}$	km/hr	165		262	193	158
Range	km	2,100	1,405	3,335	3,220	1,100
RC	km/min	3.9	10.5	5.0	2.6	1.26
S	m <sup>2</sup>	23.52	17.3	34.85	24.15	18.8
b	m	9.84	8.13	8.22	8.38	9.46
AR	---	4.1	3.82	1.9	2.9	4.8
W/S	N/m <sup>2</sup>	2,711	4,410	3,795	3,378	2,452
T/W	---	0.70	0.58	0.45	0.51	0.37
Load limits	---	-3/+9	-3/+7	-3/+9	-3/+8	N/A
Ceiling	km	12.5	16	17.0	12.9	11.0

### 1.5.3 Discussion and Conclusion

The aircraft have similar configurations with the exception of the Mirage III, a delta wing. Based on the selected aircraft, there is no preference in wing position given the aircraft feature low, mid, and high-wing configurations. The capabilities of the aircraft differ from one to another. Some can transition easily to a light attack aircraft with the addition of munitions for air or ground attacks. All aircraft are capable as ferry or escort planes. Others are capable of aerial surveillance and other light missions.

When comparing flight perimeters and performance, all the planes vary from one degree to another. Most of the planes are between 34 and 70 kN empty weight, and depending on the design, each plane has

a takeoff weight of 46 to 135 kN. The maximum speed, rate of climb, and service ceiling of each of the aircraft are a result of the design's wing and thrust loading.

A low-wing loading equates to a larger wing, which produces more lift and drag. More lift is good for low speed performance, rate of climb, and potential service ceiling, but a larger wing carries a greater drag penalty. Coupled with inadequate available thrust or inefficient engines, this results in lower max speeds and service ceiling.

The planes vary in wing area, which can be attributed to designer's choice during the design process. The choices could have been in favor of reducing drag (smaller wing) for increase speed performance, or a larger wing for better lift characteristics for maneuvering. The other sizing parameters would have been determined from a performance matching graph method. A matching graph is used to plot important parameters as functions of wing loading and thrust to weight ratio. Using the plotted curves, the design space of an aircraft can be narrowed down to a smaller area that meets specific design constraints. Using the design point found in the matching graph, a designer can determine sizing parameters such as wing area wing span, power or thrust required, aspect ratio, etc.

The comparison of previous aircraft gives a good baseline of what the proposed AMT configuration, capabilities, and flight performance parameters should be. The proposed aircraft must meet the minimum requirements of the USAF and have the capability to integrate future technologies. The AMT must be a better platform for student pilots transitioning from basic flight training to advanced training. The critical design parameters will be maneuverability and speed. The difficulty with maneuverability will be to ensure the structure of the aircraft can sustain the g-loads in high-g maneuvers. Speed is an issue, because most of the training flights are subsonic. Demanding supersonic capabilities from an aircraft that mostly flies subsonic leads to difficult design choices for engineers.

## **2. Configuration Design**

### **2.1 Comparative Study of Similar Airplanes**

The aircraft presented in Table 2, section 1.5.2, are the comparable aircraft to investigate. The weights of the airplanes vary considerably and provide a spectrum of values that should contain the design space of the proposed aircraft for this project. The takeoff and empty weights of the aircraft in Table 2 are used in the following weight sizing chapter.

Similarities and differences in configuration choices are noticeable from a visual inspection of the aircraft. All the aircraft have a conventional tricycle landing-gear, aft buried engine(s), and conventional horizontal stabilizer. Tricycle landing-gear offers the most ground stability for the fewest number of wheels and struts. More than three wheels will increase the aircraft's weight. Less than three will require wing supports to maintain a level plane during ground roll and parking. Engines are placed inside the fuselage to reduce additional drag as compared to externally mounted engines.

The main configuration differences of the aircraft are the wing location, number of engines, crew, and vertical stabilizers. The comparable aircraft have low-, mid-, and high-wing placements. Low-wings are selected for more maneuverability. Low-wings also allow for shorter and lower weight landing-gear due to reduced ground clearance. Mid-wings are selected for neutral stability and more ground clearance for underwing mounts over the low-wing. High-wings offer the most stability and ground clearance. Though stability is good, increased stability reduces the controllability of the aircraft.

The number of engines is determined based on available engines in the market to meet specific thrust requirements of a design. The number of crew on mission complexity. For training, an additional crew member is needed for instructing. The number of vertical stabilizers are determined based on height restrictions. Military hanger and door heights restrict the height of the aircraft. For this reason, designers would choose to split a single larger vertical fin into two smaller vertical fins. If con

Though the comparable aircraft look similar, there are distinct differences. There is not a single configuration combination that makes the best airplane. There are tradeoffs between design choices that a designer will determine by weighing the pros and cons. There are many ways to select an aircraft's configuration, though certain design choices are better for specific missions. Hence, this is why many planes look similar when they are designed for the same or similar missions.

#### **2.1.1 Wing Configuration**

Both advanced trainer and fighter aircraft require maneuverability. From the three possible wing locations a mid or low-wing are the best options. A high-wing is not ideal because it is favored for stability. Since stability and control are interdependent, a more inherently stable aircraft tends to have lower controllability. A low-wing is ideal for increased controllability. A low-wing also offers potential storage volume for landing-gear. The design requires supersonic flight, which generally equates to thinner wing profiles. This eliminates the option of storing the landing-gear in the wing.

The ideal choice for this design is a mid-wing. A mid-wing offers neutral stability and control. The main negative effect of a mid-wing is the structural integration into the fuselage while considering engine inlets and structure. The compromise of complex structure integration is worth the downside to gain on neutral stability and control.

#### **2.1.2 Empennage Configuration**

The empennage configuration will be a conventional design for an advanced trainer type aircraft. There will be a horizontal and two vertical stabilizers. A rear horizontal is favored over a canard for pilot visibility

and over a T-tail's tendency to have deep stall. Two vertical stabilizers are selected to help reduce the overall height of the aircraft. Having two vertical fins also help to reduce coupled pitch and yaw modes. This is accomplished by the shorter moment arm, when compared to a single larger vertical fin. The negative effect of two vertical stabilizers is a reduction in aerodynamic efficiency by having vertical stabilizers with lower aspect ratios.

### 2.1.3 Propulsion System

The propulsion system will be integrated in the aft fuselage section. Having an internal engine will reduce aerodynamic drag over externally mounted engines. Placing the engine in the back of the aircraft also presents problems. One of the problems is the need for an intake duct, which can have efficiency losses when compared to an externally mounted engine. The other problem is a reduction in ease of maintenance for the engine, due to the engine enclosed by the aircraft's structure.

### 2.1.4 Landing-Gear

The landing-gear will be a conventional tricycle configuration. For supersonic capabilities, the wing will be thinner with less storage capacity. Also, a mid-wing will require longer landing-gear when compared with a low-wing or fuselage integrated landing-gear. Therefore, landing-gear integrated with the wing will not be a good choice. There will be a single nose wheel with steering capabilities for taxiing purposes. Two rear wheels will be specifically placed aft of the aircraft cg to ensure proper stability during ground roll.

### 2.1.5 Proposed Configuration

The above configuration design choices are presented in Figure 2. The wing will be swept for reduced drag in the transonic and supersonic envelopes and tapered for reduced wing root bending moments. The aircraft will feature a conventional tail with a fully moving horizontal stabilizer. Two vertical stabilizers are selected to reduce the overall height of the aircraft. A single internal fuselage engine is selected for reduced drag. The design will incorporate a conventional tricycle landing-gear configuration.

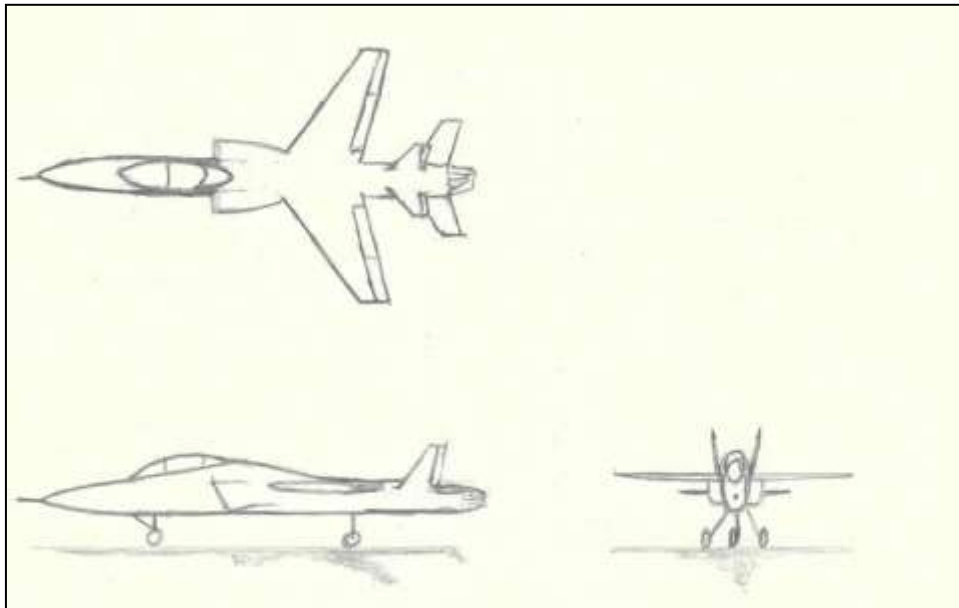


Figure 2. Initial AMT design sketches

### 3. Weight Sizing

#### 3.1 Mission Weight Estimates

##### 3.1.1 Database for Takeoff and Empty Weights from Similar Airplanes

The previous ten comparable aircraft are used as a database for takeoff and empty weights. The weight values presented in Table 3 are from [6] through [16].

Table 3. Empty and takeoff weights of comparable aircraft

Airplane	Type	W <sub>E</sub> (kN)	W <sub>TO,max</sub> (kN)
M-346	Supersonic Trainer/ Light Fighter	45.2	93.2
Scorpion	Trainer/ Light Fighter	56.5	97.9
T-38 Talon	Supersonic Trainer	32.1	53.9
T-45 Goshawk	Trainer	43.7	62.7
T-50 Golden Eagle	Supersonic Trainer	63.5	120
Yak-130	Supersonic Trainer/ Light Fighter	45.1	101
F-5 Tiger	Light Fighter	42.7	110
Mirage III	Light Fighter	69.1	134
A-4 Skyhawk	Light Fighter	46.5	109
L-39 Albatros	Light Fighter	34.9	44.7

##### 3.1.2 Determination of Weight Regression Coefficients A and B

Historic data has demonstrated there exists a linear base 10 logarithmic relationship between aircraft TO and empty weight, shown by equation (3.1) [17].

$$\log_{10} W_{TO} = A + B \cdot \log_{10}(W_E) \quad (3.1)$$

Where, A and B are the regression coefficients of the logarithmic equation. Using the data in Table 3, the base 10 logarithm is taken for the TO and empty weights of the aircraft. The data is plotted, see Figure 3. Using Excel trend line, a linear equation is fitted to the plotted data. From the equation the coefficients A and B are determined.

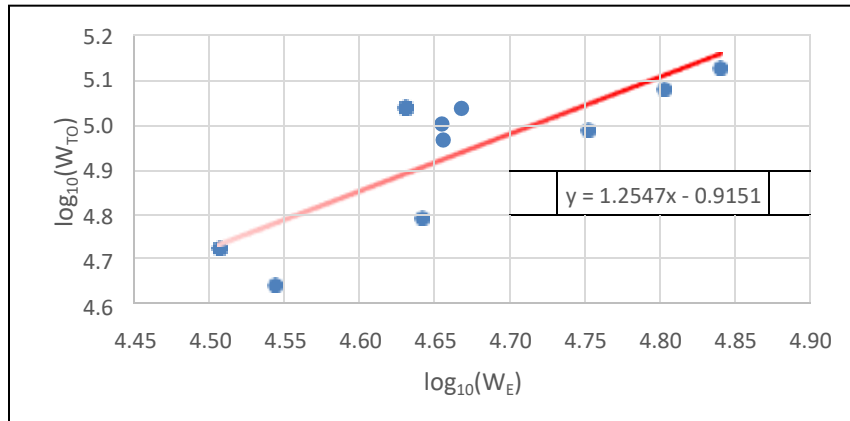


Figure 3. Determining A and B coefficients

From Figure 3, the regression coefficients are found to be:  $A = -0.9151$  and  $B = 1.254$ . From table 2.15 in [17], the regression coefficients for a military jet trainer are,  $A = 0.6632$  and  $B = 0.8640$ . The regression coefficients for a jet fighter are:  $A = 0.1362$  and  $B = 0.9505$ . Comparing the results obtained from Figure 3 to previous data, there is a large discrepancy between the numbers. This can be attributed to the data used in [17] is much older. A combination of technology and improved structural materials have made planes better. For this project, the results obtained from Figure 3 will provide more accurate approximations.

### 3.1.3 Determination of Mission Weights

#### 3.1.3.1 Manual Calculation of Mission Weights

A method for approximating  $W_E$ ,  $W_F$ , and  $W_{TO}$  is the fuel fraction method [17]. The method uses the following steps and equations:

1. Determine the mission payload weight,  $W_{PL}$ .
  - Passengers and baggage
  - Cargo
  - Military: guns and munitions
  - Special equipment
2. Make an educated guess for  $W_{TO}$ .
3. Determine the mission fuel weight  $W_F$ .

$$W_F = W_{F_{used}} + W_{F_{res}} = (1 - M_{ff})W_{TO} + W_{F_{res}} \quad (3.2)$$

$$M_{ff} = \frac{W_1}{W_{TO}} \prod_{i=1}^{i=7} \frac{W_{i+1}}{W_i} \quad (3.3)$$

Where the subscript  $i$  indicates the flight profile phase.

4. Calculate a tentative value for  $W_{OE}$ .

$$W_{OE_{tent}} = W_{TO_{guess}} - W_F - W_{PL} \quad (3.4)$$

5. Calculate a tentative value for  $W_E$ .

$$W_{E_{tent}} = W_{OE_{tent}} - W_{tfo} - W_{crew} \quad (3.5)$$

The value for  $W_{tfo}$  can be up to 0.5% of  $W_{TO}$  or this variable can be neglected at this point in the sizing process.

6. Calculate  $W_E$  using  $W_{TO}$  guess and the regression coefficients  $A$  and  $B$ .

$$W_E = \text{inv.log}_{10} \left( \frac{\log_{10}(W_{TO}) - A}{B} \right) \quad (3.6)$$

7. Compare  $W_E$  and  $W_E$  tentative, if the difference is greater than 0.5%, repeat steps 2 through 6 until convergence.

Since the aircraft being designed is for training, weapons are not required. Considering any munitions in the design would lead to an oversized plane to support such a payload. A plane designed with munitions would ultimately increase the lifecycle cost of the plane because a larger plane not only has more parts to assemble but also burns more fuel. The primary goal of the AMT is to improve the pilot's flight skills

through training and flight exercises, and be purpose built for the mission. If weapons are considered in the design, the aircraft would be a blend of trainer and fighter. Thus, it would increase the capabilities of the aircraft but would reduce effectiveness as a trainer.

To determine the mission phase fuel fractions, tables [17] are provides for various aircraft flight phases and flight parameters. Figure 4 shows a typical flight profile for a military trainer. Table 2.1 in [17], lists fuel fractions for all flight phases except cruise and loiter.

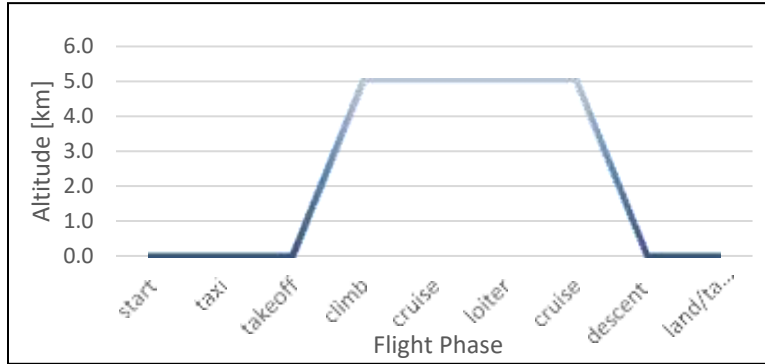


Figure 4. Basic flight profile

To determine the fuel fraction for cruise and loitering, equations (3.7) and (3.8) are used, respectfully.

$$\frac{W_i}{W_{i+1}} = \exp \left[ -R_{cr} \left( \frac{c_j}{V_{cr}} \right) \left( \frac{1}{L/D_{cr}} \right) \right] \quad (3.7)$$

$$\frac{W_i}{W_{i+1}} = \exp \left[ -E_{ltr} \cdot c_{j,ltr} \left( \frac{1}{L/D_{ltr}} \right) \right] \quad (3.8)$$

An additional fuel fraction parameter is added to the calculations to account for fuel reserves. From the T-X program requirements, the aircraft must contain enough fuel reserves for 45 minutes of flight at cruise conditions.

The initial  $W_{TO}$  guess is 40.0kN. Iterations are done from steps two through six until the fuel fraction method and the regression method converged to 0.5% or less difference. This calculation results in:

- $W_{TO} = 44.9\text{kN}$
- $W_E = 27.4\text{kN}$
- $W_F = 15.4\text{kN}$

### 3.1.3.2 Mission Weights Using the AAA Program

The AAA program is based on the aircraft design methods [17], [19]. The fuel fractions of the flight profile phases are presented in Figure 5. The regression coefficients A and B are determined from the aircraft presented in Table 3. The weight of the aircraft and the coefficients A and B are presented in Figure 6. The loglog plot of the aircraft's  $W_{TO}$  and  $W_E$  are shown in Figure 7. Figure 8 shows the output of the aircraft's weights from the AAA program.

Mission Profile	$M_{ff}$
Warmup	0.9900
Taxi	0.9900
Take-off	0.9900
Climb	0.9342
Cruise	0.9447
Loiter	0.9357
Cruise	0.9447
Descent	0.9900
Land/Taxi	0.9500

Figure 5. AAA – Flight profile weight fractions

Empty Weight - Take-off Weight Table					
#	Manufacturer	Airplane Name	$W_{TO}$ [N]	$W_E$ [N]	Reference
1	Aermacchi	M-346	93167.0	45210.0	
2	Textron	Scorpion	97874.0	56488.0	
3	Northrop	T-38	53939.0	32069.0	
4	McDonnell Douglas	T-45	62667.0	43739.0	
5	Lockheed Martin/KAI	T-50	129626.0	63451.0	
6	Yakovlev	Yak-130	100914.0	45112.0	
7	Northrop	F-5	109838.0	42660.0	
8	Dassault	Mirage III	134336.0	69139.0	
9	Douglas	A-4	109250.0	46485.0	
10	Acro Vedebody	L-39	44720.0	34913.0	

Output Parameters			
A	<input type="text" value="0.7495"/>	B	<input type="text" value="1.2546"/>

Figure 6. AAA – Regression coefficients from comparable aircraft

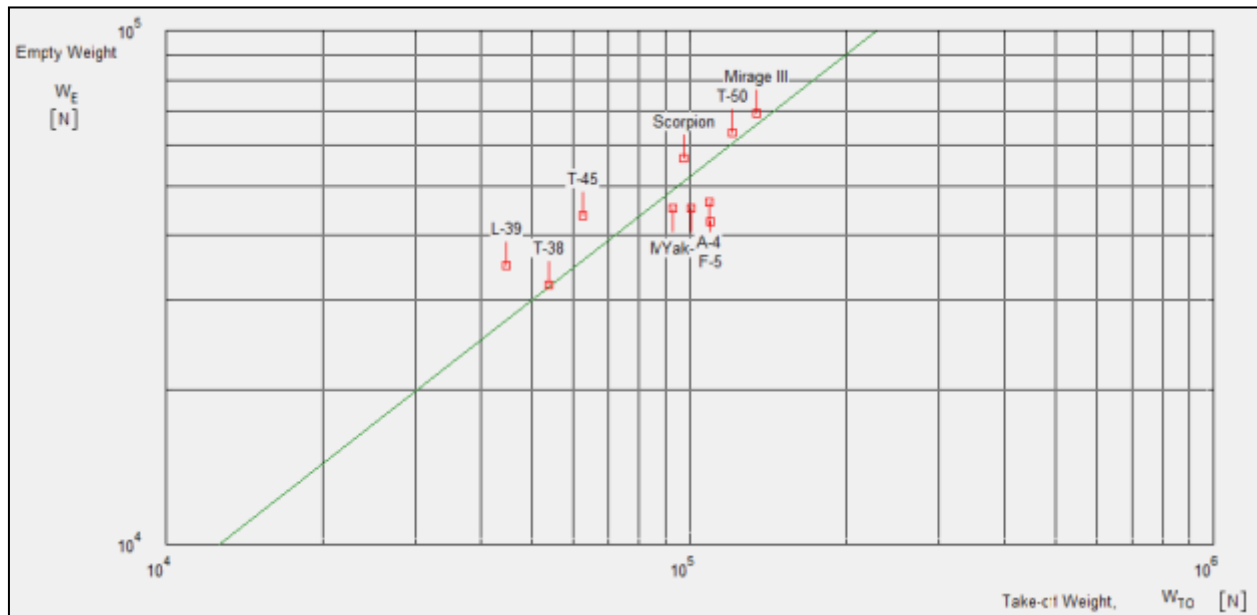


Figure 7. AAA – LogLog plot of comparable aircraft for  $W_E$  and  $W_{TO}$

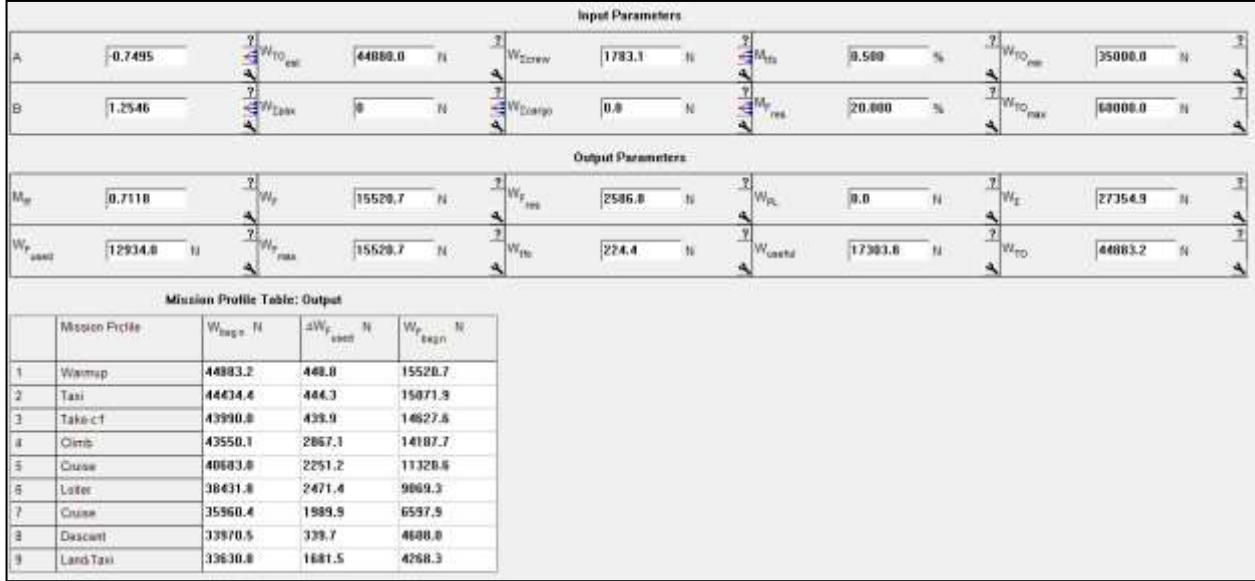


Figure 8. AAA – weight output

Comparing the manual calculations to the results obtained from the AAA program, the difference in values are not significant. This confirms the values for the takeoff, fuel, and empty weights by three different methods: weight regression, fuel fraction, and computer program.

### 3.2 Takeoff Weight Sensitivities

#### 3.2.1 Manual Calculation of Takeoff Weight Sensitivities

The takeoff weight sensitivities can be derived from equation (3.1). The empty weight can be expressed by equation (3.9). All the following equations are taken from [17].

$$W_E = C \cdot W_{TO} + D \quad (3.9)$$

Where,

$$C = 1 - (1 + M_{res})(1 - M_{ff}) - M_{tfo} \quad (3.10)$$

$$D = W_{PL} + W_{crew} \quad (3.11)$$

Substituting equation (3.9) into (3.1) results in equation (3.12)

$$\log_{10} W_{TO} = A + B \cdot \log_{10}(C \cdot W_{TO} + D) \quad (3.12)$$

The sensitivity of takeoff weight to any parameter of interest can be expressed as the derivative of equation (3.12), which is shown in equation (3.13). Where  $y$ , represents a parameter of interest.

$$\frac{\partial W_{TO}}{\partial y} = \frac{B \cdot W_{TO}^2 \cdot \frac{\partial C}{\partial y} - B \cdot W_{TO} \cdot \frac{\partial D}{\partial y}}{C(1 - B)W_{TO} - D} \quad (3.13)$$

If  $y = W_{PL}$ ,  $\partial C / \partial W_{PL} = 0$  and  $\partial D / \partial W_{PL} = 1$ . Equation (3.13) reduces to equation (3.14).

$$\frac{\partial W_{TO}}{\partial W_{PL}} = \frac{B \cdot W_{TO}}{D - C(1 - B)W_{TO}} \quad (3.14)$$

The sensitivity of the takeoff weight to empty weight can be directly derived from equation(3.1), resulting in equation (3.15)

$$\frac{\partial W_{TO}}{\partial W_E} = B \cdot W_{TO} \left\{ \text{inv. log}_{10} \left[ \frac{\log_{10}(W_{TO}) - A}{B} \right] \right\}^{-1} \quad (3.15)$$

Equation (3.13) reduces to equation (3.16) for the following parameters: range, endurance, L/D, and specific fuel consumption.

$$\frac{\partial W_{TO}}{\partial y} = \frac{B \cdot W_{TO}^2 \cdot \frac{\partial y}{\partial y}}{C(1 - B)W_{TO} - D} \quad (3.16)$$

The derivative of equation (3.10) is the following:

$$\frac{\partial C}{\partial y} = (1 + M_{res}) \left( \frac{\partial M_{ff}}{\partial y} \right) \quad (3.17)$$

Where  $\partial M_{ff}/\partial y$  is:

$$\frac{\partial M_{ff}}{\partial y} = M_{ff} \left( \frac{W_i}{W_{i+1}} \right) \left( \frac{\partial (W_{i+1}/W_i)}{\partial y} \right) \quad (3.18)$$

The weight ratios can be expressed in terms of the Breguet's range and endurance equations, as shown in equations (3.19) and (3.20).

$$R = \ln \left( \frac{W_i}{W_{i+1}} \right) = R \cdot c \left( V_j \right) \frac{L}{D}^{-1} \quad (3.19)$$

$$E = \ln \left( \frac{W_i}{W_{i+1}} \right) = E \cdot c_j \left( \frac{L}{D} \right)^{-1} \quad (3.20)$$

The combination of equations (3.16), (3.17), (3.18), and (3.19) or (3.20) results in equations (3.21) and (3.22).

$$\frac{\partial W_{TO}}{\partial y} = F \cdot \frac{\partial R}{\partial y} \quad (3.21)$$

$$\frac{\partial W_{TO}}{\partial y} = F \cdot \frac{\partial E}{\partial y} \quad (3.22)$$

Where F is represented by equation (3.23).

$$F = -B \cdot W_{TO}^2 [C \cdot W_{TO}(1 - B) - D]^{-1} (1 + M_{res}) M_{ff} \quad (3.23)$$

The sensitivity of takeoff weight to range can be expressed using equations (3.19) and (3.21) to form equation (3.24).

$$\frac{\partial W_{TO}}{\partial R} = F \cdot c_j \left( V \frac{L}{D} \right)^{-1} \quad (3.24)$$

The sensitivity of takeoff weight to endurance can be expressed using equations (3.20) and (3.22) to form equation (3.25).

$$\frac{\partial W_{TO}}{\partial E} = F \cdot c_j \left( \frac{L}{D} \right)^{-1} \quad (3.25)$$

The sensitivity of takeoff weight to L/D can be expressed using equations (3.19) and (3.21) to form equation (3.26).

$$\frac{\partial W_{TO}}{\partial \left( \frac{L}{D} \right)} = -F \cdot R \cdot c_j \left( V \left( \frac{L}{D} \right) \right)^{2-1} \quad (3.26)$$

The sensitivity of takeoff weight to specific fuel consumption can be expressed using equations (3.19) and (3.21) to form equation (3.27).

$$\frac{\partial W_{TO}}{\partial c_j} = F \cdot R \left[ V \left( \frac{L}{D} \right) \right]^{-1} \quad (3.27)$$

The calculated weight sensitivities are listed in Table 4.

Parameter	Units	Eq.	Calculated
$\frac{\partial W_{TO}}{\partial W_{PL}}$	N/N	(3.14)	6.10
$\frac{\partial W_{TO}}{\partial W_E}$	N/N	(3.15)	2.06
$\frac{\partial W_{TO}}{\partial R_{cr}}$	N/km	(3.24)	28.2
$\frac{\partial W_{TO}}{\partial E_{ltr}}$	N/hr	(3.25)	22,805
$\frac{\partial W_{TO}}{\partial \left( \frac{L}{D} \right)_{cr}}$	N/(N/N)	(3.26)	-1,622
$\frac{\partial W_{TO}}{\partial c_{j_{ltr}}}$	N/(N/N/hr)	(3.27)	16,220

### 3.2.2 Calculation of Takeoff Weight Sensitivities using the AAA Program

The AAA program determines weight sensitivities very quickly. Under the weight sizing tab there is a tab for sensitivities. Clicking the sensitivities tab shows the weight sensitivities presented in Figure 9. Comparing the manual calculations results of section 3.1.3.1 to the AAA results,  $W_{TO}$ ,  $W_E$ , and  $W_F$  have a difference of less than 1.0%. The results show a good approximation for the three weights. Table 5 presents a summary of the calculated sensitivities to the sensitivity output of the AAA program. The fourth column

shows the percent difference between the calculations and AAA. Overall the sensitivities calculated match well with the AAA program results. The AAA program does not specify the method for calculations. The discrepancies with the last four sensitivities in Table 5 could be attributed to rounding errors in the manual calculations.

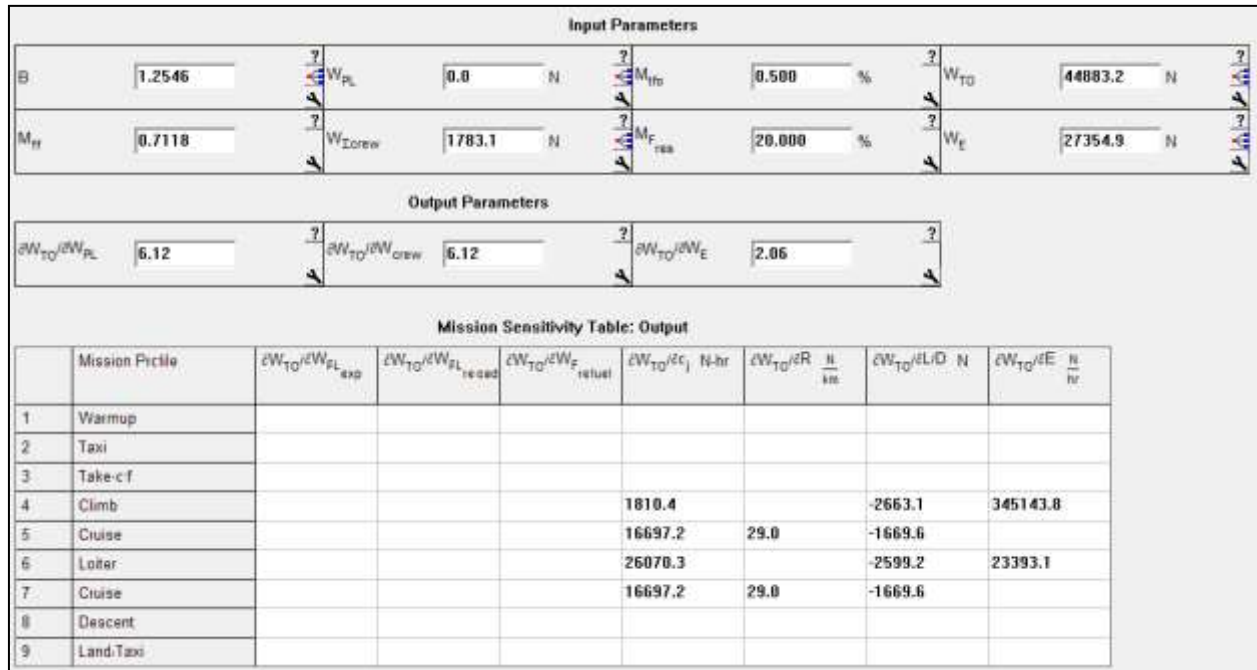


Figure 9. AAA – sensitivity output

Table 5. Sensitivity comparison

Parameter	Calculated	AAA	% Diff.
$\frac{\partial W_{TO}}{\partial W_{PL}}$	6.10	6.12	0.3
$\frac{\partial W_{TO}}{\partial W_E}$	2.06	2.06	0
$\frac{\partial W_{TO}}{\partial R_{cr}}$	28.2	29.0	2.7
$\frac{\partial W_{TO}}{\partial E_{ltr}}$	22,805	23,393	2.5
$\frac{\partial W_{TO}}{\partial (\frac{L}{D})_{cr}}$	-1,622	-1669.6	2.8
$\frac{\partial W_{TO}}{\partial C_{j_{ltr}}}$	16,220	16,697.2	2.9

### 3.2.3 Trade Studies

Regardless of a military trainer’s mission, the beginning and end of the flight will be the same. The aircraft will startup, taxi, take off, climb, cruise to training exercise airspace, perform training exercise, cruise back to airport, descend, land, taxi, and shutdown. The main parameter that will change between training missions will be flight time, which corresponds to fuel burned. Though fuel weight will affect all flight phases, the cruise and training mission execution will be affected the most.

Using the fuel fractions determined in section 3.1.3.1, the weight of the aircraft was determined for the end of climb and beginning of descent. The range and endurance of the aircraft, for cruise and training exercise, were determined for increased fuel weights. The tradeoffs are presented in Figure 10 and Figure 11.

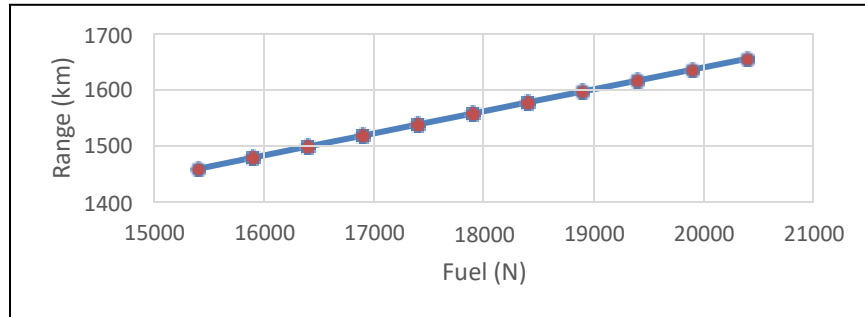


Figure 10. Range versus payload and fuel mass

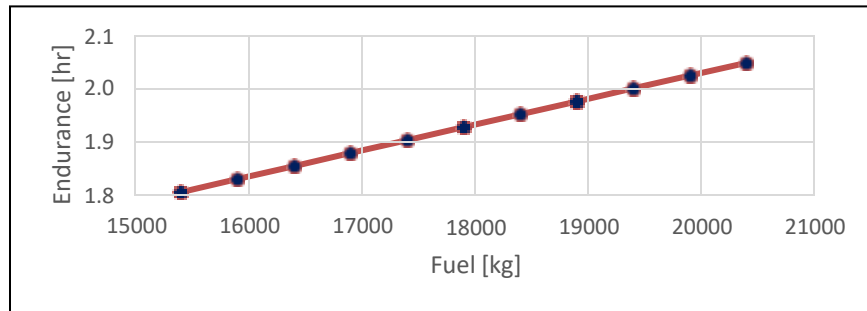


Figure 11. Endurance versus payload and fuel mass.

The Breguet range and endurance equations are simple to understand. Both the range and endurance are proportional to the difference between the initial and final weights. Increasing the amount of fuel extends the flight range and time of the aircraft. However, the performance of the aircraft cannot be determined by the equations. Increasing the takeoff weight, with additional fuel, will require greater takeoff distances and lower climb performance. Since the aircraft is limited to a specific  $C_{L,max}$ , the increase in the required lift must be produced by increasing the dynamic pressure. Additional trade studies could have been performed but simple equation analysis of the Breguet range (3.28) and endurance (3.29) equations can determine how parameters change in relation to others.

$$R = \left(\frac{V}{c}\right) \left(\frac{L}{D}\right) \ln \left(\frac{W_i}{W_f}\right) \quad (3.28)$$

$$E = \left(\frac{1}{c}\right) \left(\frac{L}{D}\right) \ln \left(\frac{W_i}{W_f}\right) \quad (3.29)$$

Considering equation (3.28), range increases if specific fuel consumption decreases or if  $L/D$  increases. This follows that range increases with a more efficient fuel burn or a greater lift-to-drag ratio. If the range is held constant, then the takeoff weight increases with specific fuel consumption or a decrease in  $L/D$ . This makes sense because a poorer lift-to-drag ratio or less efficient fuel burn will require more fuel to fly the same range.

Considering equation (3.29), endurance increases if  $L/D$  increases or specific fuel consumption decreases. Similar to range, the aircraft can fly longer with a better lift-to-drag ratio or more efficient fuel

burn. If the endurance is held constant, then the takeoff weight increases with increased specific fuel consumption or decreased L/D. Analogous to range, to fly the same amount of time more fuel must be carried if the lift-to-drag ratio decreases or fuel consumption is less efficient.

### 3.3 Conclusion

The calculations and analysis performed in the previous sections show a reasonable first approximation for the critical weight parameters of the aircraft. Most of the manual calculations agree with the AAA program results. In succeeding design phases, the weights determined in this report will be adjusted in the refinement of the aircraft's design. Based on the calculations and the analysis completed in this report, the following weights will be used to further refine the design.

- $W_{TO} = 44.9\text{kN}$  (10,090lbs)
- $W_E = 27.4\text{kN}$  (6,160 lbs)
- $W_F = 15.4\text{kN}$  (3,460 lbs)

## 4. Performance Sizing

Performance sizing is the process of analyzing performance constraints to determine the relationship of the thrust-to-weight ratio and wing loading for an aircraft. The general performance constraints that are considered: stall speed, takeoff distance, landing distance, climb, speed, and maneuvering. Depending on the type of aircraft, other performance parameters may be added. Each of these constraints can be represented by equations involving various parameters, such as Oswald efficiency, aspect ratio, aerodynamic coefficients, etc. At this point in the design process the various parameters are unknown and will require engineering judgement to assume reasonable variables for the analysis. Not all the constraints depend on T/W or W/S.

To determine the T/W and W/S for the different performance constraints, the requirements for performance must be defined. Table 6 lists the performance constraints found in [1] and [2]. Both references do not specify an exact value for stall or max speed. The max speed constraint was chosen to give the aircraft supersonic capability. This was not a specific design requirement, but research indicated an advanced trainer with supersonic capability provides upcoming fighter pilots with additional experience in supersonic flight regime. The performance requirements that will be evaluated are presented in Table 6.

Table 6. Aircraft performance requirements

Parameter	Requirement	Conditions
$V_{ST}$	N/A	NA
$s_{TO}$	1,950 m (6,400 ft)	<ul style="list-style-type: none"> <li>Wet runway</li> <li>Alt = ~2.3 km</li> <li>50ft obstacle</li> </ul>
$s_{La}$	2,130 m (7,000 ft)	<ul style="list-style-type: none"> <li>Wet runway</li> <li>Alt = ~2.3 km</li> <li>80% <math>W_F</math></li> </ul>
$CGR_{TO}$	33 m/km (200ft/nMile)	<ul style="list-style-type: none"> <li>Alt = ~2.3 km</li> </ul>
RC	2.54 m/s (500 ft/min)	<ul style="list-style-type: none"> <li>Subsonic</li> </ul>
RC	5.08 m/s (1,000 ft/min)	<ul style="list-style-type: none"> <li>Supersonic</li> </ul>
G-load	7	<ul style="list-style-type: none"> <li>50% <math>W_{F,full}</math></li> <li>Alt = ~4.6 km</li> <li><math>M \leq 0.9</math></li> </ul>
$\omega$	12.5°/sec	<ul style="list-style-type: none"> <li>50% <math>W_{F,full}</math></li> <li><math>M \leq 0.9</math></li> </ul>
$R_{bank}$	1,372m (4,500 dt)	<ul style="list-style-type: none"> <li>50% <math>W_{F,full}</math></li> <li><math>M \leq 0.9</math></li> </ul>
$M_{max}$	1.5	<ul style="list-style-type: none"> <li>Alt &lt; 5,5 km</li> </ul>
$C_j$	0.088 kg/N-hr (0.864 lbm/(lbf-hr))	<ul style="list-style-type: none"> <li>Cruise</li> </ul>
$C_j$	0.20 kg/N-hr (1.98 lbm/(lbf-hr))	<ul style="list-style-type: none"> <li>With AB</li> </ul>

## 4.1 Manual Calculation of Performance Constraints

### 4.1.1 Stall Speed

The stall speed of an aircraft is only a function of wing loading, air density, and  $C_{L,max}$ . The stall speed is derived from the lift equation:

$$L = \frac{1}{2} \rho_{\infty} \cdot V_{\infty}^2 \cdot S \cdot C_L$$

Assuming steady-state level conditions and substituting weight for lift, the stall speed of an aircraft is represented by equation (4.1) [17].

$$V_{st} = \sqrt{\frac{2(W/S)}{\rho \cdot C_{L,max}}} \quad (4.1)$$

A stall speed of 52.1m/s is selected. This value is a few units above the average stall speeds for the comparison aircraft used in previous sections. The density for the calculation is at sea-level,  $1.225\text{kg/m}^3$ . A range of  $C_{L,max}$  is selected based on typical military advanced trainers and fighter aircraft, ranging from 1.2 to 1.6. Figure 12 is the thrust-to-weight versus wing loading plots obtained. The arrows indicate the side of the line that satisfies the requirement.

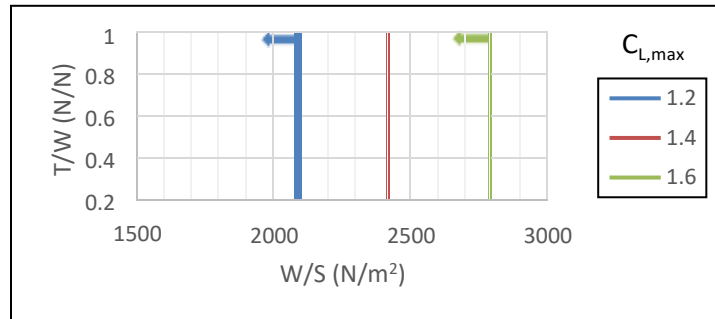


Figure 12. Stall speed performance sizing graph

### 4.1.2 Takeoff Distance

The takeoff distance for military aircraft is composed of the rolling TO distance plus the ground distance to clear a 50 ft obstacle. For the T-X program requirements [2], the takeoff distance and flight conditions are given in Table 6. The TO distance is derived from the forces acting on the aircraft. The resulting equation is (4.2) [18].

$$s_{TO} = \frac{1.44 \cdot W_{TO}^2}{g \cdot \rho_{\infty} \cdot S \cdot C_{L,max} \{T - [D + \mu_r(W_{TO} - L)]\}} \quad (4.2)$$

The negative acting forces, drag and rolling friction, can be assumed to be much less than the force due to thrust [18]. This simplification reduces equation (4.2) to equation (4.3).

$$s_{TO} = \frac{1.44(W_{TO}/S)}{g \cdot \rho_{\infty} \cdot C_{L,max} \cdot (T/W_{TO})} \quad (4.3)$$

For calculations, the following is assumed:

- gravitational force is  $9.807\text{m/s}^2$

- sea-level density
- $1.2 < C_{L,max} < 1.6$
- $W/S$  from  $500 < W/S < 3500 \text{ N/m}^2$

The resulting curves are shown in Figure 13.

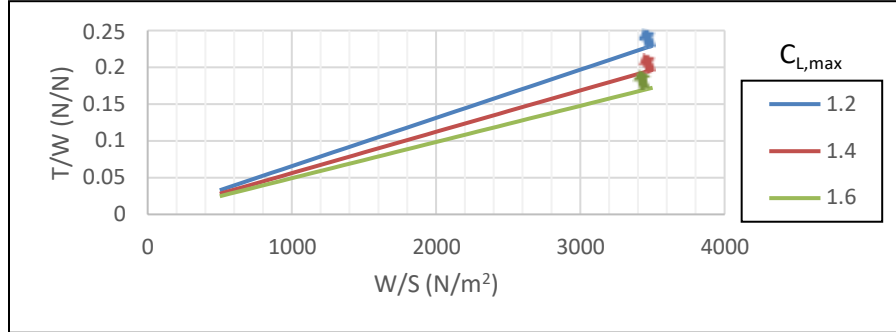


Figure 13. Takeoff distance performance sizing graph

#### 4.1.3 Landing Distance

The derivation for landing distance is the same as takeoff distance. The only differences are no thrust force, unless the aircraft will have thrust reversers, and the rolling friction coefficient. If the aircraft will have brakes, then the rolling friction coefficient must account for the braking friction coefficient. At this stage in the design, there will be no thrust reverser and the aircraft will have brakes.

Equation (4.4) is used for landing distance [18]. A paved runway has a rolling friction coefficient of 0.02 [18]. If an airplane is equipped with breaks, the value is 0.4 or 20 times. A wet runway must be considered [2]. Engineering textbooks list the wet asphalt/rubber friction coefficient as 20-25% less than the dry friction coefficient. For these calculations,  $\mu_r$  is chosen as 0.3. A range of  $C_{L,max}$  is chosen based on the stall speed calculations. The landing weight can be approximated as 80% of the takeoff weight [17]. Figure 14 shows the wing loading for the scenarios calculated.

$$s_{La} = \frac{1.69 \cdot W^2}{g \cdot \rho_{\infty} \cdot S \cdot C_{L,max} [D + \mu_r (W_{La} - L)]} \quad (4.4)$$

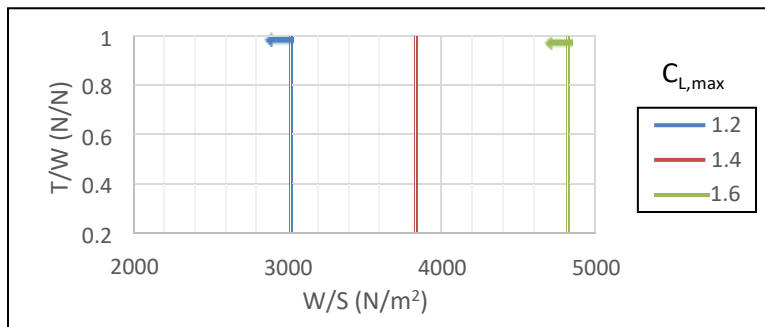


Figure 14. Landing distance performance sizing graph

#### 4.1.4 Drag Polar Estimation

The drag polar shows the relationship between the lift and drag coefficients. The drag coefficient is composed of three terms: skin friction drag, induced drag due to lift, and wave drag [18].

$$C_D = C_{D_o} + C_{D_i} + C_{D_w}$$

At this point in the aircraft sizing process the skin friction drag can be approximated using statistical data for similar aircraft. The lift induced drag is a function of the  $C_L$ , Oswald efficiency ( $e$ ), and wing AR. To calculate the lift induced drag a range of  $C_L$  values are selected between 0.0 and 1.6, and the Oswald efficiency and AR can be approximated using similar class of aircraft. For trainers and fighter aircraft [17] lists Oswald efficiencies around 0.8,  $C_{D_o}$  around 0.025 to 0.05, and aspect ratio around 4 to 6.

Wave drag is a function of airfoil nose radius, wing sweep, and wing taper. At this point there is no design for a wing therefore, [18] recommends approximating the wave drag for a flat plate for initial performance sizing. An assumption of the flat plate wave drag is that the angle of attack is small, less than  $13^\circ$ . The wave drag is a function of angle of attack and Mach number. The simplified approximate form for the wave drag coefficient is equation (4.5).

$$C_{D_w} = C_{D_o} + \frac{C_L^2}{\pi \cdot e \cdot AR} + \frac{4\alpha^2}{\sqrt{M^2 - 1}} \quad (4.5)$$

subsonic  
supersonic

Figure 15 is the drag polar for the takeoff configuration. Skin friction drag increases due to deployed landing-gear and high-lift devices (HLD). Figure 16 is the drag polar for the clean configuration. Figure 17 is the drag polar considering wave drag.

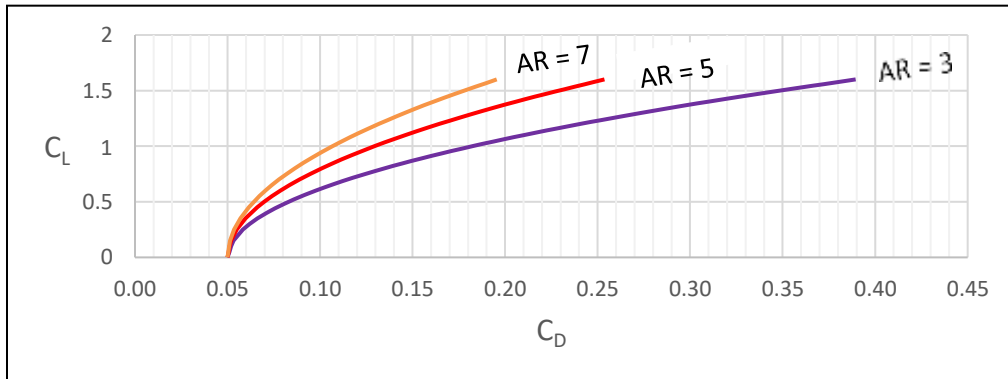


Figure 15. Takeoff and landing drag polar

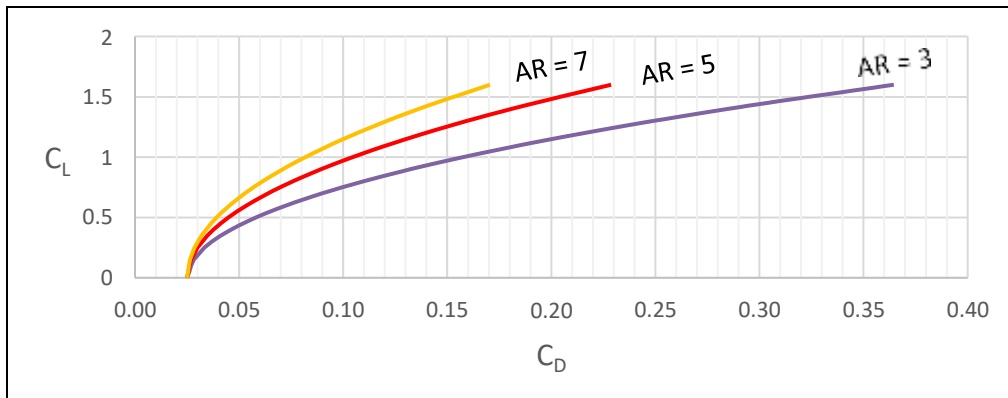


Figure 16. Clean drag polar

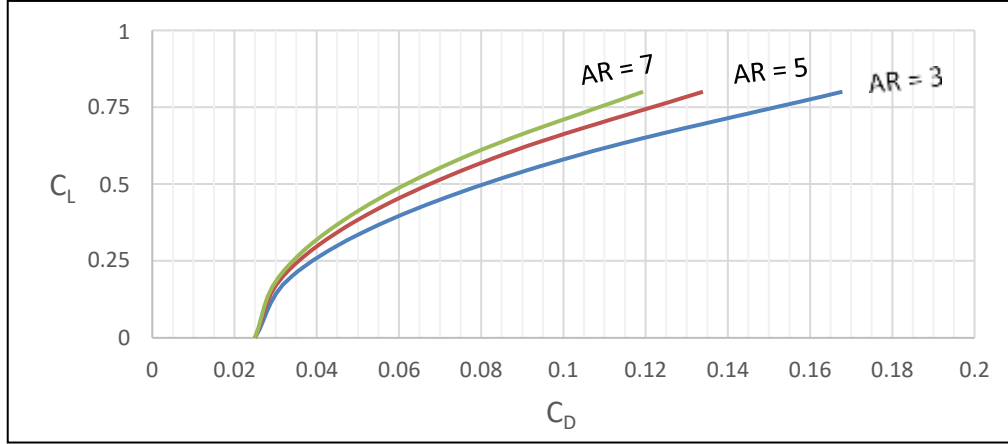


Figure 17. Supersonic drag polar

#### 4.1.5 Climb Constraints

##### 4.1.5.1 Rate of Climb

The rate of climb for an aircraft is determined from the excess power and weight by the following equation [18].

$$RC = \frac{\text{excess power}}{W} = \frac{P_{av} - P_{req}}{W} = \frac{V(T - D)}{W}$$

The above rate of climb equation can be rewritten in terms of the thrust-to-weight ratio and the drag-to-weight ratio.

$$RC = V_{cli} \left( \frac{T}{W} - \frac{D}{W} \right)$$

Assuming the lift generated by the aircraft is not significantly greater than the weight, the weight in the denominator of the drag term can be replaced with lift, and  $V_{cli}$  can be replaced by the equation for velocity.

$$RC = V_{cli} \left( \frac{T}{W} - \frac{D}{L} \right)$$

$$V = \sqrt{\frac{2(W/S)}{C_L \rho_\infty}}$$

Substituting in the velocity equation and the aerodynamic coefficients, the rate of climb is a function of wing loading, freestream density,  $C_L$  for climb, and the lift to drag ratio. The rate of climb equation can then be expressed with equation (4.6) [18]. For takeoff climb,  $C_{L,cli}$  is the same as the takeoff configuration and has a corresponding lift-to-drag ratio as determined using the takeoff drag polar.

$$RC = \sqrt{\frac{2(W/S)}{\rho_\infty \cdot C_{L,cli}}} \left( \frac{T}{W} - \frac{1}{\left(\frac{C_L}{C_D}\right)_{cli}} \right) \quad (4.6)$$

### 4.1.5.2 Climb Gradient

The climb gradient is the ratio of vertical distance traveled per time over the horizontal distance traveled per time. This relation can be expressed as the rate of climb over the horizontal velocity.

$$\text{CGR} = \frac{h}{V_{cr}} = \frac{RC}{V_{cr}}$$

The climb gradient can be expressed by equation (4.7) [18]. The design requirements specify the climb gradient at takeoff. Equation (4.7) can be solved for RC and substituted into equation (4.6). Substituting the correct variables for density, lift, and drag, the wing loading, and thrust-to-weight ratio relation can be determined.

$$\text{CGR} = \frac{RC}{V_{cr}} \quad (4.7)$$

From the requirements listed in Table 6, there are three: takeoff, subsonic cruise, and supersonic cruise. Figure 18 shows the T/W and W/S for the three requirements. For the climb gradient calculation, parameters are selected on the proposed altitude and the most efficient lift-to-drag ratio as determined from clean and supersonic drag polars.

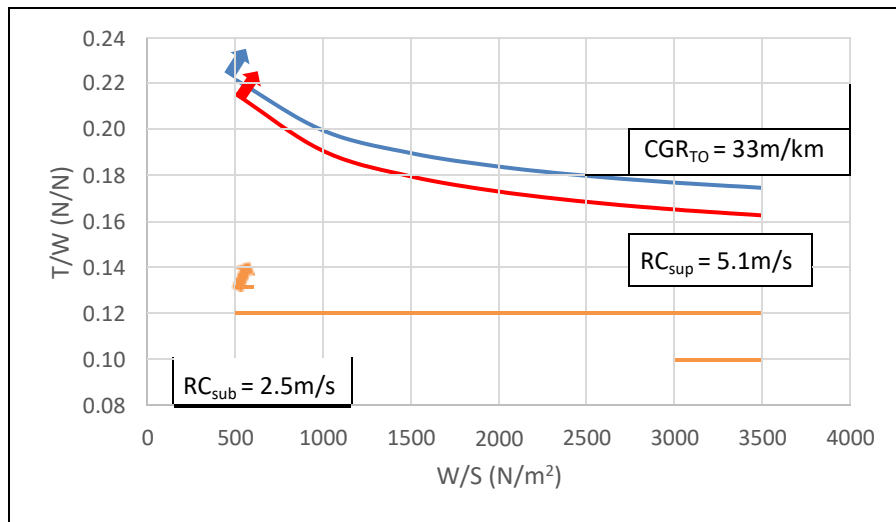


Figure 18. Climb requirement performance sizing graph

### 4.1.6 Speed Constraint

In the steady-state cruise condition the thrust equals the drag and weight is equal to lift. The following relation can be expressed:

$$\frac{T}{W} = \frac{D}{L} = \frac{C_D}{C_L}$$

Substituting in the equation for the expanded drag coefficient:

$$\frac{T}{W} = \frac{1}{C_L} \left( C_{D_o} + \frac{C_L^2}{\pi \cdot e \cdot AR} + \frac{4\alpha^2}{\sqrt{M^2 - 1}} \right) = \frac{C_{D_o}}{C_L} + \frac{C_L}{\pi \cdot e \cdot AR} + \frac{4\alpha^2}{C_L \sqrt{M^2 - 1}}$$

Substituting the lift coefficient equation into the above equation results in equation (4.8) [19]. This equation is not for calculating the speed of the aircraft. The speed of the aircraft is contained in the dynamic pressure term. Equation (4.8) is a thrust-to-weight and wing-loading relation dependent on the freestream velocity masked in the drag coefficient equation.

$$\frac{T}{W} = \frac{q_{\infty} \cdot C_{D_0}}{W/S} + \frac{W/S}{q_{\infty} \cdot \pi \cdot e \cdot AR} + \left( \frac{q_{\infty}}{W/S} \right) \frac{4\alpha^2}{\sqrt{M^2 - 1}} \quad (4.8)$$

subsonic  
supersonic

The dynamic pressure is determined from the conditions at altitude and Mach number indicated. The angle of attack is determined from the  $C_L$  corresponding to the wing loading, dynamic pressure, and the change in  $C_L$  with respect to angle of attack. Figure 19 shows the T/W and W/S relation for the Mach number of 1.25 and 1.5.

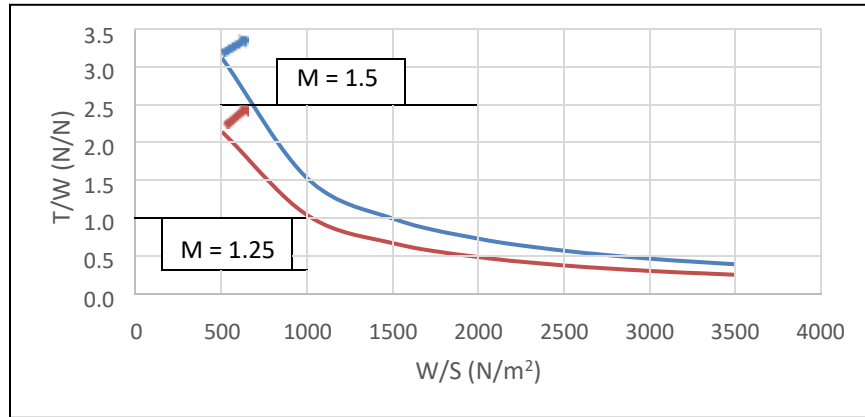


Figure 19. Speed requirement performance sizing graph

#### 4.1.7 Maneuvering Constraint

The turn rate is expressed by equation (4.9) [18]. The radius of the turn can be expressed by equation (4.10) [18]. These two equations are only functions of the gravitational force, flight speed, and g-loading (n).

$$\omega = \frac{g_0 \sqrt{n^2 - 1}}{V_{\infty}} \quad (4.9)$$

$$R = \frac{V_{\infty}^2}{g_0 \sqrt{n^2 - 1}} \quad (4.10)$$

To determine the thrust-to-weight ratio and wing loading for a maneuver, the same derivation is used as for the speed requirement in section 4.1.6. To perform the maneuver there must be sufficient thrust to overcome the drag of the aircraft at the g-load. This results in equation (4.11) [17].

$$\frac{T}{W} = \frac{q_{\infty} \cdot C_{D_0}}{W/S} + \frac{(W/S)n^2}{q_{\infty} \cdot \pi \cdot e \cdot AR} \quad (4.11)$$

The turn rate and turn radius requirements calculate flight speeds well below the maximum speed from the previous section and are therefore satisfied. The T/W and W/S relation for the high-g maneuver is the critical maneuver requirement to analyze. Figure 20 shows the T/W and W/S relation for the high-g maneuver at varying AR.

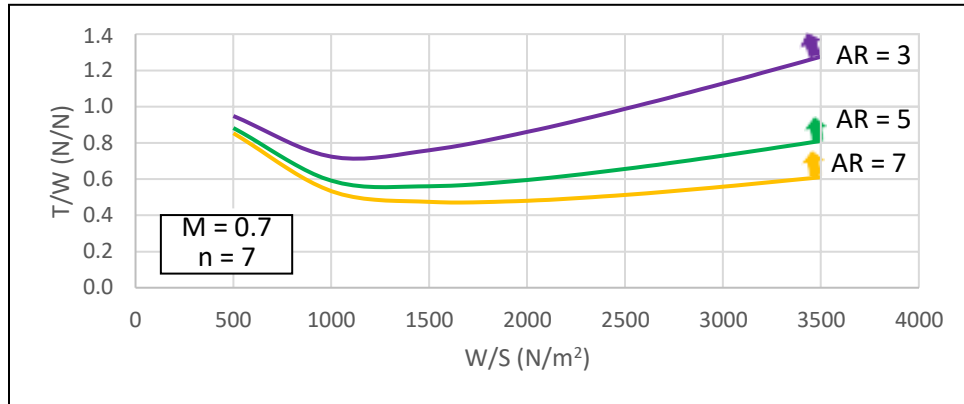


Figure 20. Maneuvering performance sizing graph

## 4.2 Calculation of Performance Constraints with the AAA Program

The AAA program is used to verify the calculations and the results obtained from section 4.1. The input parameters for each performance constraint are taken from the manual calculations. The results from AAA are shown in the following sections. The input screen dumps are in the top of the figures and the bottom is the performance sizing graphs for the performance requirements.

### 4.2.1 Stall Speed

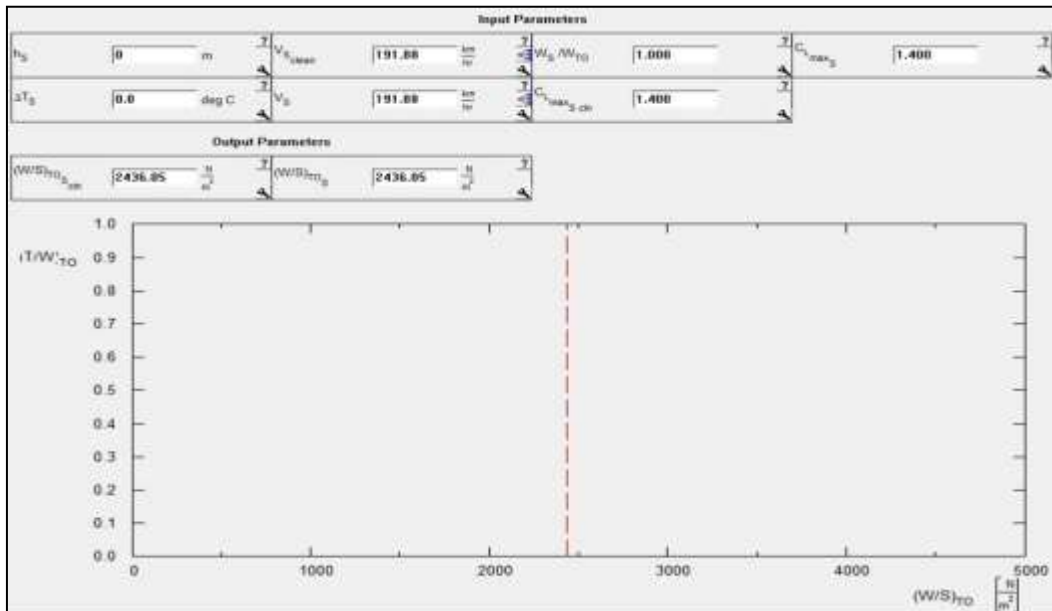


Figure 21. AAA – Stall T/W versus W/S

### 4.2.2 Takeoff Distance

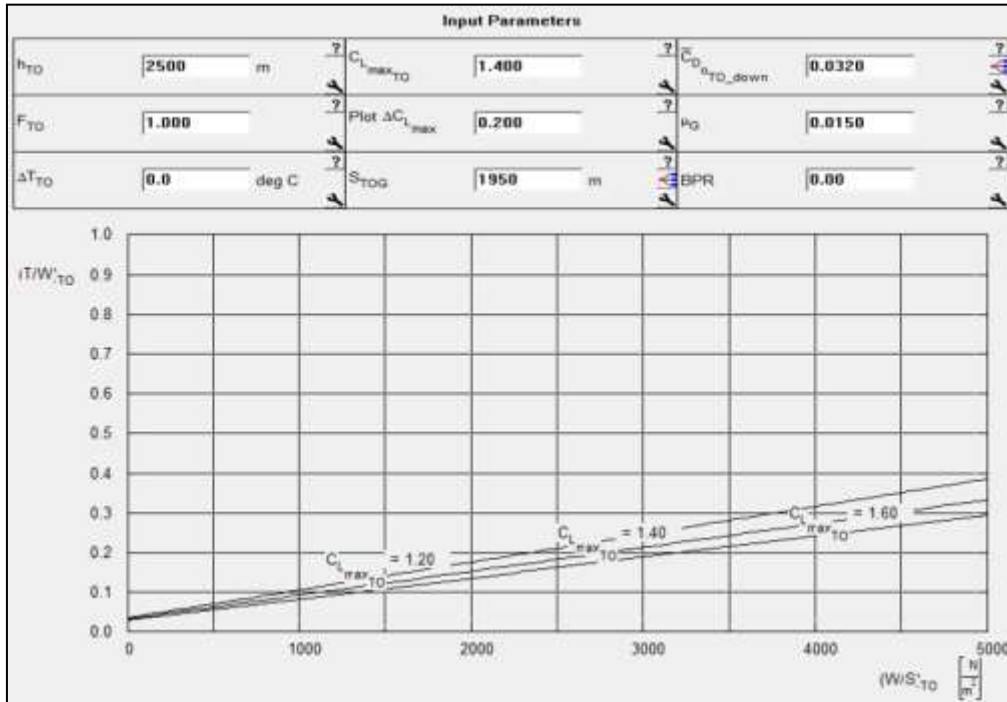


Figure 22. AAA – Takeoff distance T/W versus W/S

### 4.2.3 Landing Distance

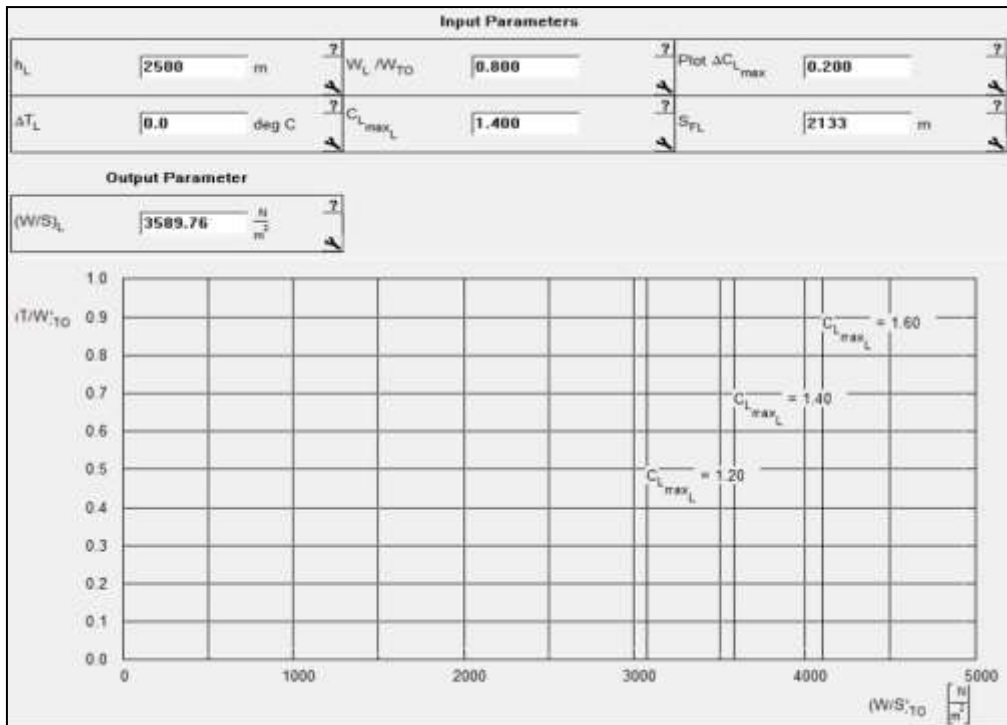


Figure 23. AAA – Landing distance T/W versus W/S

#### 4.2.4 Drag Polar Estimation

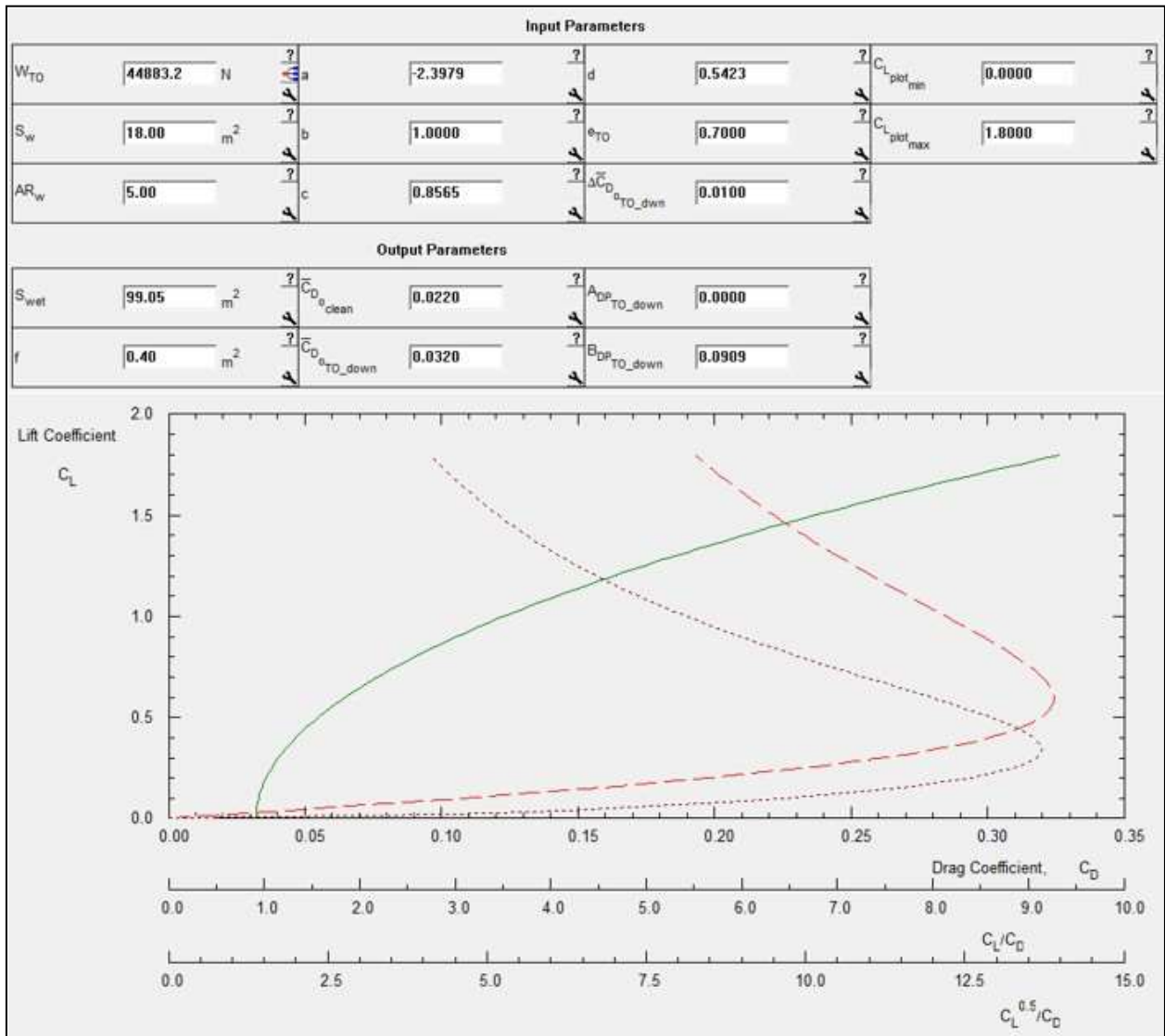


Figure 24. AAA – Takeoff drag polar

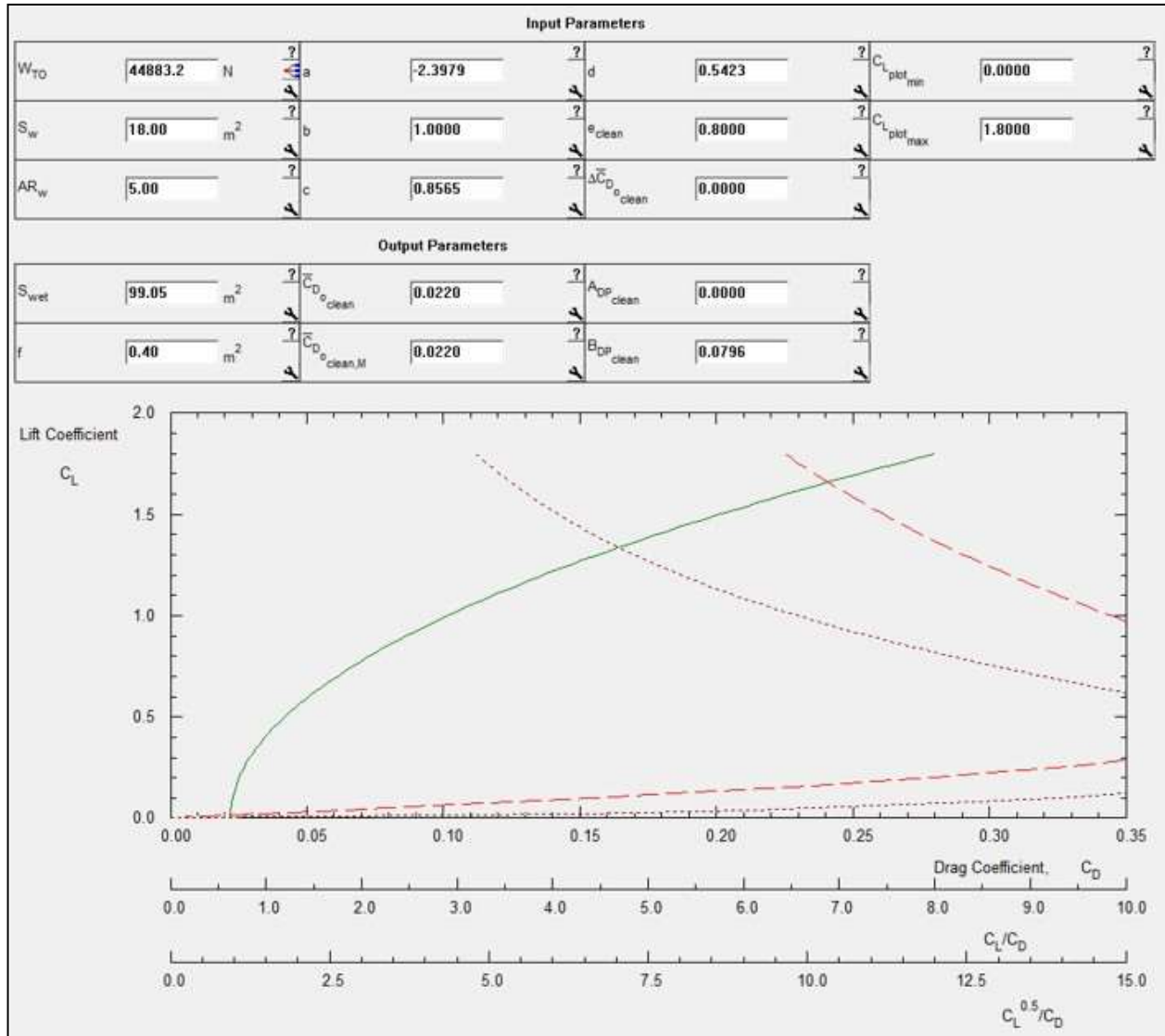


Figure 25. AAA – Clean drag polar

### 4.2.5 Climb Constraints

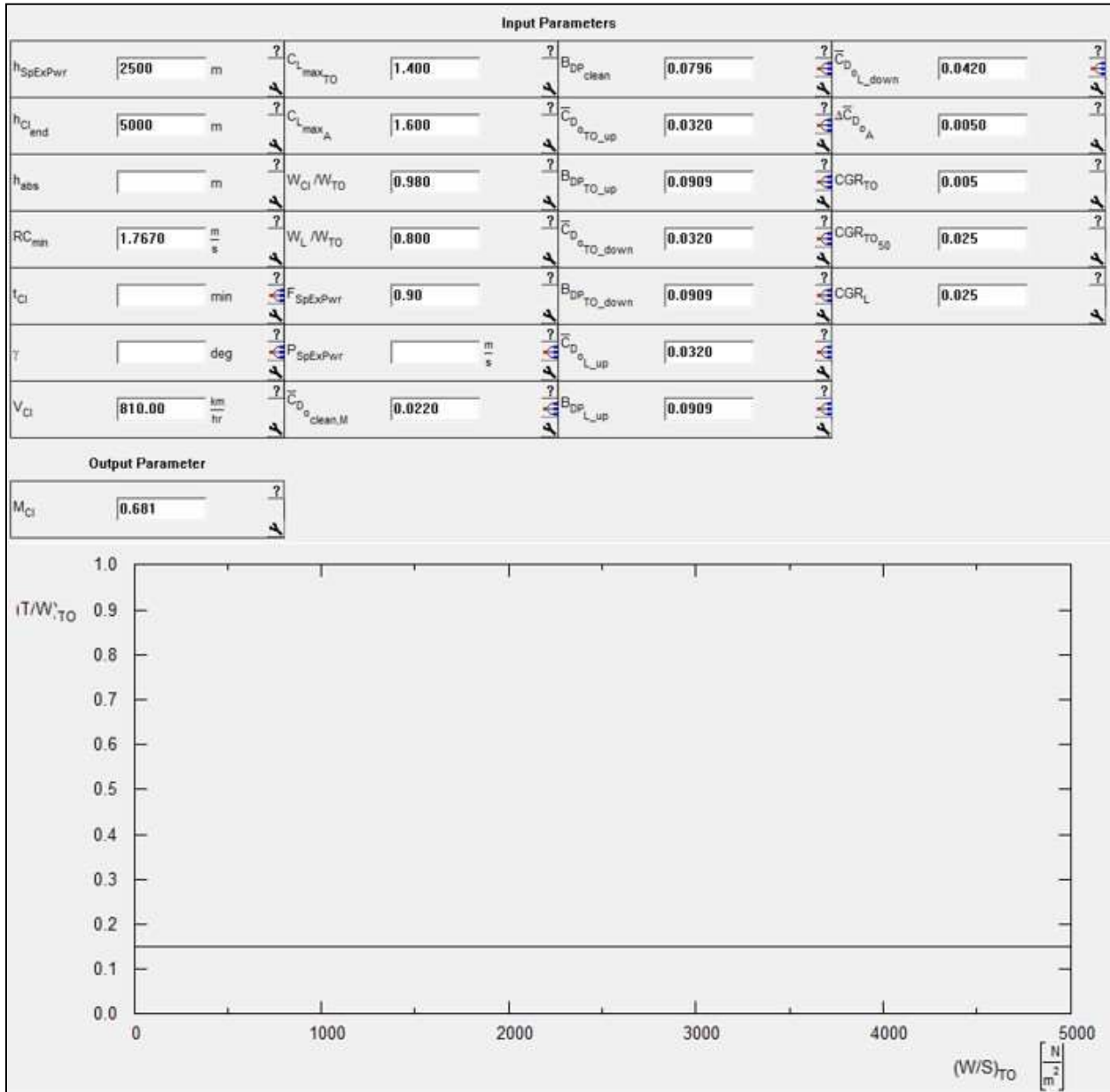


Figure 26. AAA – Takeoff climb T/W versus W/S

#### 4.2.6 Speed Constraint

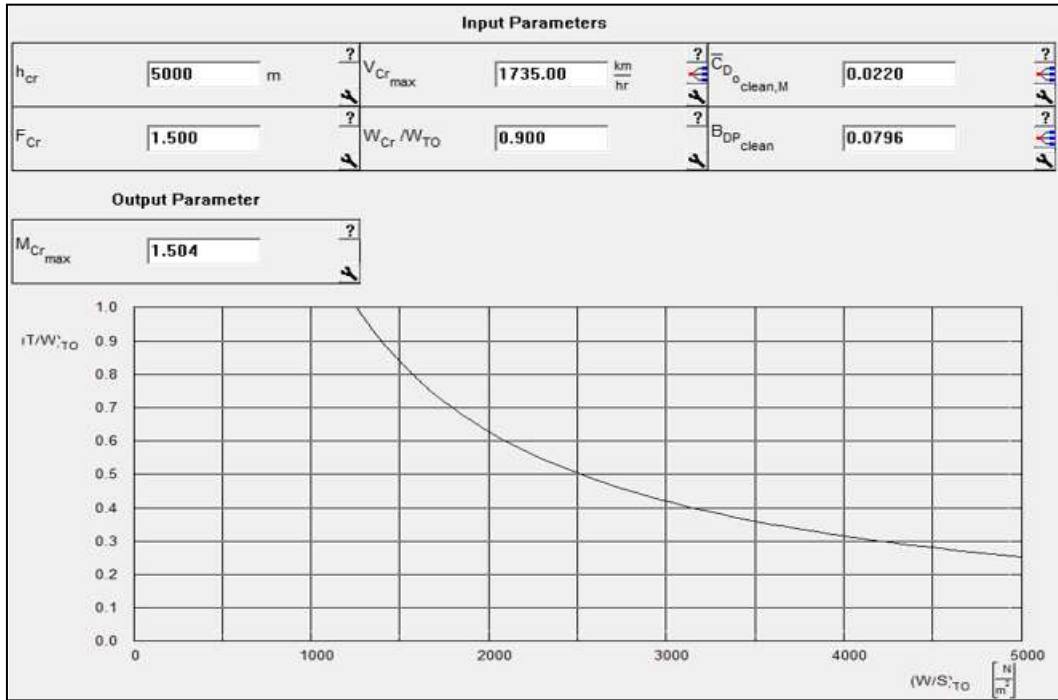


Figure 27. AAA – Speed T/W versus W/S

#### 4.2.7 Maneuvering Constraint

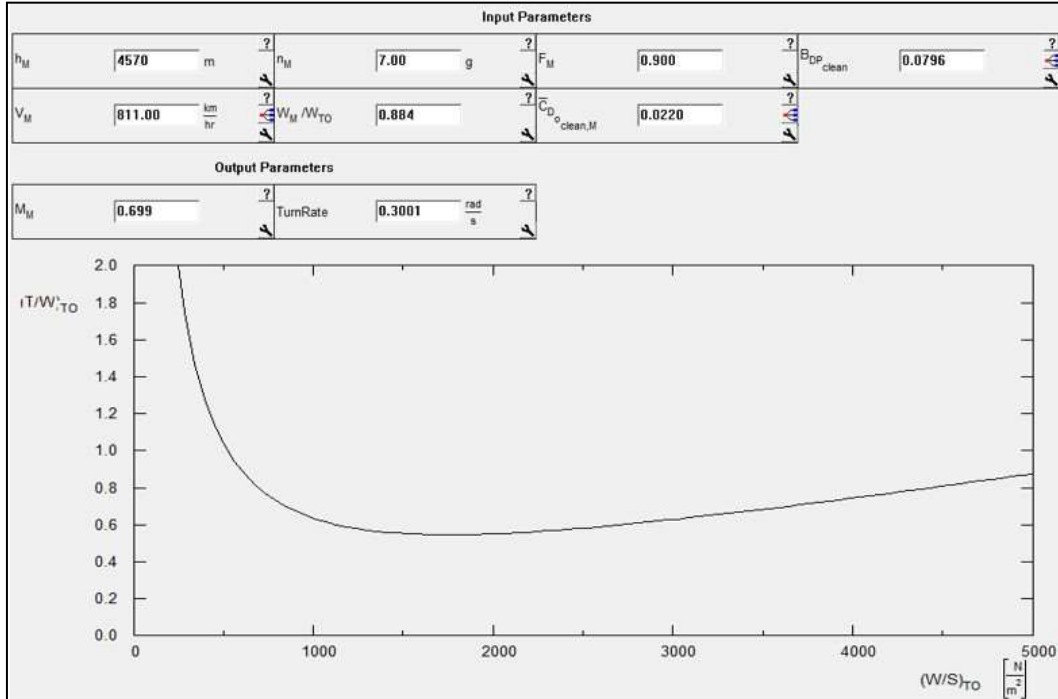


Figure 28. AAA – 7g maneuver T/W versus W/S

### 4.3 Summary of Performance Constraints

The combined performance sizing graphs from AAA are presented in Figure 29 and the manual calculations combined performance sizing graph is presented in Figure 30.

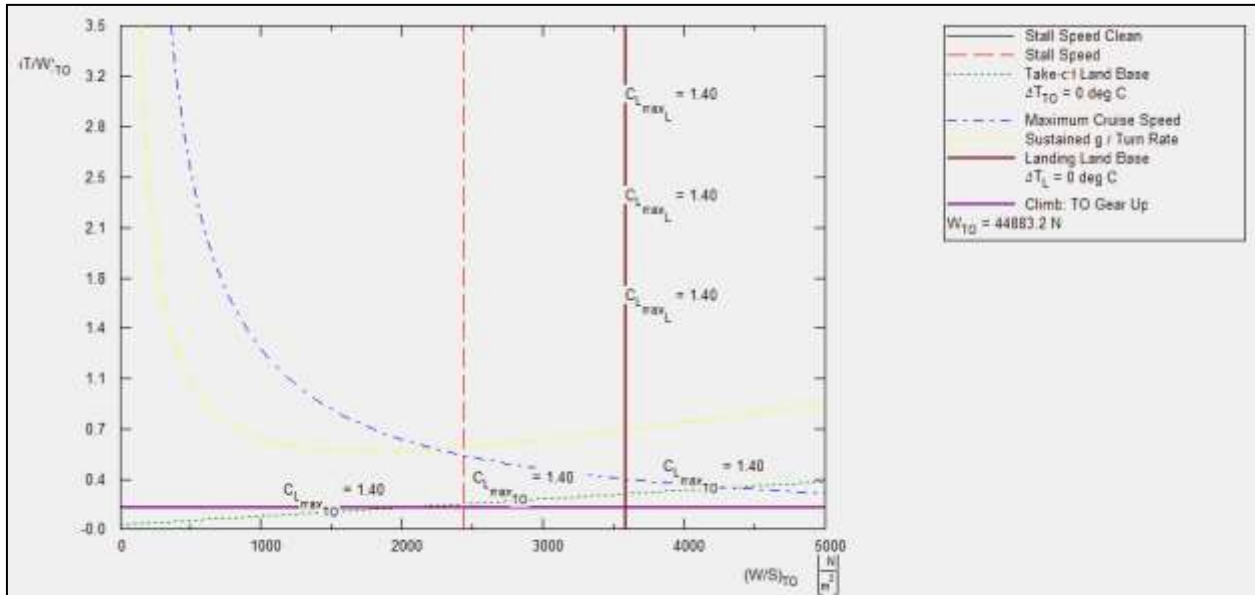


Figure 29. AAA – Performance sizing graph

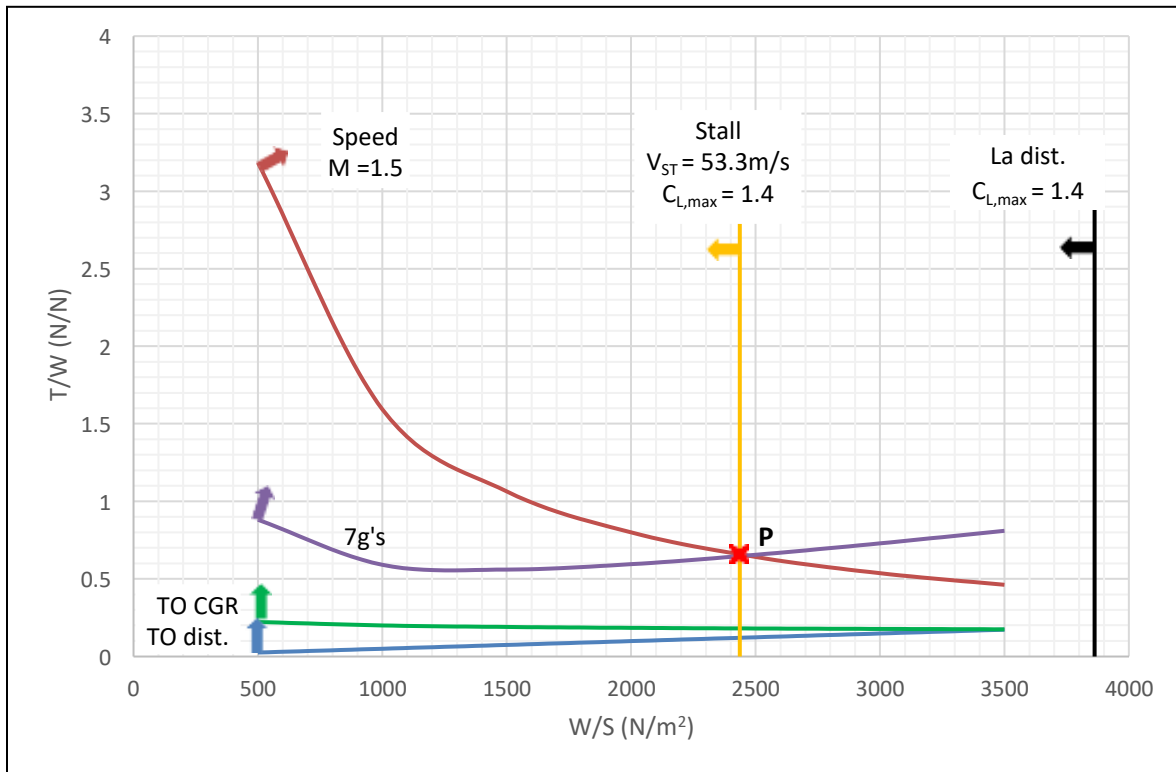


Figure 30. Hand calculation performance sizing graph

From the design point in Figure 30, indicated by the red star, the wing-loading is determined to be  $2,436 \text{ N/m}^2$  and the thrust-to-weight ratio is determined to be  $0.659 \text{ N/N}$ . The design point is selected at the

intersection of maximum speed, high-g maneuver, and stall speed. At this point, all other performance sizing requirements are met as indicated by the arrows in Figure 30.

Using the design point, the performance is calculated for each of the performance categories using the equations presented in section 4.1. Table 7 lists the indicated performance correlating to the design point. The takeoff and land distance, and takeoff climb are evaluated at 2.5km because some USAF bases at higher altitudes ranging from 7,500 to 8,000 ft (~2.5 km). The other parameters are evaluated at the same conditions used for the performance sizing analysis.

Table 7. Performance at design point

Parameter	Value	Units	Condition
W <sub>TO</sub>	44,920	N	Takeoff
	10,100	lb	
T/W	0.659	N/N	Takeoff
			Sea-level
T	29,600	N	Sea-level
	6,655	lb	
W/S	2,436	N/m <sup>2</sup>	Takeoff
	50.9	Lbs/ft <sup>2</sup>	Sea-level
S	18.4	m <sup>2</sup>	---
	198	ft <sup>2</sup>	
V <sub>ST</sub>	53.3	m/s	Sea-level
	175	ft/s	C <sub>L,max</sub> = 1.4
S <sub>TOG</sub>	405	m	Alt = 2,500m (8,200ft)
	1,330	ft	C <sub>L,max</sub> = 1.4
S <sub>LaG</sub>	716	m	Alt = 2,500m (8,200 ft)
	2,350	ft	C <sub>L,max</sub> = 1.4
CGR <sub>TO</sub>	540	m/km	Alt = 2,500m, C <sub>L,max</sub> = 1.4
	2,850	ft/nMile	
RC <sub>sub</sub>	65.2	m/s	Alt = 4,570m (15,000ft)
	12,835	ft/min	
RC <sub>sup</sub>	69.8	m/s	Alt = 5,486m (18,000ft)
	13,740	ft/min	
V <sub>max</sub>	478	m/s	Alt = 5,486m (18,000ft)
	1,570	ft/s	
M <sub>max</sub>	1.5	---	Alt = 5,486m (18,000ft)
n	7.1	---	Alt = 5,486m (18,000ft)

## 4.4 Propulsion System Selection

### 4.4.1 Propulsion System Type

The type of propulsion system can be determined from an altitude versus Mach number plot as depicted by Figure 31, which shows the types of propulsion systems used based on Mach number envelopes correlating to the maximum velocity at altitude.

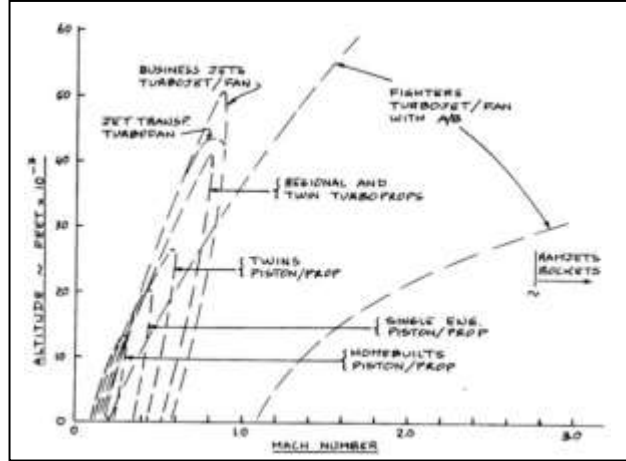


Figure 31. Mach altitude plot [19] To create an altitude versus Mach or velocity graph, equation (4.12) [18] is used. The relationship is derived from the thrust = drag equation, but neglecting wave drag. Using the density at various altitudes the maximum velocity can be determined based on the design point determined from the previous section. The speed of sound at altitude is calculated by equation (4.13). The maximum Mach at altitude is calculated by the  $V_{max}$  at altitude divided by the speed of sound at altitude.

$$V_{max} = \frac{\sqrt{\left(\frac{T}{W}\right)_{max} \left(\frac{W}{S}\right) + \left(\frac{W}{S}\right) \sqrt{\left(\frac{T}{W}\right)_{max}^2 - \frac{4C_D}{\pi \cdot e \cdot AR}}}{\rho_{\infty} \cdot C_{D_0}} \quad (4.12)$$

$$a_{alt} = \sqrt{\gamma_{air} \cdot \mathcal{R}_{air} \cdot T_{alt}} \quad (4.13)$$

The  $M_{max}$  versus altitude for the design point is shown in Figure 32. Comparing Figure 32 to Figure 31, for the design point of the aircraft a turbofan or turbojet must be considered for the propulsion system to achieve the required thrust of the design point.

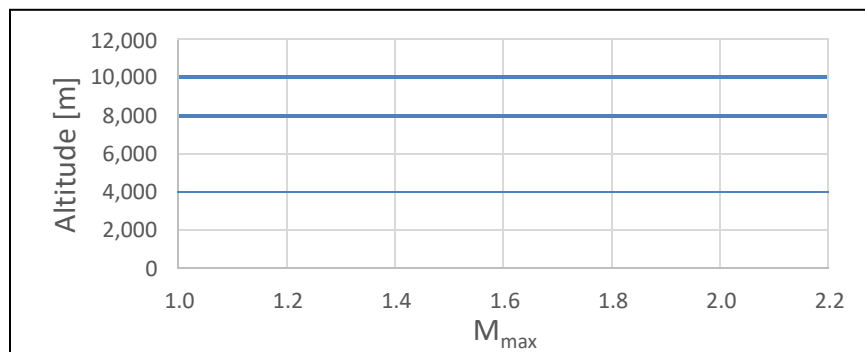


Figure 32. Mach versus altitude

#### 4.4.2 Number of Engines

The number of engines required depends on the available thrust an engine can produce or designing a new engine to satisfy the requirement. Since the lead times for new engines are long and expensive, a list of currently produced engines for military applications is compiled, see Table 8. The design point resulted in having a thrust requirement of about 29.6 kN.

The Pratt and Whitney (P&W) F135 is currently used in the F-35 program. The F135 meets all the requirements but is simply oversized for the application. The P&W F100 has a significant amount of thrust and meets the specific fuel consumption requirements but is oversized for the application. The GE F404 has been used in various Boeing aircraft and the F-117. The F404 is a viable option but has a greater mass than other options, so it will not be considered.

The Eurojet EJ200 is used in the Typhoon fighter. The EJ200 is selected because it has the lowest mass compared to the other engines and it meets the specific fuel consumption and thrust requirements. Further analysis and design refinement will determine if a larger engine must be considered if the required thrust increases over the available thrust of the EJ200

Table 8. Possible engines

Engine	T <sub>AB</sub> (kN)	T (kN)	Mass (kg)	C <sub>j</sub> (kg/(N*hr))	C <sub>j</sub> AB (kg/(N*hr))	# of Engines Required
P&W F135	190	125	1,700	0.089	N/A	1
P&W F100	130	79	1,737	0.077	0.20	1
GE F404	79	49	1,036	0.083	0.18	1
EJ200	90	60	1,000	0.082	0.17	1

#### 4.5 Summary of Performance Sizing

The critical design parameters have been determined from the weight and performance sizing. These values are listed in Table 9. The propulsion system analysis determined the engine of choice would be the EJ200. If thrust required increases over the available thrust of the EJ200, then the F100 engine will be considered.

Table 9. Summary of critical parameters

Parameter	Value	Units
W <sub>TO</sub>	44.9(10.0)	kN(klbs)
W <sub>F</sub>	15.4(3.46)	kN(klbs)
W <sub>E</sub>	27.5(6.18)	kN(klbs)
T <sub>req</sub>	29.6(6.65)	kN(klbs)
S <sub>req</sub>	18.4(198)	m <sup>2</sup> (ft <sup>2</sup> )

## 5. Fuselage Design

The purpose of this section is to develop a general understanding of the cockpit layout and approximate fuselage shape. The main components are the crewmen, engine, and adequate space for subsystems. The design methodology has been developed from historical and adapted industry standards [20]. Military standards were also considered as additional references [1], [3], [4].

### 5.1 Layout Design of the Cockpit

#### 5.1.1 Dimensions and Weights for Crew Members

The design requires the cockpit to fit two crew members, one pilot and one instructor. The average military crewman weighs 180lbs (801N) plus about 20lbs (89N) for gear [20]. Therefore, the total weight of a crewman and gear is 200lbs (890N). An average standing male crewman is shown in Figure 33, and Table 10 lists the dimensions corresponding to Figure 33. The average body width of a male across the shoulders is 533mm, at the elbows 561mm, and at the hips 457mm [20].

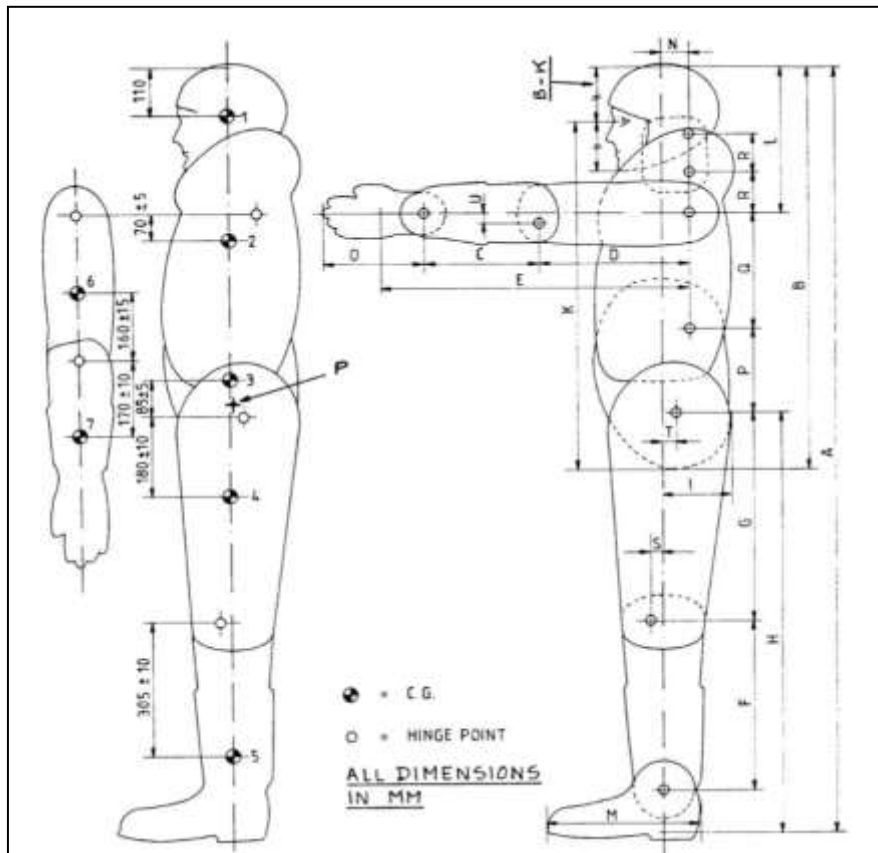


Figure 33. Standing crewman dimension relations [20]

Table 10. Dimensions for male crew members (mm) [20]

Dimension	1	2	3
A	1600	1750	1900
B	870	920	990
C	230	255	280
D	300	335	370
E	620	685	750
F	350	390	430
G	435	475	515
H	850	950	1050
I	140	150	160
K	760	805	875
L	300	330	360
M	300	325	350
N	50	60	70
O	200	220	240
P	190	200	210
Q	260	270	280
R	80	90	100
S	25	300	30
T	20	30	30
U	20	20	20

Figure 34 shows a sitting crewman, and Table 11 lists the corresponding dimensions. The columns in Table 10 and Table 11 represent the dimensions of an average person. If female pilots are being considered, then all male crewman dimensions and weights should be adjusted by a factor varying from 0.80 to 0.85 [20].

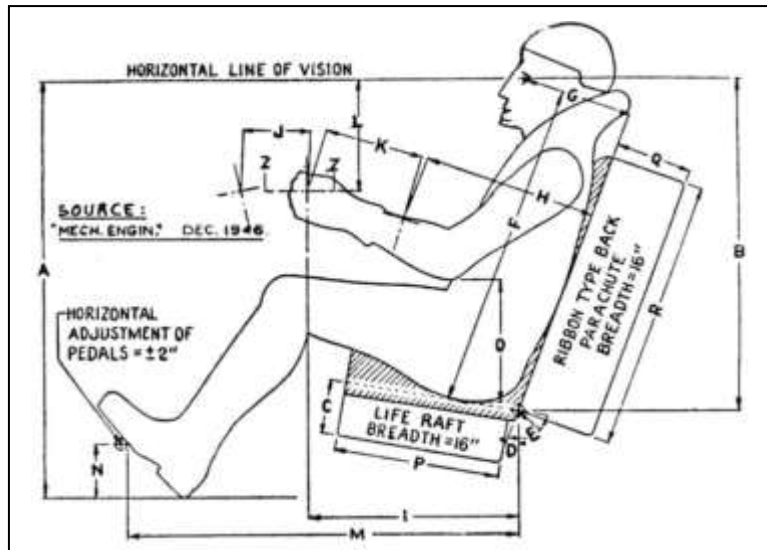


Figure 34. Sitting crewman dimension relations [20]

Table 11. Sitting dimensions for male crew members (mm) [20]

Dimension	1	2	3	4
A	940	991	1041	1092
B	768	781	800	806
C	127	127	127	127
D (deg)	21	19	16	16
E (deg)	101	101	101	101
F	756	768	787	794
G	254	248	248	254
H	368	349	343	330
I	483	483	483	483
J	152	152	152	152
k	229	229	229	229
L	292	349	394	445
M	914	889	876	876
N	127	127	127	127
O	235	235	235	235
P	381	381	381	381
Q	178	178	178	178
R	635	635	635	635

Using the dimensions in the third column (column heading, 2), a three-dimensional footprint of a sitting crewman is modeled using Solidworks. The model is shown in Figure 35.

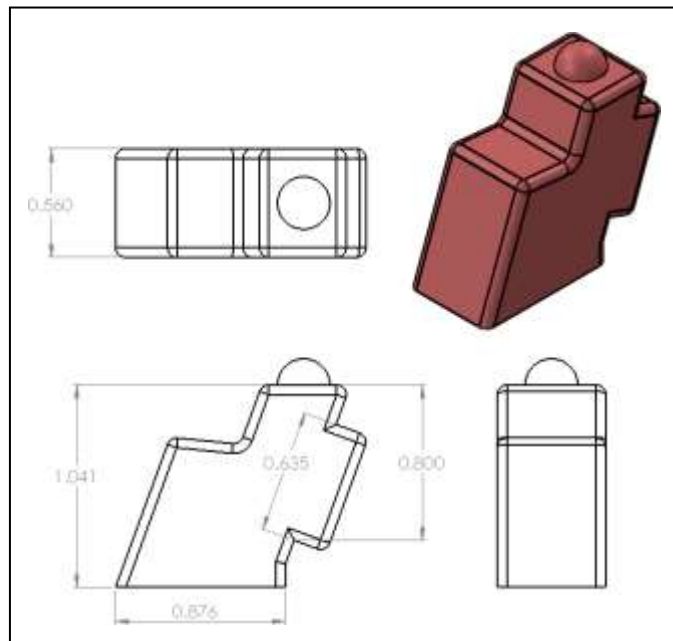


Figure 35. Crewman space sitting position

### 5.1.2 Layout of Cockpit Seating and Cockpit Controls

The layout of the cockpit depends on the dimensions of the pilot and visibility. The recommended seat arrangement for military trainers and fighters is shown in Figure 36. For the class of aircraft in the design,

ejection seats must be considered. Figure 37 and Figure 38 show the ejection seat requirements. Figure 39 shows the typical military trainer and fighter cockpit layout.

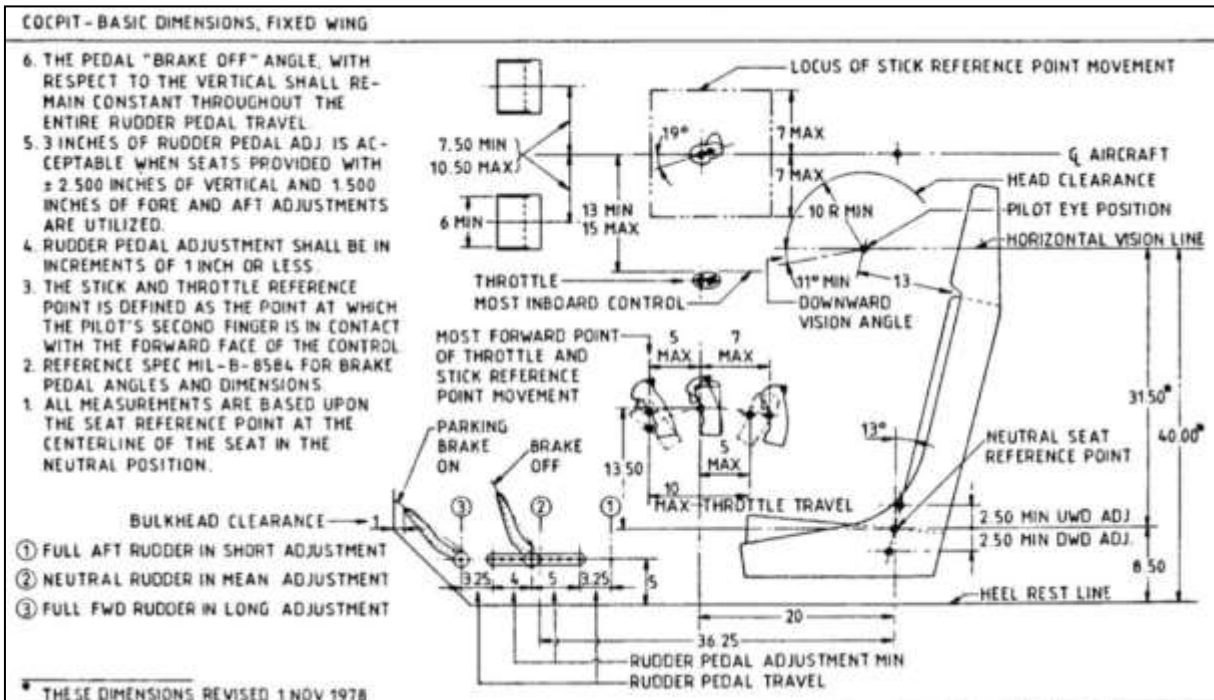


Figure 36. Recommended seat arrangement for military [20]

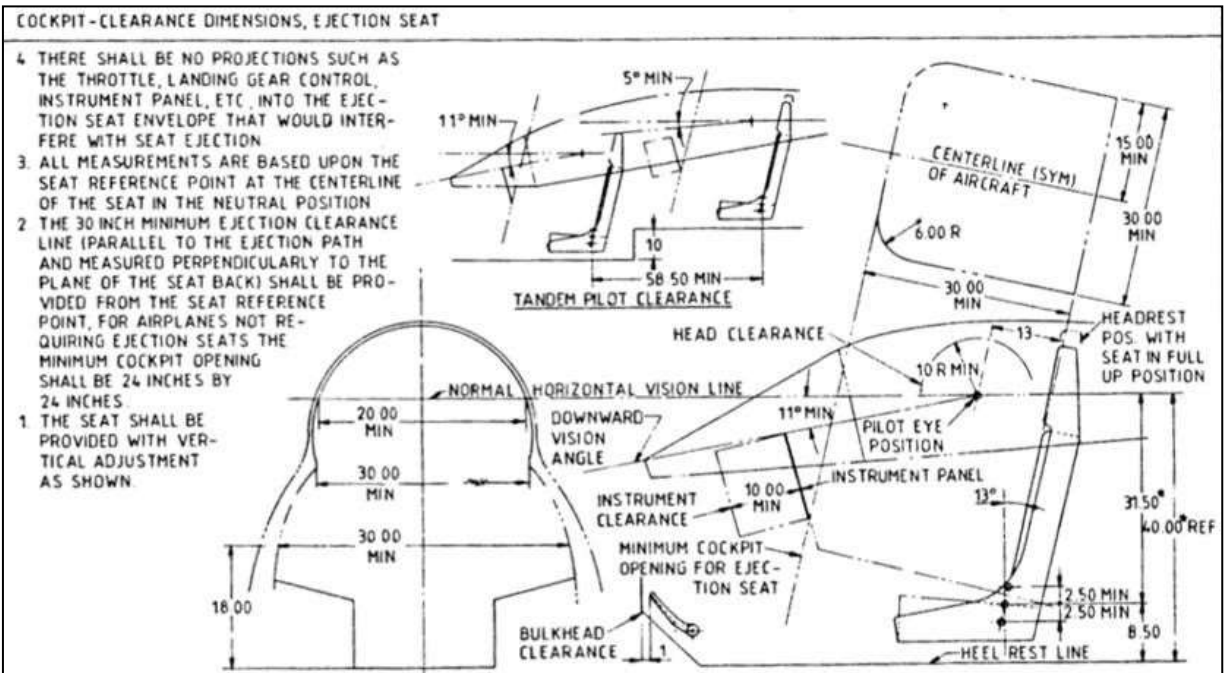


Figure 37. Recommended clearances for ejection seats [20]

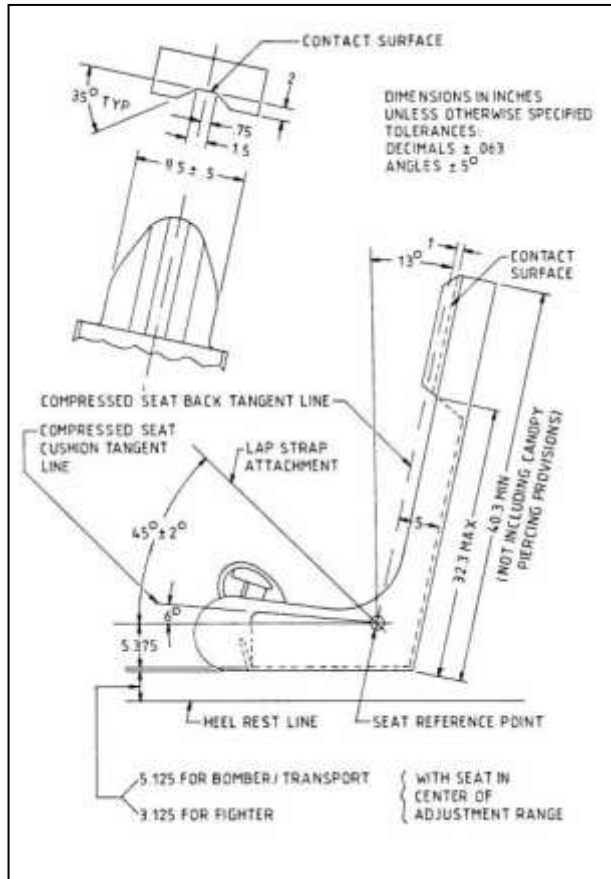


Figure 38. Typical ejection seat dimensions [20]

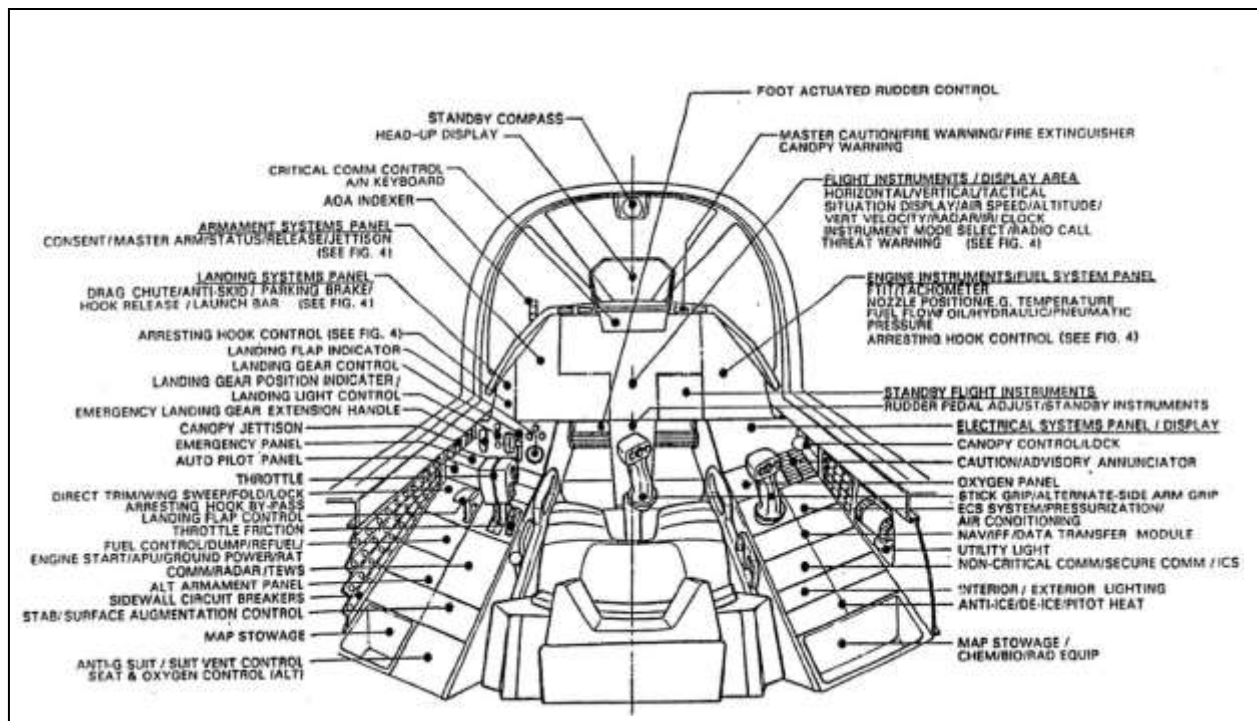


Figure 39. Fighter/attack cockpit arrangement [3]



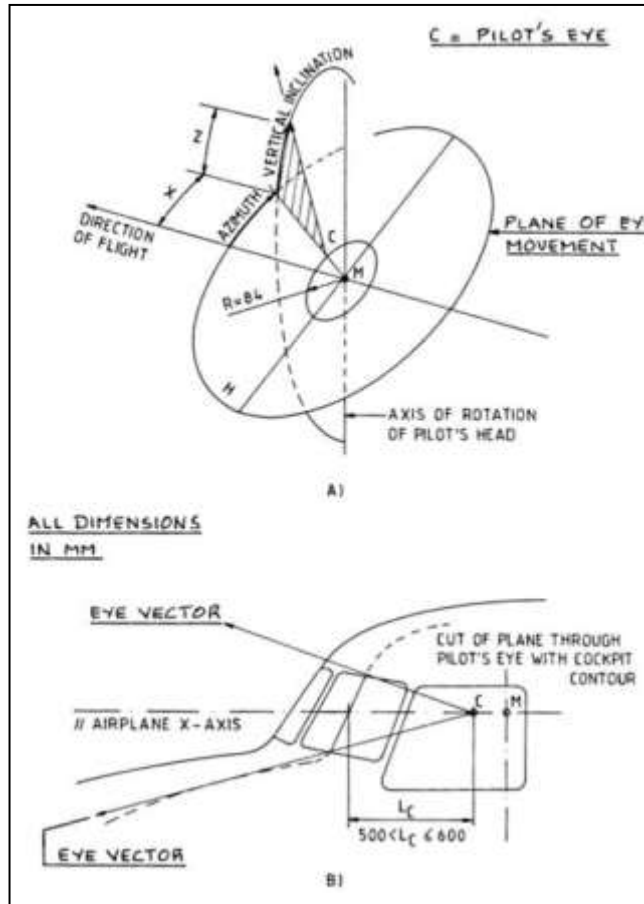


Figure 41. Definition of radial eye vectors [20]

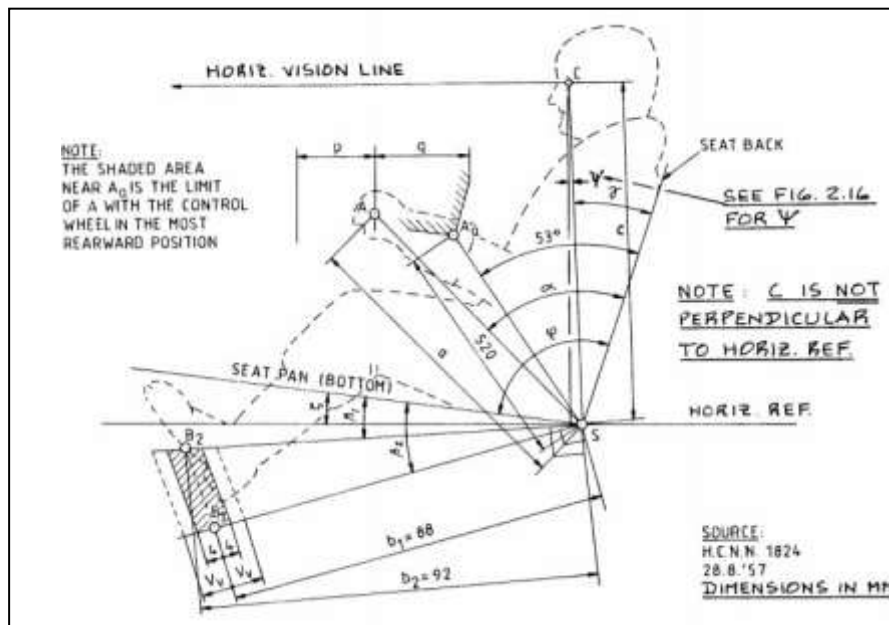


Figure 42. Recommended seat arrangement [20]

### 5.1.4 Cockpit Layout

Figure 43 to Figure 45 are cutaways of the drawings for better viewing of the cockpit. A military trainer is smaller in comparison to a large commercial transport plane and the ratio of cockpit to fuselage size is considerably larger. The cockpit of a military trainer from a visual inspection is 30 to 50% of the fuselage. Therefore, individual drawings or zoomed-in dimensional drawings of the cockpit were not necessary.

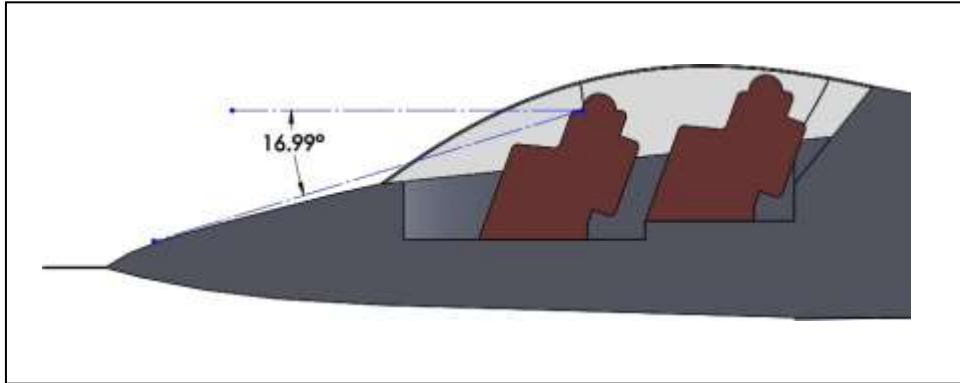


Figure 43. Cockpit cutaway side view

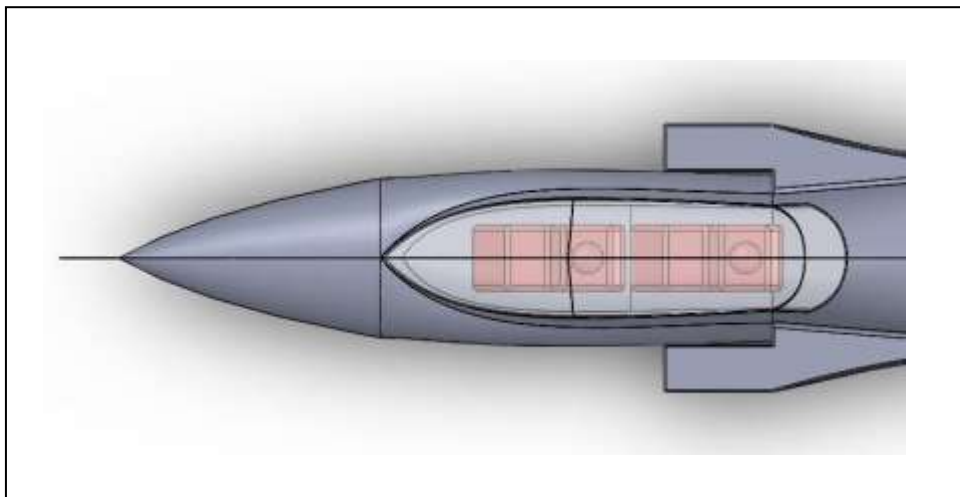


Figure 44. Cockpit cutaway top view

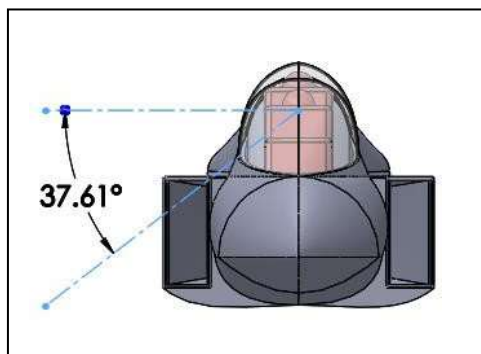


Figure 45. Cockpit cutaway front view

## 5.2 Layout Design of the Fuselage

The fuselage design used the T-50 Golden Eagle side view as a reference shape. Most of the fuselage design was completed in section 5.1. The only other main feature to consider is the engine. The engine placement was previously determined in the configuration design, chapter 3. The engine cutout that can be seen in Figure 46 was sized from the outer dimensions of the EJ200 engine. The manufacturer lists the dimensions as 4.0 m long and the maximum diameter of 0.737 m. Figure 47 through Figure 49 are the side, top, and front views. Figure 50 shows the preliminary engine intake ducts. Figure 51 is an isometric view. Dimensional drawings can be found in the closing chapter.

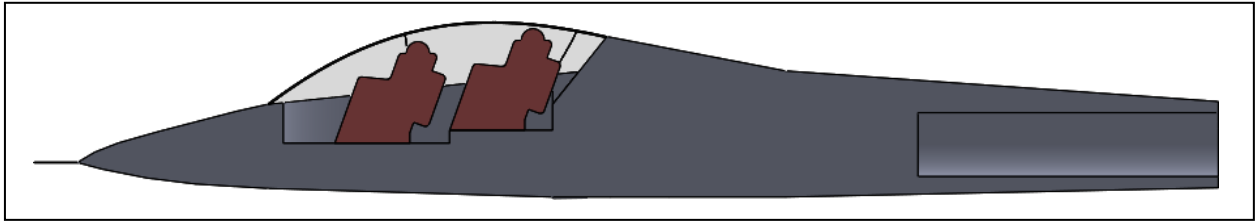


Figure 46. Fuselage cutaway side view.

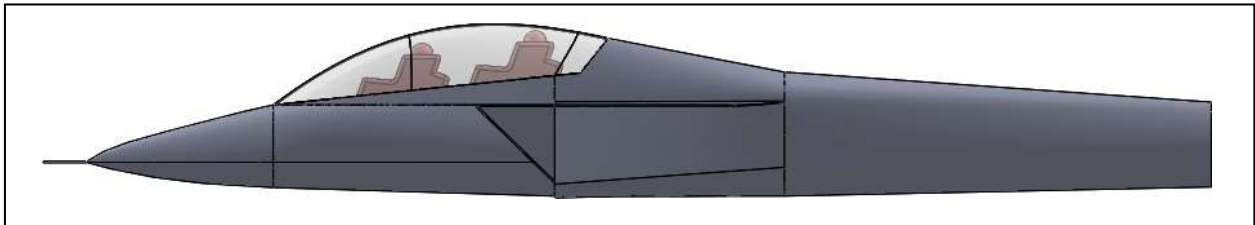


Figure 47. Fuselage side view

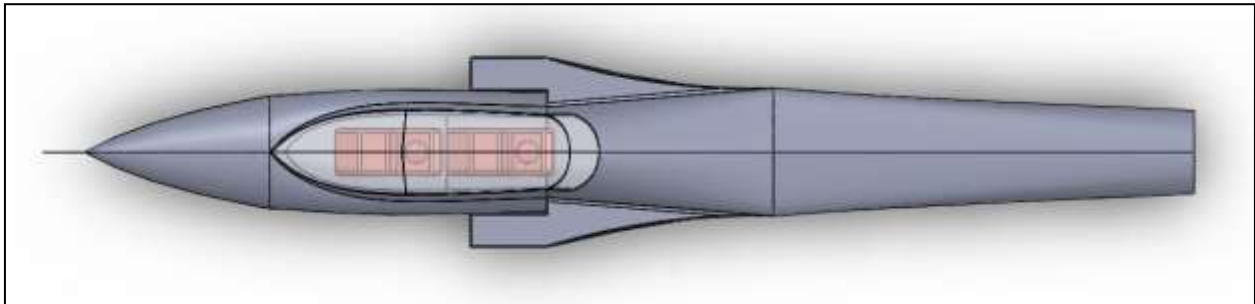


Figure 48. Fuselage top view

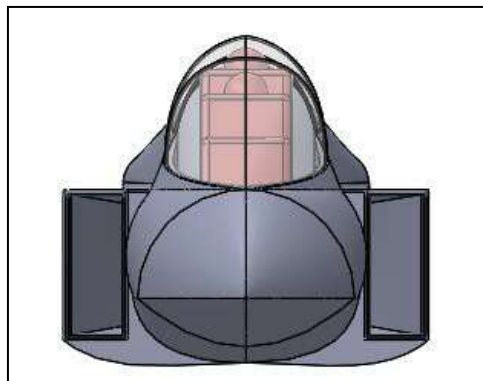


Figure 49. Fuselage front view

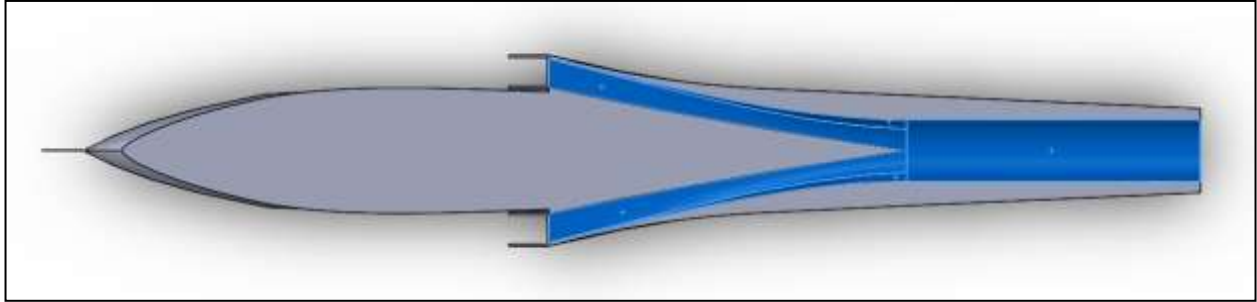


Figure 50. Preliminary engine intake ducts

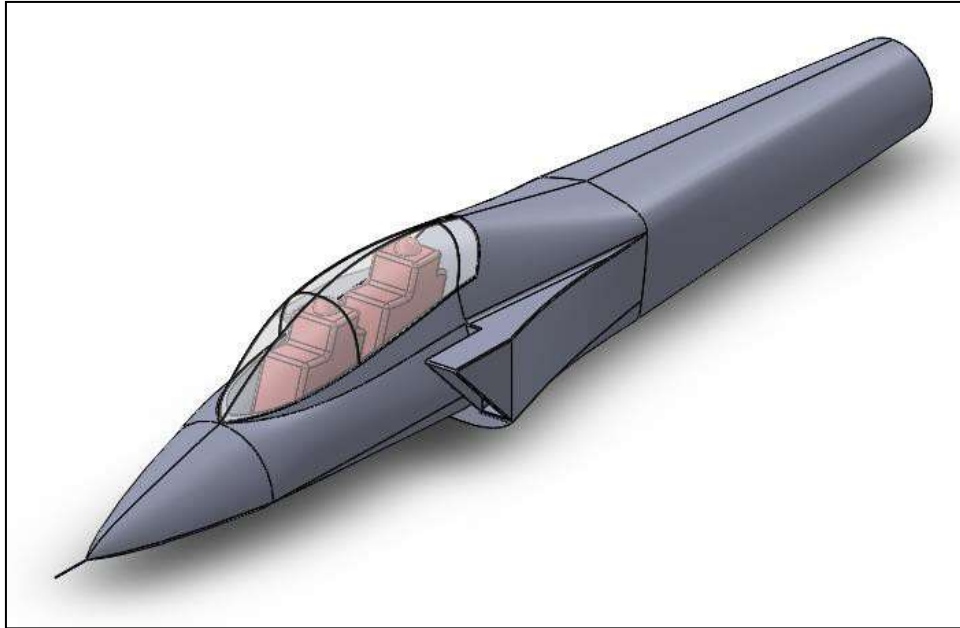


Figure 51. Fuselage isometric view

### 5.3 Summary of Fuselage Design

The overall fuselage design is determined based on pilot viewability and engine placement. The general design of the fuselage is used as a baseline that will require refinement as other features are added, such as the wing, empennage, etc. The integration of the wing structure and landing-gear may require a redesign of the engine intakes. The current design utilizes two intakes on each side of the cockpit.

The overall fuselage design is based on similar class of aircraft. These aircraft are those considered in the comparable aircraft section, such as the Lockheed Martin T-50 Golden Eagle, Textron Scorpion, Aermacchi M-346, etc. The aircraft have been certified to military requirements and therefore are a good reference to base the cockpit and fuselage design on.

## 6. Wing Design

The purpose of this chapter is to develop the general geometry of the wing and control surface sizing. Through the proceeding analysis and calculations, the following wing parameters are determined: aspect ratio, thickness ratio, taper ratio, airfoil, wing incidence, geometric twist, and overall shape. Based on the wing design appropriate high-lift devices and control surfaces will be sized.

### 6.1 Wing Planform

During the configuration design, the wing planform was selected to be a mid-wing. The proposed design requires transonic cruise capability. For the transonic cruise, analysis must be completed to determine the ratio of sweep angle to airfoil thickness ratio using equation (6.1). As a figure of merit, the weight of the wing can be estimated with equation (6.2) [21].

$$\frac{M_{cr}^2 \cos^2(\Lambda)}{\sqrt{1 - M_{cr}^2 \cos^2(\Lambda)}} \left\{ 2.64(t/c) \left( \frac{\gamma + 1}{2} \right) \left[ \frac{1}{\cos(\Lambda)} + \frac{0.34C_L}{\cos^3(\Lambda)} \right] \right\} + \frac{M_{cr}^2 \cos^2(\Lambda)}{1 - M_{cr}^2 \cos^2(\Lambda)} \left[ \left( \frac{\gamma + 1}{2} \right) \frac{1.32(t/c)^2}{\cos(\Lambda)} \right. \\ \left. + M_{cr}^2 \cos^2(\Lambda) \left\{ 1 + \left( \frac{\gamma + 1}{2} \right) \left[ \frac{0.68C_L}{\cos^2(\Lambda)} + \left( \frac{0.34C_L^2}{\cos^2(\Lambda)} \right) \right] \right\} \right] - 1 = 0 \quad (6.1)$$

$$W_w = 3.08 \left[ \frac{K_w \cdot n_{ult} \cdot W_{T0}}{(t/c)_{max}} \right] \left\{ \left( \tan(\Lambda) - \frac{2(1 - \lambda)}{AR(1 + \lambda)} \right)^2 + 1.0 \right\} \cdot 10^{-6} \quad \left\{ AR(1 + \lambda) \right\}^{0.593} S_w^{0.741} \quad (6.2)$$

Where  $K_w = 1.0$  for fixed wing or 1.175 for swing wings,  $\Lambda$  is wing sweep angle to the leading-edge, and  $n_{ult}$  is ultimate load factor.

Using equations (6.1) and (6.2), the relationship between wing sweep angle, thickness ratio, and weight are determined, see Table 12. The calculation is based on sea-level conditions and  $M = 0.85$ . A higher Mach number than the previously determined cruise is used assuming some subsonic flight exercises will exceed the cruise Mach. Based on the design choices, the relationship between wing sweep and thickness ratio can be seen in Figure 52. Figure 53 shows the relationship of wing sweep angle versus wing weight as a percentage of takeoff weight.

Table 12. Wing sweep angle versus thickness ratio

$\Lambda$ [deg]	$t/c$	$W_w$ [N]
0	0.0554	2968
10	0.0628	2670
20	0.0866	2223
30	0.130	1848
40	0.195	1632
50	0.2836	1598
60	0.3928	1799
70	0.516	2483
80	0.6323	5140
90	0.404	N/A

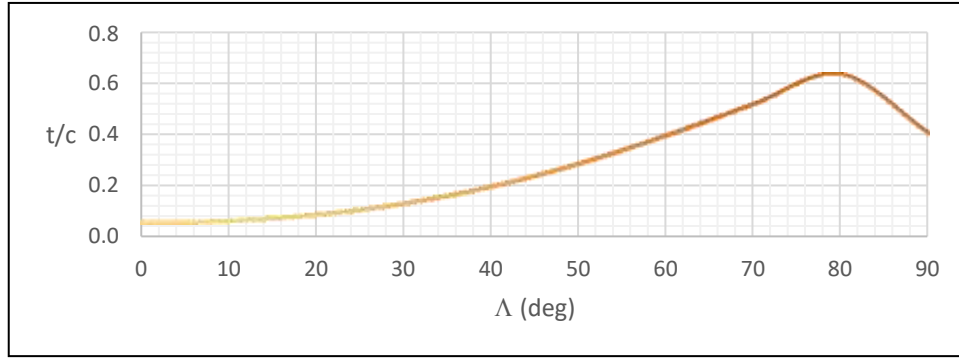


Figure 52. Wing sweep versus airfoil thickness ratio

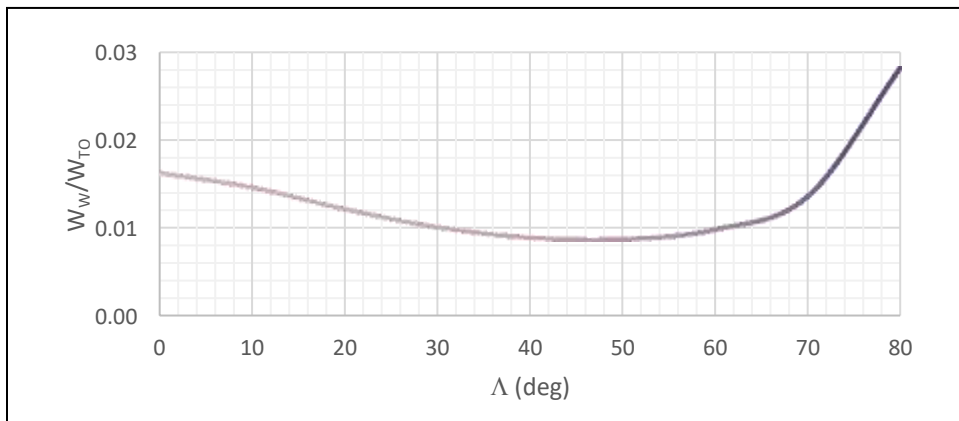


Figure 53. Wing weight percent of takeoff weight versus wing sweep angle

When considering airfoils, a thickness ratio of more than 20% results in large increases of drag. Based on the analysis presented in Table 12, wing sweep of more than 40 degrees should not be considered since it shows a relationship of more than 20% thickness ratio. Also having a considerable amount of wing sweep would lead to reduced low speed aerodynamic performance of the wing. In consulting the wing geometry tables in chapter 6 [19], wing sweep of this class of aircraft range from 0° to 60°. From the tables in chapter 8 [19], the comparable aircraft thickness ratios ranged from 6% to 15%. Based on the analysis and comparable aircraft, the wing sweep angle is selected to be 35° to the leading-edge and a thickness ratio of 8%.

## 6.2 Airfoil Selection

Selecting an airfoil for a wing requires an in-depth analysis of all the critical flight phases: takeoff, low speed, supersonic speeds, ect. Such analysis is beyond the scope for this project, but a discussion is necessary to convey the important design criteria that must be considered when selecting an airfoil or developing the geometry for a new airfoil.

The wing of an aircraft can be considered to have two or three sections depending on the complexity of the design. Depending on the wing's performance requirements, each section's airfoil shape would be customized to achieve the desired performance. The important variables to consider for each section of the wing are: drag coefficient, desired lift coefficient, critical Mach number, and pitching moment coefficient [19].

For the purpose of this project, a single airfoil will be considered. The performance sizing was completed considering a  $C_{L,max}$  of 1.4. This is not considered a high value for an airfoil to obtain. Since the

AMT is being designed with supersonic capabilities, the selected airfoil should consider features that help to reduce wave drag. From supersonic thin airfoil theory, the wave drag coefficient is calculated by equation (6.3) [22].

$$C_{D,w} = \frac{4}{\sqrt{M_\infty^2 - 1}} \left[ \alpha^2 + \overline{\alpha_c(x)^2} + \overline{\left( \frac{t}{c} \right)^2} \right] \quad (6.3)$$

Where  $\alpha$  is the angle of attack,  $\alpha_c(x)$  is the mean square of the camber line, and  $\left( \frac{t}{c} \right)$  is the mean square of the thickness distribution. Based on equation (6.3), symmetrical and low thickness ratio airfoils are more favorable for transonic and supersonic flight regimes to serve the purpose of reducing wave drag.

Another critical aspect to consider is the leading-edge of the airfoil. This is because when the flow across the wing is supersonic, the leading-edge determines if the shock wave is attached or detached. A detached bow shock will have greater wave drag than an attached one and require a more powerful propulsion system. An airfoil with a rounded leading-edge would be considered a subsonic leading-edge, and a sharp leading-edge would be considered a supersonic leading-edge.

Determining whether to consider airfoils with a supersonic or subsonic leading-edge is a tricky design choice for the AMT because most of the flying would be subsonic. A supersonic leading-edge has very poor low speed performance. This is because at low speeds and increased angles of attack, the flow will detach as it goes around sharp leading-edge and then reattach. This is considered a leading-edge stall. As the angle of attack is increased, the length of the detached flow increases until the flow is fully detached and there is a complete stall. This can result in abrupt and violent stall characteristics for the wing. Considering a pilot coming in for a landing, an abrupt stall could result in a crash.

These are some of the important parameters and design features to consider when selecting an airfoil(s). For the purpose of this project and analysis, a NACA 0008 airfoil will be used, shown in Figure 54.



Figure 54. NACA 0008

The aerodynamic polars for various Reynolds numbers are shown in Figure 55 and Figure 56, which are obtained from airfoiltools.com. Airfoiltools.com uses Xfoil software.

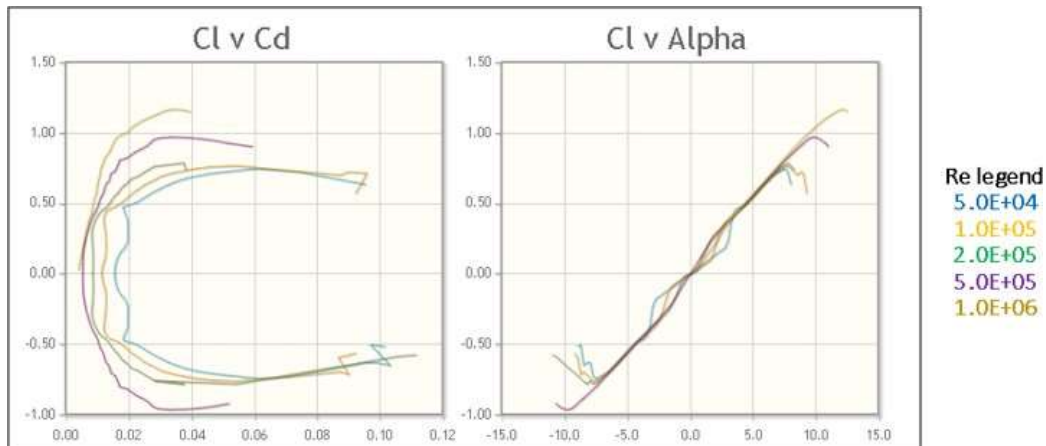


Figure 55. NACA 0008 aerodynamic polars

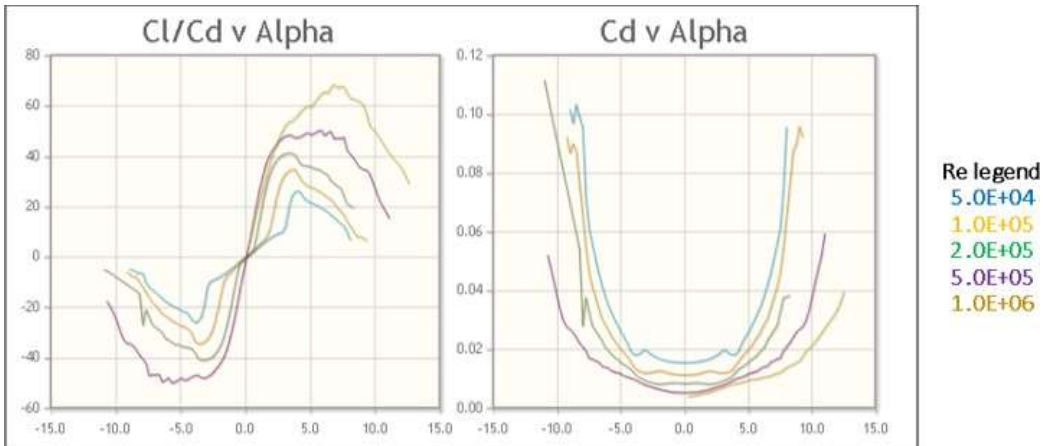


Figure 56. NACA 0008 aerodynamic polars

The aerodynamic polars presented in Figure 55 and Figure 56 are verified by performing an airfoil analysis on the NACA 0008 with the XFLR5 program. XFLR5 is a program built on the Xfoil software with a user-friendly interface. The results obtained, see Figure 57, are similar to airfoiltools.com. This makes sense because they are obtained using the same software.

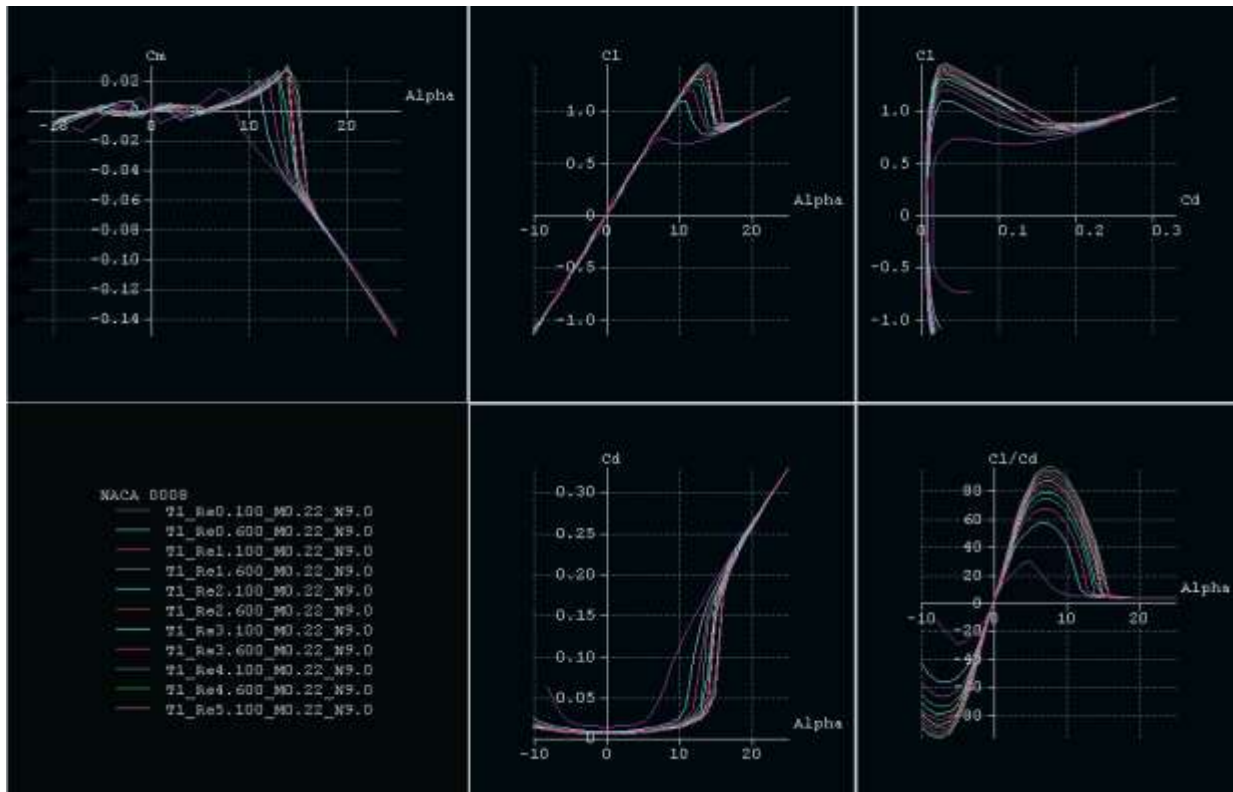


Figure 57. NACA 0008 coefficient polars from XFLR5

### 6.3 Wing Geometry

The wing design evaluation is completed to ensure that the wing's design  $C_{L_{max}}$  is obtained. During takeoff and landing, there is more drag and the flight speeds are low. Therefore, a greater  $C_L$  values is

required to obtain the necessary lift. For the AMT, a  $C_{L_{\max}}$  of 1.4 was determined in the performance sizing for takeoff and landing. Since the AMT is primarily designed to traverse a range of different flight conditions, and is more maneuverable in comparison to a transport plane, a clean  $C_{L_{\max}}$  is not as critical when compared to takeoff and landing. The landing  $C_{L_{\max}}$  is also not as critical, because the plane is lighter in comparison to the takeoff configuration. Therefore, satisfying the takeoff requirement will also satisfy the landing requirement.

Though the clean  $C_{L_{\max}}$  is not critical, a reasonable value must still be considered which will be used to size the high-lift devices. Though the airfoil results are promising, 3D effects reduce the aerodynamic performance of a wing, when compared to an 2D airfoil. From performance sizing the wing area and aspect ratio have been determined to be 18.4m<sup>2</sup> and 5, respectfully. The wing span is calculated using equation (6.4) and is found to be 9.60m.

$$AR = \frac{b^2}{S} = \frac{b}{c_{ave}} = \frac{2b}{c_r(1 + \lambda)} \quad (6.4)$$

A common practice in wing design is to incorporate chord taper along the wing span to reduce the wing root bending moment. This helps to reduce the required structure and offers weight saving advantages. The taper ratio is defined by equation (6.5). For the AMT a taper ratio of 0.25 will be used.

$$\lambda = c_t/c_r \quad (6.5)$$

Given the span, taper ratio, and aspect ratio, the root chord is 3.07m, from equation (6.4). The mean aerodynamic chord is calculated using the root chord length and taper ratio with equation (6.6) [22]. The mean aerodynamic chord is 2.15m.

$$\bar{c} = \frac{2}{3} c_r \frac{(1 + \lambda + \lambda^2)}{1 + \lambda} \quad (6.6)$$

The chord tip is calculated with the taper ratio and the root chord length from equation (6.5). Table 13 summarizes the developed wing geometry.

Table 13. Preliminary wing geometry

Parameter	Value
S	18.4 m <sup>2</sup>
b	9.60 m
$\bar{c}$	2.15 m
$c_r$	3.07 m
$c_t$	0.768 m
$\Lambda_{LE}$	35°
$\lambda$	0.25

## 6.4 Wing Design Evaluation

Based on the airfoil analysis, a wing with a clean  $C_{L_{\max}}$  of 1.0 can be achievable. The recommended increase to account for tail (or canard) trim is 5 to 10 percent [19]. Therefore, a clean  $C_{L_{\max}}$  of 1.05 would be ideal. A straight wing  $C_{L_{\max}}$  is calculated using equation (6.7).

$$C_{L_{\max W}} = k_\lambda \frac{c_{l_{\max r}} + c_{l_{\max t}}}{2} \quad (6.7)$$

The maximum sectional lift coefficient of the wing root and tip, and the wing taper correction factor ( $k_\lambda$ ) is determined using the AAA program. These are found to be:

- $c_{l_{max_r}}$  1.25
- $c_{l_{max_t}}$  1.19
- $k_\lambda$  0.968

The above values result in a  $C_{L_{max_w}}$  of 1.18. Because the AMT has a swept wing, the  $C_{L_{max_w}}$  must be correct for sweep using equation (6.8). If the quarter-chord sweep angle is greater than  $35^\circ$ , then another method should be employed [19].

$$C_{L_{max_{swept}}} = C_{L_{max_{unswept}}} \cos(\Lambda_{c/4}) \quad (6.8)$$

The corrected  $C_{L_{max_w}}$  is 1.02. Comparing this value to the desired value of 1.05, the difference is less than 5%. If the difference between the desired and calculated  $C_{L_{max}}$  is greater than 5%, and if the clean  $C_{L_{max}}$  value is critical, then a design change is recommended [19]. The above calculations are verified with the AAA program, which uses the same or similar methods. Figure 58 through Figure 60 are the screen dumps of the navigation process through the AAA verification.

Input Parameters					
Altitude	4570 m	$c_{r_w}$	3.07 m	$(t/c)_{r_w}$	8.00 %
$\Delta T$	0.0 deg C	$c_{l_w}$	0.77 m	Root Airfoil	NACA 4 & 5 Digit Symmetric
$V_{S_{clean}}$	811.00 $\frac{km}{hr}$	$(t/c)_{t_w}$	8.00 %	Tip Airfoil	NACA 4 & 5 Digit Symmetric
Output Parameters					
$Re_{r_w}$	32.5014 $\times 10^5$	$Re_{t_w}$	8.1227 $\times 10^6$		
$c_{l_{max_{rw}}}$	1.253	$c_{l_{max_{tw}}}$	1.100		

Figure 58. AAA – Airfoil  $c_{l,max}$

Input Parameters			
$b_w$	9.60 m	$\Lambda_{c/w}$	30.1 deg
$c_{r_w}$	3.07 m	$x_{apex_w}$	0.00 m
$c_{t_w}$	0.77 m	$y_{offset_w}$	0.00 m
Output Parameters			
$S_w$	10.44 m <sup>2</sup>	$y_{mpc_w}$	1.92 m
$AR_w$	5.00	$x_{mpc_w}$	1.34 m
$\lambda_w$	0.25	$\Lambda_{LE_w}$	35.0 deg
$z_w$	2.15 m	$\Lambda_{TE_w}$	12.4 deg

Figure 59. AAA – Wing geometry

Input Parameters			
$C_{l_{max_{rw}}}$	1.253	$C_{r_w}$	3.07 m
$C_{l_{max_{tw}}}$	1.188	$C_{t_w}$	0.77 m
$\Lambda_{c/w}$	30.1 deg	$f_{couple}$	1.10
		$C_{l_{max_{clean}}}$	1.050
Output Parameters			
$\lambda_w$	0.25	$C_{L_w_{max_{clean}}}$	1.021
$K_{L_w}$	0.968	$C_{L_w_{max}}$	1.021

Figure 60. AAA – Wing  $C_{L_{max}}$

## 6.5 Design of the High-Lift Devices

The purpose of the high-lift devices is to increase a wing's  $C_{L_{max}}$  to the required takeoff and landing  $C_{L_{max}}$ . Some modern fighters utilize leading and trailing-edge high-lift devices for improved maneuverability. The USAF wants an advanced trainer that prepares pilots for modern aircraft. The AMT will employ both a leading-edge nose flap and trailing-edge flap to offer more maneuverability, when compared to designs without such devices. The following is the method and analysis for sizing the AMT's high-lift devices as presented in chapter 7 [19] and chapter 8 [24].

The first step is to determine the incremental change in  $C_{L_{max}}$  for takeoff and landing from the clean  $C_{L_{max}}$  using equation (6.9).

$$\Delta C_{L_{Max}} = 1.05 (C_{L_{max_{TO,La}}} - C_{L_{max}}) \quad (6.9)$$

The factor of 1.05 is to account for trim penalties associated with balancing the aircraft [19]. From performance sizing, a takeoff  $C_{L_{max}}$  of 1.4 was determined. Using the 1.02  $C_{L_{max}}$  of the wing determined in the previous section, the  $\Delta C_{L_{max}}$  is 0.40. The change in sectional maximum lift coefficient must be

calculated to determine the sectional lift coefficient,  $\Delta c_l$ . The change in maximum sectional lift coefficient is calculated with equation (6.10).

$$\Delta c_{l_{\max}} = \frac{\Delta c_{l_{\max}} S}{K_{\Lambda}} \left( \frac{\partial}{\partial f} \right) \quad (6.10)$$

The wing sweep factor,  $K_{\Lambda}$ , is calculated with equation (6.11).

$$K_{\Lambda} = [1 - 0.08 \cos^2(\Lambda_{c/4})] \cos^{0.75}(\Lambda_{c/4}) \quad (6.11)$$

The flapped wing area is defined in Figure 61 and the ratio of the flapped wing area to total wing area can be calculated using equation (6.12).

$$\frac{S_f}{S} = \frac{(\eta_o - \eta_i)[2 - (1 - \lambda)(\eta_i + \eta_o)]}{1 + \lambda} \quad (6.12)$$

The spanwise flap locations  $\eta_o$  and  $\eta_i$  are non-dimensional values from the centerline with respect to the half-span.

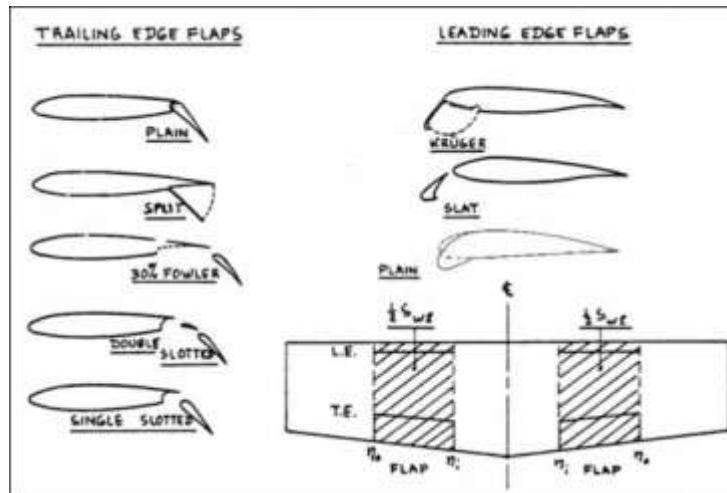


Figure 61. Wing flapped area [24]

For maximum maneuverability, the leading-edge and trailing-edge flaps should span the total wing span, minus the intersection area of the wing and fuselage. The problem with this is, the sectional lift would increase across the wing span. Any increase in outboard wing lift would increase the wing root bending moment and would require increasing the wing's structure to support the load. Therefore, the flapped wing area will be considered to cover half of the wing span extending off the fuselage. Approximately where the wing will be placed, the fuselage is about 0.85m from the centerline of the aircraft. Therefore, the spanwise location  $\eta_i$  is 0.1875 correlating to 0.9 m from the centerline. With  $\eta_i = 0.1875$ ,  $\eta_o$  is 0.6875.

Using equation (6.12), the ratio of flapped wing area to total wing area is found to be 0.537. From equation (6.11), the wing sweep factor is 0.843. With these two values,  $\Delta c_{l_{\max}}$  is found to be 0.876.

### 6.5.1 Trailing-Edge Flaps

The required change in sectional lift coefficient ( $\Delta c_{l_{\text{req}}}$ ) for a trailing-edge flap is related to the  $\Delta c_{l_{\max}}$  by equation (6.13).

$$\Delta c_{l_{req}} = \frac{\Delta c_{l_{max}}}{K} \quad (6.13)$$

The factor K is determined using Figure 62. The trailing-edge flap should be approximately 20-30% of the wing's sectional chord. This will allow a reasonable amount of space for a rear wing support spar. The arrows in Figure 62 show the indicated values used in the trailing-edge flap sizing. The colors correlate to corresponding parameter values in figures that follow used for the trailing-edge flap sizing.

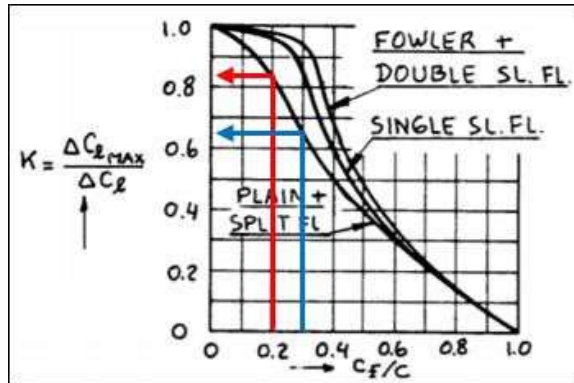


Figure 62. Relation of flap chord ratio and K factor [19]

The design sectional lift coefficient incremental increase for plain flaps, is related to the derivative of the sectional lift coefficient with respect to flap deflection ( $c_{l_{\delta_f}}$ ), flap deflection ( $\delta_f$ ), and flap chord ratio correction factor K' by equation (6.14).

$$\Delta c_{l_{des}} = c_{l_{\delta_f}} \cdot \delta_f \cdot K' \quad (6.14)$$

The  $c_{l_{\delta_f}}$  is related to the flap chord ratio and airfoil thickness by Figure 63. The flap deflection, flap chord ratio, and factor K' are related by using Figure 64.

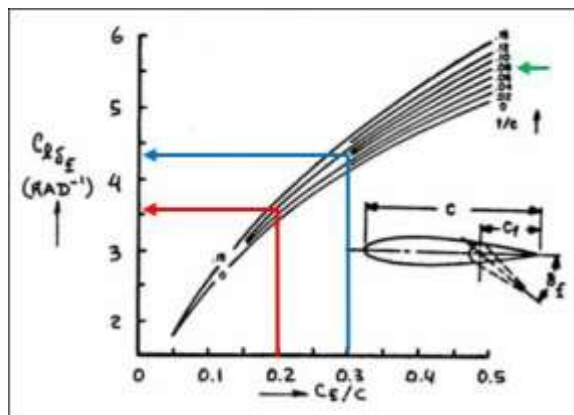


Figure 63. Effect of thickness ratio and flap chord ratio on  $c_{l_{\delta_f}}$  [19]

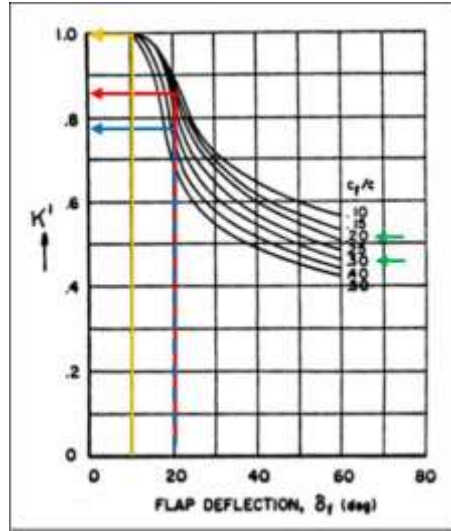


Figure 64. Effect of trailing-edge flap deflection and flap chord ratio on  $K'$  [19]

Based on flap chord ratios of 0.2 and 0.3 selected, the corresponding  $c_{l_{\delta_f}}$  is found with Figure 63. Deflected flaps can be thought of as giving the wing variable camber. Cambered airfoils have higher  $C_{L_{max}}$  and greater lift-curve slopes. This also correlates to increased drag. To help keep the drag rise to a minimum, low flap deflections of  $10^\circ$  and  $20^\circ$  are selected. The correlating factor  $K'$  is found in Figure 64. Table 14 lists the determined values from Figure 62 through Figure 64. The parameters that meet the design are highlighted in green.

Table 14. Effect of flap chord ratio and K factor on  $\Delta c_l$ .

Parameter	Values				Units
	Red Arrows		Blue Arrows		
$c_f/c$	0.2		0.3		N/A
K	0.83		0.64		N/A
Req. $\Delta c_l$	1.04		1.35		N/A
$C_{l_{\delta_f}}$	3.6		7.4		1/rad
$\delta_f$	10	20	10	20	deg
$K'$	1.0	0.86	1.0	0.79	N/A
Des. $\Delta c_l$	0.628	1.08	0.768	1.21	N/A

### 6.5.2 Leading-edge Flaps

The leading-edge flaps are evaluated using the method presented in chapter 8 [24] for plain nose flaps. The change in sectional lift is a function of nose flap deflection angle ( $\delta_{nf}$ ) and the derivative sectional lift with respect to the nose flap deflection angle ( $c_{l_{\delta_{nf}}}$ ), represented by equation (6.15)

$$\Delta c_{l_{nf}} = c_{l_{\delta_{nf}}} \cdot \delta_{nf} \quad (6.15)$$

The  $c_{l_{\delta_{nf}}}$  is related to the nose flap chord ratio by Figure 65. Three values of nose flap ratio are selected for evaluation: 0.1, 0.2, and 0.23. Figure 66 shows how  $\Delta c_{l_{nf}}$  varies with flap deflection angle for the three selected values of  $c_{nf}/c$ . Table 15 lists the selected design parameters.

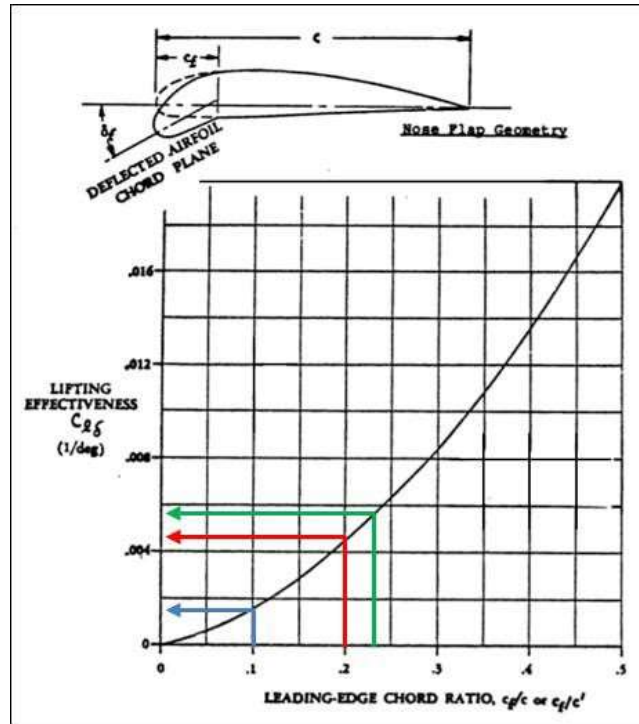


Figure 65. Effect of leading-edge flap chord ratio on  $c_{l,\delta}$  [24]

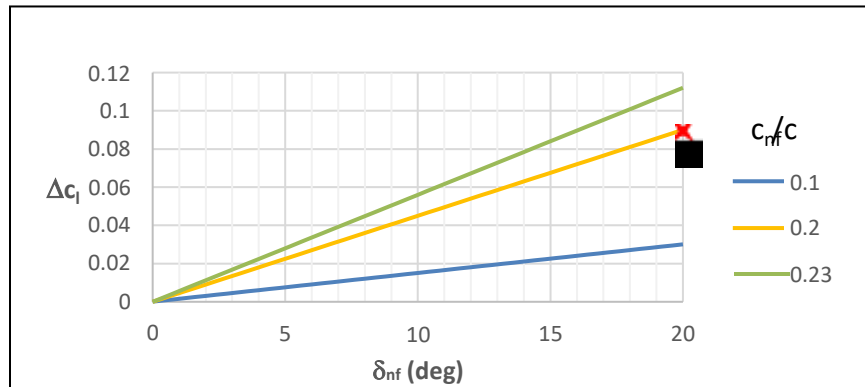


Figure 66. Effect of  $\delta_{nf}$  and  $c_{nf}/c$  on  $\Delta c_l$

Table 15. Nose flap parameters

Parameter	Value
$c_{nf}/c$	0.2
$\delta_{TO}$	20°
$\Delta c_{l_{nf}}$	0.90

### 6.5.3 High-Lift Devices Evaluation

The  $C_{L_{max_{TO}}}$  is verified by combining equations (6.9), (6.10), and (6.14) to form equation (6.16).

$$C_{L_{max_{TO}}} = \frac{(\Delta c_{l_{TE}} \cdot K_{TE} + \Delta c_{l_{LE}} \cdot K_{LE}) K_{\Lambda} (S_f/S)}{1.05} + C_{L_{max_{clean}}} \quad (6.16)$$

This is the reverse process of determining  $\Delta c_{l_{des}}$  for the trailing-edge flaps. For the design choices of the leading-edge and trailing-edge flaps, the AMT's calculated  $C_{L_{max_{TO}}}$  is 1.44. This satisfies the performance sizing requirements.

## 6.6 Design of the Lateral Control Surfaces

Based on the tables in chapter 8 in [19], ailerons for this type of aircraft have a wing half span of 20 to 100 % but average to about 40% on the outer half of the wing. The aileron chord length ranges from 10 to 40 %. For the initial design, the aircraft's ailerons will extend off the trailing-edge flaps and have an aileron chord ratio of 20%. The last step is to place the main spars of the wings. The clearance between spars and control surfaces is recommended to be at least 0.5% of the chord length [19]. The leading-edge spar is placed at the quarter-chord, and the trailing-edge spar is placed 5.0cm from the trailing-edge flap and aileron.

## 6.7 Drawings

The summation of the analysis and the design choices for the wing geometry have resulted in the half wing drawing presented in Figure 67. The drawings show the dimension call-outs of the proposed geometry. The quarter-chord, spar, and aileron locations are shown as well.

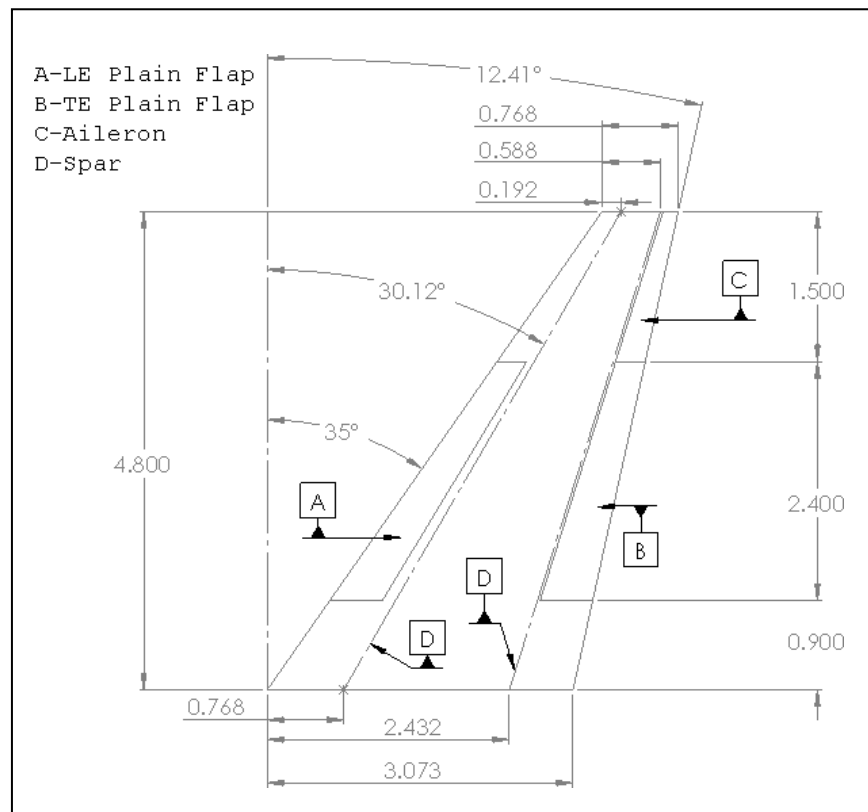


Figure 67. Proposed wing geometry , dimensions in meter

The analysis and design completed for the wing provides a good baseline. There is one more critical parameter to check. The wing volume is utilized for control surface subsystems and fuel storage. The fuel volume can be approximated with equation (6.17) [23].

$$\text{Vol}_{WF} = 0.54 \left(\frac{S^2}{b}\right) \left(\frac{t}{c}\right)_r \frac{1 + \lambda_w \sqrt{\tau_w} + \lambda_w^2 \cdot \tau_w}{(1 + \lambda_w)^2} \quad (6.17)$$

The fuel volume approximation is based on historical data. If a more accurate approximation is needed or if the calculated value is too close to previous estimations a different method should be employed [23]. Equation (6.17) is only a function of wing area, span, root thickness ratio, taper ratio, and thickness taper ratio,  $\tau_w$ . The thickness taper ratio is defined with the following equation using the wing root and tip thickness ratios.

$$\tau_w = \frac{(t/c)_t}{(t/c)_r}$$

The fuel volume is calculated to be 1.29m<sup>3</sup>. From the weight sizing analysis, the fuel required with reserves was 15.4kN. The average density of jet fuel is 800kg/m<sup>3</sup>, based on Figure 68. This correlates to 1.96m<sup>3</sup>. Based on the results, about 1/3 of the fuel will have to be stored in the fuselage. But, since a significant volume of the wing intersects with the fuselage, most of the fuel will have to be stored in the fuselage. Another option would be to increase the wing size to accommodate the fuel, but this will result in more drag for a larger wing therefore, the current design will remain as is.

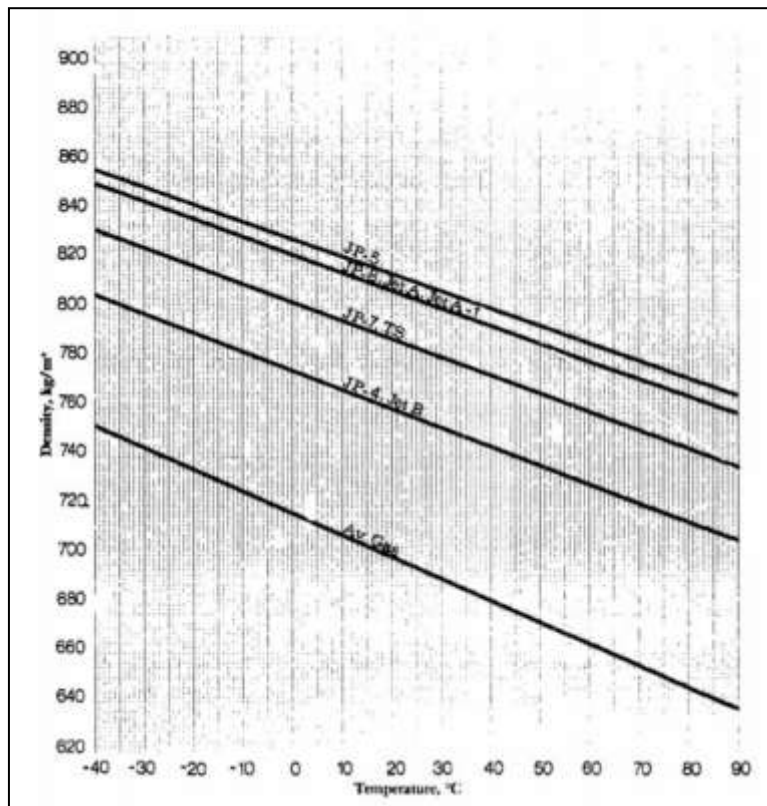


Figure 68. Aviation jet fuel densities versus temperature [25]

## 6.8 Discussion and Conclusion

At this point in the design the fuselage and wing have been determined. Using the geometry determined in the wing design, a 3D wing is modeled in Solidworks. Combining the fuselage and the wing, the proposed combination can be seen in Figure 69 through Figure 71. The exact position of the wing is an approximation.

The exact x-location and z-location of the wing may be adjusted for adequate stability and control. This will be determined in the static stability and control section.

The proposed position of the wing root's leading-edge is near the back of the cockpit and the vertical position is approximately at the top of the engine inlets. The incidence of the wing root was selected to be three-degrees which offers  $C_L$  for cruise. The wing tip has a negative two-degrees incidence to help reduce washout effects and to help maintain aileron controllability in low speed high angles of attack.

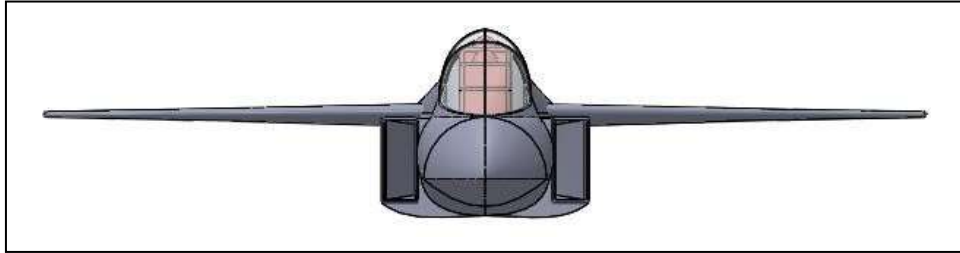


Figure 69. AMT front view fuselage and wing

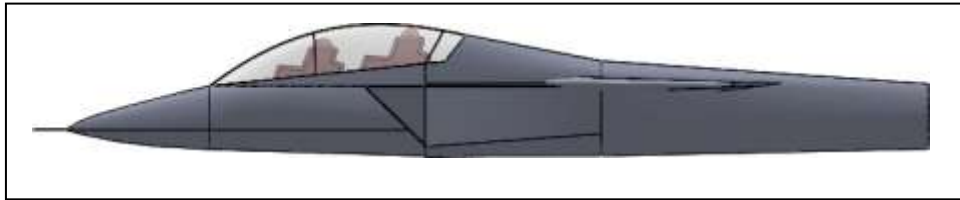


Figure 70. AMT side view fuselage and wing

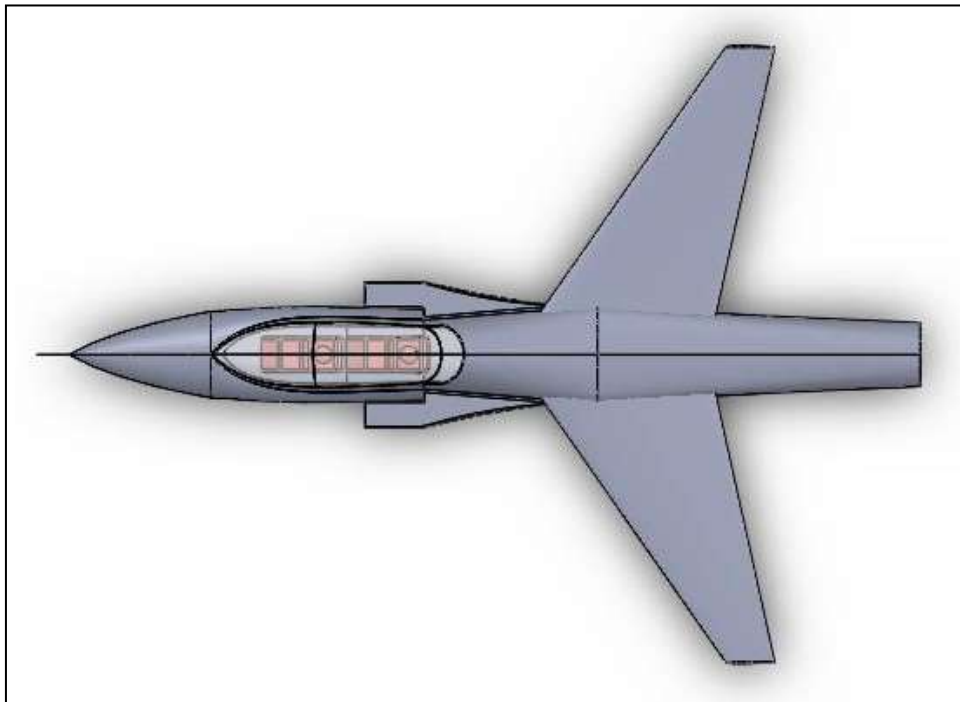


Figure 71. AMT top view fuselage and wing

From a visual inspection the wing appears to be a reasonable size in relation to the fuselage. Additional analysis on the wing must be completed using the area ruling method to ensure adequate supersonic performance. Table 16 summarizes the wing geometry determined in this chapter.

Table 16. Summarized wing geometry

<b>Parameter</b>	<b>Value</b>	<b>Units</b>
Area	18.4 (198)	m <sup>2</sup> (ft <sup>2</sup> )
Aspect Ratio	5.0	N/A
Span	9.60 (41.5)	m (ft)
Mean Chord	2.15 (7.05)	m (ft)
Root Chord	3.07 (10.1)	m (ft)
Tip Chord	0.768 (2.52)	m (ft)
c/4 Sweep	30.1	deg
LE Sweep	35.0	deg
Thickness Ratio	8.0	%
Root Incidence	3.0	deg
Tip Incidence	-2.0	deg
LE flap % ½ span	50	%
LE flap % chord	20	%
TE flap % ½ span	50	%
TE flap % chord	20	%
Outer Aileron % ½ Span	31.25	%
Aileron % Chord	20	%

## 7. Empennage Design

The purpose of this chapter is to develop the preliminary sizing of the empennage. The empennage is responsible for trimming the aircraft in pitch, and to maintain directional yaw control. The horizontal stabilizer and vertical fins are determined using tail volume coefficients. There are no elevators to size because a fully moving horizontal will be used. The rudder control surface is sized similarly to the wing control surfaces.

### 7.1 Overall Empennage Design

The horizontal stabilizer and vertical fins are sized using the tail volume coefficient method [19]. The tail volume coefficient method sizes the empennage surfaces from wing geometry and tail volume coefficients of historical data. The only required wing parameters needed to size the empennage is the wing span, area, and mean chord length from Table 16 (previous section). The tail volume coefficients are expressed by equations (7.1) and (7.2). Equations (7.1) and (7.2) can be rearranged into equations (7.3) and (7.4) to solve for the area of the stabilizer and vertical fin.

$$V_h = \frac{x_h \cdot S_h}{S \cdot \bar{c}} \quad (7.1)$$

$$V_v = \frac{x_v \cdot S_v}{S \cdot b} \quad (7.2)$$

$$S_h = \frac{\bar{V} \cdot S \cdot \bar{c}}{x_h} \quad (7.3)$$

$$S_v = \frac{\bar{V} \cdot S \cdot b}{x_v} \quad (7.4)$$

The only parameters not defined in equation (7.3) and (7.4) are the reference lengths and tail volume coefficients. The reference lengths for the stabilizer and vertical are defined as the distance between the quarter-chord and wing's root leading-edge. The tail volumes are selected based on historical aircraft, see Table 17. The empennage tail volumes are sized from the average of the historical aircraft. The empennage reference lengths are estimated based on what looks reasonable, which will be verified in the stability and control analysis. For the purpose of this calculation, the moment arm of the horizontal will be 6.0m and the vertical will be 4.5m. Solving equation (7.3) and (7.4) results in a stabilizer and fin areas summarized in Table 18 and Table 19.

Table 17. Tail volumes of comparable aircraft

Aircraft	$\bar{V}$	$\bar{V}$
F-14	0.40	0.06
F-15	0.20	0.098
F-16	0.30	0.094
Dassault Alphajet	0.43	0.084
Aero L-39	0.58	0.083
Average	0.38	0.084

### 7.2 Design of the Horizontal Stabilizer

Class I horizontal sizing follows the methods in chapter 8 of [19], this is completed based on historical aircraft and designer's choice. For advanced trainers and fighters, the horizontal AR of comparable aircraft

range between 2.5 and 4.0. Comparing the historical aircraft, the leading-edge sweep angle of the horizontal stabilizer ranges from 25° to 45°. The horizontal sweep angle should be greater than the wing's sweep to ensure the horizontal maintains pitch control at high angles of attack. For advanced trainers and fighters, the horizontal taper ratio ranges from 0.16 to 1.0.

The horizontal stabilizer is not a lifting surface and therefore it has no  $C_L$  requirement to satisfy. The average thickness ratio for this class of aircraft is about 10%. The airfoil to be used for the design will be a NACA 0010. Analogous to the airfoil discussion in the wing design chapter, the actual airfoil profile would be determined from an in-depth analysis of the critical flight conditions. Since maneuverability is an important requirement, no dihedral is considered at this point in the design. Also, no incidence angle is considered because the horizontal will be a fully moving stabilizer. Sizing of the horizontal stabilizer uses the same equations used to size the wing. Table 18 summarizes the horizontal geometry determined.

Table 18. Horizontal stabilizer geometry

Parameter	Value	Units
Aspect Ratio	3	N/A
Area, $S_h$	2.51(27.0)	m <sup>2</sup> (ft <sup>2</sup> )
Span, $b_h$	2.75(9.02)	m(ft)
MAC, $\bar{c}_h$	0.971(3.19)	m(ft)
Root c	1.31(4.30)	m(ft)
Tip c	0.523(1.72)	m(ft)
LE Sweep	40	deg
Taper Ratio	0.4	%
Airfoil	NACA 0010	N/A
Dihedral Angle	0	deg
Incidence Angle	0	deg

### 7.3 Design of the Vertical Stabilizer

Sizing the vertical fin follows the same procedure as the horizontal stabilizer, chapter 8 [19]. For a vertical fin, the sizing usually consists of only one fin. The AMT will feature two smaller fins, and to account for the efficiency loss of splitting the total area, the total vertical fin area is increased by 10%. For advanced trainers and fighters with twin vertical stabilizers, the vertical AR of comparable aircraft range between 0.4 and 2.9. An aspect ratio of 1.5 is selected. The comparable aircraft have a range of vertical quarter-chord sweep angles from 0° to 60°. This design will utilize a leading-edge sweep angle of 45°. The average thickness ratio for this class of aircraft is 10-15% and utilizes a symmetrical airfoil.

For vertical fins, only an incidence is required for propeller airplanes. This is because the flow through the propeller induces a sideslip flow on the vertical fin. To correct for this, an incidence is placed to balance the directional stability of the airplane. Since the AMT is not in this class of aircraft no incidence is required. The dihedral angle is defined as the projected geometric-plane of the aerodynamic surface and the XY-plane of the aircraft reference frame. A dihedral angle of 75° is selected to reduce the interference from the canopy wake. Table 19 summarizes the vertical fin geometry.

Table 19. Vertical fin geometry

Parameter	Value	Units
Aspect Ratio	1.5	N/A
Area, $S_v(2)$	3.64(39.2)	m <sup>2</sup> (ft <sup>2</sup> )
Span, $b_v(1)$	1.65(5.41)	m(ft)
MAC, $\bar{c}(1)$	1.17(3.84)	m(ft)
Root c	1.57(5.15)	m(ft)
Tip c	0.629(2.06)	m(ft)
LE Sweep	45	deg
Taper Ratio	0.4	%
Airfoil	NACA0010	N/A
Dihedral Angle	75	deg
Incidence Angle	0	deg

#### 7.4 Design of the Longitudinal and Directional Controls

The longitudinal control surface as previously mentioned will be a fully moving horizontal stabilizer. This design concept was realized during the flights of the X-1, see Figure 72. Initially the plane's horizontal incident angle was fixed with elevator control surfaces. In a flight at  $M = 0.94$ , pilot Chuck Yeager noted elevator ineffectiveness. Jack Ridley, an engineer on the test flight team, determined this was due to shocks forming across the horizontal stabilizer. The solution was to incorporate a fully moving horizontal stabilizer, which proved to be successful. The stabilator, or flying tail, is now a predominate feature seen on most conventional empennage supersonic aircraft.



Figure 72. X-1 aircraft

The initial estimate for sizing of the rudder is completed using historical data of similar aircraft. Tables 8.8b and 8.9b [19], the length of the rudder root is 20 to 50 % the vertical fin's chord length and the rudder tip section is 30 – 50%. The design of the AMT's rudder will be 40%. Typical designs utilize the entire span of the vertical stabilizer for the rudder length. Considering structure and mechanical features, the rudder will be 90 % of the span, and positioned 5% from the root and tip edges.

#### 7.5 Horizontal Stabilizer and Vertical Fin Geometry Drawings

Figure 73 shows the NACA0010 profile selected for the horizontal stabilizer and vertical fins. Figure 74 is the horizontal stabilizer geometry as summarized in Table 18. Figure 75 is the vertical fin geometry as outlined in Table 19.



Figure 73. NACA 0010 profile

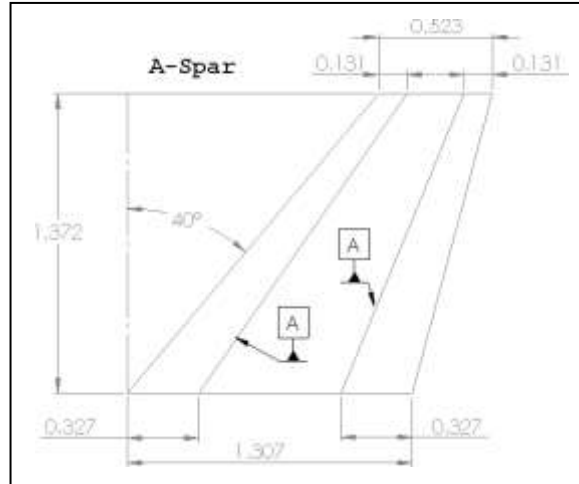


Figure 74. Horizontal stabilizer geometry drawing , units in meters

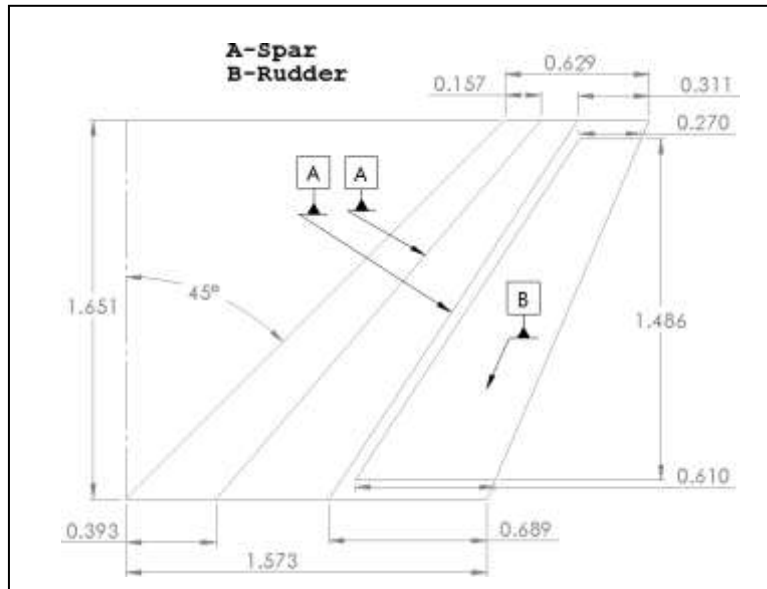


Figure 75. Vertical stabilizer geometry drawing , units in meters

## 7.6 AMT Views with Horizontal and Vertical Stabilizers

The sizing of the horizontal and vertical stabilizers has resulted in the updated CAD model presented in Figure 76 through Figure 78.

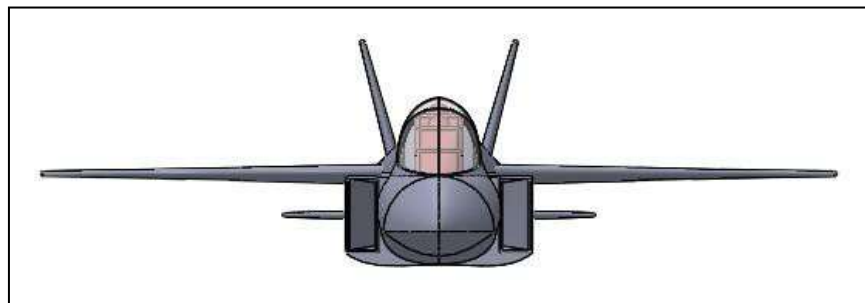


Figure 76. AMT front view with empennage

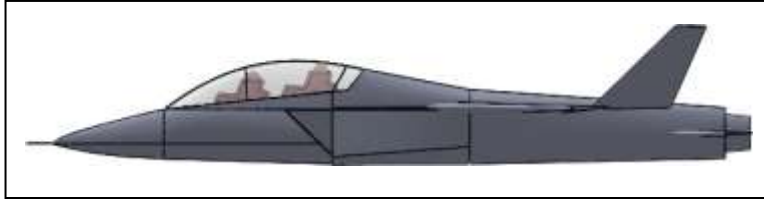


Figure 77. AMT side view with empennage

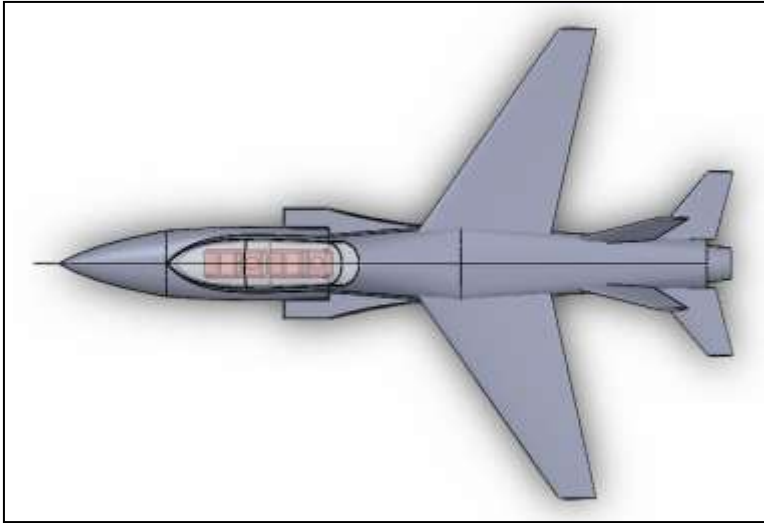


Figure 78. AMT top view with empennage

## 7.7 Discussion and Conclusion

The critical geometry for the aircraft's aerodynamic surfaces has been determined. From a visual inspection, the wing, horizontal stabilizer, vertical fin and fuselage appear proportionally correct with respect to one another. The static stability and control analysis will help to refine the design to adjust the sizing of the flight surfaces.

The horizontal stabilizer area for comparable aircraft is  $1.9$  to  $14\text{m}^2$  ( $20$ - $150\text{ft}^2$ ). The proposed design has a horizontal stabilizer area of about  $2.51\text{m}^2$  ( $27.0\text{ft}^2$ ). The horizontal stabilizer moment arm for comparable aircraft is  $2.7$  to  $7.3\text{m}$  ( $9$ - $24\text{ft}$ ). The AMT's horizontal moment arm is  $6.0\text{m}$ . Since the horizontal's area is on the lower end of the comparable aircraft range, the moment arm corresponding to the higher range of the comparable aircraft moment arm makes sense.

The vertical stabilizer area for comparable aircraft is  $1.4$  to  $14\text{m}^2$  ( $15$ - $150\text{ft}^2$ ). The current design has a total vertical stabilizer area of about  $3.64\text{m}^2$  ( $\text{ft}^2$ ). The vertical stabilizer moment arm for comparable aircraft is  $3.0$  to  $7.6\text{m}$  ( $10$ - $25\text{ft}$ ). The AMT's moment arm is  $4.5\text{m}$ , which is in the low-mid range of the comparable aircraft. This could be a hint at needing a design correction, but the directional stability analysis will provide better reasoning to correct the design if needed.

The sizing and analysis completed in this section gives an estimation of the geometry for the horizontal and vertical stabilizers. The proposed geometry is within the range of expected values for similar type of aircraft. The proposed configuration of the aircraft is only an estimate and will be used as a baseline to further refine the design. The analysis to be completed in the S&C section will help to determine if the position and area of the wing, stabilator, and vertical stabilizer are acceptable for the design.

## 8. Class I Weight and Balance and Landing-Gear Design

The purpose of this chapter is to estimate the weight and locations of the different weight groups. Based on the weight and location of the various components, the aircraft cg is determined. Based on the aircraft cg location, Class I landing gear design is performed. The Class I method includes: positioning the landing-gear to meet ground stability criterion, sizing the tires and struts, and verifying the configuration fits the aircraft model.

### 8.1 Weight and Balance

#### 8.1.1 Estimation of the Center of Gravity Location for the AMT

The cg of the AMT is approximated using the weight fraction method [21]. The method is a top-level estimation of component weights based on similar existing aircraft. The purpose of the method is to rapidly estimate aircraft component weights without requiring large engineering man-hours. The comparable aircraft component weights [21] have been converted to S.I. units from the given Imperial units. Table 20 lists the aircraft and their component weights. The takeoff weight is adjusted to only account for the components listed in the table. The weight groups of the comparable aircraft are averaged, see column *Average*, and the weight group averages are converted to a fraction with respect to the total weight average, see column  $FF/W_{tot}$ .

Table 20. Similar aircraft component weights (N)

Aircraft	T-38	F-4	F-15	F3H-2	F/A-18	*Harrier	Average	FF/W <sub>TO</sub>
Fuselage	8,829	14,541	9,052	13,651	20,839	9,163	12,679	0.135
Wing	3,403	9,697	12,018	7,557	16894	6,418	9,331	0.099
Empennage	1,357	2,976	1,463	2,891	4203	1,655	2,424	0.026
Nose LG	<u>610</u>	<u>1,210</u>	<u>1,320</u>	<u>1,157</u>	2784	<u>1,486</u>	1,428	0.015
Main LG	<u>1,423</u>	<u>2,824</u>	<u>3,079</u>	<u>2,699</u>	6076	<u>3,011</u>	3,186	0.034
Fixed Equipment	8,709	11,890	12,192	18,642	22,836	12,130	14,400	0.153
Trapped Fuel & Oil	276	320	<u>388</u>	<u>470</u>	<u>749</u>	<u>454</u>	443	0.005
Propulsion sub-components	3287	3621	6,014	2811	8820	5,435	4,998	0.053
Engine	4,617	15519	16,217	13,429	19100	16,969	14,308	0.152
Fuel	17,418	29,637	16,280	31,136	48,305	34,512	29,548	0.314
Crew	1779	890	890	890	1779	1779	1334	0.014
<b>W<sub>tot</sub></b>	49,929	92,234	78,024	94,443	150,607	91,233	92,745	1.00

The AMT's aircraft type, advanced trainer, resembles a small fighter type class of aircraft. Some fighter planes are selected for this purpose. Total weights are calculated from the component weights used. Expendable payloads (armaments) and external fuel stores of the similar aircraft are not considered in total aircraft weight because the AMT does not have these components. The underlined values for the landing-gear were given as total weights [21] for landing-gear. Therefore, the nose and main landing-gear are approximated at 30 and 70 percent of the total weight for the purpose of placing component cg's.

Certain components of the AMT are known, such as crew and the engine. The other weight groups that are unknown are estimated using the weight fractions listed in Table 20. Using the determined  $W_{TO}$  from chapter 4 weight sizing, the unknown weight groups are multiplied by their weight fractions from Table 20. The weights for the various groups are shown in the *Weights* column in Table 21.

The cg locations of the main components are estimated, based on reasonable judgement, or determined from the Solidworks CAD model (wing, fuselage, empennage, engine, and crew). The cg of the modeled parts is found with the *mass properties* tool in Solidworks. The side view of the proposed AMT is shown in Figure 79.



Figure 79. Aircraft side view with coordinate system

A coordinate system has been placed 5.0m ahead and 5.0m below the aircraft nose to allow space for changes in the design. This is done to ensure that as the design is refined, the components' location does not change sign (+/-) with respect to the reference point. The locations of the components are taken from this reference point. The aircraft cg is estimated by summing the moments and dividing by the sum of the component weights or the total weight, see equation (8.1).

$$r_{cg} = \frac{1}{W_{tot}} \sum_i r_i \cdot W_i \quad (8.1)$$

The equation is applied for each X, Y, and Z direction. Where r represents the X, Y, or Z position of the component. Table 21 lists the weight of the components and their location. There is a difference in total weight from the value determined in the weight sizing chapter. This is because the weight fractions of the engine and crew are greater than the comparable aircraft used for the calculation. Figure 80 is a top view of the model with component cg markings and descriptions. Figure 81 is a side view of the same model.

Table 21. Component weights, coordinates from reference point, and weight fractions

Component	Weight (N)	X (m)	Y (m)	Z (m)	FF/W <sub>tot</sub>
Fuselage	6,053	11.60	0.0	5.21	0.120
Wing	4,455	13.97	0.0	5.48	0.089
Empennage	1,157	17.33	0.0	5.88	0.023
Nose Gear	682	7.70	0.0	4.15	0.014
Main Gear	1,521	13.90	0.0	4.05	0.030
Fixed Equipment	6,875	10.10	0.0	5.50	0.140
Trapped Fuel & Oil	211	12.40	0.0	5.50	0.003
Propulsion Subsystems	2,386	12.60	0.0	5.15	0.047
Engine	9,807	16.55	0.0	5.16	0.195
Fuel	15,391	12.45	0.0	5.25	0.306
Crew	1,783	9.40	0.0	5.66	0.035
<b>W<sub>tot</sub></b>	<b>50,322</b>	<b>12.95</b>	<b>0.0</b>	<b>5.256</b>	<b>1.0</b>

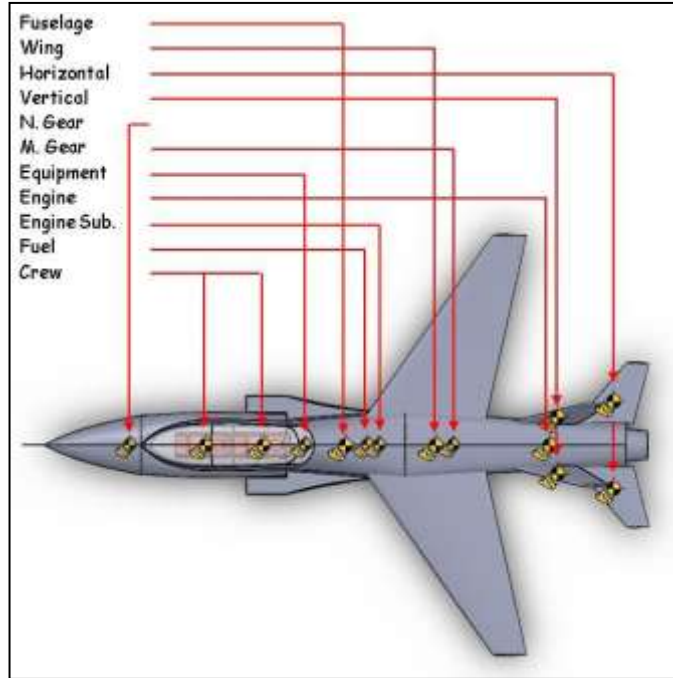


Figure 80. Top view with component center of gravity

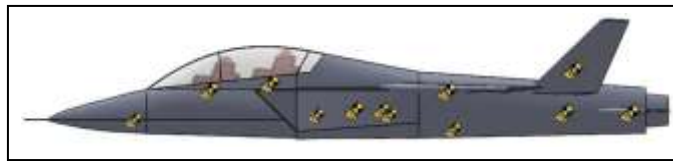


Figure 81. Side view with component center of gravity

### 8.1.2 Center of Gravity Location for Various Loading Scenarios

Using the tabulated values in Table 21 and equation (8.1), the aircraft cg is determined for different loading scenarios. Figure 82 shows the change in  $X_{cg}$ , with respect to the reference point, for loading and unloading scenarios. Table 22 lists the cg location based on Figure 82. The cg travel for various loading and unloading scenarios does not change significantly. The x-position of the cg ranges from 12.96 to 13.38m resulting in about 40cm of travel for the loading scenarios., Advanced trainers and fighters typically have a cg travel of 10 to 20 percent of the wing mean aerodynamic chord, [19] page 243. The mean aerodynamic chord of the wing is 2.15m which corresponds to a cg travel of 21.5 to 43.0cm. The AMT's cg travel is within this margin.

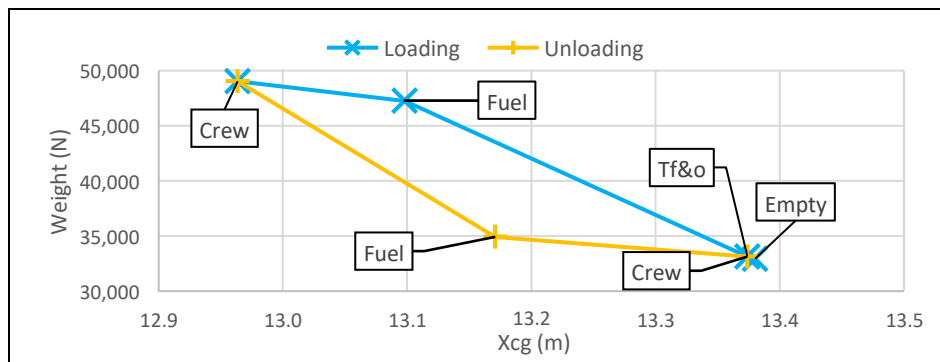


Figure 82.  $X_{cg}$  travel from ref. point for different loading scenarios

Table 22. Center of gravity location for loading and unloading scenarios from reference point

Loading	Weight (N)	X <sub>cg</sub> (m)	Y <sub>cg</sub> (m)	Z <sub>cg</sub> (m)
Empty	32,936	13.38	0.0	5.24
Trapped F&O	33,148	13.37	0.0	5.24
Fuel	48,539	13.08	0.0	5.24
Crew	50,322	12.95	0.0	5.26
Unloading	Weight (N)	X <sub>cg</sub> (m)	Y <sub>cg</sub> (m)	Z <sub>cg</sub> (m)
Fuel	34,931	13.17	0.0	5.26
Crew	33,148	13.37	0.0	5.24

## 8.2 Landing-Gear Design

### 8.2.1 Landing-Gear Configuration, Tip-Over, and Ground Clearance Criteria

The general landing-gear configuration was determined in configuration design, chapter 3. A conventional tricycle landing-gear configuration was selected. For conventional tricycle landing-gear there are general criteria that must be satisfied to ensure the aircraft is stable during ground operations. The main landing-gear must be aft of the cg but not too far such that significant stabilator deflection is required during take-off rotation. Figure 83 shows the recommended angle between aircraft cg and the main landing-gear is 15°. Lateral stability must also be satisfied by ensuring the main gear wheels form an angle with the most aft cg position of less than 55°, as shown in Figure 84.

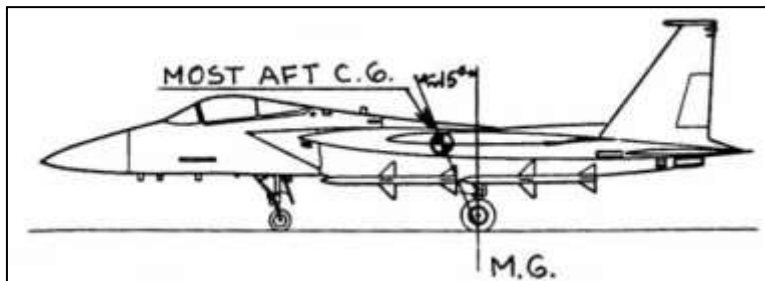


Figure 83. Tricycle gear longitudinal tip-over criterion [19]

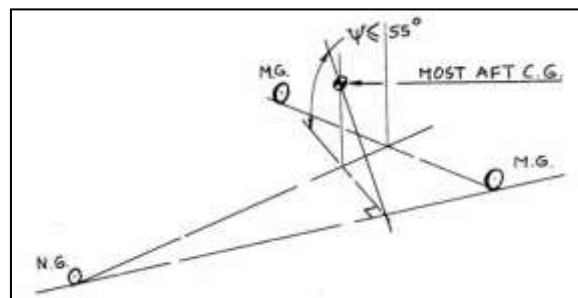


Figure 84. Tricycle gear lateral tip-over criterion [19]

Ground clearance is another criterion that must be considered. Figure 85 shows the longitudinal and lateral ground clearance criterion. For longitudinal criterion, the angle between the ground, main gear, and tail should be greater than 15°, and the lateral criterion is that the angle between the ground, main gear, and wing or wing mounted objects must be greater than 5°.

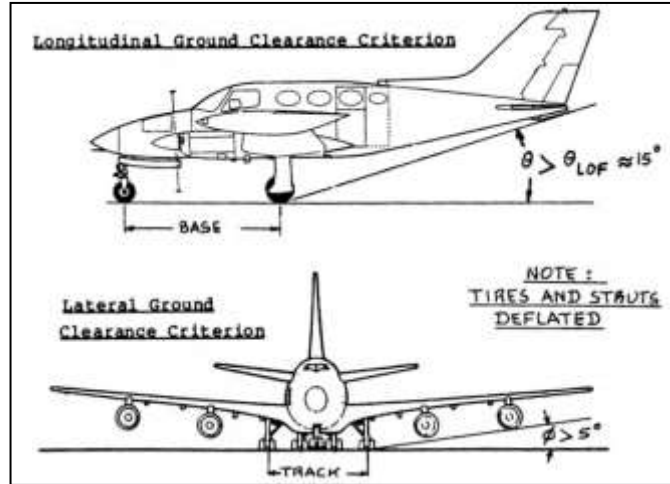


Figure 85. Ground clearance criterion [19]

The lateral ground clearance criteria are satisfied with an angle of about 31.2°. The longitudinal criteria is satisfied with an angle of 16.3°. The tip-over criterion is satisfied if the main gear is at least 0.574m from the centerline of the aircraft. The main gear will be placed 1.10m from centerline of the fuselage.

### 8.2.2 Length and Diameter of Struts, and Tire Specifications

The strut and tire sizing depend on the maximum load (P) per strut. The maximum load per strut for the nose gear is calculated with equation (8.2), and the main gear is calculated with equation (8.3). The variable  $n_s$  is the number of struts. Figure 86 shows the definition of the dimensional quantities used in the equations. The dimension  $l_n$  is 5.68 m and the dimension  $l_m$  is 0.520m. The maximum load per strut for the nose gear is 7.70kN and the maximum load per strut for the main gear is 21.3kN.

$$P_n = \frac{W_{TO} \cdot l_m}{l_m + l_n} \quad (8.2)$$

$$P_m = \frac{W_{TO} \cdot l_n}{n_s (l_m + l_n)} \quad (8.3)$$

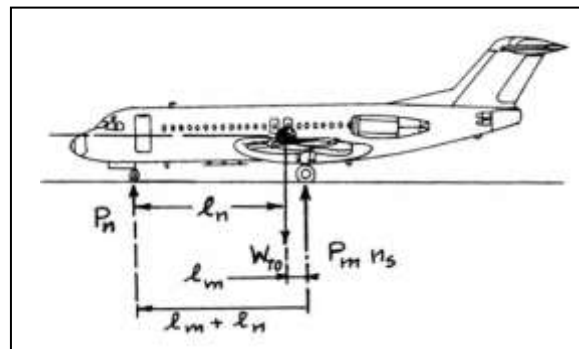


Figure 86. Landing-gear position and symbols [19]

The size of the tires can be estimated from similar aircraft using the ratio of maximum load per strut and take-off weight. The nose gear ratio is 0.10. Comparing this ratio to similar aircraft, [19] table 9.2 page 224, the tire dimensions should be a diameter of 43.2cm and width of 11.2cm. The ratio for the main gear is 0.90. Using the same table from [19], the main landing-gear tire dimensions should be a diameter of

59.2cm and a width of 16.5cm. Based on similar aircraft, one tire will be used for the nose gear and two tires will be used for the main gear, one for each side. Since this is a military aircraft, [6] recommends a type VII tire, which is typical for the class of aircraft or aircraft tires with high pressure loads.

The length of the strut depends on the landing-gear longitudinal and lateral criterion. From the aircraft component weight break down, estimates of the landing-gear position have been determined and the estimated lengths can be calculated using the dimensional relations. The diameter of the strut can be estimated from equation (8.4) [26], which is based off statistical data of produced aircraft. The units for the equation are in ft and lbs. The equation directly below (8.4) is the same equation converted to SI units, cm and N.

$$d_s = 0.041 + 0.0025\sqrt{P_{n,m}} \quad (8.4)$$

$$d_s = 1.25 + 0.036\sqrt{P_{n,m}}$$

Using the maximum load per strut calculated in the previous section, the minimum diameter of the nose landing-gear strut is 3.8cm and the minimum main landing-gear struts are 6.6cm.

### 8.2.3 Landing-Gear Drawings

Using landing-gear drawings in [19] and [26], landing-gear configuration and positions are sketched in Solidworks. Figure 87 shows a side view of the proposed landing-gear configuration. Figure 88 is a back view of the nose gear, and Figure 89 is a back view of half the main gear. The other main gear was not drawn because it is a mirror image about the aircraft centerline. In the figures, the deployed landing-gear are shown with solid lines and the retracted gear are shown with split lines, also called construction lines. Table 23 summarizes the landing-gear and tire design choices.

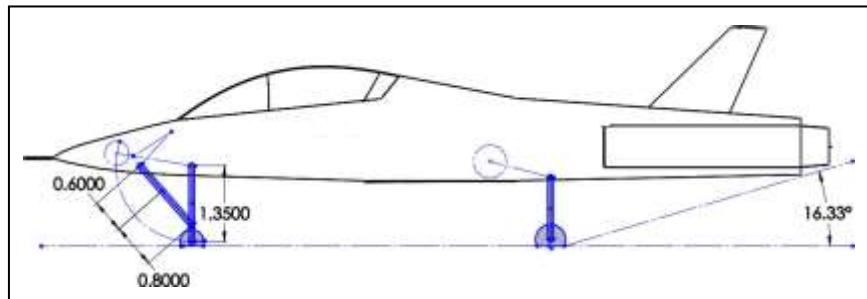


Figure 87. Side view of landing-gear

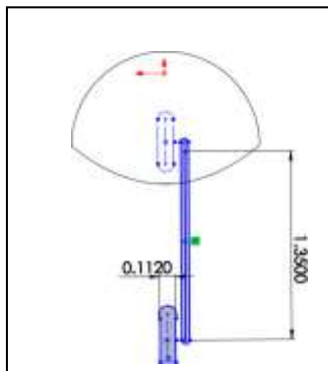


Figure 88. Back view of nose landing-gear

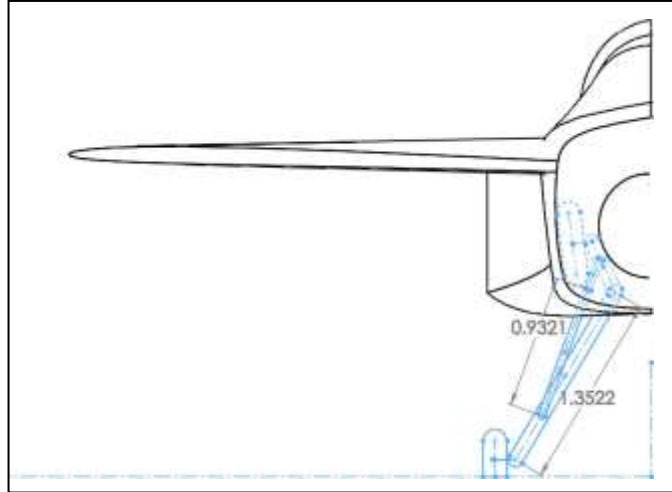


Figure 89. Back view of main landing-gear

Table 23. Landing-Gear parameters

Parameter	Units	Nose Gear	Main Gear
Maximum Load, P	N(lbs)	7,710(1,730)	21,310(4,780)
$P_n/W_{TO}$	---	0.15	---
$P_{m\Omega}/W_{TO}$	---	---	0.85
Number of Struts	---	1	2
Strut Length	m(ft)	1.35(4.43)	1.35(4.43)
Strut Diameter	cm(in)	>3.2(81.3)	>6.6(2.6)
Tire Type	---	VII	VII
Tire Diameter	cm(in)	43.2(17.0)	59.2(23.3)
Tire Width	cm(in)	11.2(4.41)	16.5(6.50)

### 8.3 Discussion and Conclusion

Through the iteration of determining the landing-gear and the component positions, the landing-gear meets the criterion as discussed in [19], [26]. Since the weight and balance was completed during the landing-gear design process, there are no significant changes from the initial W&B and the final proposed configuration. Based on the loading and unloading scenarios, the change in the cg location is manageable. Based on Figure 89, the spacing between the intake duct and exterior wall of the fuselage is very tight. In future iterations of the design, landing-gear fairings would be included to better accommodate the space required.

The strut sizing completed in this section is a first iteration sizing which estimated the length based on landing-gear criterion and strut diameter based on statistical data. Proper sizing of the strut requires a more in-depth structural analysis. The tire sizing was based on comparable aircraft with similar maximum loading ratios. The W&B completed only reflects the distribution of weight groups. The analysis completed does not reflect the stability and control of the aircraft in flight.

## 9. Longitudinal and Directional Stability and Control

The analysis of the longitudinal and directional stability and control (S&C) is to determine if the proposed design has satisfactory inherent S&C. If a design cannot meet such requirements, then a redesign of some aspect must be completed. De facto stability is a design compensation of poor stability with an augment control system. Though computing technology today allows designers to create augmented control systems, which can correct for subpar stability, inherent stability helps to simplify designs and reduce costs. The longitudinal and directional stability is related to the pitch and yaw axis of the aircraft, respectfully.

### 9.1 Static Longitudinal Stability

The longitudinal stability of an aircraft is related to the static margin (SM). The static margin of an aircraft is the non-dimensional distance, with respect to the mean aerodynamic chord, between the aircraft's aerodynamic center (ac) and center of gravity (cg), or the negative change in the moment coefficient with respect to the change in the lift coefficient. The static margin of an aircraft is expressed by equation (9.1) [19].

$$SM = \bar{x}_{cA/C} - \bar{x}_{gA/C} = - \frac{\partial C_{M_{A/C}}}{\partial C_{L_{A/C}}} \quad (9.1)$$

Large transport and general aviation aircraft tend to have a static margin of about 10%. More maneuverable aircraft tend to have a static margin less than 5%, and sometimes negative which must be augment by a control law system. The AMT's static margin is selected to be 5%. Therefore, the configuration must be checked that this is satisfied or close enough not to warrant a redesign.

From weight and balance, the approximate cg of the aircraft is known. The ac of the aircraft is calculated with equation (9.2) [19]. The aircraft ac is a sum of the contributing aerodynamic surfaces about the pitch axis. The contributions to an aircraft's ac are the fuselage, wing, tail, and canard, if applicable. The AMT is a conventional trainer/fighter configuration, so the ac of the aircraft will depend on the fuselage, wing, and tail. Therefore, equation (9.3) will be used for the AMT.

$$\bar{x}_{cA/C} = \frac{C_{L_{\alpha wf}} \bar{x}_{c wf} + C_{L_{\alpha h}} \bar{x}_{c h} + C_{L_{\alpha c}} \bar{x}_{c c}}{C_{L_{\alpha wf}} + C_{L_{\alpha h}} + C_{L_{\alpha c}}} \quad (9.2)$$

$$\bar{x}_{cA/C} = \frac{\bar{x}_{c wf} + \frac{C_{L_{\alpha h}}}{C_{L_{\alpha wf}}} \left(1 - \frac{d\varepsilon_h}{d\alpha}\right) \frac{S_h}{S} \bar{x}_{c h}}{1 + \frac{C_{L_{\alpha h}}}{C_{L_{\alpha wf}}} \left(1 - \frac{d\varepsilon_h}{d\alpha}\right) \frac{S_h}{S}} \quad (9.3)$$

$\bar{x}_{c wf}$  is the non-dimensional location of the wing and fuselage ac, which is estimated with equation (9.4). All nondimensional x values are taken from the reference point described in chapter 8, with respect to the wing's mean aerodynamic chord.

$$\bar{x}_{c wf} = \bar{x}_{c w} + \Delta \bar{x}_{c f} \quad (9.4)$$

The proceeding discussion will be to define the other variables and the calculated values for the AMT.

### 9.1.1 Determination of Wing-Fuselage Aerodynamic Center with Monk's Method

The change in ac due to the fuselage is approximated using from equation (9.5).  $\partial M/\partial \alpha$  is approximated using Monk's Method [24], with equation (9.6). Combining equations (9.5) and (9.6) results in equation (9.7).

$$\Delta x_{ac_f} = - \frac{\partial M / \partial \alpha}{q S \cdot c C_{L_{\alpha_w}}} \quad (9.5)$$

$$\frac{\partial M}{\partial \alpha} = \frac{q C_{L_{\alpha_w}}}{2.92} \sum_{i=1}^{i=13} w_i^2 \left( \frac{\partial \varepsilon}{\partial \alpha_i} \right) \Delta x_i \quad (9.6)$$

$$\Delta x_{ac_f} = - \frac{1}{2.92 \cdot S \cdot c} \sum_{i=1}^{i=13} w_i^2 \left( \frac{\partial \varepsilon}{\partial \alpha_i} \right) \Delta x_i \quad (9.7)$$

The shift in the aircraft's ac due to the fuselage is a result of the upwash ahead of the wing and the downwash behind the wing. This assumes the horizontal stabilizer has a negligible effect to the airflow based on the scale of the wing's contribution.

The geometric relationships in equation (9.7) are determined using Figure 90. Figure 91 is used to approximate the downwash gradient of the forward fuselage sections. Curve (1) is used for panels 1-4 and curve (2) is used for panel 5. Equation (9.8) is used to approximate the downwash gradient for the aft wing sections. For ease of calculation,  $(1 - \partial \varepsilon / \partial \alpha)$  in equation (9.8) can be approximated with a value of 0.6 to 0.7 [19]. 0.65 will be used for the calculation.

$$\left( \frac{\partial \varepsilon}{\partial \alpha_i} \right) = \frac{x_i}{x_h} \left( 1 - \frac{\partial \varepsilon}{\partial \alpha} \right) \cong \frac{x_i}{x_h} 0.65 \quad (9.8)$$

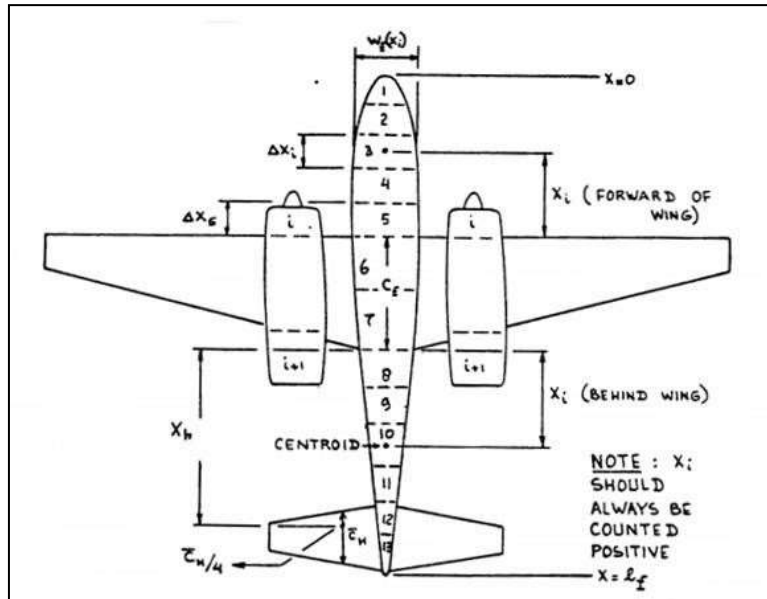


Figure 90. Parameter definitions for Monk's method [24]

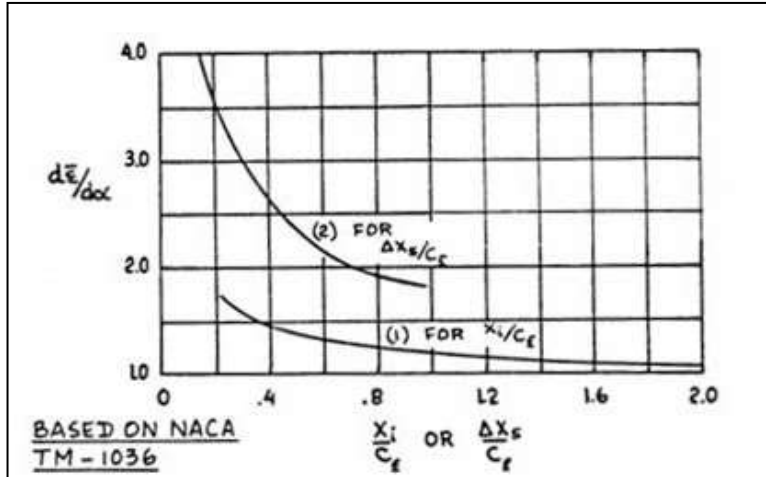


Figure 91. Effect of fuselage (or nacelle) segment location on upwash gradient [24]

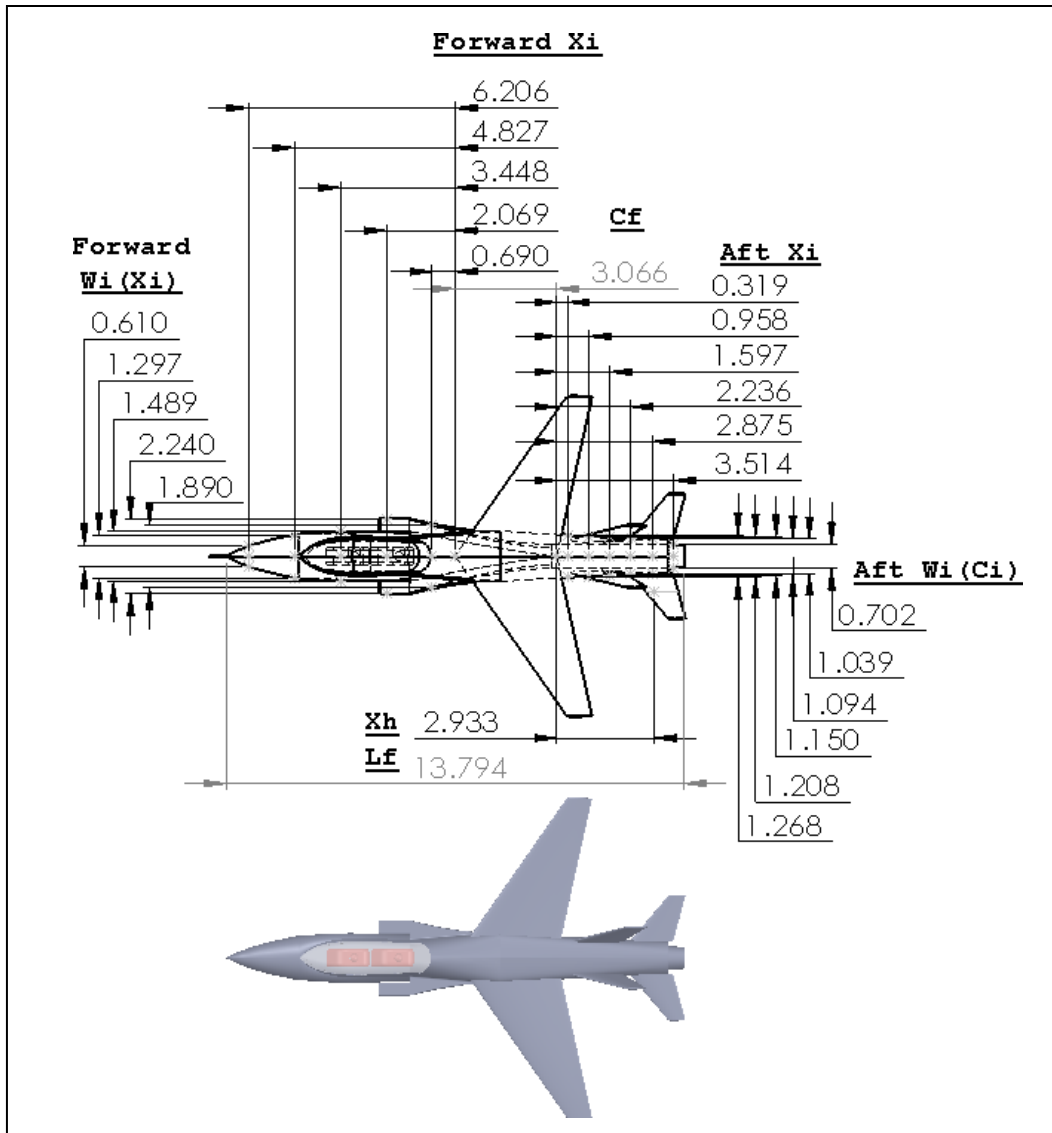


Figure 92. Layout of AMT's fuselage for Monk's method

$\Delta \bar{x}_{cf}$  is determined to be -0.264m using the dimensional callouts in Figure 92.  $x_{acw}$  is calculated with equation (9.9). The parameter  $n_{ac}$  is defined in Figure 93, and is calculated with the equation (9.10) for a swept straight tapered wing. Based on the wing geometry determined in chapter six, the location along the wing span of the mean aerodynamic chord is determined with equation (9.11).

$$x_{acw} = x_{LE_{ref}} + n_{ac} \quad (9.9)$$

$$n_{ac} = \bar{c} / 4 + y \tan(\Lambda_{LE}) \quad (9.10)$$

$$y_c = \frac{b(c_r - \bar{c})}{2c_i(1 - \lambda)} \quad (9.11)$$

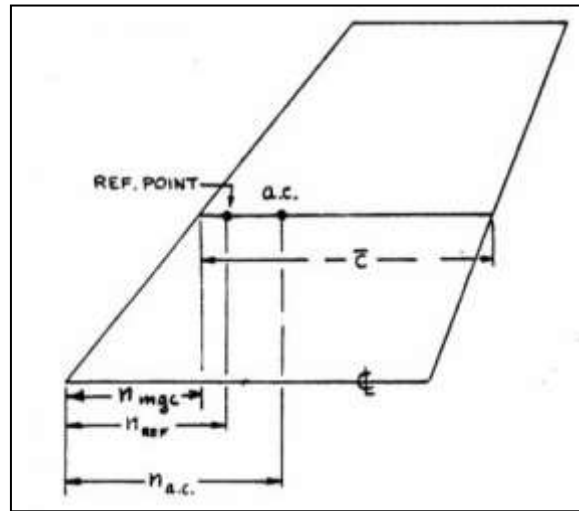


Figure 93. Wing parameter relations [26]

Using the Solidworks CAD model, the wing's leading-edge root distance from the reference point is 11.3m. Adding the wing's  $n_{ac}$  and non-dimensionalizing results in  $\bar{x}_{cw} = 6.0m$ . The resulting nondimensional ac of the wing and fuselage combined is  $\bar{x}_{cwf} = 5.74$ . The remaining variables to determine are the lift-curve slopes of the wing and the horizontal, and the downwash gradient.

### 9.1.2 Wing and Horizontal Lift-Curve Slopes

The lift-curve slope of a wing, in units of 1/rad, can be approximated from thin airfoil theory and geometry using equation (9.12) [22]. Equation (9.12) applies to straight tapered wings with quarter-chord sweep of less than 35°. The variable  $\beta$  is calculated with equations (9.13) [22] for subsonic flight.

$$C_{L\alpha} = \frac{2\pi \cdot AR}{2 + \sqrt{4 + (AR \cdot \beta)^2 \left(1 + \frac{\tan^2(\Lambda_{(t/c)_{max}}}{\beta^2}\right)}} \quad (9.12)$$

$$\beta = \sqrt{1 - M^2} \quad (9.13)$$

The wing's lift-curve slope for a range of subsonic Mach numbers is shown in Figure 94 and tabulated in Table 24. This trend has been verified by experiments in [27]. The lift-curve slope for the horizontal is determined with the same method and is tabulated in Table 24

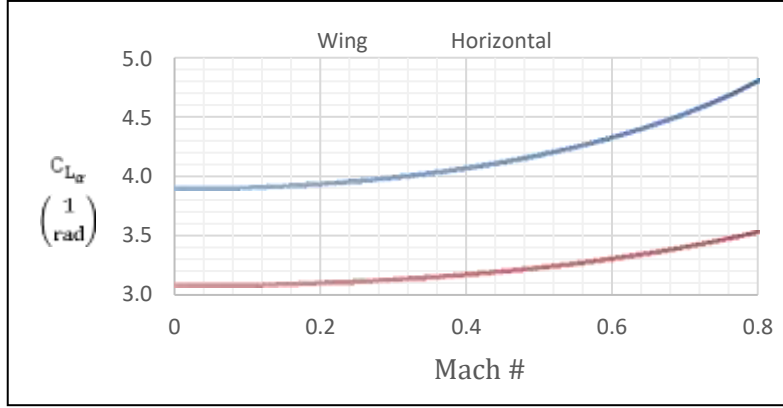


Figure 94. Change in wing and horizontal lift-curve slope due to Mach number

Table 24. Values of wing and horizontal lift-curve slopes for Mach number correction

Mach #	$C_{L_{\alpha_w}}$ (1/rad)	$C_{L_{\alpha_h}}$ (1/rad)
0.1	3.907	3.084
0.2	3.937	3.100
0.3	3.990	3.129
0.4	4.068	3.171
0.5	4.176	3.227
0.6	4.323	3.301
0.7	4.521	3.397
0.8	4.793	3.521

### 9.1.3 Downwash Gradient at Horizontal Stabilizer

The final variable to define is the downwash gradient. The downwash gradient on the horizontal stabilizer is determined using equation (9.14) [24].

$$\frac{\partial \varepsilon}{\partial \alpha} = 4.44 \left[ \{K_{AR} \cdot K_{\lambda} \cdot K_h \sqrt{\cos(\Lambda_{c/4})}\}^{1.19} \right] \frac{(C_{L_{\alpha_w}})_{@M}}{(C_{L_{\alpha_w}})_{@M=0}} \quad (9.14)$$

The K coefficients are calculated with the equations (9.15) through (9.17) [24].  $K_{AR}$ ,  $K_{\lambda}$ , and  $K_h$  are found to be 0.139, 1.32, and 1.03, respectfully.

$$K_{AR} = \frac{1}{AR} - \frac{1}{1 + AR^{1.7}} \quad (9.15)$$

$$K_{\lambda} = \frac{10 - 3\lambda}{7} \quad (9.16)$$

$$K_h = \frac{1 - \left| \frac{(z_h)_{\text{from } w_{\text{root LE}}}}{b} \right|}{\left( \frac{2(x_h)_{\text{from } w_{c/4}}}{b} \right)^{1/3}} \quad (9.17)$$

Using the range of  $C_{L_{\alpha_w}}$  from Table 24, which correlate to Mach number, the downwash gradient on the horizontal stabilizer is plot versus Mach number. The results obtained from equation (9.14) are shown in Figure 95.

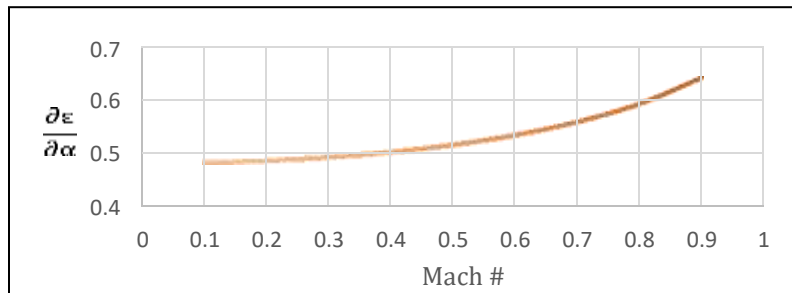


Figure 95. Change in tail downwash due to Mach number

### 9.1.4 Static Margin

All the variables are known that are required to solve equations (9.1) and (9.2). Based on the current configuration, and the results of Figure 94 and Figure 95, the static margin for the subsonic flight regime is shown in Figure 96 for three weight configurations. The change in cg used for the calculation is based on fuel used, which assumes the same point location for the fuel as determined in the weight and balance chapter.

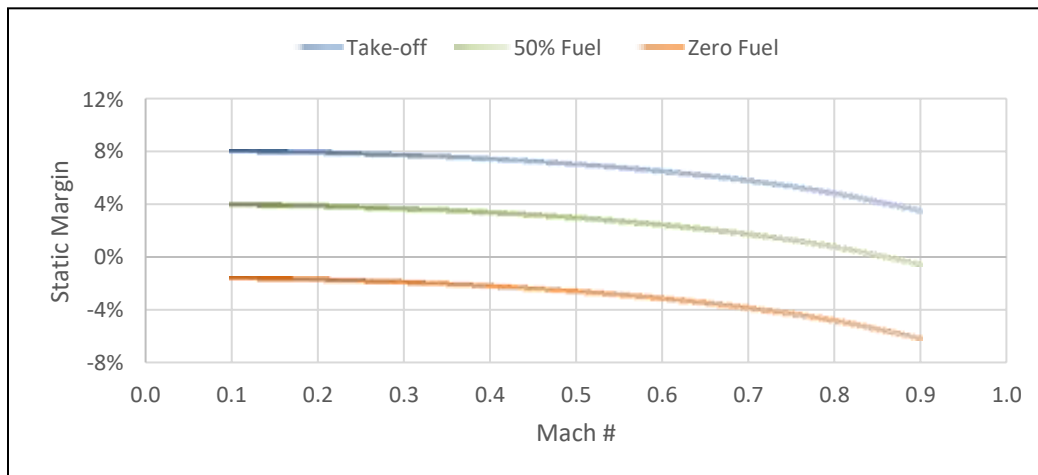


Figure 96. Effect of Mach number on static margin

The decrease in static margin can be attributed to the forward shift in the aerodynamic center of the lifting surfaces as the flight speed increases [27]. The calculation done with equation (9.1) does not account for the shift in the lifting surfaces' aerodynamic centers. The decrease in the static margin can be attributed to the ratio of the lift-curve slopes decreasing with Mach number. In a produced aircraft, there would be a subsystem which would pump fuel around to maintain an acceptable SM. Based on the results, the AMT has sufficient SM at this point in the design process.

### 9.1.5 Longitudinal X-plot

The purpose of an X-plot is to vary the horizontal stabilizers moment arm or horizontal area to move the aircraft's ac forward or aft to obtain an acceptable static margin for longitudinal stability. Since the lifting surfaces are aerodynamic, any adjustment should result in a greater change of aircraft ac than cg.

### 9.1.5.1 X-plot by Horizontal Moment Arm

For this analysis, the conditions found in the previous section for  $M = 0.6$  are used. Table 25 lists the incremental change used for each configuration. The lift-curve slopes and downwash used for the analysis correspond to  $M = 0.6$  listed in Table 24 and Figure 95. For each change in the horizontal position, the aircraft cg must be recalculated to account for the adjustment. The calculation for the aircraft ac follows the same method used in section 9.1.4. The resulting X-plot is shown in Figure 97

Table 25. Incremental change in horizontal position for X-plot

	TO	50% Fuel	0% Fuel
$\Delta x_{ac_h}$ (m)	-0.2	0.3	0.8

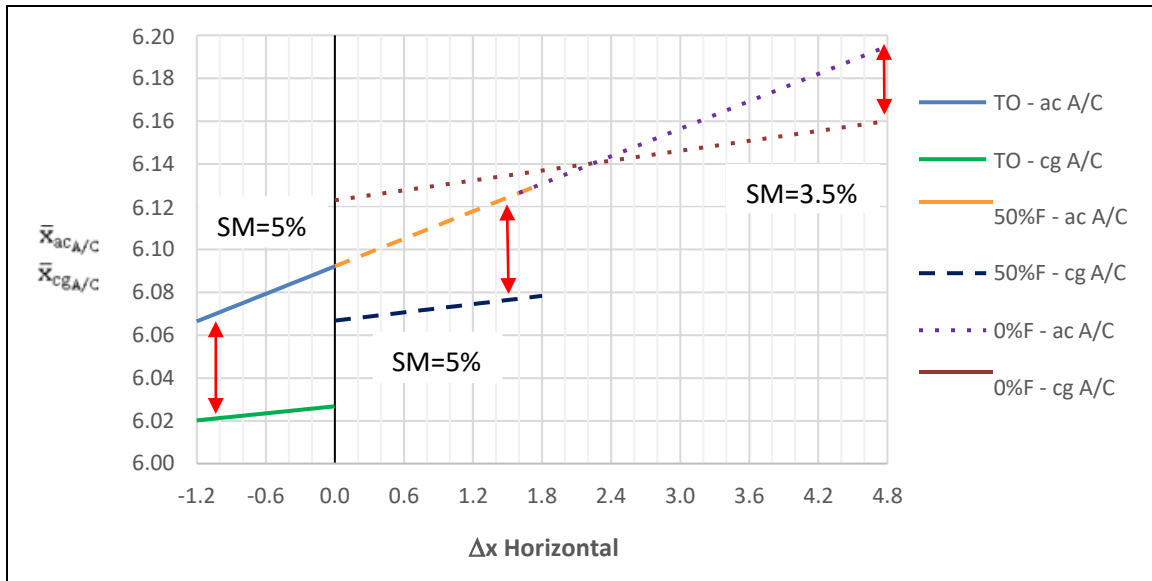


Figure 97. X-plot for change in horizontal position

### 9.1.5.2 X-plot by Horizontal Area

Varying the horizontal area will also change the aircraft's overall cg. To approximate the change in weight, the horizontal's area is assumed to be proportional to the horizontal's weight. Based on this assumption, the weight of the tail can be corrected for change in horizontal area with equation (9.18).

$$W_h = \left( \frac{S_h}{S_h} \right) W_h \quad (9.18)$$

The tilde in equation (9.18) is used to indicate the reference base value used for the initial weight and horizontal area. The  $\tilde{x}_{CA/C}$  and  $\tilde{x}_{CGA/C}$  is calculated with the same method as before. The result of the X-plot for a  $\Delta S_h$  is shown in Figure 98.

Table 26. Incremental change in horizontal area for X-plot

	TO	50% Fuel	0% Fuel
$\Delta S_h$ (m <sup>2</sup> )	-0.15	0.2	0.5

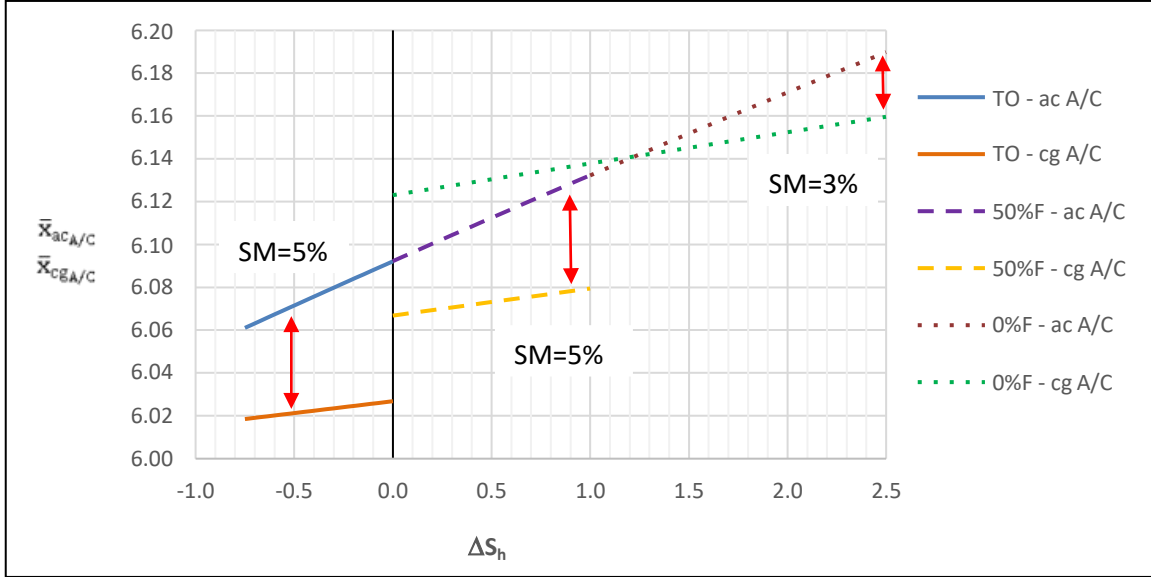


Figure 98. X-plot for change in horizontal area

## 9.2 Static Directional Stability

The directional stability of an aircraft is determined by the change in the yawing moment coefficient with respect to sideslip angle. This is calculated with equation (9.19) [19]. Since the AMT has two vertical fins, the total fin area will be used in equation (9.19). Also, since the vertical fins have dihedral, the projected area on the aircraft XZ-plane must be determined. The corrected equation is (9.20).

$$C_{n\beta} = C_{n\beta_{wf}} + C_{L\alpha_v} \left( \frac{S_v}{S} \right) \left( \frac{x_v}{b} \right) \quad (9.19)$$

$$C_{n\beta} = C_{n\beta_{wf}} + C_{L\alpha_v} \left( \frac{S_{v,tot} \cdot \sin(\Gamma_v) x_v}{S} \right) \left( \frac{x_v}{b} \right) \quad (9.20)$$

### 9.2.1 Fuselage Contribution to the Yawing Moment Coefficient due to Sideslip

The analysis completed for the empennage sizing has resulted in all the necessary geometry. The only term that must be determined is the contributions of the wing-fuselage combination,  $C_{n\beta_{wf}}$ . For preliminary design purposes,  $C_{n\beta_w}$  is very small and can be considered zero [24], unless the directional stability is being analyzed at high angles of attack, which is not the case. Therefore,  $C_{n\beta_{wf}}$  is only depend on the fuselage contributions which is calculated with equation (9.21) based on empirical data [24].

$$C_{n\beta_f} = -57.3K_N \cdot K_{R_1} \left( \frac{S_{B_s} \cdot l_f}{S \cdot b} \right) \quad (9.21)$$

$K_N$  is determined using Figure 99.  $K_{R_1}$  is a correction factor due to Reynold's number which is determined using Figure 100. The read arrows in Figure 99 indicate the path taken to determine  $K_N$ . Figure 99 also provides the geometry relations to be used in determining  $K_N$ .  $C_{n\beta_f}$  was found to be -0.218.

Table 27. Aircraft parameters for fuselage yawing-moment coefficient due to sideslip

$S_{B_s}$ (m <sup>2</sup> )	$l_f$ (m)	$h_1$ (m)	$h_2$ (m)	$w_f$ (m)	$x_m$ (m)
17.70	13.80	1.72	1.27	2.24	8.06

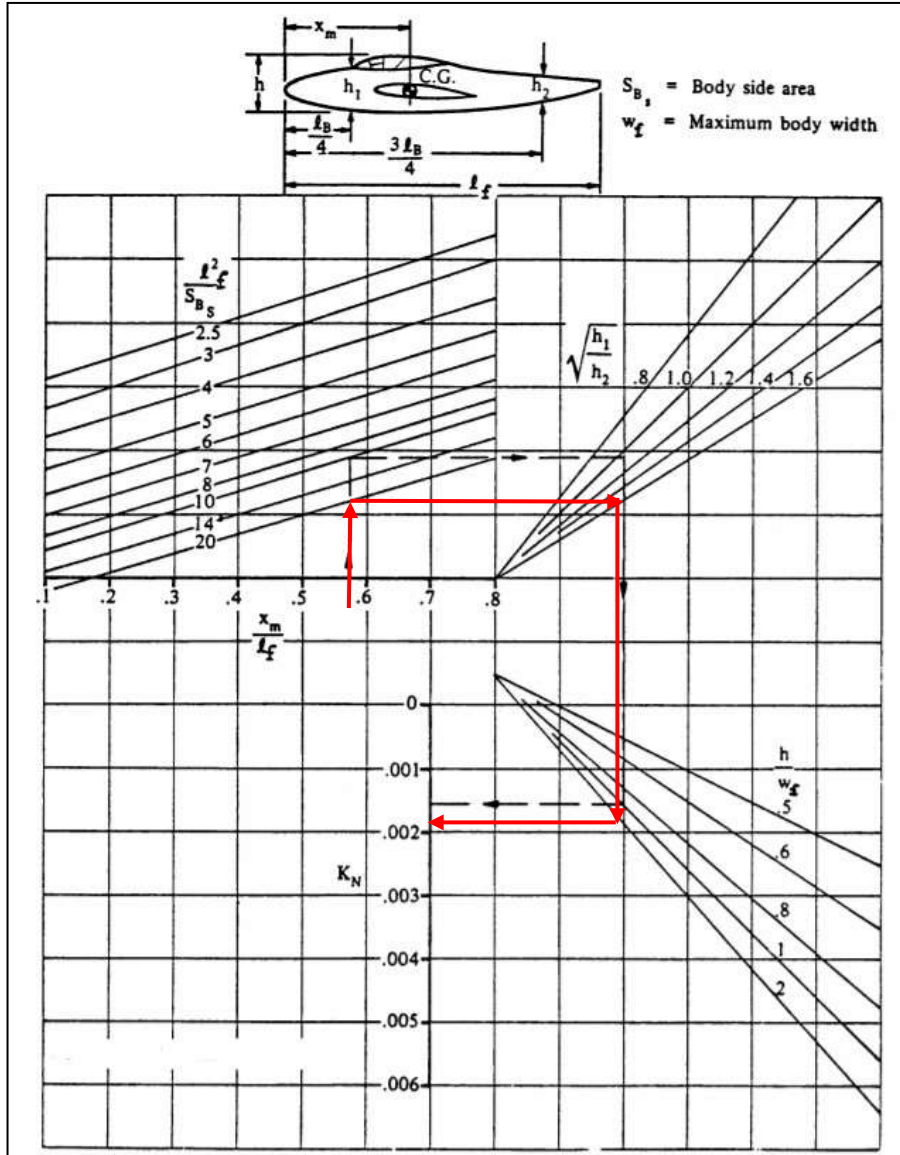


Figure 99. Wing-fuselage interference with directional stability [19]

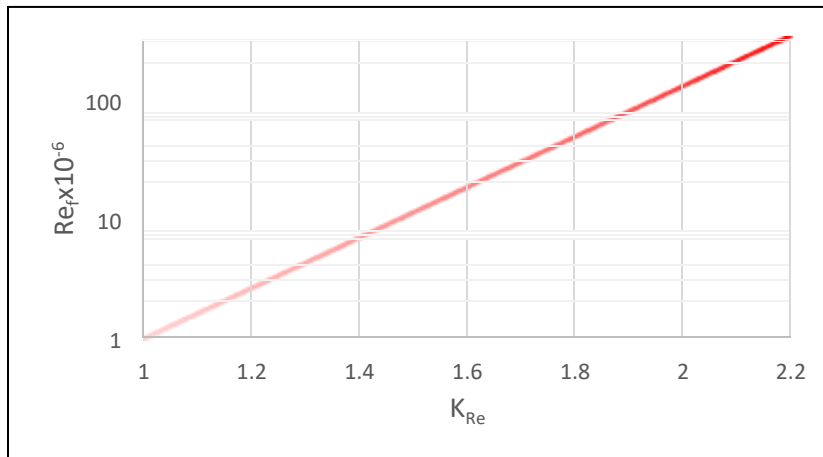


Figure 100. Fuselage Reynolds number versus  $K_{R1}$  reproduced from [29]

### 9.2.2 Vertical Fin Lift-Curve Slope

The only parameter not known in equation (9.19) is  $C_{L_{\alpha_v}}$ . Similar for the wing and horizontal, the lift-curve slope of the vertical fin is determined from equation (9.12). Figure 101 shows the Mach number and geometry effects for the vertical fins lift-curve slopes.

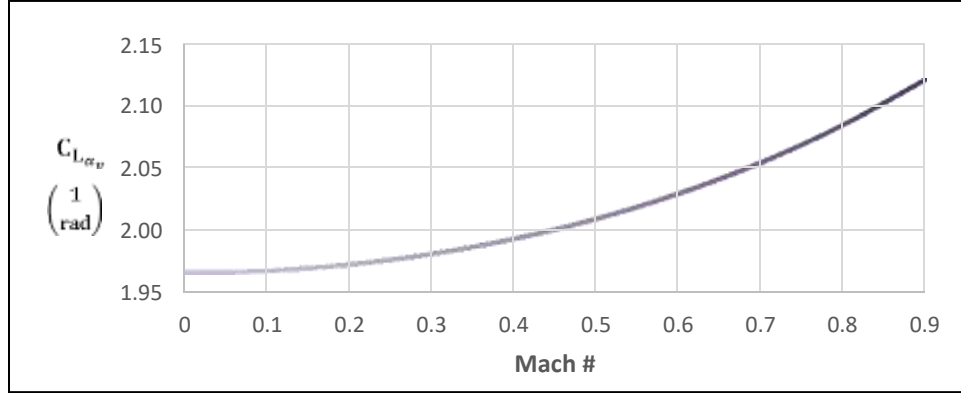


Figure 101. Mach number effect on vertical fin lift-curve slope

### 9.2.3 Directional X-plot

For inherent directional stability,  $C_{n_{\beta}}$  should be 0.001/deg [19]. The evaluation of equation (9.20) for varied Mach numbers leads to Figure 102, which shows the AMT is inherently unstable. In such cases, the vertical tail area or moment arm could be increased to regain inherent directional stability. In varying these two variables, the requirement to obtain inherent stability would require a total tail area increase of 150% and an increase in the moment arm by 30%. Since the AMT is a modern fighter which will have a feedback control system, de facto stability will be employed.

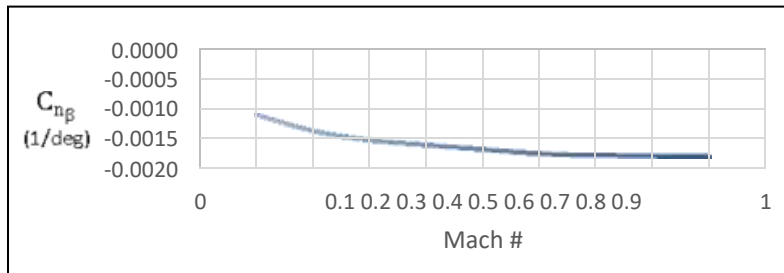


Figure 102. Mach effect on change in yawing moment wrt sideslip angle

### 9.2.4 Sideslip to Rudder Feedback Gain

For de facto directional stability, the sideslip to rudder feedback gain must be satisfied by equation (9.22) [19]. The rudder control yaw moment derivative is calculated with equation (9.23) [28]. The term  $\eta_v$ , is the ratio of the vertical's dynamic pressure to freestream. The term  $\tau$ , is the lift-curve slope corrective factor for deflected control surfaces and is approximated using Figure 103.

$$K_{\beta_r} = \frac{0.001 - C_{n_{\beta}}}{C_{n_{\delta_r}}} < 5 \frac{\text{deg}}{\text{deg}} \quad (9.22)$$

$$C_{n_{\delta_r}} = -\eta_v \bar{V} \frac{\partial C_{L_v}}{\partial \delta_r} = -\eta_v \bar{V} C_{L_{\alpha_v}} \tau \quad (9.23)$$

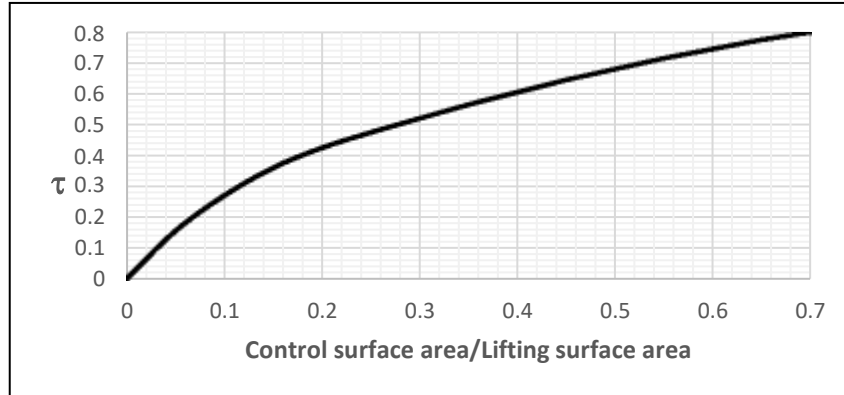


Figure 103. Control surface effectiveness parameter  $\tau$  reproduced from [28]

The dynamic pressure ratio for the vertical tail is assumed to be one for simplicity of calculation. The tail volume coefficient was previously determined in the empennage sizing. The control surface area to lifting surface area for the AMT is about 35% therefore  $\tau_v$  is taken as 0.57 from Figure 103. Equation (9.22) is solved for the 50% fuel configuration, the resulting sideslip to rudder feedback gain is shown in Figure 104.

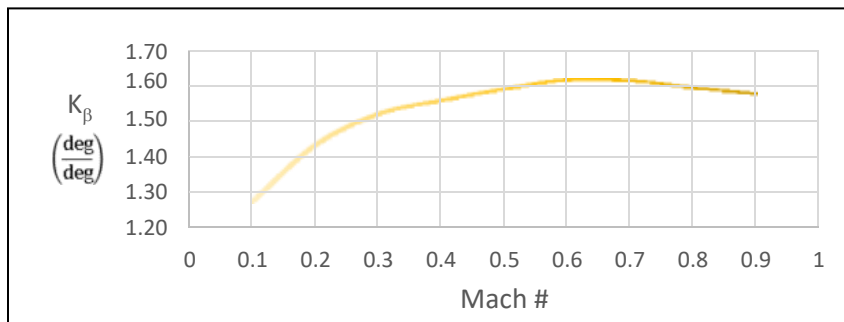


Figure 104. Mach number effect on  $K_\beta$

The AMT is a single engine aircraft so, there is no requirement for engine out minimal speed or directional control. Based on the calculations, there is no need for any redesign because the AMT has sufficient directional control by meeting the sideslip feedback gain criteria of  $K_\beta$  less than 5 deg/deg.

### 9.3 Discussion and Conclusion

The longitudinal stability has an acceptable SM for the current configuration of around 5%. The SM was evaluated for three values of fuel capacity: full, 50%, and 0%. Modern aircraft utilize fuel location management systems which would help to limit the movement in aircraft cg due to fuel burn. Corrective methods were completed with adjustments in horizontal moment arm and horizontal area to show how to correct a configuration for inefficient SM.

The directional stability showed inefficient sideslip control without control surface feedback. Though not shown, performing vertical tail moment arm or area adjustments resulted in too large a configuration change. To obtain inherent directional stability, the product of the vertical moment arm and area would have to be 2.0-2.5 times greater than the current configuration. Since modern aircraft utilize feedback control systems, de facto stability criteria was followed. The current configuration resulted in acceptable sideslip to rudder feedback gain.

## 10. Refined Drag Polars

The purpose of this chapter is to establish a better approximation for the AMT's drag polars than previously determined in the performance sizing chapter. The drag polar is a visual representation of the lift to drag relationship. The analysis will cover airplane zero-lift, zero-lift drag increments due to HLD and landing-gear, and compressibility drag. The compressibility drag approximation methods requiring the application of the area rule.

### 10.1 Airplane Zero-Lift Drag

The aircraft zero-lift drag is determined by computing the wetted area of all the components [19]. The following equations are used to estimate the wetted area of components. The figures below each set of equation define how the variables not previously defined should be measured.

*Planforms (wing, tail, canard, fin, and pylon)*

$$S_{\text{wet,plf}} = 2 \cdot S_{\text{exposed,plf}} \left\{ 1 + \frac{0.25(t/c)_r(1 + \tau\lambda)}{1 + \lambda} \right\} \quad (10.1)$$

$$\tau = \frac{(t/c)_r}{(t/c)_t} \quad \lambda = c_t/c_r$$

*Cylindrical Fuselage*

$$S_{\text{wet}_f} = \pi \cdot D_f \cdot l_f \left( 1 - \frac{2}{\lambda_f} \right)^{2/3} \left( 1 + \frac{1}{\lambda_f^2} \right) \quad (10.2)$$

*Streamlined Fuselage*

$$S_{\text{wet}_f} = \pi \cdot D_f \cdot l_f \left( 0.5 + 0.135 \left( \frac{l_n}{l_f} \right)^{2/3} \right) \left( 1.015 + \frac{0.5}{\lambda_f^{1.5}} \right) \quad (10.3)$$

$$\lambda_f = l_f/D_f$$

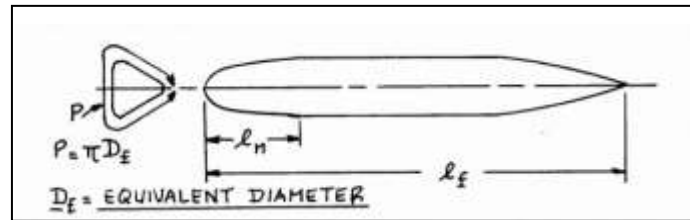


Figure 105. Definition of fuselage variables [19]

*Fan Cowl*

$$S_{\text{wet,fan}} = l_n \cdot D_n \left\{ 2 + 0.351 \left( \frac{l_n}{D_n} \right) + 0.81 \left( \frac{l_n D_{hl}}{l_n D_n} \right) + 1.15 \left[ 1 - \left( \frac{l_n}{D_n} \right) \right] \left( \frac{D_g}{l_g} \right) \right\} \quad (10.4)$$

*Gas Generator*

$$S_{\text{wet,gg}} = \pi \cdot l_g \cdot D_g \left\{ 1 - \frac{1}{3} \left[ 1 - \left( \frac{D_{eg}}{D_g} \right) \right] \left[ 1 - 0.18 \left( \frac{D_g}{l_g} \right) \right] \right\}^{5/3} \quad (10.5)$$

Plug

$$S_{\text{wet,plug}} = 0.7\pi l_p D_p \quad (10.6)$$

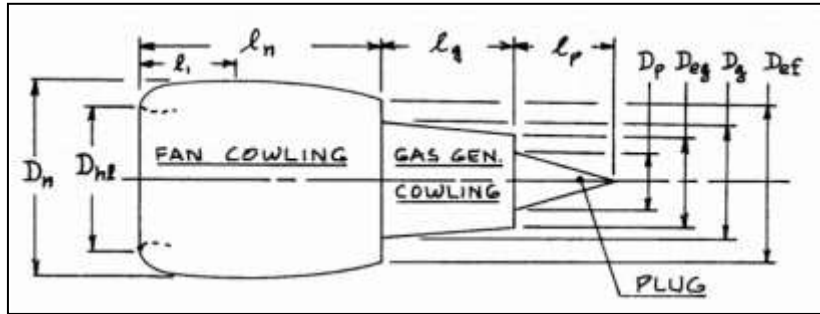


Figure 106. Nacelle geometry [19]

The total wetted area of the aircraft is the sum of the components minus the intersection area of the components. In the case of the AMT, the wetted area is determined from the Solidworks CAD model. Using Solidworks mass properties, the exposed, or wetted, surface area of the aircraft is found to be 173.8m<sup>2</sup> (1,870ft<sup>2</sup>). Using Figure 107, the equivalent parasite area (f) is determined by how streamlined the aircraft is and the aircraft wetted area. Figure 107 is based off historical data and is recreated for simpler interpretation. The horizontal line in Figure 107 is selected based on the grouping of similar class of aircraft in the original figure. The equivalent parasite area is 0.418m<sup>2</sup> (4.5ft<sup>2</sup>).

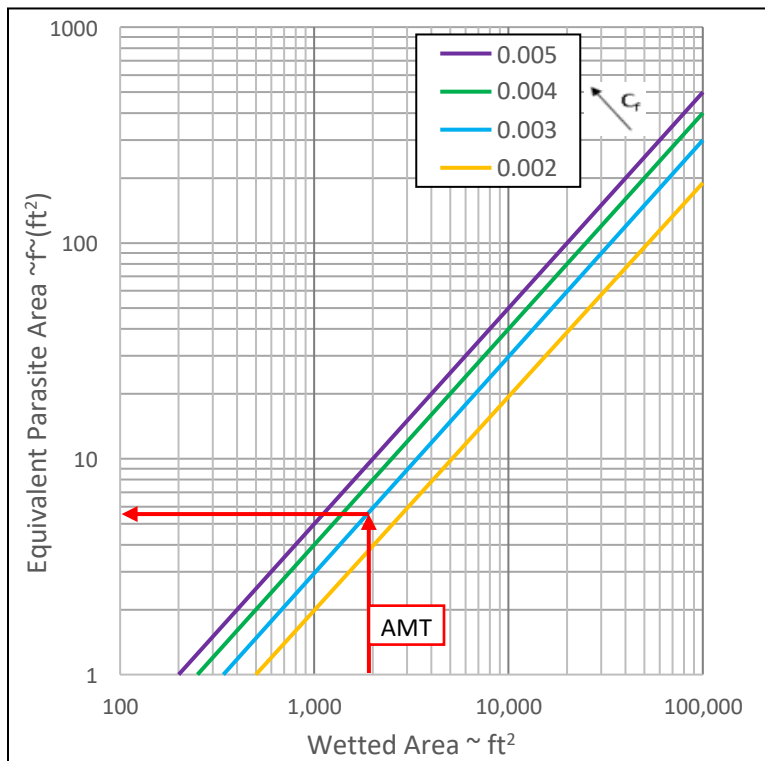


Figure 107. Effect of equivalent skin friction on wetted and parasite area reproduced from [17]

The clean zero-lift drag is calculated by equation (10.7) [17].

$$C_{D_0} = f/S \quad (10.7)$$

Based on the wing area determined in performance sizing, 18.44m<sup>2</sup>, the clean C<sub>D</sub> is calculated to be 0.023.

## 10.2 Low Speed Drag Increments

### 10.2.1 High-lift Devices Drag Increment

#### 10.2.1.1 Trailing-edge Flaps

The incremental drag increase due to flaps is calculated with equation (10.8), which is a combination of profile drag and lift induced drag. The equation assumes only low speed flight where the HLDs are used. The profile drag is determined with equation (10.9) [24]. The term  $\Delta C_{d_{p_{\Lambda_c/4=0}}}$  is the incremental drag increase of the 2D profile and is determined using Figure 108, for plain flaps. The incremental induced drag for a flap is calculated with equation (10.10). The factor K in equation (10.10) is determined with Figure 109, for interrupted flaps.

$$\Delta C_{D_{flap}} = \Delta C_{D_{prof_{flap}}} + \Delta C_{D_{i_{flap}}} \quad (10.8)$$

$$\Delta C_{D_{prof_{flap}}} = \Delta C_{d_{p_{\Lambda_c/4=0}}} \cos(\Lambda_c/4) \frac{S_{flap}}{S} \quad (10.9)$$

$$\Delta C_{D_{i_{flap}}} = (K \cdot \Delta C_{L_{flap}})^2 \cos(\Lambda_c/4) \quad (10.10)$$

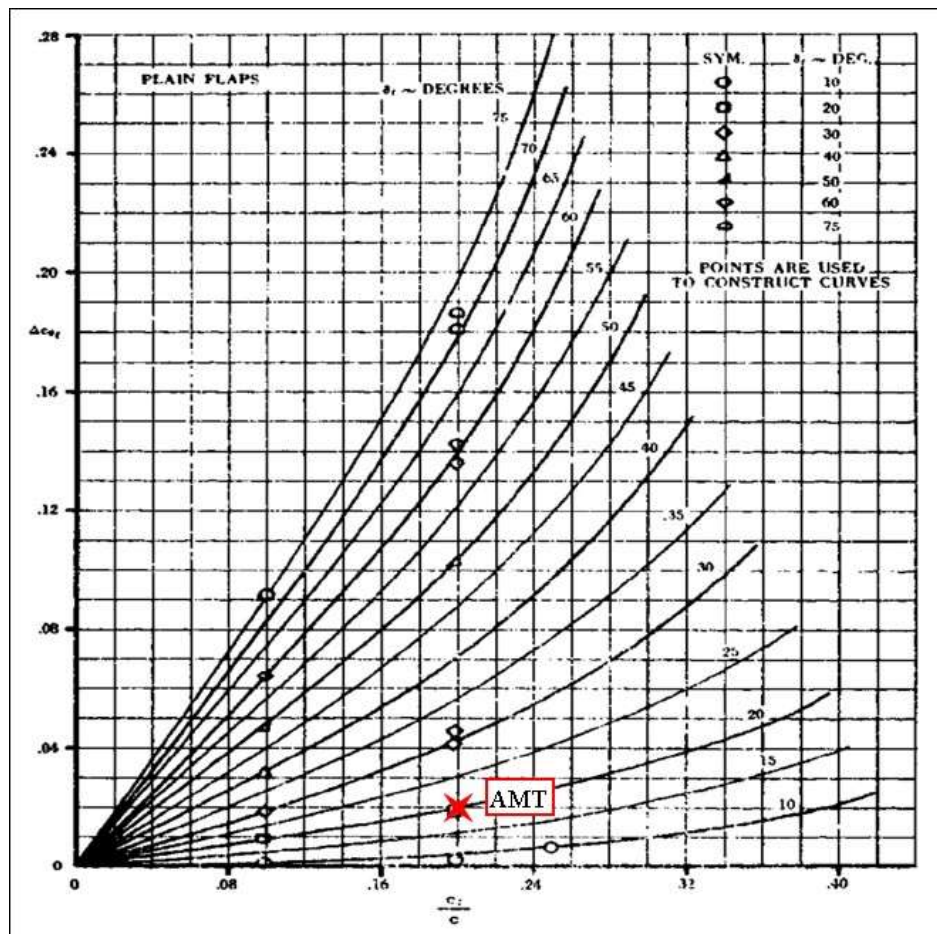


Figure 108. Plain flap profile drag increase [29]

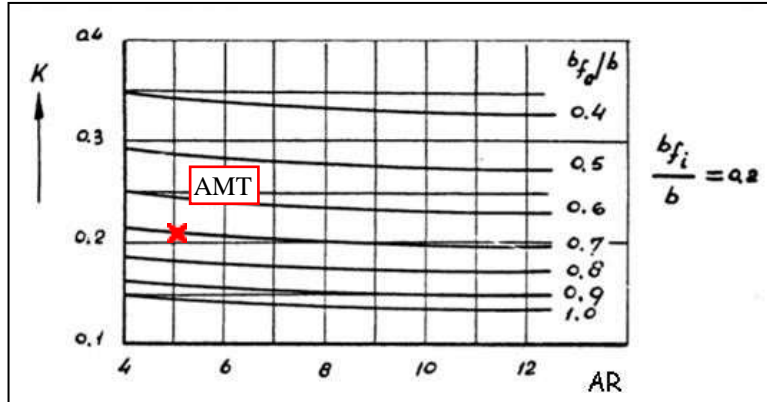


Figure 109. Interrupted flap induced drag factor [24]

From the wing design chapter, the trailing-edge flaps have a length of 20% chord. With a 20° deflection,  $\Delta C_{d_{P\Lambda_{c/4}=0}}$  is found to be 0.02 from Figure 108. The quarter-chord sweep angle is 30.1° and the wing-to-flap area ratio is 0.537. The resulting profile drag increase is 0.0093.

The K value determined from Figure 109 is about 0.21. The change in wing lift due to deflected trailing-edge flaps is determined to be 0.387 from section 6.5. The resulting induced drag of the trailing-edge flaps is 0.070.

### 10.2.1.2 Leading-edge Flaps

Based on the current references used, there is no simplified method to calculate plain leading-edge flap incremental drag increases.

### 10.2.1.3 Resulting High-lift Devices' Incremental Drag Increase

Using equation (10.8), the resulting drag increase due to deployed trailing-edge flaps is 0.079. The drag increase due to deployed HLD range from 0.055 – 0.075 [17]. The calculation performed for the trailing-edge plain flap may indicate a conservative estimation. The value obtained for the trailing-edge flaps will be assumed the total incremental drag increase for the HLDs.

### 10.2.2 Deployed Landing-Gear Drag

The AMT's landing-gear is retractable and does not feature any streamlining of the struts or wheels. The zero-lift drag can be estimated between 0.015 and 0.025 [17]. A more in-depth approach for calculating the additional drag due to deployed landing-gear is provided in [24] but upon exploring the method, some calculated parameters fell outside the limits of the statistical plots provided. As a result, the simpler method is employed by assuming a value based on historical data [19], which estimates  $\Delta C_{D_{o,gear}}$  between 0.015 and 0.025. Due to non-streamlining of the struts and wheels, the AMT will use  $\Delta C_{D_{o,gear}} = 0.025$ .

## 10.3 Compressibility Drag

The Class I method for transonic compressibility drag [19], rely on statistical data as presented in Figure 110. Due to the complexity of compressibility drag, more accurate methods require experimental testing or CFD analysis. The advanced trainer/fighter class of aircraft have negligible compressibility drag effects in the subsonic regime  $0.6 < M < 0.8$ . Since the subsonic cruise Mach number is about 0.7, the AMT's subsonic cruise compressibility drag will be considered zero.

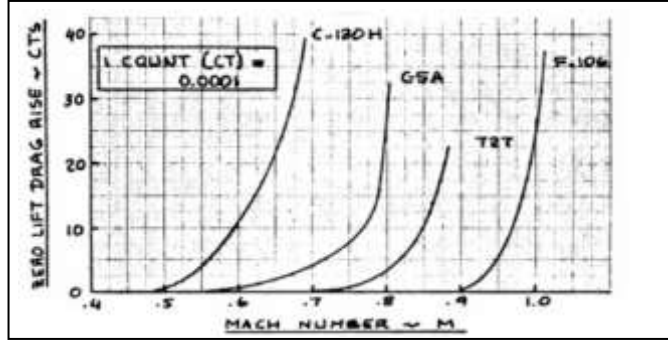


Figure 110. Zero-lift drag rise versus Mach number for various aircraft [19]

### 10.3.1 Supersonic Contributions

The three following sections of 10.3.1 outlines the theory used to approximate wave drag components in equation (10.11). The critical components of the AMT are the wing, fuselage, and empennage surfaces. The theory used is only applicable when correct “area ruling” is applied. The theories are taken from [24].

$$C_{D_{\text{super}}} = C_{D_{\text{ow}}} + C_{D_{\text{ofus}}} + C_{D_{\text{oemp}}} + C_{D_{L_w}} + C_{D_{L_{\text{fus}}}} + C_{D_{L_{\text{emp}}}} \quad (10.11)$$

#### 10.3.1.1 Wing Contributions

The wing’s zero-lift is a function of skin friction drag and wave drag, and is calculated with equation (10.12). The skin friction component is calculated with equation (10.13). The skin friction coefficient is found from Figure 111 based on the mean chord’s Reynolds number.

$$C_{D_{\text{ow}}} = C_{D_{f_w}} + C_{D_{\text{wave}_w}} \quad (10.12)$$

$$C_{D_{f_w}} = c_{f_w} \frac{S_{\text{wet}}}{S} \quad (10.13)$$

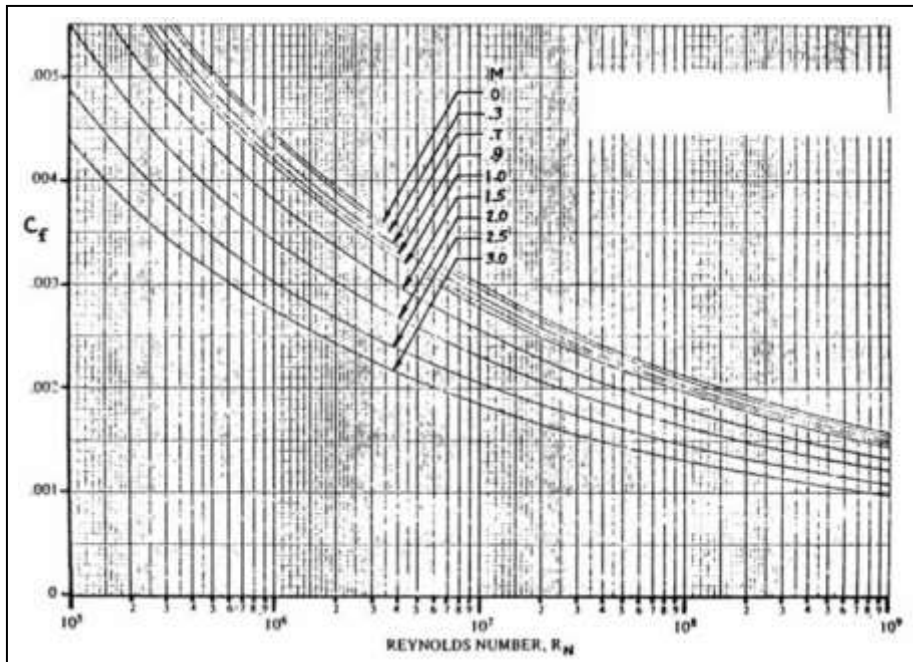


Figure 111. Reynolds number effect on turbulent mean skin-friction coefficient [24] taken from [29]

The wing's wave drag component is calculated with equation (10.14) or (10.15) depending on whether the wing's leading-edge is supersonic or subsonic, as defined by Figure 112. The basic wing (bw) variables are defined in Figure 113. The leading-edge drag coefficient is determined from Figure 114. The effective thickness ratio is calculated with equation (10.16).

*Supersonic Leading-Edge*

$$C_{D_{\text{wave}_w}} = C_{D_{\text{LE}}} + \frac{16\{t/c_{\text{eff}}\}^2 S_{\text{bw}}}{3\sqrt{M^2 - 1}} \left(\frac{S}{S}\right) \quad (10.14)$$

*Subsonic Leading-Edge*

$$C_{D_{\text{wave}_w}} = C_{D_{\text{LE}}} + \frac{16}{3} \{t/c_{\text{eff}}\}^2 \cot(\Lambda_{\text{LE}}) \left(\frac{S_{\text{bw}}}{S}\right) \quad (10.15)$$

$$t/c_{\text{eff}} = \frac{\int_0^{b/2} \{t/c(y)\}^2 c_{\text{bw}}(y) dy}{\sqrt{S_{\text{bw}}/2}} \quad (10.16)$$

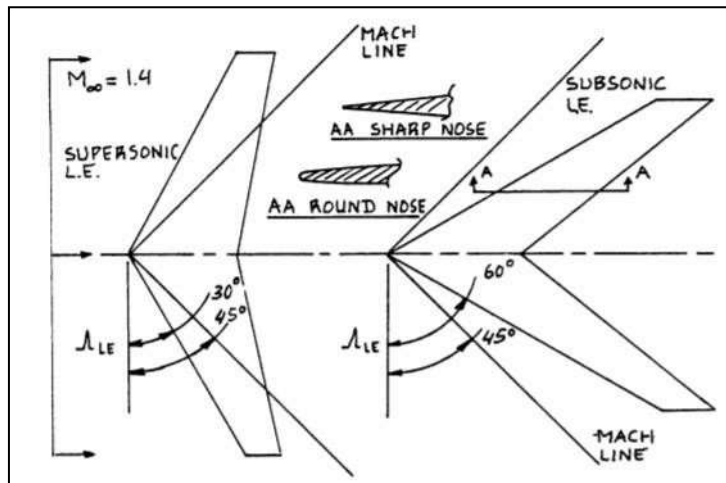


Figure 112. Definition of supersonic and subsonic leading-edge [24]

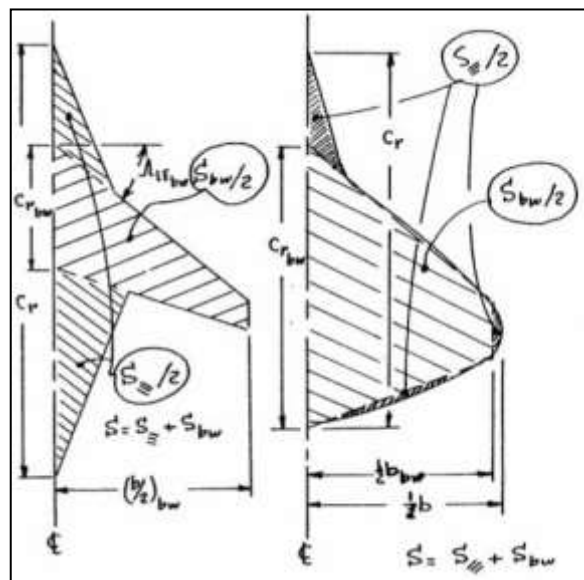


Figure 113. Definition of basic wing [24]

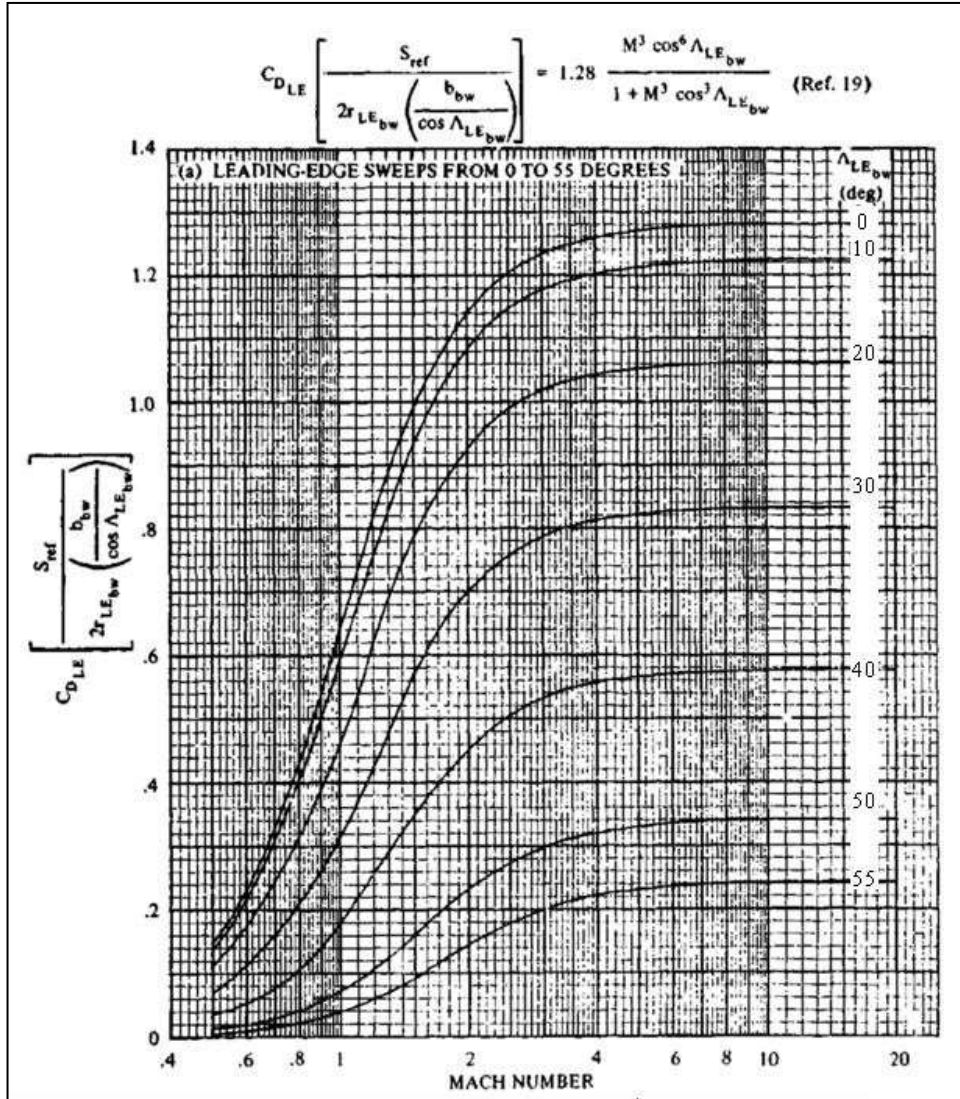


Figure 114. Leading-edge pressure drag [29]

The lift induced drag of the wing is calculated with equation (10.17). The term  $C_D / C_L^2$  is found with the following process:

1. Calculate equation (10.18)
2. Calculate (p) with equation (10.19)
3. Use Figure 115 to find the curly bracket term in equation (10.20)
4. Solve equation (10.20) with the appropriate terms.

$$C_{D_{Lw}} = \left( \frac{C_{D_L}}{C_L^2} \right) C_L^2 \quad (10.17)$$

$$\frac{b \cdot \beta}{2c_r} = \frac{b\sqrt{M^2 - 1}}{2c_r} \quad (10.18)$$

$$p = \frac{S}{b \cdot c_r} \quad (10.19)$$

$$\frac{C_{D_L}}{C_L^2} = \left\{ \pi \cdot AR \left( \frac{C_{D_L}}{C_L^2} \right) \frac{p}{p+1} \right\}_{\text{term}} \frac{1+p}{p \cdot \pi \cdot AR} \quad (10.20)$$

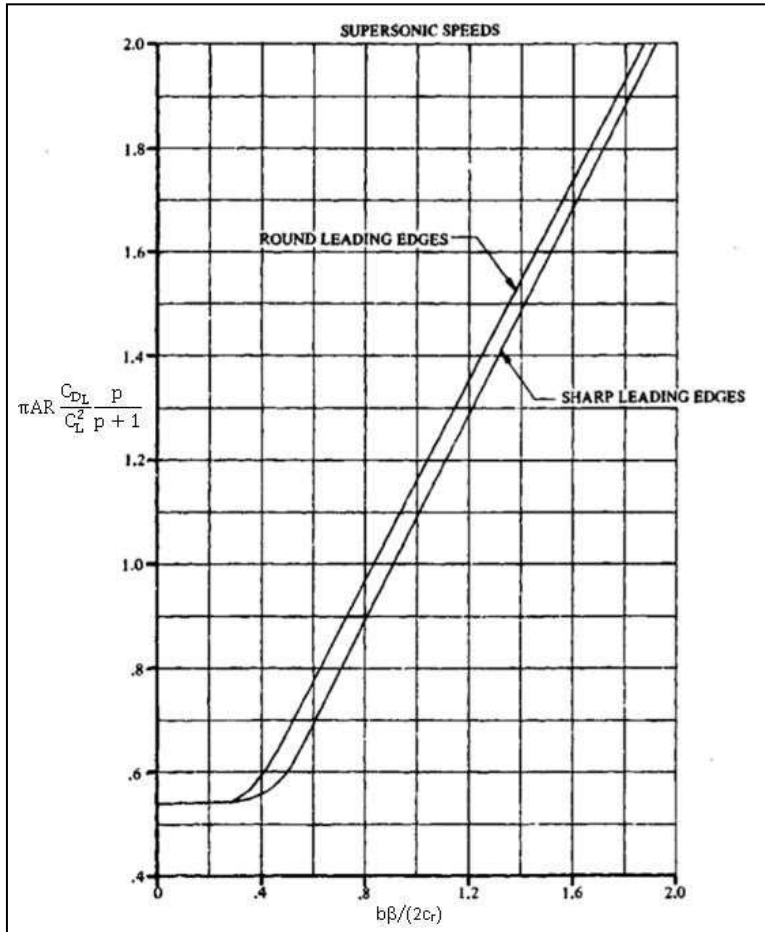


Figure 115. Supersonic drag due to lift for straight tapered wings [29]

### 10.3.1.2 Fuselage Contributions

The fuselage zero-lift drag is estimated with equation (10.21). The skin-friction coefficient is estimated from Figure 111. The fuselage areas ( $S_{\text{subscript}}$ ) are defined in Figure 116. The drag coefficients  $C_{D_{N_2}}$  and  $C_{D_A}$  are estimated using Figure 117. The inference drag  $C_{D_{A(NC)}}$  is estimated from Figure 118. The fuselage base drag is estimated with Figure 119. These approximations assume the cross-sectional area distribution is smooth. This is verified in section 10.3.2.

$$C_{D_{o_{\text{fus}}}} = \left\{ C_{f_{\text{fus}}} \frac{S_{\text{wet}_{\text{fus}}}}{S_{\text{fus}}} + C_{D_{N_2}} + C_{D_A} + C_{D_{A(NC)}} + C_{D_{b_{\text{fus}}}} \right\} \frac{S_{\text{fus}}}{S} \quad (10.21)$$

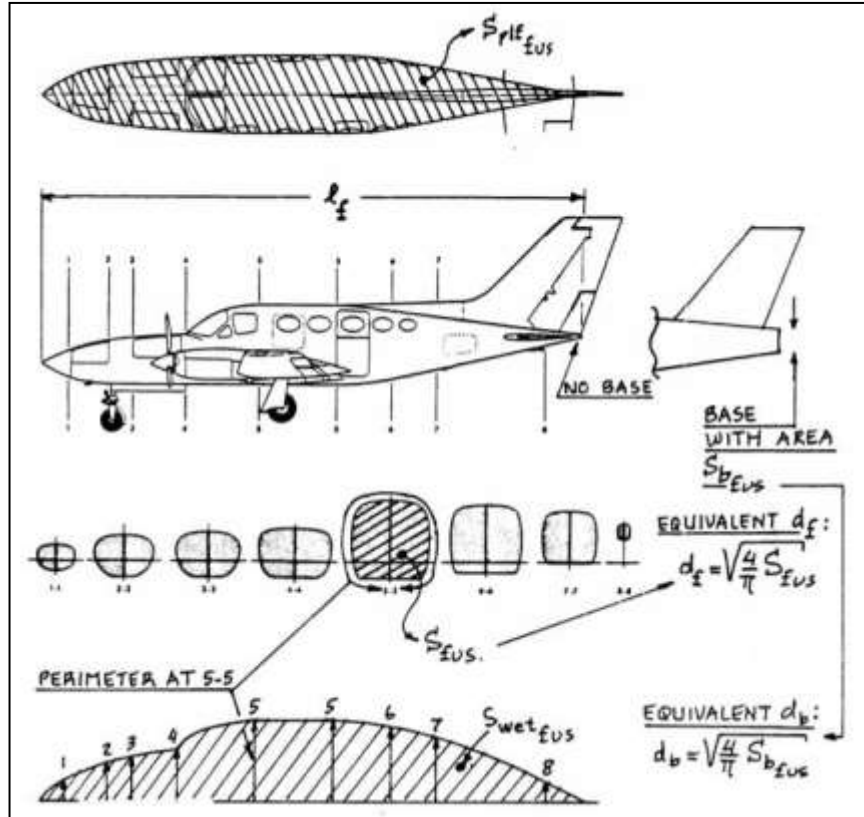


Figure 116. Fuselage parameters defined [24]

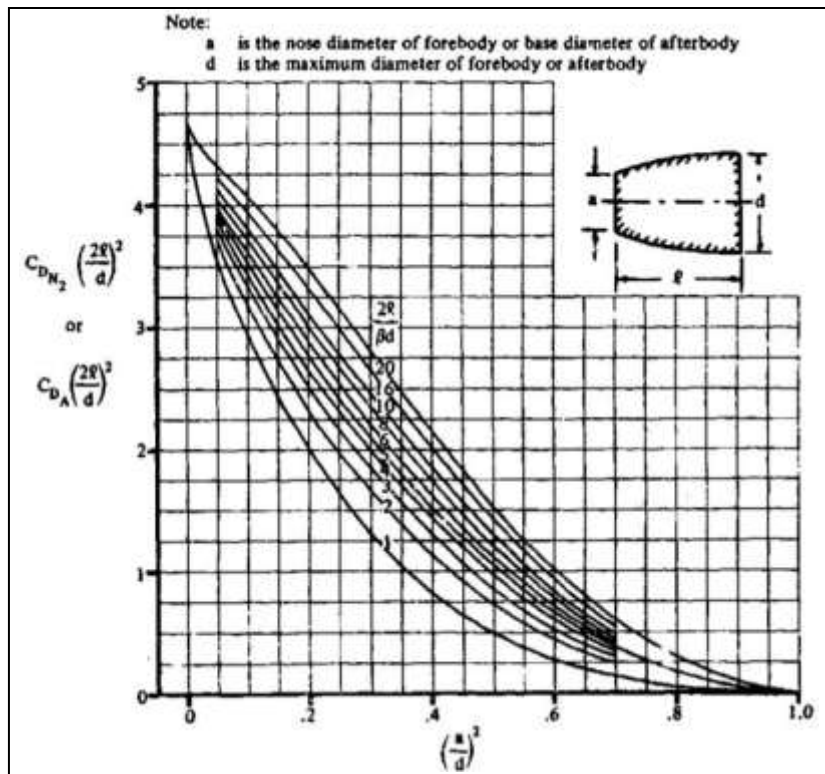


Figure 117. Drag of slender fore or aft bodies [29]

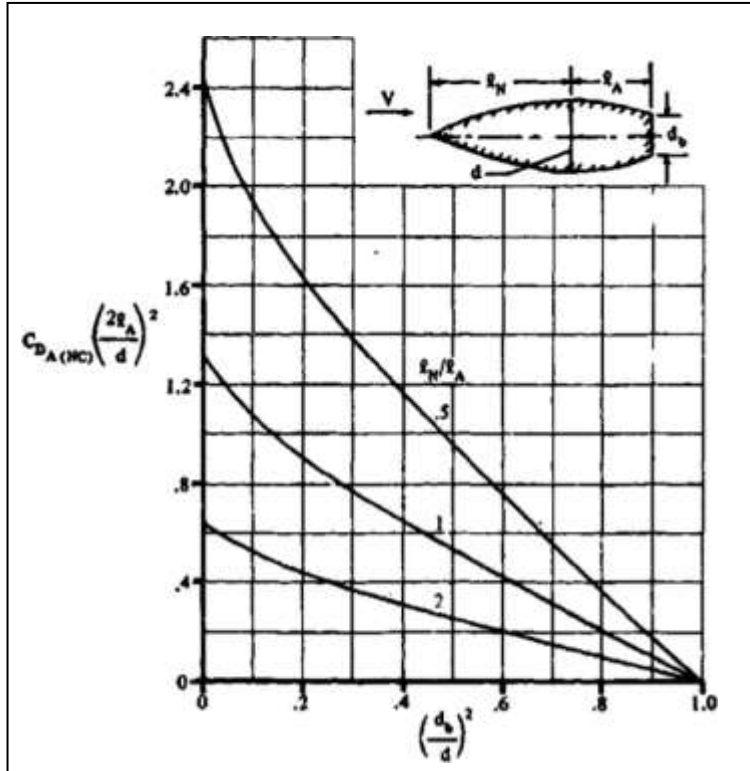


Figure 118. Interference drag of pointed forebody with truncated aftbody [29]

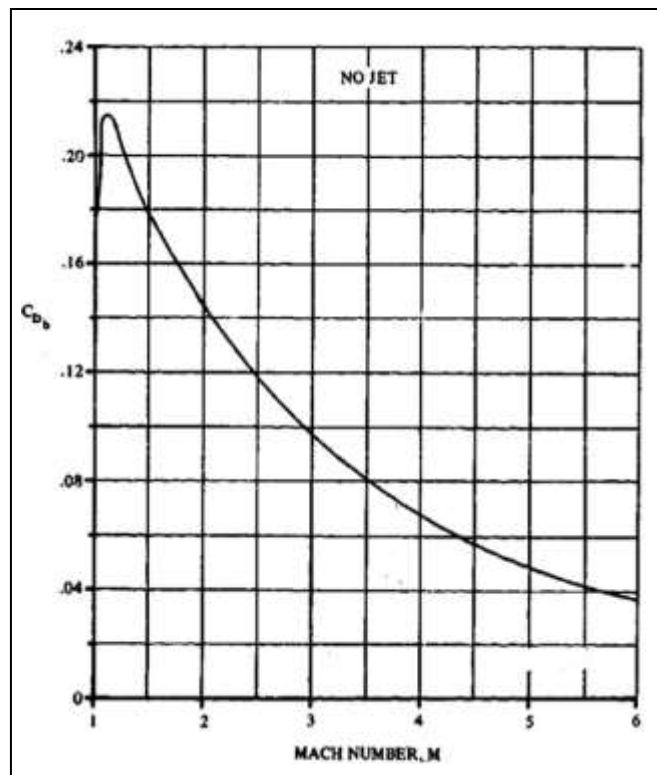


Figure 119. Bodies of revolution base drag [29]

The lift induced drag of the fuselage is estimated with equation (10.22). The parameter F is 1.0 for circular cross-sections. For elliptical cross-sections, equation (10.23) is used. Where a is the major axis and b is the minor axis. The cross flow drag coefficient is estimated from Figure 120

$$C_{D_{L_{fus}}} = F \left\{ 2\alpha^2 \frac{\Delta b_{fus}}{S} + c_{d_c} \frac{\Delta p_{lfus}}{S} |\alpha|^3 \right\} \quad (10.22)$$

$$F = \frac{a}{b} \cos^2(\omega) + \frac{b}{a} \sin^2(\omega) \quad (10.23)$$

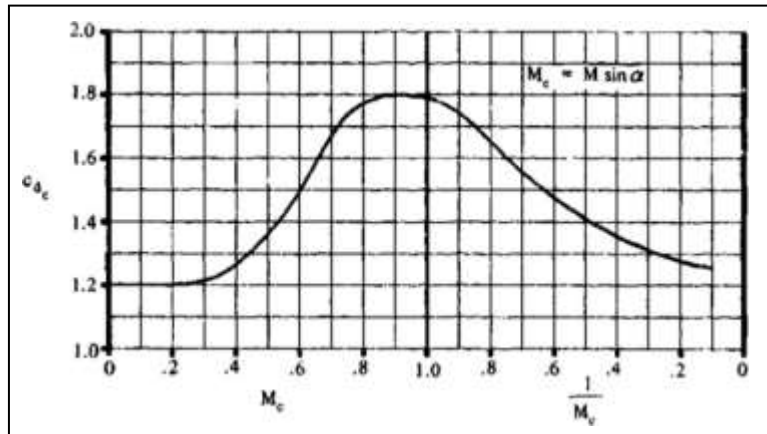


Figure 120. Steady-state cross flow drag coefficient [29]

### 10.3.1.3 Empennage Contributions

The empennage drag is a sum of each surface and is estimated with equation (10.24). The zero-lift drag of each empennage surface is estimated with equation (10.25). The friction coefficient for each surface is approximated from Figure 111. The wave drag components follow the same method used for the wing using equations (10.14) through (10.16).

$$C_{D_{emp}} = \sum_i \{ (C_{D_{oemp}})_i + (C_{D_{Lemp}})_i \} \quad (10.24)$$

$$(C_{D_{oemp}})_i = (C_{f_{emp}})_i \frac{(S_{wetemp})_i}{S} + C_{D_{empwave}} \quad (10.25)$$

The lift induced drag is estimated using equation (10.26). This is the same method used for the wing, which uses equations (10.17) through (10.20)

$$(C_{D_{Lemp}})_i = \left( \frac{C_{D_L}}{C_L} \right)_{emp_i}^2 (C_{Lemp})_i^2 \quad (10.26)$$

### 10.3.2 Area Ruling

The “area rule” is credited to R.T. Whitcomb during the 1950s for the purpose of understanding and reducing wave drag in the transonic flow regimes. Whitcomb’s experiments showed that compressibility drag increases when an aircraft’s cross-sectional area distribution is not smooth, and the wave drag of an aircraft is comparable to a body of revolution with the same cross-sectional area distribution [24]. Otto Frenzl, in Germany, and Wallace Hayes, in The United States, were also discovering the same area rule methodology around the time of Whitcomb.

Further research was performed to expand the area ruling to the supersonic flow regime. The supersonic area rule requires determining the aircraft cross-sectional area with respect to the intersection of the Mach cone [30]. The method explains that if the area distribution normal to the flow is known then the area of the Mach cone intersection can be expressed by equation (10.27). the Mach line angle ( $\mu$ ) is defined by equation (10.28).

$$S(\mu) = \frac{S_{\text{norm}}}{\sin(\mu)} \quad (10.27)$$

$$\mu = \arcsin \left( \frac{1}{M} \right) \quad (10.28)$$

The cross-sectional area of the AMT is determined from the Solidworks CAD model. A feature in Solidworks allows for cutting the model, then using the *measure* feature (in evaluate tab) to determine the area. In some cases, this does not work because the section cut reveals geometry that is “not really there.” In these cases, the section properties are used and is found on the same *evaluate* ribbon. The section cuts can be seen between Figure 121 and Figure 122.

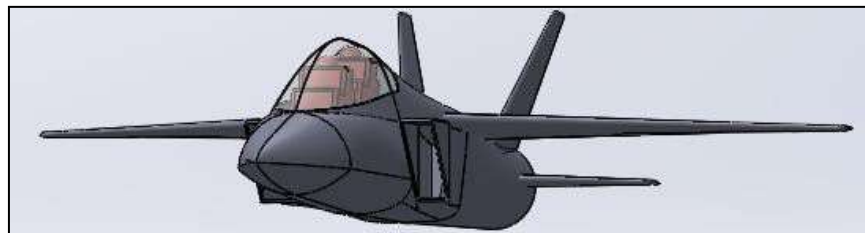


Figure 121. AMT Solidworks model

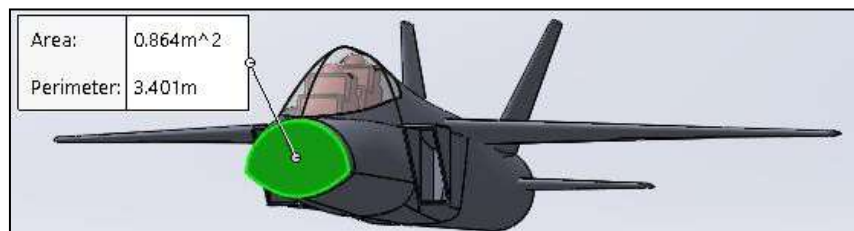


Figure 122. Solidworks cut view and measure feature

Cuts are made along the AMT in increments of 0.5m with the exception of specific intersection points along the fuselage: canopy, engine inlets, wing, horizontal stabilizer, and vertical fin. In these cases, the specific starting and end points are used as the section cut. In cases where components overlap, each part’s “cut” area is determined and the overlapping area is subtracted from the summation of the components’ areas. This can be seen in Figure 123. The AMT’s cross-sectional area distribution is shown in Figure 124

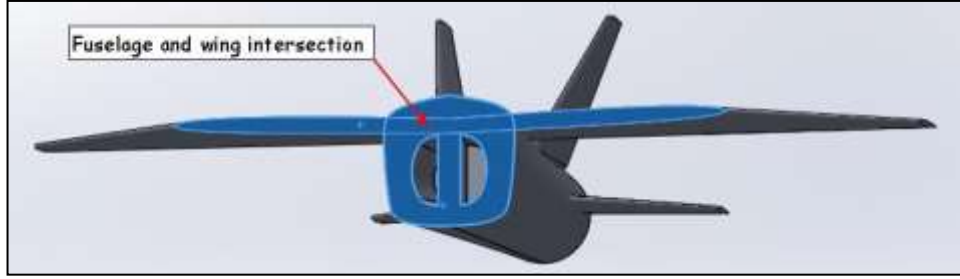


Figure 123. AMT, cut at wing-fuselage intersection

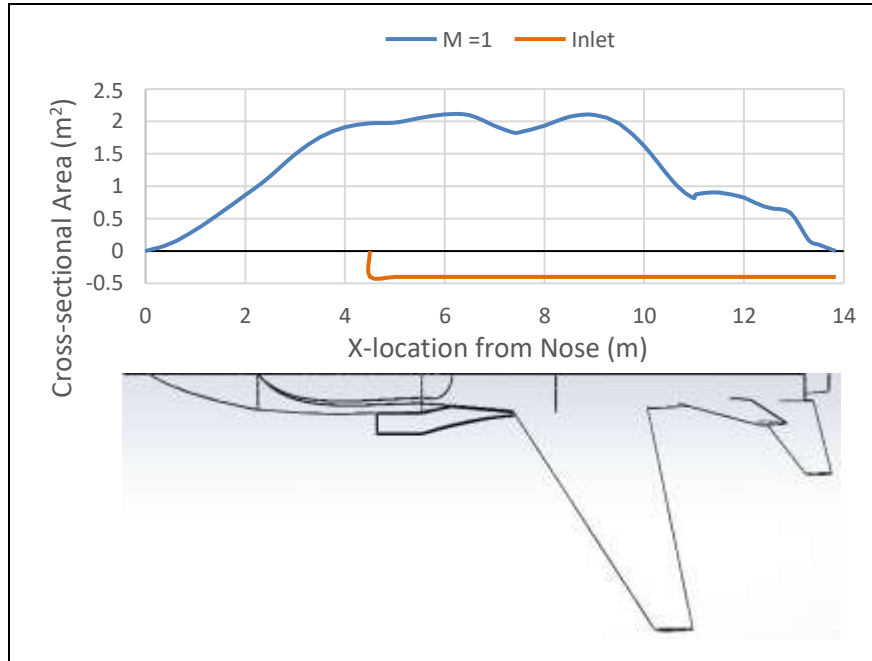


Figure 124. AMT area distribution

Based on the area distribution in Figure 124, there is some non-smoothness that needs to be corrected. The area rule is applied for the Sears-Haack body [24], [31]. A type-I Sears-Haack body radius is calculated with equation (10.29).

$$r(x)_{S-H} = r_{\max}\{4 \cdot x(1 - x)\}^{0.75} \quad (10.29)$$

The comparison of a type-I Sears-Haack Body is made with the AMT's non-dimensional values shown in Figure 125. Applying the area rule, the fuselage's cross-sectional area needs to be reduced around the canopy, wing tip, and the empennage. The cross-sectional area needs to be increased at the wing's leading-edge root and between the wing trailing-edge and vertical stabilizers.

In Solidworks, the different lofts and guide curves are adjusted to correct for the non-smoothness area distribution. The area ruled AMT's non-dimensional values can be seen with the red curve in Figure 125. Applying equation (10.28), the area distributions for  $M = 1.25$  and  $M = 1.5$  are obtained as shown in Figure 126. The resulting equivalent body of revolutions' thickness-to-length ratio for the three conditions is listed in Table 28.

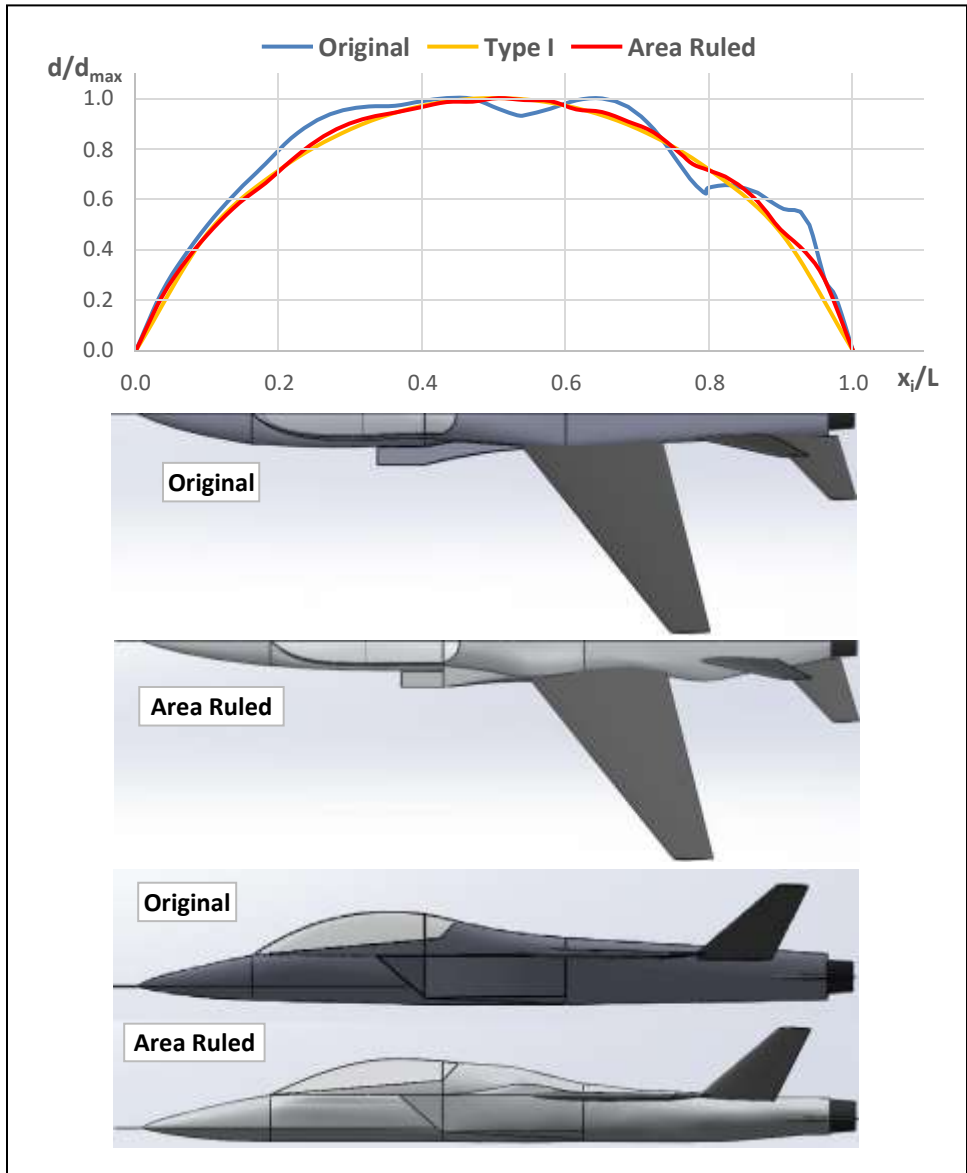


Figure 125. AMT non-dimensional diameter comparison to Sears-Haack type-I

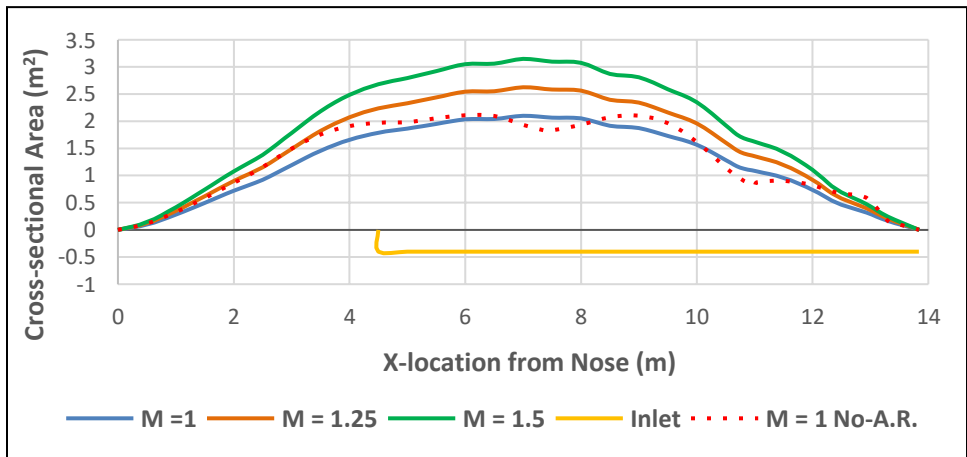


Figure 126. AMT's cross-sectional area distributions

Table 28. AMT's equivalent bodies of revolution thickness ratio for Mach condition

	M = 1.0	M = 1.25	M = 1.5
$d_{\max}/L$	0.118	0.132	0.145

## 10.4 AMT Drag Polars

### 10.4.1 Clean

The clean zero-lift drag was determined to be 0.023. The Oswald efficiency factor was approximated as 0.8 previously for the performance sizing and the aspect ratio is 5.0. The resulting drag polar equation for the clean configuration is equation (10.30).

$$C_D = 0.023 + 0.0796C_L^2 \quad (10.30)$$

### 10.4.2 Takeoff and Landing

The takeoff and landing configuration introduces additional drag as a result of deployed flaps and landing-gear. With deployed flaps, the zero-lift drag increase was determined as 0.079 in 10.2.1. The deployed flaps also reduce the Oswald efficiency and the reduction can be 5.0-10.0% [17]. From the clean value of 0.8,  $e$  will assume to be 0.73 for the takeoff and landing configuration. From section 10.2.2, the landing-gear contribution to the zero-lift drag was determined to be 0.025. The resulting drag polar equation is (10.31).

$$C_D = 0.127 + 0.0872C_L^2 \quad (10.31)$$

### 10.4.3 Supersonic

#### 10.4.3.1 Wing Contributions

Following the procedure outlined in 10.3.1.1, the wing's supersonic zero-lift drag is determined to be 0.0607 and 0.0624 for  $M = 1.25$  and  $M = 1.5$ , respectfully. The lift induced drag coefficient is determined to be 0.220 and 0.308 for  $M = 1.25$  and  $M = 1.5$ , respectfully. The resulting drag polar equations for  $M = 1.25$  and  $M = 1.50$  are (10.35) and (10.36).

$$M = 1.25$$

$$C_{D_w} = 0.0607 + 0.220C_L^2 \quad (10.32)$$

$$M = 1.50$$

$$C_{D_w} = 0.0624 + 0.308C_L^2 \quad (10.33)$$

#### 10.4.3.2 Fuselage Contributions

Following the procedure outlined in 10.3.1.2, the fuselage's supersonic zero-lift drag is determined to be 0.0831 and 0.0658 for  $M = 1.25$  and  $M = 1.5$ , respectfully. Equation (10.22) is used for the fuselage's contribution to lift induced drag. Since the drag polar equations are function of  $C_L$ , the supersonic flatplate  $C_L$  equation will be used to approximate  $\alpha$  in equation (10.22), by equation (10.34). This relation is only valid for small angles of attack, less than  $13^\circ$ . This correlate to a max  $C_L$  of 0.8 with equation (10.34). The resulting fuselage contributions of the drag polar equations are (10.35) and (10.36).

$$C_L = \frac{4\alpha}{\sqrt{M^2 - 1}} \rightarrow \alpha = \frac{C_L}{4} \sqrt{M^2 - 1} \quad (10.34)$$

$$M = 1.25$$

$$C_{D_{fus}} = 0.0831 + 0.0024C_L^2 + 0.012C_L^3 \quad (10.35)$$

$$M = 1.50$$

$$C_{D_{fus}} = 0.0658 + 0.0064C_L^2 + 0.045C_L^3 \quad (10.36)$$

#### 10.4.3.3 Horizontal Stabilizer Contributions

Following the procedure outlined in 10.3.1.3, the horizontal's supersonic zero-lift drag is determined to be 0.0846 and 0.0858 for  $M = 1.25$  and  $M = 1.5$ , respectfully. The lift induced drag coefficients are calculated to be 0.239 and 0.343 for  $M = 1.25$  and  $M = 1.5$ , respectfully. The resulting horizontal contributions of the drag polar equations are

$$M = 1.25$$

$$C_{D_h} = 0.0846 + 0.239C_L^2 \quad (10.37)$$

$$M = 1.50$$

$$C_{D_h} = 0.0858 + 0.343C_L^2 \quad (10.38)$$

#### 10.4.3.4 Vertical Fins Contributions

Following the procedure outlined in 10.3.1.3, the horizontal's supersonic zero-lift drag is determined to be 0.0707 and 0.0717 for  $M = 1.25$  and  $M = 1.5$ , respectfully. The vertical fins are assumed to not have any lift induced drag contributions due to their orientation.

$$M = 1.25$$

$$C_{D_v} = 0.0707 \quad (10.39)$$

$$M = 1.50$$

$$C_{D_v} = 0.0717 \quad (10.40)$$

#### 10.4.3.5 Supersonic Drag Polar Equation

Combining the drag polar equations obtained between sections 10.4.3.1-10.4.3.4 results in the aircraft drag polar equations (10.41) and (10.42).

$$M = 1.25$$

$$C_D = 0.299 + 0.462C_L^2 + 0.0121C_L^3 \quad (10.41)$$

$$M = 1.50$$

$$C_D = 0.286 + 0.657C_L^2 + 0.0452C_L^3 \quad (10.42)$$

#### 10.4.4 Drag Polars

Figure 127 is the resulting drag polars for the clean, takeoff and landing,  $M = 1.25$ , and  $M = 1.50$  as determined from equations (10.30), (10.31), (10.41), and (10.42).

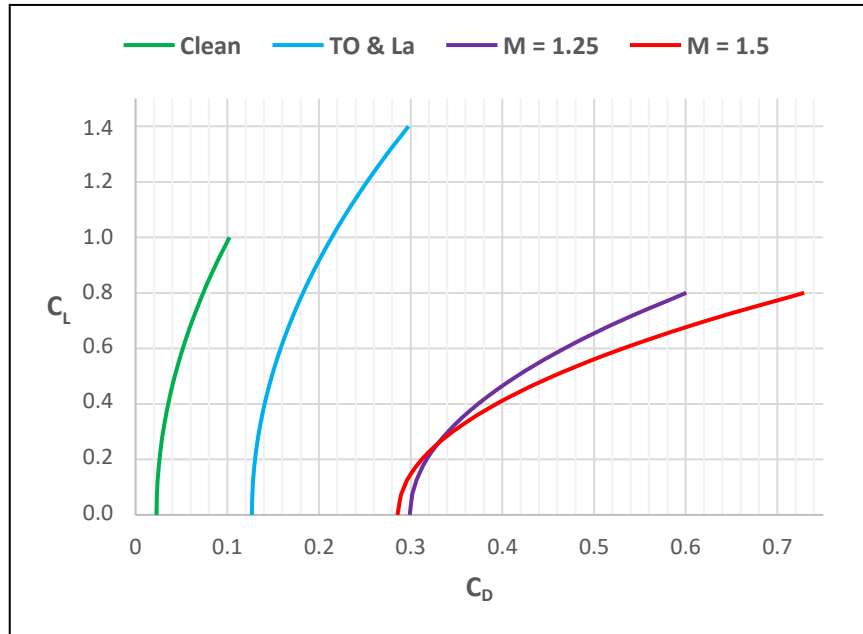


Figure 127. AMT drag polars

## 10.5 Discussion and Conclusion

The clean subsonic drag polar should be a reasonable approximation. The zero-lift skin friction drag calculated should be a reasonable value due to the surface area of the AMT was determined using a 3D CAD model, and the method used is based on statistical data. Due to the assumption for landing-gear drag, a more accurate method must be researched to determine a more realistic value for the drag increase due to landing-gear deployment. The large increase in drag due to deployed HLD was expected and can be attributed to the additional vortices created by the break in the trailing-edge of the wing. This would create eight additional vortices, four on the wing's trailing-edge where the flap is deflected down and four at the flap's trailing-edge. To obtain more accurate approximations, computer simulations or wind tunnel testing would be required.

The initial geometry resulted in a non-smooth cross-sectional area distribution, and therefore area ruling was applied to the AMT. After many small adjustments and iterations, the cross-sectional area distribution now resembles a Type-I Sears-Haack body. This is necessary because the supersonic drag equations assume the body of interest has an equivalent body of revolution with a smooth cross-sectional area distribution. As experiments by Whitcomb showed equivalent bodies of revolution had similar drag coefficients as an area ruled wing-body model.

The skin friction approximations, for supersonic drag of the major aircraft components, are considered over approximations because the skin friction coefficients used are for turbulent boundary layers. The theory used for the supersonic drag approximations are a result of extensive research and testing for the USAF [29]. The lower zero-lift drag obtain under  $M = 1.5$  conditions, in comparison to  $M = 1.25$ , is expected. This is because as the Mach number increases from sonic conditions, the drag coefficient tends to decrease as a result of fewer unstable shocks around the body and high dynamic pressure. As discussed with the subsonic polars, computer simulations or wind tunnel testing would be required to obtain better approximations.

## 11. V-n Diagram

V-n diagrams are used to describe the flight envelop and provide design load limits with corresponding speeds. Based on the V-n plots, flight load limits can be quickly determined based on speed or design restrictions. Load limits are generally specific to the type of aircraft. For an advanced trainer there are four primary speeds to determine and their corresponding load limit: stall, maneuvering, maximum level flight, and dive speed.

### 11.1 Load Limits

For military trainers, [32] lists the positive load limit as 7.5g up to the dive limit speed, the negative load limit as -3.0g up to maximum level speed, and -1.0g at the dive limit speed.

### 11.2 Stall Speed

The stall speed of an aircraft is calculated with equation (11.1) [21]. Where the maximum load force coefficient is calculated with equation (11.2) [21].

$$V_s = \sqrt{\frac{2(W/S)}{\rho \cdot C_{N_{\max}}}} \quad (11.1)$$

$$C_{N_{\max}} = \sqrt{C_{L_{\max}}^2 + C_{D@C_{L_{\max}}}^2} \quad (11.2)$$

The maximum load force coefficient with deployed HLD is 1.47 and in the clean configuration is 1.01. Table 29 lists the stall speeds for the clean and deployed HLD configuration for 3 altitudes.

Table 29. AMT stall speed for given altitudes for clean and HLD configurations

Altitude km(kft)	Clean, m/s (ft/s)	HLD, m/s (ft/s)
0.0(0.0)	65.6(215)	54.4(178)
2.5(8.2)	74.2(243)	61.5(202)
5.0(16.4)	84.6(277)	70.1(230)

### 11.3 Design Maneuvering Speed

The design maneuvering speed must satisfy equation (11.3). Using the stall speeds in Table 29, the minimum maneuvering speeds for positive and negative g-loads are shown in Table 31.

$$V_A \geq V_s \sqrt{n_{\lim}} \quad (11.3)$$

Table 30. AMT minimum maneuver speed for given altitudes for clean and HLD configurations

Altitude km(kft)	Positive g-load		Negative g-load	
	Clean, m/s (ft/s)	HLD, m/s (ft/s)	Clean, m/s (ft/s)	HLD, m/s (ft/s)
0.0(0.0)	180(589)	149(488)	114(373)	94.1(309)
2.5(8.2)	203(666)	168(553)	129(422)	107(349)
5.0(16.4)	232(760)	192(630)	147(480)	121(398)

## 11.4 Maximum Level Flight Speed

The maximum level flight speed is defined as the maximum speed attainable ( $V_H$ ) in basic level flight, while using the maximum available thrust with afterburners or augment thrust device [33]. Therefore, the maximum speed can be derived from thrust is equal to drag. Given that the thrust is also a function of altitude, a relation for the change in thrust must be derived. Equation (11.4) is the general thrust equation for a jet engine [34].

$$F_T = (\dot{m}_o + \dot{m}_f)V_e - \dot{m}_o \cdot V_\infty + (P_e - P_a)A_e \quad (11.4)$$

Where the subscripts of the mass flow rates are the air (o) and fuel (f). The velocities are the exit velocity of the jet engine and the freestream velocity. For the most efficient thrust, the jet exhaust would be perfectly expanded so the exit pressure is equal to the atmosphere pressure. The thrust equation can be rewritten in terms of only the freestream and exit velocities, the fuel-to-air mass flow ratio, and the air mass flow rate by equation (11.5).

$$F_T = \dot{m}_o [(\dot{m}_{f/o} + 1)V_e - V_\infty] \quad (11.5)$$

Generally, jet engines are rated at sea-level conditions. Therefore, to perform analysis at altitude for a given engine's sea-level thrust, the thrust at altitude can be divided by the sea-level thrust, which gives the following relation.

$$\frac{F_{T_{alt}}}{F_{T_{sea}}} = \frac{\dot{m}_{o_{alt}} [(\dot{m}_{f/o} + 1)V_e - V_\infty]}{\dot{m}_{o_{sea}} [(\dot{m}_{f/o} + 1)V_e - V_\infty]}$$

Assuming the thrust being compared has the same fuel-to-air mass flow ratio, engine exit velocity, and freestream velocity, the following relation can be made:

$$\frac{F_{T_{alt}}}{F_{T_{sea}}} = \frac{\dot{m}_{o_{alt}}}{\dot{m}_{o_{sea}}} = \frac{\rho_{alt} \cdot V_\infty \cdot A}{\rho_{sea} \cdot V_\infty \cdot A}$$

Therefore, the thrust at altitude can be represented by the sea-level thrust rating and the ratio of the air densities by equation (11.6)

$$F_{T_{alt}} = \left(\frac{\rho_{alt}}{\rho_{sea}}\right) F_{T_{sea}} \quad (11.6)$$

Now to find the maximum speed the thrust is equal to drag. Using the drag coefficient equations from section 10.4.3.5, the thrust is equal to drag.

$$T = D = (C_{D_o} + K_1 C_L^2 + K_2 C_L^3) q_\infty$$

Substituting in the relation for  $C_L$  in terms of wing loading, the above equation is transformed into the following relation:

$$T = \left\{ C_{D_o} + K_1 \left[ \frac{W/S}{q_\infty} \right]^2 + K_2 \left[ \frac{W/S}{q_\infty} \right]^3 \right\} q_\infty$$

The above equation can then be transformed into a cubic relation, equation (11.7), and solved for the dynamic pressure. The velocity equation can be written as a function of dynamic pressure and density by equation (11.8).

$$0 = C_{D_0} \cdot q_\infty^3 - T \cdot q_\infty^2 + K_1(W/S)^2 q_\infty + K_2(W/S) \quad (11.7)$$

$$V = \sqrt{\frac{2q_\infty}{\rho}} \quad (11.8)$$

A range of altitudes are used from 0 to 10km. Correcting for the change in thrust with equation (11.6) and substituting in the appropriate variables from the drag polar equations (10.41) and (10.42), equation (11.7) is solved for the freestream dynamic pressure. The results are shown in Table 31. Solving equation (11.8) for the dynamic pressure results in the maximum speed in the final row of Table 31. The last two columns Mach conditions indicate which drag polar is used for the calculation.

Table 31. Dynamic pressure solution to equation (11.7) and  $V_H$

Altitude (km)	Density (kg/m <sup>3</sup> )	Dynamic Pressure (Pa)	
		M=1.25 conditions	M=1.5 conditions
0	1.225	264,172	276,165
2.5	0.9570	206,348	215,708
5.0	0.7364	158,767	165,958
7.5	0.5572	120,086	125,510
10.0	0.4135	89,065	93,066
<b><math>V_H</math>, m/s (ft/s)</b>		656(2,150)	671(2,200)

### 11.5 Dive Limit Speed

The dive speed is defined as the maximum allowable speed while in a dive [33]. [21] This value is typically 25% greater than the maximum speed, as shown by equation (11.9) [21].

$$V_L = 1.25V_H \quad (11.9)$$

Solving equation (11.9) with the maximum velocity obtained in the previous section results in the dive limit speed 820 and 839m/s based on the  $M = 1.25$  and  $M = 1.50$  drag polar equations, respectfully.

### 11.6 V-n Plot

The initial curve from  $V = 0$  and  $n = 0$ , is calculated with equation (11.10) [32]. Combining the values obtained in sections 11.2 to 11.5, the resulting V-n plots for the AMT are shown in Figure 128 for the clean configuration and in Figure 129 for deployed HLD in the low subsonic speed regime.

$$n = \frac{\rho \cdot V^2}{2(W/S)} C_{N_{\max \text{ or } \min}} \quad (11.10)$$

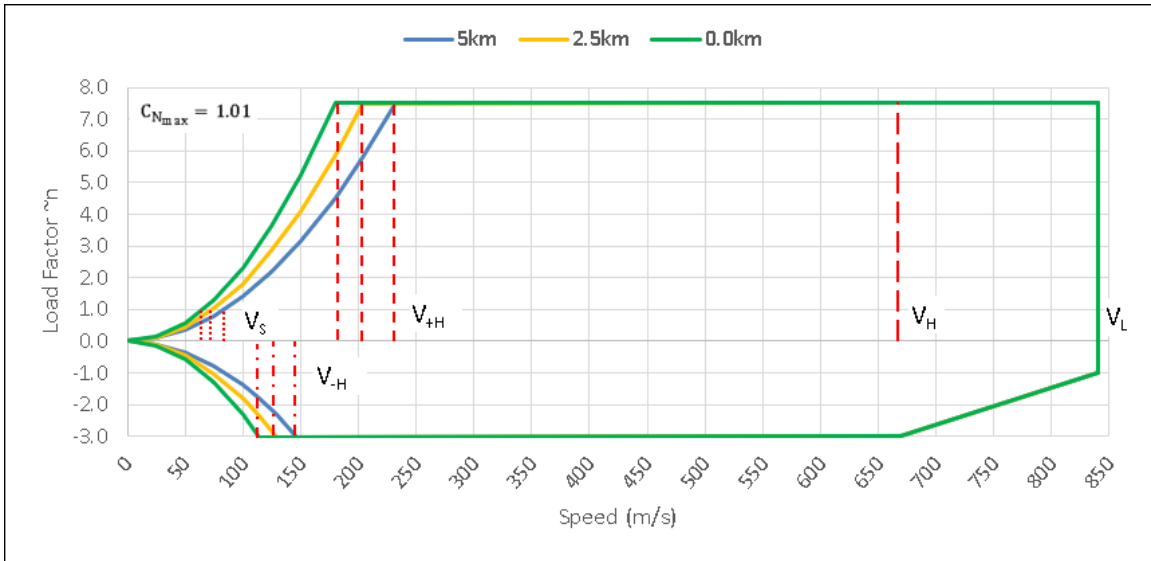


Figure 128. AMT clean configuration V-n diagram

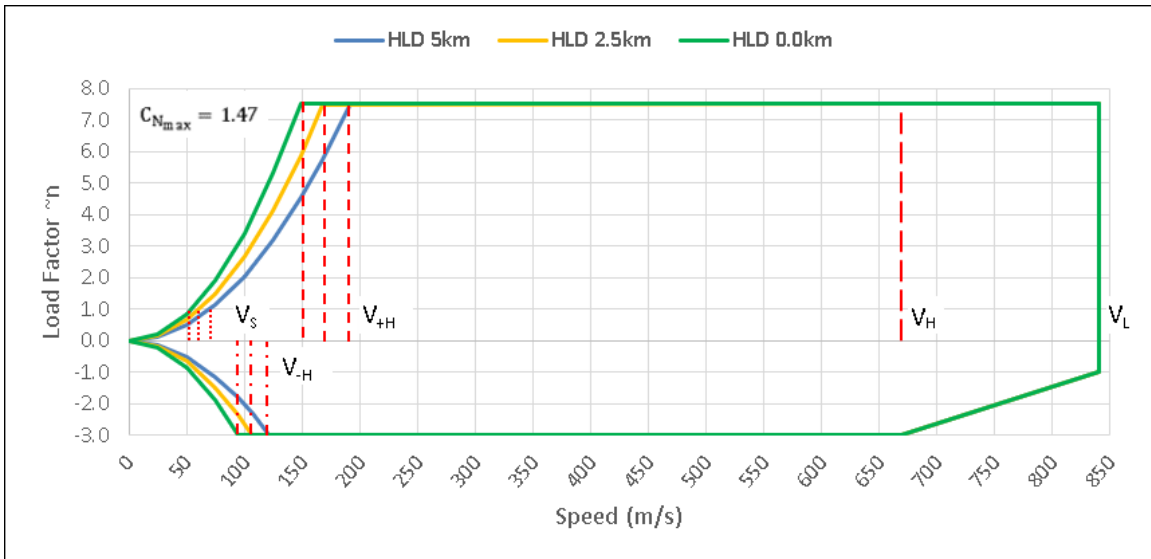


Figure 129. AMT deployed HLD configuration V-n diagram

## 11.7 Discussion and Conclusion

From initial performance sizing, the design max speed was  $M = 1.5$  at exercise altitude. Based on the engine selection, with afterburners the AMT is capable of  $M = 1.9$  to  $M = 2.1$  for the theoretical calculations performed in 11.4. The engine selected was based on the fact that clean sheet designed engines take many years to develop and obtain certification. From a design perspective, the options are to invest in a new purpose-built engine design or rely on what is available in the market today.

For military trainers and fighters, the critical parameters are the max and dive limit speeds. Since these types of aircraft are design with the intent of high g-loads, wind gust speeds are not critical to determine. The left sides of the V-n plots are reasonable due to the well-known aerodynamics at low subsonic speeds. The right-side velocity limits, of max and limit dive speed, are really approximations due to the complexity of supersonic flows. The actual values would be determined with structural load limits and proper wind tunnel testing. The real design limit speeds would be determined with prototype testing.

## 12. Class II Weight and Balance

The purpose of this chapter is to develop more accurate weight estimations than previously determined in Class I W&B. This requires a more detailed breakdown of weight components and layout. Once the components have been placed, the same method as Class I is used to determine the aircraft cg. The moments and products of inertia are estimated, and the performance is reevaluated based on the criteria at the end of section 4.5 with the updated design parameters.

Note for the following calculations, all the weight estimation equations were developed using English units [21]. Therefore, the SI units of the AMT are converted to English to use the equations and are converted back after the calculations. The SI units use sea-level gravity as the reference. The equations used are for military trainer or fighter class of aircraft [25].

### 12.1 Known and Previous Weights

The known weights from previous design chapters are listed in Table 32. These include the crew, fuel, trapped fuel and oil, and the engine. The first three were approximated previously and the engine weight is given by the manufacture specifications. The other weights that are required is the estimated takeoff and empty weights. These will be used for the first iteration. Once the weight estimation of the components are determined, a new takeoff and empty will be used to iterate on the equations that require these parameters.

Table 32. Known and previous weights

Parameter	Weight, N(lbs)
Crew (2)	1,780(400)
Fuel	15,390(3,450)
Trapped F&O	211(47.4)
Engine	9,800(2,200)
W <sub>TO</sub>	50,322(11,290)
W <sub>E</sub>	32,935(7,390)

### 12.2 Revised Weight Estimates

#### 12.2.1 Structural Weight

The structural weight is a sum of the wing, empennage, fuselage and landing-gear as shown with equation (12.1). For other aircraft classes, additional component terms may be added as necessary to equation (12.1).

$$W_{str} = W_w + W_{emp} + W_{fus} + W_{lg} \quad (12.1)$$

##### 12.2.1.1 Wing

The wing weight is approximated with equation (6.2), which is reproduced below. All the wing's geometry is used from wing design chapter 6. The first iteration calculates the wing to 3,970N(890.6lbs).

$$W_w = 3.08 \left[ \left\{ \frac{K_{wn_{ult}} W_{TO}}{(l/c)_m} \right\} \left\{ \left( \tan(\Lambda_{LE}) - \frac{2(1-\lambda)}{AR(1+\lambda)} \right)^2 + 1.0 \right\} \cdot 10^{-6} \right]^{0.593} \left\{ AR(1+\lambda) \right\}^{0.89} S_w^{0.741}$$

##### 12.2.1.2 Empennage

The horizontal and vertical fins weight are approximated with equations (12.2) and (12.3). The 1.1 multiplier in equation (12.2) is to account for variable incidence stabilizer. In cases where the horizontal is

fixed, the multiplier is 1.0. The velocity dive limit is taken from the previous chapter. The horizontal and vertical fins' weight are calculated to be 409N(91.8lbs) and 607N(136lbs), respectfully.

$$W_h = 1.1S_h \left\{ 3.81 \frac{S_h^{0.2} \cdot V_{dL}}{1000[\cos(\Lambda_{c/2_h})]} - 0.287 \right\} \quad (12.2)$$

$$W_v = S_v \left\{ 3.81 \frac{S_v^{0.2} \cdot V_{dL}}{1000[\cos(\Lambda_{c/2_h})]} - 0.287 \right\} \quad (12.3)$$

### 12.2.1.3 Fuselage

The fuselage weight is approximated with equation (12.4). The term  $\bar{q}_L$  is the dynamic pressure dive limit as determined from the dive limit velocity in the previous chapter. The air density used for the dynamic pressure is taken at 5.0km. The length and height of the fuselage are taken from the CAD model, as 13.85m (45.4ft) and 1.70m (5.58ft), respectfully. The 14.51 multiplier in equation (12.4) is a correction factor that accounts for fuselage mounted inlets. For other type of mounted inlets [21] should be consulted. The first iteration of the fuselage weight is calculated to be 6,486N (1,455lbs).

$$W_{fus} = 14.51 \left( \frac{\bar{q}_L}{100} \right)^{0.245} \left( \frac{W_{TO}}{1000} \right)^{0.98} \left( \frac{\ell_{fus}}{h_{fus}} \right)^{0.61} \quad (12.4)$$

### 12.2.1.4 Landing-Gear

The landing-gear weight is approximated with equation (12.5). The first iteration of the landing-gear weight is calculated to be 2,079N (466.3lbs)

$$W_{lg} = 62.21 \left( \frac{W_{TO}}{1000} \right)^{0.84} \quad (12.5)$$

### 12.2.1.5 Structure Weight Summary

Table 33. AMT structure weight summary

Parameter	Weight, N(lbs)
Wing	3,970(890.6)
Horizontal	409(91.8)
Vertical Fins	608(136)
Fuselage	6,486(1,455)
Landing-Gear	2,079(466.3)
Total	13,550(3,040)

### 12.2.2 Powerplant Weight

The powerplant weight is a sum of the engine, air induction system, ramp (for supersonic aircraft), and fuel system, as shown in equation (12.6).

$$W_{pwr} = W_{eng} + W_{ai} + W_{ramp} + W_{fs} \quad (12.6)$$

### 12.2.2.1 Air Induction and Ramp System

The air induction system and intake ramp are approximated with equations (12.7) and (12.8), respectfully. The duct coefficient ( $K_d$ ) is 1.0 for curved cross sections and 1.33 for flat cross sections. The air induction system is calculated to be 767N (172lbs). The ramp intake is calculated to be 365N (81.9lbs).

$$W_{ai} = 11.45(\ell_{duct} \cdot N_{inl} \cdot \sqrt{A_{inl} K_d})^{0.7331} \quad (12.7)$$

$$W_{ramp} = 4.079\{\ell_{ramp} \cdot N_{inl} \cdot \sqrt{A_{inl}}\}^{1.201} \quad (12.8)$$

### 12.2.2.2 Fuel Management System

The fuel system is responsible for reducing cg change due to fuel burn. The fuel system is approximated using equation (12.9). The coefficient  $K_{fsp}$  is the density of the fuel. The USAF specifies JP-8 fuel, which has an average density of 820 kg/m<sup>3</sup> [25], this converts to about 6.8 lbs/gal. These are the appropriate units for equation (12.9). For other types of fuel systems, [25] can be consulted for appropriate fuel densities. The fuel system is calculated to be 652N (146lbs).

$$W_{fs} = 41.6 \left\{ \frac{W_F}{100K_{fsp}} \right\}^{0.818} + 7.91 \left\{ \frac{W_F}{100K_{fsp}} \right\}^{0.854} \quad (12.9)$$

### 12.2.2.3 Propulsion System

The propulsion system is composed of the engine controls and the starting system. Depending on the system, additional terms may be added to equation (12.10). The engine controls and electric starter are approximated from equation (12.11) and (12.12), respectfully. The propulsion system is calculated to be 396N (88.9lbs).

$$W_p = W_{ec} + W_{ess} \quad (12.10)$$

$$W_{ec} = 1.08(\ell_{fus} \cdot N_e)^{0.792} \quad (12.11)$$

$$W_{ess} = 38.93(W_{eng}/1000)^{0.918} \quad (12.12)$$

### 12.2.2.4 Powerplant Weight Summary

Table 34. AMT powerplant weight summary

Parameter	Weight, N(lbs)
Engine	9,800(2,200)
Air Induction	767(172)
Ramp Inlet	365(81.9)
Fuel Management System	652(146)
Propulsion system	396(88.9)
Total	11,990(2,690)

### 12.2.3 Fixed Equipment Weight

The fixed equipment weight is the sum of the appropriate components for the aircraft being designed. For the AMT equation (12.4) is used. Each of the components are explained in the following sub-sections.

$$W_{feq} = W_{fc} + W_{iae} + W_{els} + W_{api} + W_{ox} + W_{fur} + W_{aux} \quad (12.13)$$

### 12.2.3.1 Flight Control System

The flight control system is approximated with equation (12.14). For aircraft designs without a horizontal tail or with a variable sweep wing, the constant of 138 must be correct, see [25] pg. 100. The first iteration is calculated to be 2,478N (556lbs).

$$W_{fc} = 138 \left( \frac{W_{TO}}{1000} \right)^{0.581} \quad (12.14)$$

### 12.2.3.2 Instrumentation, Avionics, and Electronics

The instrumentation, avionics, and electronics are approximated with equation (12.15). The first iteration is calculated to be 918N (206lbs).

$$W_{iae} = 120 + 20N_{eng} + 0.006W_{TO} \quad (12.15)$$

### 12.2.3.3 Electrical System

The electrical system is approximated with equation (12.16). The first iteration is calculated to be 1,116N (250lbs).

$$W_{els} = 426 \left( \frac{W_{fs} + W_{iae}}{1000} \right)^{0.51} \quad (12.16)$$

### 12.2.3.4 Air-conditioning, Pressurization, and Anti-Icing Systems

The air-condition, pressurization, and anti-icing systems are approximated with equation (12.17). The first iteration calculation is 623N (140lbs).

$$W_{api} = 202 \left\{ \frac{W_{iae} + W_{crew}}{1000} \right\}^{0.53} \quad (12.17)$$

### 12.2.3.5 Oxygen System

The oxygen system is approximated with equation (12.18). The first iteration calculation is 212N (47.6lbs).

$$W_{ox} = 16.9(N_{crew})^{1.494} \quad (12.18)$$

### 12.2.3.6 Furnishings

Furnishings for trainers and fighters include ejection seats, insulation, trim panels, lighting, etc. The furnishings are approximated with equation (12.19). The first iteration is calculated to be 3,520N (789lbs).

$$W_{fur} = \underbrace{22.9 \left( \frac{N_{crew} \cdot \bar{q}_L}{100} \right)^{0.77}}_{\text{ejection seats}} + \underbrace{107 \left( \frac{N_{crew} \cdot W_{TO}}{100,000} \right)^{0.503}}_{\text{other}} \quad (12.19)$$

### 12.2.3.7 Auxiliary Gear

The auxiliary gear is used to account for other equipment not in the other categories and manufacturers variation. The auxiliary gear weight is approximated with equation (12.20). The first iteration is calculated to be 346N (77.5lbs).

$$W_{aux} = 0.01W_E \quad (12.20)$$

### 12.2.3.8 Fixed Equipment Weight Summary

Table 35. AMT fixed equipment weight summary

Parameter	Weight, N(lbs)
Flight Control System	2,480(556)
Instrumentation, Avionics, and Electronics	918(206)
Electrical System	1,116(250)
Air-conditioning, Pressurization, and Anti-Icing Systems	623(140)
Oxygen System	212(47.6)
Furnishings	3,520(789)
Auxiliary Gear	344(77.2)
Total	9,210(2,065)

## 12.3 Iterated Weight Summary

The equations used in section 12.2 that are function of  $W_{TO}$  must be iterated upon to determine a converged value for the empty weight. After three iterations, the difference between the initial and final values for  $W_E$  is less than 0.5%. When comparing the Class I to the final iteration of Class II weight sizing, the takeoff weights had a difference of 6%.

Many of the structure equations are based on much older aircraft that were manufactured with heavier materials. Composite parts can be 15 to 25% lighter than the older materials, and aluminum-lithium as 10% lighter [17]. Since the publishing of Roskam's *Airplane Design* series, large improvements in composite technology and manufacturing techniques make the claims more reasonable. Boeing has claimed approximately a 20% savings in weight, as a result of composite material use, as compared to aluminum alloys.

Since composite parts will be used in the AMT's structure, a conservative 5% reduction of the structure component weights will be employed. Table 36 summarizes the final iteration values along with the  $W_E$  and  $W_{TO}$ .

**Table 36. Summary of class I and class II AMT component weights with percent change**

Parameter	Weight, N(lbs)		%Change
	Class I	Class II	
Wing	4,455(999)	3,955(887)	-11
Horizontal		389(87)	
Vertical Fins	1,157(260)	577(129)	-17
Fuselage	6,083(1,358)	6,310(1,415)	+4.2
Landing-Gear	2,203(494)	2,110(473)	-4.2
Total	13,870(3,111)	13,340(2,293)	-1.3
Engine	9,800(2,200)	9,800(2,200)	0.0
Air Induction		767(172)	
Ramp Inlet		365(81.9)	
Fuel Management System	2,386(535)	701(157)	-6.6
Propulsion system		396(89)	
Total	12,190(2,735)	12,040(2,700)	-1.3
Flight Control System		2,595(582)	
Instrumentation, Avionics, and Electronics		943(210)	
Electrical System		1,140(255)	
Air-conditioning, Pressurization, and Anti-Icing Systems	6,875(1,542)	627(140)	+37
Oxygen System		212(48)	
Furnishings		3,530(790)	
Auxiliary Gear		355(80)	
Total	6,875(1,542)	9,400(2,110)	+35
Fuel	15,390(3,450)	15,390(3,450)	0.0
Crew	1,783(400)	1,783(400)	0.0
<b>W<sub>E</sub></b>	32,940(7,390)	34,990(7,850)	+6.7
<b>W<sub>TO</sub></b>	50,322(11,290)	52,160(11,700)	+4.4

The largest discrepancy between Class I and Class II weight sizing is the fixed equipment. After a review of the Class I weight fraction method, the discrepancy is a result of the averaged comparable aircraft  $W_{TO}$  being greater than the AMT's. This resulted in a lower weight fraction. When comparing the calculated fixed equipment weight to the comparable aircraft's fixed equipment weight, the results obtained are more agreeable than the weight fractions.

With that said, the overall structure and powerplant weights have a difference from Class I of less than 5% as recommended [21]. The fixed equipment weight is acceptable based on actual fixed equipment of comparable aircraft. The calculated Class II weights will be used for the proceeding analysis.

#### 12.4 Component Centers of Gravity

Following the same method from Class I W&B, each of the components are laid out and their positions are recorded. The cg of the AMT is determined with equation (8.1). The estimated position of the component weights are listed in Table 37. The resulting cg travel for the loading and unloading scenarios is shown in Figure 130. The fuel management system helps maintain A/C cg location, which is why there is one fuel unloading, as compared to the two fuel loadings. Table 38 lists the aircraft cg locations for the loading and unloading scenarios in Figure 130.

Table 37. Class II component weights and coordinates from reference point

Component	Weight (N)	X (m)	Y (m)	Z (m)
Wing	3954	13.97	0.0	5.68
Horizontal	389	18.03	0.0	5.2
Vertical (1)	289	16.76	-0.548	6.15
Vertical(2)	289	16.76	0.548	6.15
Fuselage	6310	11.60	0.0	5.36
Landing-Gear Nose	633	9.82	0.0	4.83
Landing-Gear Main	1478	13.9	0.0	4.95
Engine	9807	16.55	0.0	5.26
Air Induction	767	12.6	0	5.2
Ramp Inlet	365	10.9	0	5.6
Fuel Management System	701	12.3	0	5.25
Propulsion system	396	15.2	0	5.2
Flight Control System	2595	14.65	0	5.6
Instrumentation, Avionics, and Electronics	943	8.05	0	5.35
Electrical System	1141	6.65	0	5.1
Air-conditioning, Pressurization, and Anti-Icing Systems	627	11.55	0	6.05
Oxygen System	212	11.15	0	5.85
Furnishings	3528	9.23	0	5.44
Auxiliary Gear	355	11.05	0	5.47
Trapped Fuel & Oil	211.4	12.89	0	4.95
Fuel, Fuselage	8,290	12.08	0.0	5.20
Fuel, Wing	7,101	13.86	0.0	5.67
Crew(1)	892	8.78	0	5.62
Crew(2)	892	10.16	0	5.77
<b>Takeoff Weight</b>	<b>52,160</b>	<b>12.99</b>	<b>0.0</b>	<b>5.39</b>

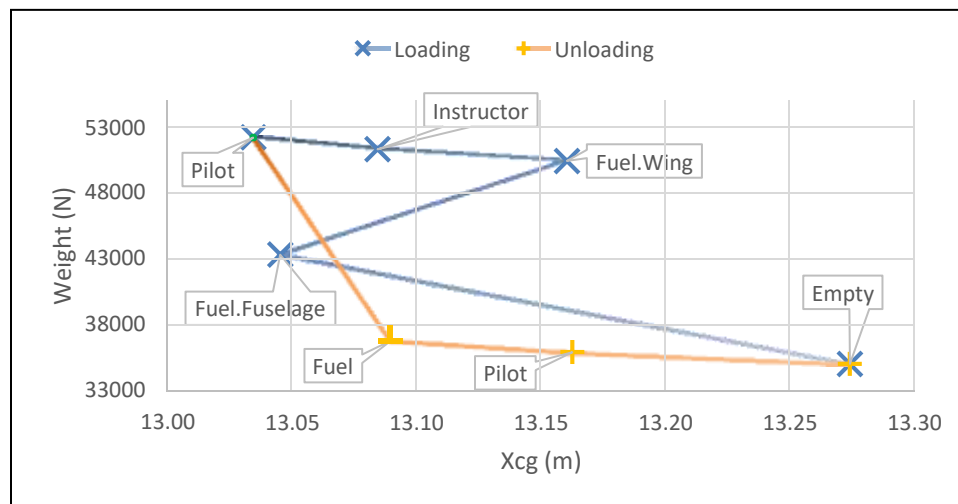


Figure 130.  $X_{cg}$  travel for Class II W&B from reference point for different loading scenarios

Table 38. Class II W&B center of gravity location for loading and unloading scenarios from reference point

<b>Loading</b>	<b>Weight (N)</b>	<b>X<sub>cg</sub> (m)</b>	<b>Y<sub>cg</sub> (m)</b>	<b>Z<sub>cg</sub> (m)</b>
Empty	34,990	13.27	0.00	5.38
Fuel <sub>Fuselage</sub>	43,280	13.01	0.00	5.34
Fuel <sub>Wing</sub>	50,380	13.11	0.00	5.38
Instructor	51,270	13.04	0.00	5.38
Pilot	52,160	12.99	0.00	5.39
<b>Unloading</b>	<b>Weight (N)</b>	<b>X<sub>cg</sub> (m)</b>	<b>Y<sub>cg</sub> (m)</b>	<b>Z<sub>cg</sub> (m)</b>
Fuel	36,770	13.09	0.00	5.40
Pilot	35,880	13.16	0.00	5.39
Instructor	34,990	13.27	0.00	5.38

### 12.4.1 Discussion

In chapter 8 it was determined that that the allowable cg travel is 22-43cm. This configuration has a cg travel of 24cm, which is acceptable. The decrease form 41cm in the Class I W&B is due to splitting the fuel between the wing and the fuselage. In the wing design chapter, it was determined the wing volume would not be adequate to contain all the fuel. In part to improve the design, an approximated volume is taken for the wing as shown by Figure 131. The fuel cell would be located between the spars and half the span of the wing. This results in a volume of 0.9m<sup>3</sup>, which is below the 1.3m<sup>3</sup> calculated in chapter 6. The fuselage fuel cell is determined to be placed aft of the cockpit between the inlet ducts as shown by Figure 132. The volume is determined from the difference of the required volume of 1.95m<sup>3</sup> and the wing volume, plus a 5% margin. This equates to the fuselage fuel cell volume equal to about 1.1m<sup>3</sup>.

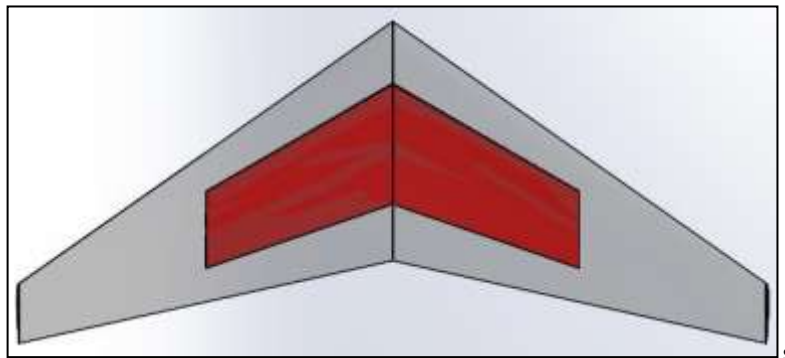


Figure 131. AMT wing fuel cell

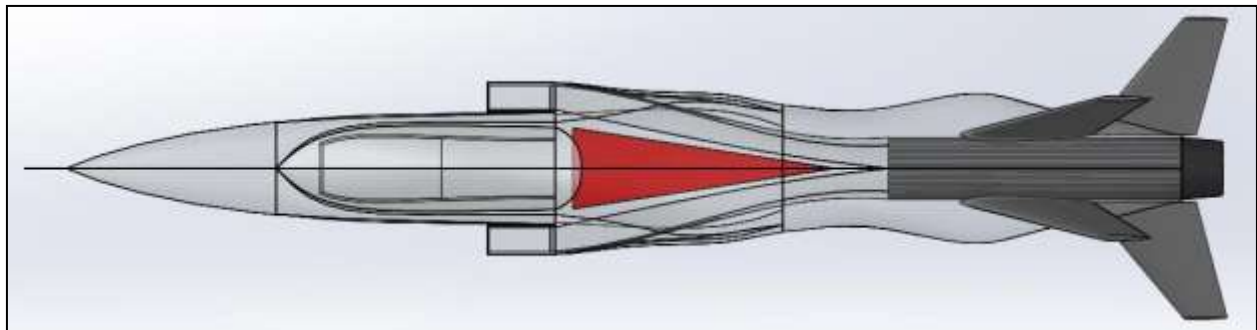


Figure 132. AMT fuselage fuel cell

The nose landing-gear has been moved aft and below the cockpit, so the nose conical area can be utilized for appropriate equipment and sensors. This was initially not considered for the Class I W&B. This is not a significant change in the design to warrant landing-gear reevaluation. The other significant change is the minimum and maximum cg travels have decrease by about 10cm. With a more forward cg, the static margin would increase providing more static longitudinal stability.

## 12.5 Aircraft Moments and Products of Inertia

The moments and products of inertia (MoI and PoI) of an aircraft are calculated with equations (12.21) through (12.26) [21]. The first terms in equation (12.21) through (12.26) are the individual components' MoI and PoI about their own cg. In the special case where a component's individual MoI and PoI is negligible and the list of components is large, the individual MoI and PoI of the components can be dropped from equations (12.21) through (12.26) [21].

$$I_{xx} = \sum_i^n I_{xx_i} + m_i \{ (y_i - y_{cg})^2 + (z_i - z_{cg})^2 \} \quad (12.21)$$

$$I_{yy} = \sum_i^n I_{yy_i} + m_i \{ (z_i - z_{cg})^2 + (x_i - x_{cg})^2 \} \quad (12.22)$$

$$I_{zz} = \sum_i^n I_{zz_i} + m_i \{ (x_i - x_{cg})^2 + (y_i - y_{cg})^2 \} \quad (12.23)$$

$$I_{xy} = \sum_i^n I_{xy_i} + m_i (x_i - x_{cg})(y_i - y_{cg}) \quad (12.24)$$

$$I_{yx} = \sum_i^n I_{yx_i} + m_i (y_i - y_{cg})(z_i - z_{cg}) \quad (12.25)$$

$$I_{zx} = \sum_i^n I_{zx} + m_i (z_i - z_{cg})(x_i + x_{cg}) \quad (12.26)$$

The individual components' MoI and PoI are unknown, and applying the simplified version of equations (12.21) through (12.26) lead to incorrect estimations. To obtain a better approximation, the Solidworks 3D model will be used. The model's components are the wing, horizontal, vertical fins, fuselage, engine, fuel and crew. All the other components' masses will be added to the overall fuselage mass. Each of the modeled components are assigned the masses determined in the Class II W&B. Using the *mass properties* in Solidworks, the approximate MoI and PoI of the AMT are determined. These values are listed in Table 39, along with the hand calculated values to see the comparison. For a comparison, The F-104 MoI [35] have been listed in Table 39. Though the F-104 is 45% heavier than the AMT, the values provide a reference to merit the approximate MoI and PoI for the AMT.

Table 39. Moments and products of inertia , units: kg·m<sup>2</sup>(slug·ft<sup>2</sup>)

Method	Configuration	I <sub>xx</sub>	I <sub>yy</sub>	I <sub>zz</sub>	I <sub>xy</sub>	I <sub>yz</sub>	I <sub>zx</sub>
By Hand	TO	325(240)	34,380(25,355)	34,090(25,140)	0.0	0.0	167(123)
	TO	4,350(3,210)	40,915(30,180)	44,030(32,470)	~0.0	~0.0	257(190)
Solidworks	50% Fuel	3,730(2,750)	39,800(29,355)	42,420(31,290)	~0.0	~0.0	100(75)
	0% Fuel	3,115(2,300)	38,640(28,500)	40,770(30,070)	~0.0	~0.0	-50(-40)
F-104	Cruise	4,880(3,600)	80,000(59,000)	81,350(60,000)	~0.0	~0.0	~0.0

## 12.6 Performance Reevaluated

The performance sizing from chapter 4 used many assumptions and simplifications. Through the design process parameters have changed, and analysis has provided better approximations that can be used for better performance approximations based on W/S and T/W. The initial drag polars considered used simplified drag polar estimation techniques. The revised drag polars provide a better approximation which should be applied to the AMT's aircraft performance. Based on the engine selected, the thrust available is significantly greater than previous sizing in section 4.3. The performance in section 4.5 is recalculated based on the analysis completed, the results are shown in Table 40. As a note, the max speed and Mach number are based off the Mach 1.5 drag polar.

Table 40. AMT performance reevaluated

Parameter	Value	Units	Condition
T <sub>AB</sub>	90.0(20.2)	kN(klbs)	Sea-level
T	60.0(13.5)		
W <sub>TO</sub>	52,160(11.7)	kN(klbs)	Sea-level
T <sub>AB</sub> /W <sub>TO</sub>	1.73	N/A	Sea-level
T/W <sub>TO</sub>	1.15		
W <sub>TO</sub> /S	2,830 (55.5)	N/m <sup>2</sup> (lb/ft <sup>2</sup> )	Takeoff Sea-level
S	18.4 (198)	m <sup>2</sup> (ft <sup>2</sup> )	N/A
V <sub>ST</sub>	56.6(186)	m/s (ft/s)	Sea-level C <sub>L,max</sub> = 1.44
S <sub>TOG</sub> w/AB	250 (810)	m (ft)	Alt = 2,500m (8,200ft) C <sub>L,max</sub> = 1.44
no AB	390 (1,280)		
S <sub>LaG</sub>	600 (1,975)	m (ft)	Alt = 2,500m (8,200 ft) C <sub>L,max</sub> = 1.44
CGR <sub>TO</sub> w/AB	1,175(7,137)	m/km(ft/nMile)	Alt = 2,500m, C <sub>L,cli</sub> = 1.2
no AB	710(4,320)		
RC <sub>sub</sub> w/AB	121(23.8)	m/s (kft/min)	Alt = 4,570m (15,000ft)
no AB	77.2(15.2)		
RC <sub>sup</sub> w/AB	23.3(4.58)	m/s (kft/min)	Alt = 5,486m (18,000ft)
no AB	11.2(2.20)		
V <sub>max</sub>	670(2,200)	m/s ft/s	Alt = 10km (32,800ft)
M <sub>max</sub>	2.1	---	Alt = 10.0km (18,000ft)
n	9.0	---	Alt = 5,486m (18,000ft)

### 13. Life-Cycle Cost Analysis

The cost analysis in the following sections uses the methods from [36]. The analysis covers prototype development cost, manufacturing and acquisition cost, operational cost, and disposal cost. Many of the cost functions were developed +30 years ago and must be corrected. The cost corrections are done with inflation rates and the cost escalation factor (CEF) defined by Figure 133. Many of the labor rates are given in [36] are for 1990s wages. To account for inflation, these values are multiplied by 1.9. The 90% increase was determined with an online inflation rate calculator.

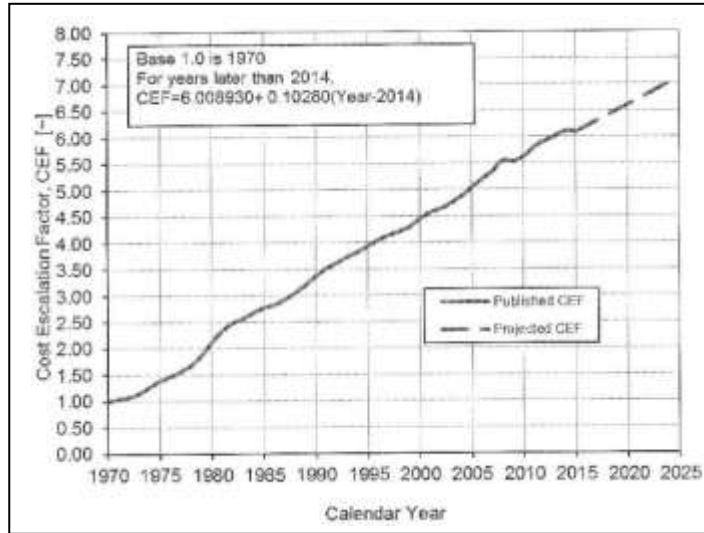


Figure 133. Change in CEF over time [36]

The life-cycle cost is approximated with equation (13.1).

$$LCC = C_{RDTE} + C_{MACQ} + C_{OPS} + C_{DISP} \quad (13.1)$$

Where,

$C_{RDTE}$	Research, development, testing, and evaluation cost (RDTE)
$C_{MACQ}$	Manufacturing and acquisition cost (MA)
$C_{OPS}$	Operational cost
$C_{DISP}$	Disposal cost

The following sections provide additional detail for each of the life-cycle cost components.

#### 13.1 Research, Development, Testing, and Evaluation Costs

The research, development, testing, and evaluation cost is approximated with equation (13.2).

$$C_{RDTE} = C_{aed_r} + C_{dst_r} + C_{pta_r} + C_{fto_r} + C_{tsf_r} + C_{pro_r} + C_{fin_r} \quad (13.2)$$

Where,

$C_{aed_r}$	airframe engineering and design cost (AED)
$C_{dst_r}$	development support and testing cost (DST)
$C_{pta_r}$	prototype test airplanes cost (PTA)
$C_{fto_r}$	flight test operation cost (FTO)
$C_{tsf_r}$	test and simulation facilities cost (TSF)

$C_{\text{pro}_r}$  RDTE profit  
 $C_{\text{fin}_r}$  RDTE finance cost

The following sections develop each of the RDTE cost contributions.

### 13.1.1 Airframe, Engineering, and Design Cost

The AED cost is approximated with equation (13.3). This is a function of:

$W_{\text{ampr}}$  aeronautical manufacturers planning report weight  
 $V_{\text{max}}$  max level speed  
 $N_{\text{rdte}}$  number of prototype testing planes  
 $F_{\text{diff}}$  design difficulty factor  
 $F_{\text{cad}}$  manufacturer CAD experience factor  
 $R_{e_r}$  average engineering rate

The constant number in the equation (13.3) is based on English units.

$$C_{\text{aed}_r} = 0.0396 W_{\text{ampr}}^{0.791} \cdot V_{\text{max}}^{1.526} \cdot N_{\text{rdte}}^{0.183} \cdot F_{\text{diff}} \cdot F_{\text{cad}} \cdot R_{e_r} \quad (13.3)$$

The ampr weight is approximately the structural weight of the aircraft, therefore the AMT's  $W_{\text{ampr}}$  is 13,340N (2,990lbs). The maximum speed was determined to be 670m/s(1,300KEAS) in chapter 11. For military planes,  $N_{\text{rdte}}$  is 6 – 20 [36]. Since the AMT is a simple conventional advanced trainer, 6 planes will be considered for the  $N_{\text{rdte}}$ . The AMT is not a complex design, so 1.0 is used for  $F_{\text{diff}}$ . Since 3D modeling is an industry normal, most manufactures should have extensive experience with CAD, so  $F_{\text{cda}}$  is 0.8. The hourly rate for an engineer was about 60USD/hr in 1990s [36]. Accounting for inflation, the  $R_{e_r}$  is assumed to be 115USD/hr. The AED cost is calculated to be \$16.1 million.

### 13.1.2 Development, Support, and Testing Cost

The DST cost generally covers windtunnel, systems, structure, propulsion, and simulation testing. The DST cost is approximated with equation (13.4). The CEF is determined from Figure 133.

$$C_{\text{dst}_r} = 0.008325 W_{\text{ampr}}^{0.873} \cdot V_{\text{max}}^{1.890} \cdot N_{\text{rdte}}^{0.346} \cdot \text{CEF} \cdot F_{\text{diff}} \quad (13.4)$$

The CEF is taken as 6.5. Using the previously determined parameters, the DST cost is calculated to be \$83.9 million.

### 13.1.3 Prototype Test Airplanes Cost

The prototype test airplanes (PTA) cost consists of:

$C_{\text{ea}_r}$  engine and avionics cost  
 $C_{\text{man}_r}$  labor cost  
 $C_{\text{mat}_r}$  materials cost  
 $C_{\text{tool}_r}$  tools cost  
 $C_{\text{qc}_r}$  quality control

The PTA is approximated with equation (13.5).

$$C_{\text{pta}_r} = C_{\text{ea}_r} + C_{\text{man}_r} + C_{\text{mat}_r} + C_{\text{tool}_r} + C_{\text{qc}_r} \quad (13.5)$$

### 13.1.3.1 Engine and Avionics Cost

The engine and avionics ( $EA_r$ ) cost is approximated with equation (13.6). This depends on the cost of the engine ( $C_{e_r}$ ), number of engines per plane ( $N_e$ ), avionics cost ( $C_{a_r}$ ), and the number of prototype test planes.

$$C_{ea_r} = (C_{e_r} \cdot N_e + C_{a_r}) \cdot N_{rdte} \quad (13.6)$$

The EJ200 is reported to cost \$8.5M by deagel.com, which reports on military and commercial aviation. Each aircraft only has one engine. For the F-14 to F-18 aircraft, avionics can cost %50 to %100 of the cost of the propulsion system. Since this is a trainer, fewer systems are needed. Therefore, the avionics cost is assumed to be %30 of the propulsion system. The engine and avionics cost is calculated to be \$66.3 million.

### 13.1.3.2 Manufacturing Labor Cost

The manufacturing labor ( $MAN_r$ ) cost is approximated with equation (13.7). The hourly rate for manufacturing labor was about 35USD/hr in 1990s [36]. Accounting for inflation, the  $R_{m_r}$  is assumed to be 66.5USD/hr.

$$C_{man_r} = 28.984 W_{ampr}^{0.740} \cdot V_{max}^{0.543} \cdot N_{rdte}^{0.524} \cdot F_{diff} \cdot R_{m_r} \quad (13.7)$$

The manufacturing labor cost is calculated to be \$90.4 million.

### 13.1.3.3 Manufacturing Materials Cost

The manufacturing materials ( $MAT_r$ ) cost is approximated with equation (13.8). The correction factor ( $F_{mat}$ ) is dependent on the type of materials used. Where  $F_{mat}$  is 1.0 for conventional aluminum alloys, 2.0 for conventional composites, and 3.0 for carbon fiber composites. The AMT will feature a combination of all three types of materials. Therefore,  $F_{mat}$  is assumed to be 2.0.

$$C_{mat_r} = 37.632 F_{mat} \cdot W_{ampr}^{0.689} \cdot V_{max}^{0.624} \cdot N_{rdte}^{0.792} \cdot CEF \quad (13.8)$$

The manufacturing materials is calculated to be \$44.1 million.

### 13.1.3.4 Tooling Cost

The tooling cost is approximated with equation (13.9). The undefined symbols are the production rate per month ( $N_{r_r}$ ) and the tooling labor rate ( $R_{t_r}$ ). The production rate per month is 0.33 may be assumed [36]. The hourly rate for tooling labor was about 45USD/hr in 1990s [36]. Accounting for inflation, the  $R_{t_r}$  is assumed to be 85.5USD/hr.

$$C_{tool_r} = 4.0127 W_{ampr}^{0.764} \cdot V_{max}^{0.899} \cdot N_{rdte}^{0.178} \cdot N_{r_r}^{0.066} \cdot F_{diff} \cdot R_{t_r} \quad (13.9)$$

The tooling cost is calculated to be \$125 million.

### 13.1.3.5 Quality Control (QC) Cost

The quality control cost is approximated as a percent of the manufacturing cost with equation (13.10)

$$C_{qc_r} = 0.13 C_{man_r} \quad (13.10)$$

The quality control is calculated to be \$11.8 million.

### 13.1.3.6 Summary of Prototype Test Aircraft Costs

The summary of the PTA costs and total PTA cost is listed in Table 41. Figure 134 shows the percent breakdown of the prototype test airplanes.

Table 41. Summary of prototype test airplanes costs

Parameter	USD \$
Engine & Avionics	66.3M
Manufacture Labor	90.4M
Manufacturing Materials	44.1M
Tooling	125M
Quality Control	11.8M
Prototype Test Airplanes Cost	338M

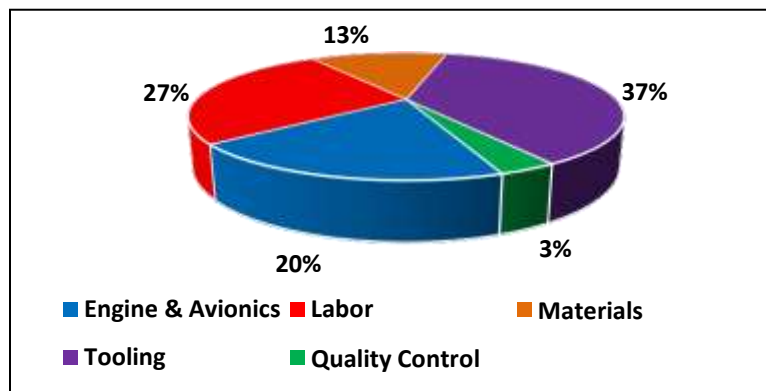


Figure 134. Prototype test airplanes cost percentages

### 13.1.4 Flight Test Operation Cost

The FTO cost is approximated with equation (13.11). For flight testing inherently unstable airplanes or stealth observability, an additional multiplier would be added to equation (13.11). The AMT does not have any complexities that would require outside the normal prototype flight testing.

$$C_{fto_r} = 0.001244W^{1.160} \cdot V_{ampr}^{1.370} \cdot N_{max}^{1.281} \cdot CEF \cdot F_{rdte} \quad \text{diff} \quad (13.11)$$

The FTO cost is calculated to be \$12.2 million.

### 13.1.5 Test and Simulation Facilities Cost

The TSF cost is to account for the building of special facilities related to a specific aircraft design. Examples of this are the B-2 and X-29. The cost of the TSF is considered a fraction of the overall RDTE cost. The AMT does not require any special facilities and therefore, this cost is \$0.

### 13.1.6 RDTE Profit

The RDTE profit is to account for the fact that a company performing the RDTE would like to make money. A recommended value to assume for profit cost is 10% of the total RDTE cost [36]. Therefore, the profit cost can be expressed by equation (13.12).

$$C_{pro_r} = F_{pro_r} \cdot C_{RDTE} \quad (13.12)$$

The profit cost is calculated to be \$56.3 million.

### 13.1.7 RDTE Finance Cost

The RDTE finance cost is to account for cost associated with borrowing money to perform the RDTE. Regardless if a well-financed company has the capital, the capital to perform the RDTE has a cost. A recommended value to assume for the finance cost is 10-20% of the total RDTE cost [36]. Therefore, the finance cost can be expressed by equation (13.13). A finance cost of 10% will be used for the AMT.

$$C_{fin_r} = F_{fin_r} \cdot C_{RDTE} \quad (13.13)$$

The profit cost is calculated to be \$56.3 million.

### 13.1.8 Summary of RDTE Costs

The total cost of RDTE is calculated with equation (13.14). The summary of the RDTE costs are listed in Table 42. The percent breakdown of the RDTE cost can be seen in Figure 135.

$$C_{RDTE} = \frac{C_{aed_r} + C_{dst_r} + C_{pta_r} + C_{fto_r}}{1 - F_{pror} - F_{fin_r}} \quad (13.14)$$

Table 42. Summary of RDTE

Parameter	USD \$
AED <sub>r</sub>	16.1M
DST <sub>r</sub>	83.9M
PTA <sub>r</sub>	338M
FTO <sub>r</sub>	12.2M
TSF <sub>r</sub>	0
RDTE Profit	56.3
RDTE Finance	56.3
RDTE Total	563M

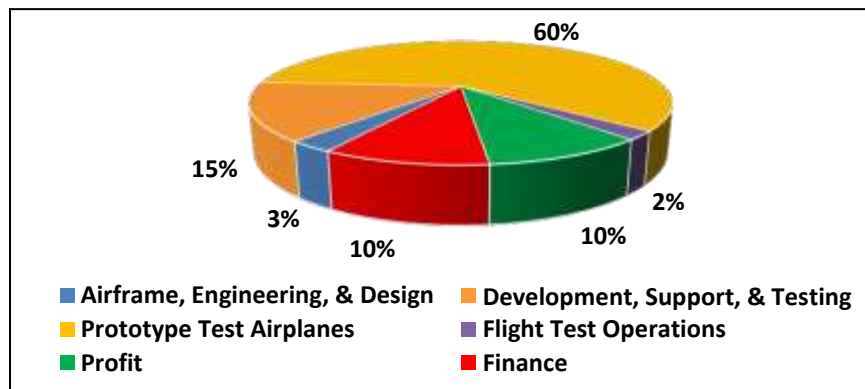


Figure 135. Research, development, testing, and evaluation cost percentages

## 13.2 Manufacturing and Acquisition Cost

The manufacturing and acquisition cost is similar to RDTE cost. Airframe engineering and design ( $C_{aed_m}$ ) is necessary to correct any problems found during the RDTE phase. The Aircraft program production ( $C_{apc_m}$ ) is the cost of producing the aircraft. The production flight test operations ( $C_{fto_m}$ ) verifies

basic handling qualities of the aircraft. Finance ( $C_{fin_m}$ ) and profit ( $C_{pro_m}$ ) costs are the same definitions as in the RDTE cost but applied to producing the aircraft. Many of the components of the MA cost approximation are the same or very similar to the cost approximations used for the RDTE. The main difference being the second subscript, where r was used for RDTE and m is used for MA.

$$C_{MA} = C_{aed_m} + C_{apc_m} + C_{fto_m} + C_{fin_m} + C_{pro_m} \quad (13.15)$$

### 13.2.1 Airframe, Engineering, and Design Cost

The  $AED_m$  is calculated similarly to the  $AED_r$  cost. The exceptions are that the number of planes to produce ( $N_{MA}$ ) is for the total production, and the  $AED_r$  cost is subtracted so as not to account for AED cost that has previously been done.

$$C_{aed_m} = 0.0396 W_{ampr}^{0.791} \cdot V_{max}^{1.526} \cdot N_{MA}^{0.183} \cdot F_{diff} \cdot F_{cad} \cdot R_{em} - C_{aed_r} \quad (13.16)$$

The USAF is asking for an initial 350 aircraft. Using the values previously determined in 13.1, the calculated  $AED_m$  cost is \$323 million.

### 13.2.2 Aircraft Production (APC<sub>m</sub>) Cost

The  $APC_m$  cost is similar to the prototype test airplanes cost.

$$C_{apc_m} = C_{eam} + C_{man_m} + C_{mat_m} + C_{tool_m} + C_{qc_m} \quad (13.17)$$

#### 13.2.2.1 Engine and Avionics Cost

The  $EA_m$  cost is approximated with equation (13.18). Equation (13.18) is similar to equation (13.6) but the number of research planes is corrected to the number of planes being manufactured.

$$C_{eam} = (C_{em} \cdot N_e + C_{ar}) \cdot N_{MA} \quad (13.18)$$

The engine and avionics cost is calculated to be \$3.87 billion.

#### 13.2.2.2 Manufacturing Labor Cost

The manufacturing labor cost is approximated with equation (13.19). The MA manufacturing labor rate is the same as the RDTE manufacturing labor rate in 13.1.3.

$$C_{man_m} = 28.984 W_{ampr}^{0.740} \cdot V_{max}^{0.543} \cdot N_{MA}^{0.524} \cdot F_{diff} \cdot R_{m_m} - C_{man_r} \quad (13.19)$$

The manufacturing labor cost is calculated to be \$671 million.

#### 13.2.2.3 Manufacturing Materials Cost

The manufacturing materials cost is approximated with equation (13.20).

$$C_{mat_m} = 37.632 F_{mat} \cdot W_{ampr}^{0.689} \cdot V_{max}^{0.624} \cdot N_{MA}^{0.792} \cdot CEF - C_{mat_r} \quad (13.20)$$

The MA manufacturing materials cost is calculated to be \$1.06 billion.

### 13.2.2.4 Tooling Cost

The MA tooling cost is approximated with equation (13.21). The production rate ( $N_{R_m}$ ) is assumed to be 0.33. The MA tooling labor rate ( $R_{t_m}$ ) is the same as the RDTE tooling labor rate.

$$C_{\text{tool}_m} = 4.0127 W_{\text{ampr}}^{0.764} \cdot V_{\text{max}}^{0.899} \cdot N_{\text{MA}}^{0.178} \cdot N_{r_m}^{0.066} \cdot F_{\text{diff}} \cdot R_{t_m} - C_{\text{tool}_r} \quad (13.21)$$

The MA tooling cost is calculated to be \$133 million.

### 13.2.2.5 Quality Control Cost

The MA quality control cost is approximated the same as the RDTE quality control with equation (13.10). The quality control is calculated to be \$87.2 million.

### 13.2.2.6 Summary of APC<sub>m</sub> Costs

The summary of the APC<sub>m</sub> costs and total APC<sub>m</sub> cost is listed in Table 43. Figure 136 shows the percent breakdown of the aircraft production costs.

Table 43. Summary of APC costs

Parameter	USD \$
Engine & Avionics	3.87B
Manufacture Labor	671M
Manufacturing Materials	1.06B
Tooling	133M
Quality Control	87.2M
Aircraft Production	5.82B

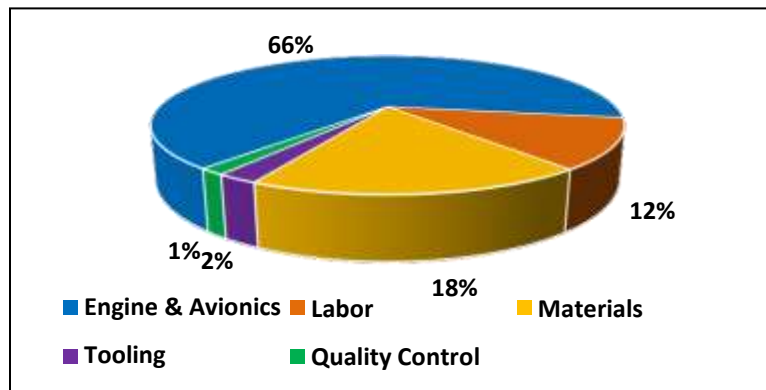


Figure 136. Aircraft production cost percentages

### 13.2.3 Production Flight Test Operations Cost

The production flight test operations (FTO<sub>m</sub>) cost is approximated with equation (13.22). The operational cost per hour ( $C_{\text{ops/hr}}$ ) is determined in section 13.3.7. The  $C_{\text{ops/hr}}$  is calculated to be \$2,400/hr. A recommended 20hrs be used for military flight test hours ( $t_{\text{pft}}$ ) [36]. The overhead factor ( $F_{\text{ftoh}}$ ) is recommended to be 4.0 when no data is available.

$$C_{\text{fto}_m} = N_{\text{MA}} \cdot C_{\text{ops/hr}} \cdot t_{\text{pft}} \cdot F_{\text{ftoh}} \quad (13.22)$$

The production flight test operations cost is calculated to be \$66.9 million.

### 13.2.4 Manufacturing Finance Cost

The manufacturing finance cost is calculated in the same manner for the RDTE finance cost using equation (13.23). The finance factor ( $F_{fin_m}$ ) is assumed to be 10%.

$$C_{fin_m} = F_{fin_m} \cdot C_{MA} \quad (13.23)$$

The manufacturing finance cost is calculated to be \$776 million.

### 13.2.5 Manufacturing Profit Cost

The manufacturing profit cost is calculated in the same fashion as the RDTE profit cost using equation (13.24). The profit factor ( $F_{prom}$ ) is assumed to be 10%.

$$C_{prom} = F_{prom} \cdot C_{MA} \quad (13.24)$$

The manufacturing profit cost is calculated to be \$776 million.

### 13.2.6 Summary of Manufacturing and Acquisition Cost

The resulting MA cost can be determined with equation (13.25). Table 44 summarizes the MA costs and Figure 137 shows the percent breakdown of the MA cost.

$$C_{MA} = \frac{C_{aed_m} + C_{apc_m} + C_{fto_m}}{1 - F_{fin_m} - F_{prom}} \quad (13.25)$$

Table 44. Summary of manufacturing and acquisition cost

Parameter	USD \$
AED <sub>m</sub>	323M
APC <sub>m</sub>	5.82B
FTO <sub>m</sub>	66.9M
MA Finance	776M
MA Profit	776M
Total Manufacturing and Acquisition Cost	7.76B

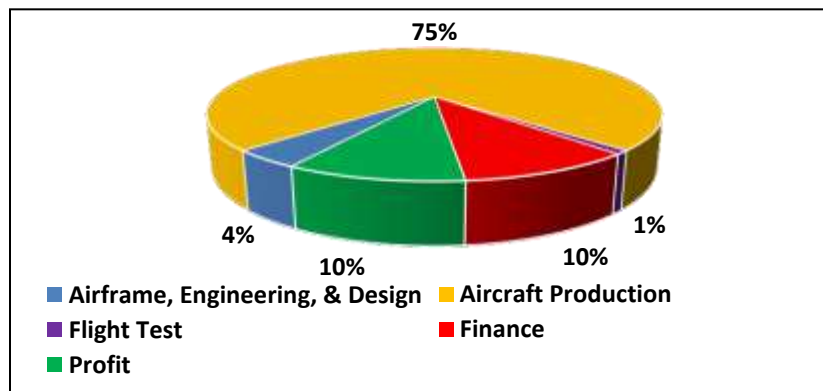


Figure 137. Manufacturing and acquisition cost percentages

### 13.3 Operating Cost

The operating cost covers all the required expenses of operating the aircraft. For a military aircraft, the significant contributors are the following:

- $C_{FOL}$  fuel, oil, and lubricants costs
- $C_{PERSDIR}$  direct personnel cost
- $C_{PERSIND}$  indirect personnel cost
- $C_{CONMAT}$  consumable materials cost
- $C_{SPARES}$  spares cost
- $C_{MISC}$  miscellaneous and other costs

The operating cost is approximated with equation (13.26). For the following sections, the calculations will use the minimum and maximum annual flight hours 600 and 1,000 for a military train [36].

$$C_{OPS} = C_{FOL} + C_{PERSDIR} + C_{PERSIND} + C_{CONMAT} + C_{SPARES} + C_{MISC} \quad (13.26)$$

#### 13.3.1 Fuel, Oil, and Lubricants (FOL) Cost

The fuel, oil, and lubricants cost is approximated with equation (13.27). This depends on the fuel price (FP), fuel density (FD), number of missions ( $N_{MISSION}$ ), number of planes in service ( $N_{SERV}$ ), and the service life of the plane ( $N_{YR}$ ).

$$C_{FOL} = 1.05W_{Fused} \cdot \frac{FP}{FD} \cdot N_{MISSION} \cdot N_{SERV} \cdot N_{YR} \quad (13.27)$$

The average fuel consumed per flight is about 1,325kg without counting the reserves fuel, as determined in chapter 3 weight sizing. The price of JP-8 is about \$3/gal [37], which equates to \$0.79/L. The converted fuel density is about 0.8kg/L. Assuming the average flight time is 1.5hrs, the number of missions is 400 to 667/yr. The number of planes in service are assumed to be about 30% of the 351 planes acquired. The service life is assumed to be half of the T-38's at 30yr. The cost of the fuel, oil, and lubricants is about \$1.66 to \$2.77 billion.

#### 13.3.2 Direct Personnel Cost

The direct personnel cost is a result of flight and maintenance crews, and is approximated using equation (13.28). It should be assumed that the crew ratio ( $R_{CR}$ ) as zero [36], [38]. There is no explanation for this in either reference. The most logical reason is that trainers are used for learning and therefore, the crews are not directly paid to operate the aircraft. Based on this, the direct personnel cost for a trainer is only a result of the maintained crews.

$$C_{PERSDIR} = N_{SERV} \cdot N_{YR} (N_{CREW} \cdot R_{CR} \cdot \$_{CREW} \cdot OHR_{CREW} + U_{ANNFLT} \cdot MHR_{FLHR} \cdot R_{MML}) \quad (13.28)$$

The annual hourly usage was previously determined to be 600hrs/yr. The maintenance manhours ( $MHR_{FLHR}$ ) is assumed to be 10 manhours/flight-hour, based on the T-38 maintenance manhours [36]. The military maintenance labor rate ( $R_{MML}$ ) in 1989 as 45USD/hr [36]. Adjusting for a 90% inflation rate to today's USD,  $R_{MML}$  is assumed to be 85USD/hr. The resulting direct personnel cost for the AMT is calculated to be \$1.53 to \$2.55 billion.

#### 13.3.3 Indirect Personnel Cost

Indirect personnel covers all other personnel required for the operation of an aircraft, which are not directly involved in the flight operations. For military trainers the fractional cost of indirect personnel is negligible since the flight missions are only for training purposes. In cases where indirect personnel cost must be considered, equation (13.29) is used.

$$C_{\text{PERSIDR}} = f_{\text{PERSIND}} \cdot C_{\text{OPS}} \quad (13.29)$$

### 13.3.4 Consumable Materials Cost

The consumable materials covers the materials used in the maintenance of the aircraft. The consumable materials cost is approximated with equation (13.30).

$$C_{\text{CONMAT}} = N_{\text{SERV}} \cdot N_{\text{YR}} \cdot U_{\text{ANNFLT}} \cdot \text{MHR}_{\text{FLHR}} \cdot R_{\text{CONMAT}} \quad (13.30)$$

The average cost of consumable materials ( $R_{\text{CONMAT}}$ ) is recommended to be taken as 6.5 USD/hr [36]. This value must be multiplied by an inflation rate to properly account for the cost. Therefore, this value is assumed to be 12.35. All other terms have been defined. The consumable materials cost is calculated to be \$222 to \$371 million.

### 13.3.5 Spares Cost

No spares are considered for the AMT. Any spares are covered under the USAF procurement of the 350 aircraft. When spares must be accounted for, equation (13.31) is used. The coefficient  $f_{\text{SPARES}}$  is determined from comparable planes in service.

$$C_{\text{SPARES}} = f_{\text{SPARES}} \cdot C_{\text{OPS}} \quad (13.31)$$

### 13.3.6 Miscellaneous Costs

The miscellaneous costs are those that don't fall under the other cost categories. Miscellaneous costs can be approximated, similar to spares or indirect personnel costs, as a fraction of the operational costs. For military aircraft, miscellaneous costs can be approximated with equation (13.32).

$$C_{\text{MISC}} = 4C_{\text{CONMAT}} \quad (13.32)$$

Base on the consumable materials cost, the miscellaneous cost is \$889 million to \$1.48 billion.

### 13.3.7 Summary of Operating Costs

The operational costs of the AMT are approximated with equation (13.33). Since different types of planes have different missions, a way to compare their costs is with the operational cost per hour. The operational cost per hour is calculated with equation (13.34). Table 45 summarizes the operational costs for the AMT. Figure 138 shows the percent breakdown of the operational costs.

$$C_{\text{OPS}} = \frac{C_{\text{FOL}} + C_{\text{PERSDIR}} + C_{\text{CONMAT}} + C_{\text{MISC}}}{1 - f_{\text{PERSIND}} - f_{\text{SPARES}}} \quad (13.33)$$

$$C_{\text{ops/hr}} = \frac{C_{\text{OPS}}}{N_{\text{SERV}} \cdot N_{\text{YR}} \cdot U_{\text{annflt}}} \quad (13.34)$$

Table 45. Summary of operational costs

Annual Flight Hours	600	1000
Parameter	US\$	
C <sub>FOL</sub>	1.66B	2.77B
C <sub>PERSDIR</sub>	1.53B	2.55B
C <sub>CONMAT</sub>	0.222B	0.371B
C <sub>MISC</sub>	0.889B	1.48B
<b>Total(US\$ Today for 30yrs)</b>	<b>4.30B</b>	<b>7.17B</b>
<b>Cost/hr</b>	<b>\$2,400/hr</b>	<b>\$2,400/hr</b>

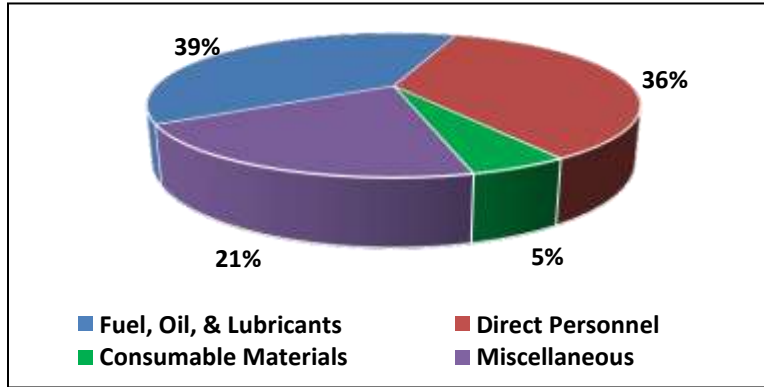


Figure 138. Operational cost percentages

### 13.4 Disposal Cost

There comes a point when an aircraft is considered not to have any value and at this point it must be disposed of. The costs associated with disposal are temporary storage, draining of liquids and oils, disassembly of engines and electronics, and cutting of the airframe. Any responsible engineer should account for these costs in the LCC of an aircraft instead of leaving such responsibilities to the future generations. There are certain components that can be recycled but the fact stands there is a cost that must be accounted for the disposal. The method to account for disposal costs is to consider a fudge factor of 1% of the total LCC by equation [36]. Upon further research, no definitive method could be found to account for the future cost of disposal. Therefore, the method provided by [36] will be used with equation (13.35)

$$C_{DISP} = 0.01LCC \quad (13.35)$$

The disposal cost is calculated to be \$128-157 million.

### 13.5 Summary of Life-Cycle Cost

Considering the disposal cost equation, the life-cycle cost is calculated by equation (13.36). Table 46 summarizes the individual costs and the life-cycle cost of the AMT. Figure 139 shows the comparison and percent breakdown of the LCC depending on the spectrum ends of the flight hours per year.

$$LCC = \frac{C_{RDTE} + C_{MA} + C_{OPS}}{0.99} \quad (13.36)$$

Table 46. Summary of LCC

Parameter	USD \$
Research, Development, Testing, and Evaluation	563M
Manufacturing and Acquisition	7.76B
Operation	4.3-7.17B
Disposal	128-157M
<b>Life-Cycle Cost</b>	<b>12.8-15.7B</b>

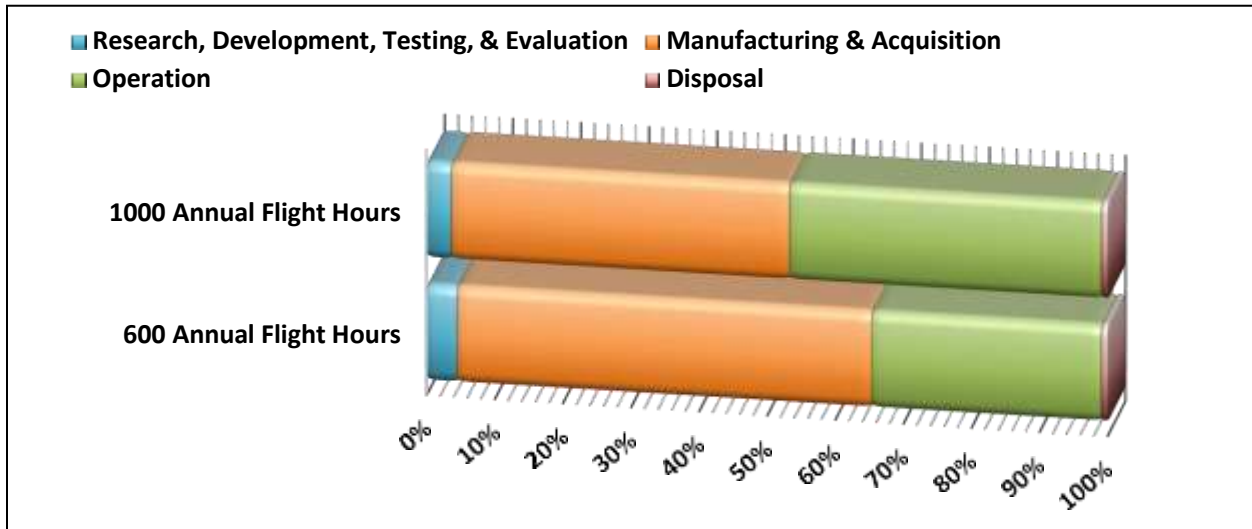


Figure 139. Life-cycle cost percentages

### 13.6 Discussion

In chapter 1, it was discussed that the USAF estimated the program would cost \$16 billion. In this comparison the approximated LCC seems reasonable. Unfortunately, the T-X program contract awarded to the Boeing-Saab partnership was for approximately \$9.2 billion [39]. This is for 351 aircraft and 46 flight simulators. In this regard, the methods used from [36] overly prices the AMT for the T-X program. This is not the whole picture.

The contract awarded to Boeing-Saab did not specify a life-cycle length or annual flight hours. These were big assumptions in the LCC approximations. Also, many of the labor rates were based off almost 30-year-old wage approximations that were corrected for the inflation. Based off section 13.2.2, the engine and avionics are a significant cost in the manufacturing of the AMT. The approximations used may be grossly overpriced. A critical stage in the next iteration of the cost analysis would be to obtain more real-world pricing for labor rates and suppliers. Overall, the estimations performed in this chapter provides a top-level starting point to develop more concrete approximations in the cost of the AMT. Finding real-world data for individual life-cycle cost contributions for military aircraft is difficult and therefore, there is no way to accurately make a comparison of the individual costs calculated.

## 14. Final Design

The purpose of this chapter is discuss environmental concerns, safety concerns, summary of the AMT's design, and compare the AMT's design to Boeing/Saab's design that secured the USAF contract for the T-X program.

### 14.1 Environmental and Economic Tradeoffs

A global concern is climate change due to man-made greenhouse gas emissions. The International Air Transport Association (IATA) reports that air travel is responsible for 2% of the world's man-made CO<sub>2</sub> emissions [40], and an estimated 11% of the total transportation emissions are related to air travel [41]. The EPA lists transportation emissions at 28% of the global emissions. As a global problem, all contributors of greenhouse gas emissions must look to reduce their emissions.

From a historical perspective, 50 years ago greenhouse gas emissions were not a public concern. The state of the world was different, and the major concerns were nuclear war with Russia. 25 years ago, the public concern grew and continues to increase to the present day. Now we live in a time where if the problem is not addressed, many scientists believe the consequences of our actions could be irreversible.

The Department of Defense (DoD) is the largest government consumer of energy and is estimated to obtain 2/3 of this energy from liquid-based fossil fuels [41]. As part of the global initiative, the DoD is looking to implement more green energy methods to reduce its CO<sub>2</sub> emissions. The reasons are to reduce the military's dependence on fossil fuels and fossil fuel supply chains [42]. Implementing more green energy reduces the military's outside dependence of energy resources, and improves the resilience and security of military bases from natural and man-made disasters [42]. Generally, the military has a large influence on research and growing technologies. With the military looking to go green, this should increase the overall funding of green technology and eventually be passed on to the public for use.

The USAF is a large consumer of fossil fuels in the military. The USAF is reported to use over 2.4 billion gallons of jet fuel annually and has approximately 260 green energy projects [43]. The goal of the green energy projects are to transform domestic military bases to net-zero energy status. Other goals are to improve the efficiency of vehicle fuel consumption and transfer some flight training to simulators. As part of the T-X program, a requirement of the USAF is to have a specific fuel consumption 10% better than the T-38 and compatible simulators to augment specific training exercises that do not require "real" flight time. One of the reasons for the USAF high fuel consumptions is the constant training and flight exercises. As a first-hand witness during an internship, with The Aerospace Corporation at Hill AF base in Utah, every day the airstrip was utilized for incoming and outgoing flights, and every two to three days, squadrons of F-35s were conducting flight exercises.

The ultimate solution to reduce military greenhouse gas emissions, is to remove the need for the military. It is not practical and there will always be the need for the military. The more practical solution is the one that is already being implemented. Researching and improving renewable energy sources. For aircraft, many manufactures are exploring biofuels, hybrid propulsion systems, and electrical propulsion. These technologies are still young but with the military looking to implement them, the industry will be receiving a good financial boost to explore these green technologies.

### 14.2 Safety and Economic Tradeoffs

The USAF current advanced trainer, the T-38, first flew in 1959. Between 1961 and 1971 over 1,100 T-38 deliveries were made to the USAF [44]. With the T-38s approaching the 50- and 60-year mark, the T-38s have required improvements and modernization to extend the life of the T-38s. A large safety concern

was T-38s with many flight hours that showed signs of structural fatigue. Upgrades for this class of T-38s are new wings and various structural improvements kits [44], see Figure 140.

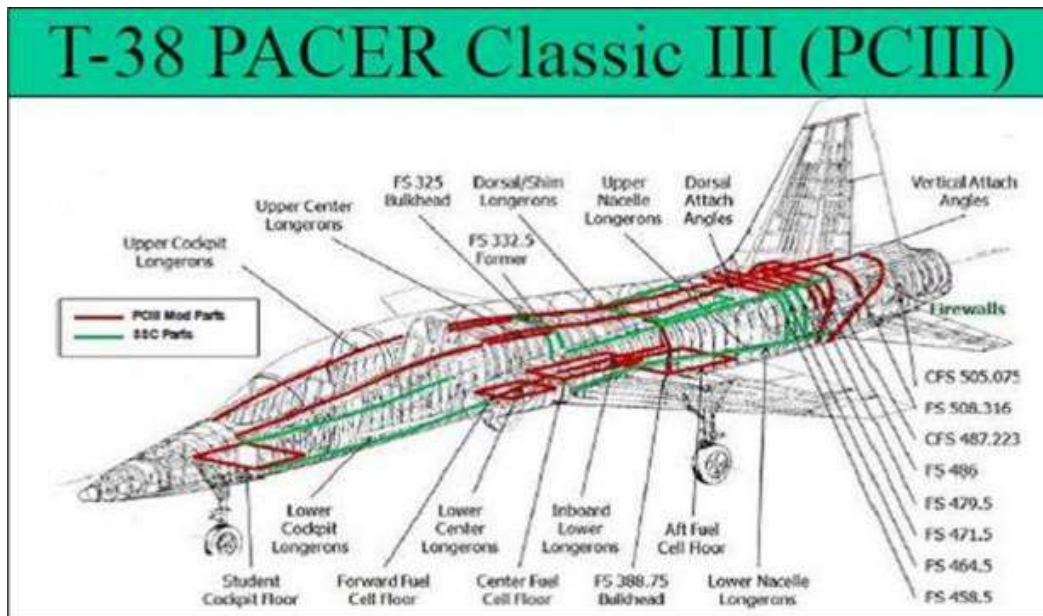


Figure 140. T-38 structure upgrades [44]

Obviously, the main safety concern for the USAF is the aging T-38 trainers and the fatigue they have endured over the 50 to 60 years of service. The idea of replacing the T-38 with a new aircraft is to eliminate these problems associated with old aircraft. The safety concerns for a new aircraft is that it is new with an unproven track record. Each subsystem needs to be tested to ensure they are reliable.

Considering the F-35, a modern aircraft in the USAF fleet which has had continued problems meeting deadlines and operational ready status [45]. This is a concern for an advanced trainer that prepares pilots going into the F-35 program. If the F-35 which first flew in the early 2000's is still working out design problems, then what is the optimism for a new plane designed to train pilots for the F-35 platform?

The safety concern for the AMT would be validating the design with flight data. Flight tests validate the various subsystems in the aircraft and ensure they are working properly. Other safety concerns, from a military viewpoint, are flight control systems and cyber safety. Many modern aircraft have augment flight control systems which must validate the programming and computers with hackable data links. Cyber safety is a concern because the aircraft can be rendered useless without a physical attack. Though the AMT is for training and will not see combat, such a concern must be addressed.

If the AMT was not a “paper” design, then upon completion of the design a prototype would be built and tested. Flight tests would ensure the performance meets the requirements and all the subsystems are working properly. The cyber security would test the vulnerability of the data links between the aircraft and the outside sources it communicates with. If there is a security issue, then it would have to be addressed.

New aircraft have always had to address the issue of safety. Which is proven and tested with in-air flight hours. Cyber safety is a more modern problem with a growing concern. This is primarily due to the available computing power now available to the public. Hackers can infiltrate networks with laptops to access systems ran by computers to cause damage. This was not a concern 50 years ago when pilots were responsible for flying, instead of computers.

### 14.3 Summary of Design Parameters and Drawings

The work completed during the aircraft design process has resulted in a preliminary design. The parameters of the AMT's design are listed in Table 47. A 3-view drawing can be found in Figure 141.

Table 47. AMT design parameters

Parameter	Value	SI Units	Value	English Units
Aircraft				
$W_{TO}$	52.2	kN	11,700	lbs
$W_E$	35.0	kN	7,850	lbs
$W_F$	15.4	kN	3,455	lbs
Length	13.78	m	45.2	ft
Ground height	3.73	m	12.2	ft
Engine - EJ200				
Length	4.0	m	13.1	ft
Intake diameter	0.74	m	2.43	ft
Mass	1,000	kg	2,200	lbs
T w/out AB	60	kN	13,460	lbs
T w/ AB	90	kN	20,190	lbs
SFC	22	g/(kN·s)	0.77	lb/(lbf·hr)
SFC w/ AB	48	g/(kN·s)	1.7	lb/(lbf·hr)
Wing				
S	18.4	m <sup>2</sup>	198	ft <sup>2</sup>
AR	5	---	5	---
b	9.60	m	31.5	ft
$\bar{c}$	2.15	m	7.05	ft
$c_r$	3.07	m	10.0	ft
$c_t$	0.768	m	2.52	ft
$\Lambda_{c/4}$	30	deg	30	deg
t/c	8%	---	8%	---
$i_r$	0	deg	0	deg
$i_t$	-5	deg	-5	deg
$\lambda$	0.25	---	0.25	---
Ailerons				
S	0.678	m <sup>2</sup>	7.30	ft <sup>2</sup>
Percent Chord	20	%	20	%
Inner Span Location	3.3	m	10.8	ft
Outer Span Location	4.8	m	15.7	ft

Parameter	Value	SI Units	Value	English Units
Horizontal/Stabilator				
S	2.51	m <sup>2</sup>	27.0	ft <sup>2</sup>
AR	3.8	---	3.8	---
b	3.54	m	11.6	ft
$\bar{c}$	0.971	m	3.18	ft
$c_r$	1.37	m	4.49	ft
$c_t$	0.915	m	3.00	ft
$\Lambda_{LE}$	40	deg	40	deg
t/c	10	%	10	%
$\lambda$	0.4	---	0.4	---
Vertical (2)				
S	1.82	m <sup>2</sup>	19.6	ft <sup>2</sup>
AR	1.5	---	1.5	---
b	1.65	m	5.41	ft
$\bar{c}$	1.17	m	3.84	ft
$c_r$	1.57	m	5.15	ft
$c_t$	0.629	m	2.06	ft
$\Lambda_{LE}$	45	deg	45	deg
t/c	10	%	10	%
$\lambda$	0.4	---	0.4	---
Rudder				
S	0.654	m <sup>2</sup>	7.04	ft <sup>2</sup>
Percent Chord	40	%	40	%
Inner Span Location	0.825	m	2.71	ft
Outer Span Location	1.57	m	5.15	ft
Nose Gear				
Strut length	1.35	m	4.43	ft
Strut diameter	<3.2	cm	<1.26	in
Tire type	VII	---	VII	---
Tire diameter	43.2	cm	1.42	ft
Tire width	11.2	cm	4.41	in
Main Gear				
Strut length	1.35	m	4.43	ft
Strut diameter	<6.6	cm	<2.60	in
Tire type	VII	---	VII	---
Tire diameter	59.2	m	1.94	ft
Tire width	16.5	m	6.50	in
Crew	2	people	2	people

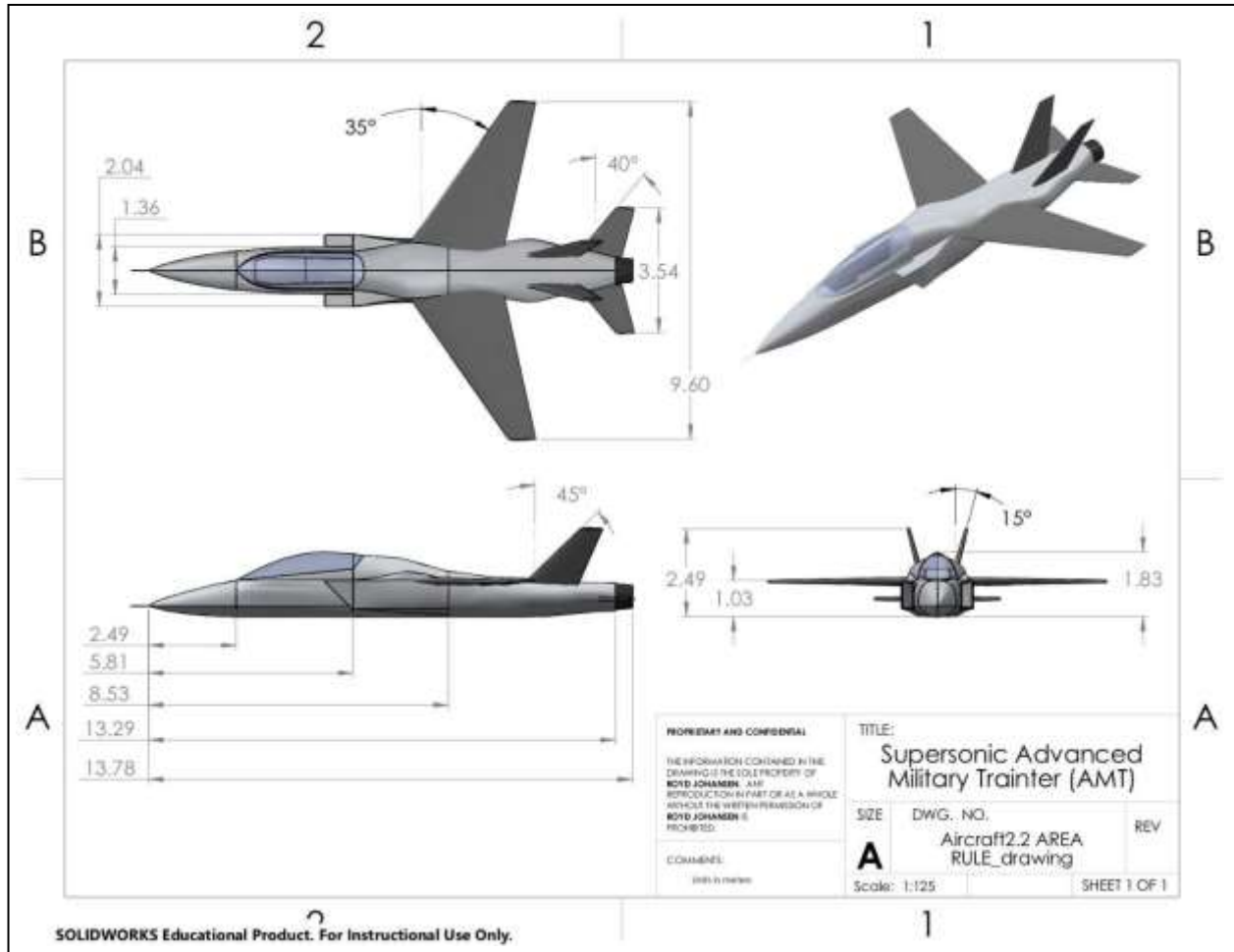


Figure 141. AMT 3-view drawing

#### 14.4 Boeing/Saab T-X Trainer

The winner of the USAF advanced trainer was by the partnership of Boeing and Saab. Since the Boeing/Saab aircraft is only at the prototype stage and it's a new military aircraft, limited data is available. One of the two prototype aircraft is shown in Figure 142 and Table 48 lists the available data on the aircraft.



Figure 142. Boeing/Saab T-X aircraft [44]

Table 48. Boeing/Saab T-X- aircraft specs

Parameter	Value	SI units	Value	English units
Crew	2	people	2	people
Length	14.15	m	46.42	ft
Wingspan	10.0	m	32.81	ft
Height	4.0	m	13.12	ft
W <sub>E</sub>	31.9	kN	7,165	lbs
W <sub>TO</sub>	53.9	kN	12,125	lbs
Engine-GE F404				
T	49	kN	11,000	Lbs
T w/ AB	79	kN	17,700	lbs
V <sub>max</sub>	1,300	km/hr	808	Mph
Range	1,840	km	990	NM
Service ceiling	15.0	km	50,000	ft
RC	10,200	m/min	33,500	ft/min

#### 14.5 Recommendations and Future Work Opportunities

Comparing the AMT to Boeing/Saab's T-X design, the designs are very similar. Which is not surprising considering they are design for the same mission. The noticeable difference is the T-X is slightly larger in length, wingspan, and takeoff weight. The AMT is sized with a greater empty weight. Based on this, there could be additional structural weight savings that are not considered in the methods of the *Airplane Design* series. This would be something that would be determined in design revisions if the AMT went into prototyping. Based on the engine selection, the AMT has a much greater performance capability due to the EJ200 having more thrust than the F404.

The design process has covered a vast spectrum of topics but there are many other areas that could be explored. A detailed structure layout was not covered, and this would be interesting to see how the structure would be incorporated into the design. Once a structural layout is determined, a structural analysis could be performed under the different loading scenarios.

The wing design did not cover an in-depth airfoil selection process. As mentioned in the chapter, this depends on a number of parameters that must be analyzed at critical flight phases. This would help determine the correct airfoil profile distribution across the wing. Once an acceptable design is determined, a small-scale model could be 3D printed and wind tunnel tested. From this, aerodynamic coefficients would be obtained and would be used to verify drag polars and other performance characteristics.

The Class II W&B helped to refine the weights of the various components, but this could be further refined. This would require a detailed breakdown of all the components, and researching which parts are available and which ones need to be built ground up. Once a more accurate subsystem and structure layout is determined, more accurate moments and products of inertia would be determined.

The last topic would be an in-depth stability and control analysis of the dynamic response of the aircraft. With a refined design of the above topics, a proper analysis of the aircraft's response at different flight conditions would be determined. The three main flight conditions to test are: low speed for landing and takeoff, subsonic maneuvering and handling characteristics, and supersonic maneuvering and handling characteristics.

## References

- [1] MIL-C-005011B, “Military Specification: Standard Aircraft Characteristics and Performance,” Retrieved September 4, 2018 from [everyspec.com/MIL-SPECS/MIL-SPECS-MIL-C/MIL-C-005011B\\_NOTICE-1\\_24080/](http://everyspec.com/MIL-SPECS/MIL-SPECS-MIL-C/MIL-C-005011B_NOTICE-1_24080/).
- [2] FA8617-16-R-6219, “System Specification for the Advanced Pilot Training Program,” Retrieved September 5, 2018 from [https://www.defensedaily.com/wp-content/uploads/post\\_attachment/137563.pdf](https://www.defensedaily.com/wp-content/uploads/post_attachment/137563.pdf)
- [3] MIL-STD-203G, “Aircrew Station Controls and Displays: Location, Arrangement and Actuation of, for Fixed Wing Aircraft,” Retrieved September 10, 2018 from [www.everyspec.com/MIL-STD/MIL-STD-0100-0299/MIL-STD-203G\\_9454/](http://www.everyspec.com/MIL-STD/MIL-STD-0100-0299/MIL-STD-203G_9454/).
- [4] MIL-STD-850B, “Aircrew Station Vision Requirements for Military Aircraft,” Retrieved September 10, 2018 from [www.everyspec.com/MIL-STD/MIL-STD-0800-0899/MIL\\_STD\\_850B\\_948/](http://www.everyspec.com/MIL-STD/MIL-STD-0800-0899/MIL_STD_850B_948/).
- [5] Freed, D., “Meet the Jets Competing to Become the Next Air Force Trainer,” *Air & Space Magazine*, Dec. 2017, Retrieved August 30, 2018 from [www.airspacemag.com/military-aviation/t-38-replacements-180967111/](http://www.airspacemag.com/military-aviation/t-38-replacements-180967111/)
- [6] Jackson, P., *Jane’s All the World’s Aircraft 2004-2005 ed.*, Jane’s Information Group Inc. Alexandria, VA, 2004.
- [7] “Aermacchi M-346 Red Air Data Sheet,” Leonardo Aircraft, Retrieved August 30, 2018 from [www.leonardocompany.com/en/-/m-346](http://www.leonardocompany.com/en/-/m-346)
- [8] “Scorpion Data,” Textron Aviation Defense, Retrieved August 31, 2018 from [www.scorpion.txtav.com/en/scorpion-jet-features](http://www.scorpion.txtav.com/en/scorpion-jet-features).
- [9] “T-38 Talon,” United States Air Force, Retrieved August 31, 2018 from [www.af.mil/About-Us/Fact-Sheets/Display/Article/104569/t-38-talon/](http://www.af.mil/About-Us/Fact-Sheets/Display/Article/104569/t-38-talon/). (2005)
- [10] “T-45A Goshawk Training Aircraft,” United States Navy. Retrieved August 31, 2018 from [www.navy.mil/navydata/fact\\_display.asp?cid=1100&tid=2000&ct=1](http://www.navy.mil/navydata/fact_display.asp?cid=1100&tid=2000&ct=1). (2016)
- [11] “Lockheed Martin T-50/FA-50 Golden Eagle,” Retrieved September 1, 2018 from [www.militaryfactory.com/aircraft/detail.asp?aircraft\\_id=513](http://www.militaryfactory.com/aircraft/detail.asp?aircraft_id=513). (2018)
- [12] “Yakovlev Yak-130,” Retrieved September 1, 2018 from [www.militaryfactory.com/aircraft/detail.asp?aircraft\\_id=966](http://www.militaryfactory.com/aircraft/detail.asp?aircraft_id=966). (2017)
- [13] “F-5 Tiger II Supersonic Fighter Aircraft,” Retrieved September 7, 2018 from [www.airforce-technology.com/projects/f-5tiger2/](http://www.airforce-technology.com/projects/f-5tiger2/)
- [14] “Mirage III,” Retrieved September 7, 2018 from [www.dassault-aviation.com/en/passion/aircraft/military-dassault-aircraft/mirage-iii/](http://www.dassault-aviation.com/en/passion/aircraft/military-dassault-aircraft/mirage-iii/)
- [15] “Douglas A-4 Skyhawk Technical Data,” Retrieved September 9, 2018 from [a4skyhawk.info/article/-technical-data](http://a4skyhawk.info/article/-technical-data)

- [16] “L-39 Albatros Trainer / Ground Attack Aircraft,” Retrieved September 9, 2018 from [www.airforce-technology.com/projects/aerol39trainer/](http://www.airforce-technology.com/projects/aerol39trainer/)
- [17] Roskam, J., *Airplane Design Part I: Preliminary Sizing of Airplanes*, DARcorporation, Lawrence, KA, 2017.
- [18] Anderson, J. D., *Introduction to Flight*, McGraw-Hill, Boston, MA, 2012.
- [19] Roskam, J., *Airplane Design Part II: Preliminary Configuration Design and Integration of the Propulsion System*, DARcorporation, Lawrence, KA, 2012.
- [20] Roskam, J., *Airplane Design Part III: Layout Design of Cockpit, Fuselage, Wing and Empennage: Cutaways and Inboard Profiles*, DARcorporation. Lawrence, KA, 2011.
- [21] Roskam, J., *Airplane Design Part V: Component Weight Estimation*, DARcorporation. Lawrence, KA, 2003.
- [22] Nicolai, L.M., *Fundamentals of Aircraft Design*, METS, Inc., 6520 Kingsland Court, CA, 95120, 1975.
- [23] Torenbeek, E., *Synthesis of Subsonic Airplane Design*, Kluwer Boston Inc., Hingham, ME, 1982.
- [24] Roskam, J., *Airplane Design Part VI: Preliminary Calculation of Aerodynamic, Thrust and Power Characteristics*, DARcorporation, Lawrence, KA, 2008.
- [25] Dunnam, M. P., et al., “Handbook of Aviation Fuel Properties,” Retrieved February 11, 2019 from [www.dtic.mil/dtic/tr/fulltext/u2/a132106](http://www.dtic.mil/dtic/tr/fulltext/u2/a132106), 1983.
- [26] Roskam, J., *Airplane Design Part IV: Layout of Landing Gear & Systems*, DARcorporation, Lawrence, KA, 2010.
- [27] Taylor, A. S., “An Analysis of Available Data on the Local Aerodynamic Centres of Aerofoils in Two- and Three-Dimensional Flow,” Aeronautical Research Council Reports and Memoranda, Retrieved February 22, 2019 from [naca.central.cranfield.ac.uk/reports/arc/rm/3000.pdf](http://naca.central.cranfield.ac.uk/reports/arc/rm/3000.pdf).
- [28] Nelson, R.C., *Flight Stability and Automatic Control*, McGraw-Hill, Boston, MA, 1998.
- [29] Hoak, D.E., et al, “USAF Stability and Control Datcom,” Flight Control Division, Air Force Flight Dynamics Laboratory, WPAFB, Ohio, Retrieved February 23, 2019 from [rahauav.com/Library/Stability-Control/USAF%20DASTCOM\\_www.rahauav.com.pdf](http://rahauav.com/Library/Stability-Control/USAF%20DASTCOM_www.rahauav.com.pdf).
- [30] Jones, R.T., “Theory of Wing-Body Drag at Supersonic Speeds,” NACA RM A53H18a, Retrieved December 10, 2018 from [ntrs.nasa.gov/archive/nasa/casi.ntrs.nasa.gov/19930092281.pdf](http://ntrs.nasa.gov/archive/nasa/casi.ntrs.nasa.gov/19930092281.pdf).
- [31] Nelson, B.D., “Design Scope for Student Supersonic Projects,” AIAA Paper-86-2638, Presented at the AIAA/AHS/ASEE Aircraft Systems, Design and Technology Meeting, Dayton, Ohio.
- [32] MIL-A-8861B, “Military Specification: Airplane Strength and Rigidity Flight Loads,” Retrieved March 14, 2019 from [everyspec.com/MIL-SPECS/MIL-SPECS-MIL-A/MIL-A-8861B\\_6743](http://everyspec.com/MIL-SPECS/MIL-SPECS-MIL-A/MIL-A-8861B_6743).

- [33] MIL-A-8860B, “Military Specification: Aircraft Strength and Rigidity,” Retrieved March 14, 2019 from [everyspec.com/MIL-SPECS/MIL-SPECS-MIL-A/MIL-A-8860B\\_6742](http://everyspec.com/MIL-SPECS/MIL-SPECS-MIL-A/MIL-A-8860B_6742).
- [34] Mattingly, J.D., *Elements of Propulsion: Gas Turbines and Rockets*, American Institute of Aeronautics and Astronautics, Reston, VA, 2006.
- [35] Roskam, J., *Airplane Flight Dynamics and Automatic Flight Controls*, DARcorporation, Lawrence, KA, 2001.
- [36] Roskam, J., *Airplane Design Part VIII: Airplane Cost Estimation*, DARcorporation, Lawrence KA, 2010.
- [37] Norquist, D., “Fiscal Year (FY) 2019 Fuel Prices,” Retrieved March 26, 2019 from [www.dla.mil/Portals/104/Documents/Energy/Standard%20Prices/Petroleum%20Prices/E\\_PetroleumStandardPricesFY19\\_181001.pdf?ver=2018-10-01-131358-203](http://www.dla.mil/Portals/104/Documents/Energy/Standard%20Prices/Petroleum%20Prices/E_PetroleumStandardPricesFY19_181001.pdf?ver=2018-10-01-131358-203).
- [38] Raymer, D.P., *Aircraft Design: A Conceptual Approach 4<sup>th</sup> Ed.*, American Institute of Aeronautics and Astronautics, Blacksburg, VA, 2006.
- [39] U.S. Department of Defense, “Contracts for September 27, 2018,” Retrieved March 30, 2019 from <https://dod.defense.gov/News/Contracts/Contract-View/Article/1647166/>.
- [40] International Air Transportation Association, “Fact Sheet: Climate Change & CORSIA,” Retrieved December 8, 2018 from [https://www.iata.org/pressroom/facts\\_figures/fact\\_sheets/Documents/fact-sheet-climate-change.pdf](https://www.iata.org/pressroom/facts_figures/fact_sheets/Documents/fact-sheet-climate-change.pdf)
- [41] Selby, G., “Military’s Shift Toward Renewable Energy,” Department of Defense. Retrieved December 8, 2018 from <http://science.dodlive.mil/2015/08/12/military-shift-toward-renewable-energy/>.
- [42] Southern Company, “How Renewable Energy Is Making Our Military Bases More Resilient,” Retrieved December 8, 2018 from <https://www.southerncompany.com/newsroom/2018/july-2018/renewable-energy-making-military-resilient.html>
- [43] Ramadan, M., “Renewable Energy in the Military,” Stanford University, Retrieved December 8, 2018 from [large.stanford.edu/courses/2016/ph240/ramadan2/](http://large.stanford.edu/courses/2016/ph240/ramadan2/).
- [44] Gertler, J., “Advanced Pilot Training (T-X) Program,” Retrieved December 8, 2018 from <https://fas.org/sgp/crs/weapons/R44856.pdf>
- [45] Clark, C., “F-35 Problems: Late IOTE, F-35A Gun Inaccurate, F-35B Tires, Threat Data, Cyber,” Breaking Defense, Retrieved December 9, 2018 from <https://breakingdefense.com/2018/01/f-35-problems-late-iote-f-35a-gun-inaccurate-f-35b-tires-threat-data-cyber/>